NASA CONTRACTOR REPORT

NASA CR

NASA CR-2599

COMPUTATION OF THE TRANSONIC PERTURBATION FLOW FIELDS AROUND TWO- AND THREE-DIMENSIONAL OSCILLATING WINGS

Warren H. Weatherill, F. Edward Ehlers, and James D. Sebastian

Prepared by
THE BOEING COMMERCIAL AIRPLANE COMPANY
Seattle, Wash. 98124
for Langley Research Center

NATIONAL AERONAUTICS AND SPACE ADMINISTRATION • WASHINGTON, D. C. • DECEMBER 1975

1. Report No.	2. Government Accession No.	3. Recipient's Catalog No.
NASA CR-2599		

4. Title and Subtitle	5. Report Date
COMPUTATION OF THE TRANSONIC PERTURBATION FLOW FIELDS AROUND TWO- AND THREE-DIMENSIONAL OSCILLATING WINGS	DECEMBER 1975
	6. Performing Organization Code
7. Author(s)	8. Performing Organization Report No.
Warren H. Weatherill, F. Edward Ehlers, and James D. Sebastian	D6-42536
	10. Work Unit No.
9. Performing Organization Name and Address	
Boeing Commercial Airplane Company P.O. Box 3707 Seattle, Washington 98124	11. Contract or Grant No. NAS1-13002
	13. Type of Report and Period Covered
12. Sponsoring Agency Name and Address	
National Aeronautics and Space Administration Washington, D.C. 20546	14. Sponsoring Agency Code Contractor Report

15. Supplementary Notes

FINAL REPORT

16. Abstract

Analytical and empirical studies of a finite difference method for the solution of the transonic flow about an harmonically oscillating wing are presented along with a discussion of the development of a pilot program for three-dimensional flow. In addition, some two- and three-dimensional examples are presented.

The procedure used consists of linearizing the partial differential equation for unsteady transonic flow by dividing the perturbation velocity potential into steady and unsteady parts. The steady potential is evaluated from a non-linear differential equation. The unsteady potential is obtained by solving a linear differential equation with coefficients that are functions of the steady-state velocity potential. The differential equation is of a mixed type, being elliptic or hyperbolic wherever the steady flow equation is elliptic or hyperbolic. Central differences were used for all derivatives except at supersonic points where a backward differencing is used for the streamwise direction. The resulting set of simultaneous equations for the velocity potential are solved using line relaxation procedures.

It was found that the number of iterations to solution convergence is sensitive to the value of over-relaxation and underrelation factors, and that there is a limit on reduced frequency, as a function of Mach number and the size of mesh regions, above which the relaxation procedure will not converge. Row relaxation was generally found to be more efficient than column relaxation. A direct solution proved to be fast and efficient for problems with small numbers of grid points. However, it has large storage requirements and it appears impractical for direct application to realistically sized problems. No improvement in solution convergence was obtained using convergence acceleration techniques. The pilot three-dimensional program for rectangular planforms was successfully applied to an aspect ratio 5 wing and the results are compared with corresponding two-dimensional and linear results.

17. Key Words (Suggested by Author(s))	18. Distribution Statement
Unsteady flow, transonic flow, oscillating wings, oscillating airfoils, flutter	Unclassified—unlimited Subject Category 02

19. Security Classif. (of this report)	20. Security Classif. (of this page)	21. No. of Pages	22. Price*
Unclassified	Unclassified	154	$6.25

For sale by the National Technical Information Service, Springfield, Virginia 22161

CONTENTS

FIGURES

FIGURES–Continued

COMPUTATION OF THE TRANSONIC PERTURBATION FLOW FIELDS AROUND TWO- AND THREE-DIMENSIONAL OSCILLATING WINGS

W.H. Weatherill, F.E. Ehlers, and J.D. Sebastian

The Boeing Company

1.0 SUMMARY

The problem of generating unsteady transonic air forces for use in flutter analyses remains a significant problem. One of the most promising procedures for solving this problem is reported by Ehlers in reference 1. It consists of a finite difference solution for the differential equation of the unsteady velocity potential. The differential equation is linear and includes coefficients that vary with respect to space, being a function of the steady flow velocity potential.

The differential equation, together with the boundary conditions, is derived in detail by Ehlers in reference 1. Ehlers also presents a finite difference solution scheme based on that used by Murman and Cole (ref. 2) and Krupp and Murman (ref. 3) for the solution of steady transonic flow. The work of reference 1 resulted in the development of the method, a pilot program for two-dimensional flow, and the calculation of several examples including both the flat-plate and NACA 64A006 airfoil. The work of this report is a direct extension of the earlier work and includes an investigation of solution parameters in order to reduce the computer resources needed to produce converged results; an extension of the two-dimensional examples of reference 1; the development of a pilot three-dimensional program; and an analysis of the dependence on frequency of the convergence of the solution scheme.

The main results of the study are as follows:

a) The number of iterations to solution convergence is sensitive to the value of overrelaxation and underrelaxation factors.

b) There is an upper limit on frequency, depending on Mach number and size of mesh region, above which the relaxation procedure will not converge.

c) Row line relaxation is more efficient than column relaxation except at combinations of Mach number and frequency for which convergence is marginal.

d) The direct solution is fast and efficient for problems with a small number of grid points. However, the storage requirements are large and incore versions are impractical for realistically sized problems, even for cases in which the flow is all subsonic. The direct solution may provide a means for avoiding or getting around the frequency limitation problem discussed in b) above.

e) A number of two-dimensional examples were calculated at Mach numbers of 0.85 and 0.9 and included flat-plate and NACA 64A006 airfoils. For the flat-plate cases, the finite difference results compare favorably with results from linear theory using the program of Rowe et al. (refs. 4 and 5). Correlation of the airfoil results with the experimental data of Tijdeman and Schippers (ref. 6) is about the same as Ehlers found in reference 1. In addition, two Freon calculations were made at M = 0.9.

f) No advantage was found in using convergence acceleration methods based on the Aitken-Shanks delta-square process.

g) A pilot three-dimensional program was developed for rectangular wings. Pressure difference coefficients are presented for an aspect ratio 5 planform in harmonic pitch. Results for a flat-plate configuration compare well with corresponding results from linear theory. Results for a NACA 64A006 configuration appear reasonable, although there are no experimental data available for correlation purposes.

2.0 INTRODUCTION

An initial attempt to apply finite difference procedures in the solution of the unsteady transonic flow problem is described by Ehlers in reference 1. This report is a sequel to that work, and includes the investigation of solution parameters in order to reduce computer resources required to obtain useful results, an extension of the two-dimensional examples of reference 1, and development of a pilot three-dimensional program.

Shortly after the publication of reference 1, Traci et al. (ref. 7) published a paper describing a second solution to the unsteady transonic problem using finite differences. They, however, obtained a different differential equation and boundary conditions by retaining only the first-order time derivative term of the differential equation. The finite difference solution procedure appears essentially the same as that used in reference 1.

The purpose of this continuing investigation is to provide a practical analytical procedure for predicting the aerodynamic forces for flutter analyses. The examples of reference 1 showed relatively good correlation with linear analytical results and experimental results. However, the amount of computer resources required to generate the results were large enough to make the procedure impractical for flutter calculations. This particular problem is significantly reduced with the use of high values of the overrelaxation factor (ORF) and sequential refinement of the finite difference mesh, as will be discussed in section 5.2.

In the present work, the unsteady transonic flow is analyzed by solving for a scaled perturbation velocity potential, φ. The velocity components of the flow, corresponding to the physical coordinates x_0, y_0, z_0 are

$$u = u_0 (1+\phi_{x_0}) \qquad v = u_0 \phi_{y_0} \qquad w = u_0 \phi_{z_0}$$

where u_0 is the freestream velocity and ϕ is the perturbation velocity potential. The scaled potential, φ, is related to the full potential, ϕ, by the relation

$$\phi = \epsilon \varphi$$

where ϵ is assumed to be a small quantity defined in terms of the airfoil thickness ratio. The differential equation for the velocity potential in unsteady transonic flow as derived by Ehlers is

$$\left\{\left[K - (\gamma+1)\varphi_{0_x}\right]\varphi_{1_x}\right\}_x + \varphi_{1_{yy}} + \varphi_{1_{zz}} - (2i\omega/\epsilon)\varphi_{1_x} + \left[\omega^2/\epsilon - (\gamma-1)i\omega\varphi_{0_{xx}}\right]\varphi_1 = 0 \qquad (1)$$

Where

φ_0 = steady velocity potential

φ_1 = unsteady velocity potential

M = Mach number

ω = reduced frequency

i = $\sqrt{-1}$

γ = specific heat ratio

ϵ = $(\delta/M)^{2/3}$ where δ is the thickness ratio or measure of camber and angle of attack

K = $(1 - M^2)/M^2\epsilon$

x,y,z are the scaled coordinates $x = x_0$, $y = \mu y_0$, $z = \mu z_0$, where x_0, y_0, z_0 are the physical coordinates and $\mu = \delta^{1/3} M^{2/3}$

Equation (1) may be rewritten as

$$\left[u\varphi_{1_x} - (2i\omega/\epsilon)\varphi_1\right]_x + \varphi_{1_{yy}} + \varphi_{1_{zz}} + q\varphi_1 = 0 \tag{2}$$

and this will be the form used throughout the report. For two-dimensional flows, equation (2) is rewritten as

$$\left[u\varphi_{1_x} - (2i\omega/\epsilon)\varphi_1\right]_x + \varphi_{1_{yy}} + q\varphi_1 = 0 \tag{3}$$

The wing shape as a function of time is written

$$z_0 = \delta f(x,y,t) \tag{4}$$

and the linearized boundary condition for the total velocity potential, φ, is

$$\varphi_z = f_x(x,y,t) + f_t(x,y,t) \tag{5}$$

For two-dimensional flow, the z_0 is replaced by y_0 and $f = f(x,t)$.

Equations (2) and (3) are rewritten as finite difference equations and solutions are obtained using relaxation procedures. The finite difference equations together with far-field boundary conditions for three-dimensional flow are presented in appendices A and B.

An important development during the course of the program was the encountering of difficulties in obtaining solution convergence–first for row relaxation, and then for certain combinations of Mach number and frequency. This led to analytical investigations of the relaxation procedures used that are discussed in section 4.0 and described in detail in appendices C through E.

Empirical investigations of the relaxation procedures are presented in section 5.0 with two-dimensional examples presented in section 6.0.

Finally, section 7.0 describes the three-dimensional pilot program together with some examples.

3.0 SYMBOLS AND ABBREVIATIONS

a, b	coefficients for y, z differences corresponding to second derivatives, with appropriate subscripts (eq. A3); also length of sides of region for finite difference solution
ADI	alternating-direction-implicit iteration scheme
b	semichord of wing
BSOR	block successive overrelaxation
c, d	coefficients for x difference corresponding to second derivative (eq. A3)
c	height of side of region for finite difference
c_{s_1}, c_{s_2}, d_{s_1}, d_{s_2}	equation (A13) in appendix A
c_{k_1}, c_{k_2}, c_{k_3}, c_{k_4}	equation (A27) in appendix A
c_1, d_1, c_2, d_2	coefficients for second-order accurate difference corresponding to first derivative (eq. A3)
ΔC_p	jump in pressure coefficient
E	coefficients in difference equations with appropriate subscripts; also used as unknown error in Von Neumann analysis
ERROR	see equation (19)
f(x,y,t)	instantaneous wing shape defined by $z_0 = \delta f(x,y,t)$
f(x,t)	instantaneous airfoil shape defined by $y_0 = \delta f(x,t)$
f_0	undisturbed wing or airfoil shape
f_1	unsteady contribution to wing or airfoil shape
F_{ij}	see equation (A6)
h	$z_{k_m} + 1 - z_{k_m}$
i,j,k	x,y,z subscripts for points in the mesh
i	$\sqrt{-1}$

i_a	x index for first mesh point behind hinge
$i_{max}, j_{max}, k_{max}$	maximum number of x,y,z mesh planes respectively
i_1	x index for trailing edge
I_w	integral defined by equation (B2)
j_m	y mesh line just below airfoil (two-dimensional configuration)
K	$(1 - M^2)/M^2 \epsilon$
k_m	z mesh plane below wing (three-dimensional configuration)
L,U	superscripts denoting lower or upper boundary on F_{ij}; also used to denote lower and upper triangular matrices resulting from matrix decomposition (sec. 5.3.2)
m	subscript used on mesh point indices to denote points adjacent to and below the airfoil or wing
M	freestream Mach number
n	number of iteration
N_x, N_y, N_z	number of mesh increments in x,y,z directions
ORF	overrelaxation factor
P(x,y)	$\varphi_{1x} + i\omega\varphi_1$ acceleration (or pressure) potential
q	$\omega^2/\epsilon - i\omega(\gamma - 1)\varphi_{0xx}$
r	overrelaxation factor
R	variable defined for equations (A18)
R_1, R_0	variables defined in equation (B4)
s	semispan of wing
s_1	$(y_{j_m+2} - y_{j_m+1})/h$
s_2	$(y_{j_m} - y_{j_m-1})/h$
u	$K - (\gamma + 1)\varphi_{0x}$
URF	underrelaxation factor

x_0, y_0, z_0	physical coordinates
x,y,z	scaled coordinates $(x_0, \mu y_0, \mu z_0)$ for the three-dimensional problem; the scaled coordinates for the two-dimensional problem are x and y, with x again being the direction of fluid flow
x_1', y_1', z_1'	variables of integration
$\bar{x},\bar{y},\bar{z}$	coordinates defined in equation (A18)
x_ℓ, x_t	coordinates of leading and trailing edges
x_a	coordinate of control surface hingeline
Δx_1	$x_i - x_{i-1}$
Δx_2	$x_{i-1} - x_{i-2}$
y_t	coordinate of wing tip
β	$\sqrt{1 - M^2}$
β_1, β_2	parameters in equation (C18)
γ	ratio of specific heats for air
$\Delta\phi_1$	jump in ϕ_1 at plane of wing or vortex wake
ϵ	$(\delta/M)^{2/3}$
δ	thickness ratio or measure of camber and angle of attack
δ_1	$x_2 - x_1$
δ_2	$x_{i_{max}} - x_{i_{max}-1}$
λ_1	$\omega M/(1 - M^2)$
μ	Scale factor on y_0 and z_0, $\mu = \delta^{1/3} M^{2/3}$
ϕ	unscaled perturbation velocity potential
φ_0	steady scaled perturbation velocity potential
φ_1	unsteady scaled perturbation velocity potential
φ_{1_W}	wake integral defined in equation (A24)
χ	acceleration or pressure potential

Ψ	fundamental source solution of integral equation for evaluation of far-field boundary conditions
ω	angular reduced frequency (semichord times frequency divided by the the freestream velocity)
ω_{cr}	critical reduced frequency (sec. 4.2)
$A \otimes B$	Kronecker product of matrices A and B (see sec. D.1.3 in app. D)

4.0 ANALYTICAL EVALUATION OF THE CONVERGENCE OF THE RELAXATION TECHNIQUES USED FOR THE UNSTEADY TRANSONIC FLOW PROBLEM

During the course of the program, a considerable effort has been made to analyze and improve upon the relaxation procedures used to solve the finite difference equations. At first this was done to ensure the convergence of the mixed-flow problem using row relaxation. It was found that a straightforward implementation of this scheme, in direct analogy to the column relaxation scheme, was divergent for the mixed-flow problem. Following the recommendations of Jameson (refs. 8 and 9), an analysis was made in which successive iterations were treated as a pseudotime variation. This analysis showed the need for the addition of time-like difference terms in the program. A summary of this work is given in section 4.1 and a detailed discussion is presented in appendix C.

The next problem was encountered in attempting to complete some of the numerical examples. In particular it was found that, for a given Mach number, there was an upper limit on the reduced frequency at which the relaxation solution converged. At higher values of frequency, the solution was found to diverge. This behavior was found to be essentially independent of the type of relaxation scheme (i.e., row or column), the mesh spacings, the relaxation factor, and whether the differential equation was purely elliptic (flat-plate configuration) or of mixed elliptic and hyperbolic type (airfoil section configuration). A matrix analysis of a simplified version of the problem revealed that there is indeed an expected frequency limitation on convergence, and this may be recognized by noting the similarity between the unsteady differential equation and the Helmholtz (or reduced wave) equation. This analysis is summarized in section 4.2 and a detailed account presented in appendix D..

Finally, a third means of analyzing relaxation procedures is the Von Neumann stability criterion. The application of this analysis method to the pertinent relaxation process generally concurs with the findings of the preceding two analyses. The details of this analysis are presented in appendix E and summarized in section 4.3.

4.1 A TIME-LIKE CHARACTERISTICS ANALYSIS

Jameson treats the difference between two consecutively iterated values of the velocity potential as a time derivative, namely:

$$\varphi_{1_{ij}}^{(n-1)} - \varphi_{1_{ij}}^{(n)} = -\Delta t \cdot \frac{\partial \varphi_{1_{ij}}^{(n)}}{\partial t} \tag{6}$$

where the superscripts denote the iteration number and the subscript i, j denotes the finite difference point. When this expression is substituted into the difference equation and all terms are expanded in a Taylor's series about the central point, a differential equation results that contains not only the terms of the original differential equation but also additional time derivatives. A study of variation with time of the solutions to this differential equation with arbitrary initial conditions will reveal some insight into how the iteration method will converge.

For flows that are subcritical, the simple straightforward difference equation developed by Murman and Cole (ref. 2) will converge whether column solution or row solution of the difference equations are used in the relaxation procedure. Column relaxation will also work for mixed flow, but row relaxation will diverge unless time-like difference terms are added. The time-like differential equations for both column and row relaxation are derived in appendix C. At elliptic points, row relaxation for sweeping toward the airfoil ($y < 0$) leads to the differential equation (C 15), i.e.

$$(u\varphi_{1_x})_x - \frac{2i\omega}{\epsilon}\varphi_{1_x} + \varphi_{1_{yy}} + q\varphi_1 + \Delta t \cdot \left[2a_j - \frac{2}{r}(a_j + b_j)\right]\varphi_{1_t} - 2\left(\frac{\Delta t}{\Delta y_j}\right)\varphi_{1_{yt}} = 0 \tag{7}$$

where $\Delta y_j = y_{j+1} - y_{j-1}$ and r is the overrelaxation parameter. The differential equation is expressed in canonical form by introducing a new time $\tau = t + \frac{\Delta t}{\Delta y_j}\, y$.

Thus

$$(u\varphi_{1_x})_x - \frac{2i\omega}{\epsilon}\varphi_{1_x} + \varphi_{1_{yy}} + q\varphi_1 - \Delta t \cdot \left[\frac{2(a_j + b_j)}{r} - 2a_j\right]\varphi_{1_\tau} - \left(\frac{\Delta t}{\Delta y_j}\right)^2 \varphi_{1_{\tau\tau}} = 0 \tag{8}$$

This equation is hyperbolic in the time and hence initial value problems are properly posed. For supersonic points, $u < 0$ and $\varphi_{1_{\tau\tau}}$ terms have the same sign rendering the equation hyperbolic in y. Since supersonic points experience only upstream influences, the equation must be made hyperbolic with respect to the variable x. This is achieved by adding difference terms of the form yielding time derivatives φ_{1xt} and φ_{1t} and choosing their coefficients so that the resulting coefficient of the $\varphi_{1_{\tau\tau}}$ term is positive. The method was employed by Jameson for the steady-state equation for the velocity potential and was found to be successful for the linear unsteady differential equation for harmonic motion discussed in this document. The inclusion of these additional terms does not affect the final solution since these terms become negligible when the solution is converged.

Introducing the time derivative terms into the difference equations for column relaxation at elliptic points leads to the following time-like differential equation for sweeping in the increasing x direction:

$$(u\varphi_{1_x})_x - \frac{2i\omega}{\epsilon}\varphi_{1_x} + \varphi_{1_{yy}} + q\varphi_1 - 2u\alpha_1\varphi_{1_{xt}} - 2(u\alpha_2 - i\omega\alpha_3)\varphi_{1_t} = 0 \tag{9}$$

where α_1, α_2, and α_3 are given in equation (C8). With the new time variable, $\tau = t + \alpha_1 x$, the equation takes the canonical form

$$(u\varphi_{1_x})_x - \frac{2i\omega}{\epsilon}\varphi_{1_x} + \varphi_{1_{yy}} + q\varphi_1 - 2(u\alpha_2 - i\omega\alpha_3)\varphi_{1_\tau} - u\alpha_1^2\varphi_{1_{\tau\tau}} = 0 \tag{10}$$

Since for elliptic or subsonic points, $u > 0$, this equation is hyperbolic in time. At hyperbolic points, backward differences are used for the x derivatives and the resulting differential equation contains no $\varphi_{1_{TT}}$ term but takes the form (eq. C11)

$$(u\varphi_{1_x})_x - 2\frac{i\omega}{\epsilon}\varphi_{1_x} + \varphi_{1_{yy}} + q\varphi_1 - 2u\frac{\Delta t}{\Delta x_1(\Delta x_1 + \Delta x_2)}\left(\frac{r-1}{r}\right)\varphi_{1_t}$$

$$+2\frac{i\omega}{\epsilon}\Delta t \cdot \left(\frac{1}{\Delta x_1} + \frac{1}{\Delta x_1 + \Delta x_2}\right)\varphi_{1_t} = 0 \tag{11}$$

where $\Delta x_1 = x_i - x_{i-1}$ and $\Delta x_2 = x_{i-1} - x_{i-2}$.

Since u is negative, this equation is parabolic in time, but hyperbolic with respect to x. To have damping at supersonic points, equation (11) indicates that r must be less than 1, and hence underrelaxation must be used at supersonic points.

4.2 A MATRIX CONVERGENCE ANALYSIS

The observed frequency-dependent limitation on the convergence of the overrelaxation method may be analyzed according to a system matrix approach. In outline, the method proceeds as follows: first, simplifying assumptions are made that replace the original problem with that of solving

$$\varphi_{1_{xx}} + \frac{1}{K}\varphi_{1_{yy}} - \frac{2i\omega}{\epsilon K}\varphi_{1_x} + \frac{\omega^2}{\epsilon K}\varphi_1 = 0 \tag{12}$$

over a rectangle of sides a, c and with φ_1 being prescribed on the sides. Then the region and differential equation are discretized using a uniform mesh and central differences, respectively, leading to a system of linear difference equations. This system is written in matrix form as $A\underline{\varphi}_1 = \overline{R}$, where $\underline{\varphi}_1$ is the vector of unknown values of φ_1 at the interior mesh points and $\overline{R}$ is a vector containing the boundary values. The elements of A are known functions of the reduced frequency, ω. A theorem is invoked that states that under certain mild assumptions, the line or block overrelaxation scheme used in the program will converge if, and only if, all the eigenvalues of A are positive; i.e., A is positive definite. To apply the theorem, the eigenvalues of A, which are, of course, also functions of ω, are determined; then the value of ω for which the smallest eigenvalue becomes zero is found. We call this value the "critical frequency" denoted by ω_{cr}, since by virtue of the theorem, it is the value of ω below which relaxation will converge and above which it will diverge.

Exact and approximate formulas for ω_{cr} derived in this way are given in appendix D. Here we give only the approximate formula, which is

$$\omega_{cr} = \pi\frac{1-M^2}{M}\left[\frac{1}{a^2} + \frac{1}{Kc^2}\right]^{1/2} \tag{13}$$

where a and c are the width and height of the mesh region. This completes the outline of the analysis, the goal of which was to find a formula for ω_{cr} to explain the frequency limitation. We now turn to validation of the formula.

A comparison of the critical frequency predicted from the analysis of the simplified problem with various computational observations is given in figure 1. The solution region in all cases was defined as the rectangle x = -2.65 to 2.75; y = -6.25 to 6.25. The approximate prediction formula given by equation (13) was used since the number of mesh points employed (at least 25 x 20) was sufficiently large in each direction so that the difference between ω_{cr} from the exact and approximate formulas is less than 1%.

With regard to the computational observation points, those indicating convergence correspond to the largest frequency for which convergence was obtained at the given Mach number. In the two airfoil cases, the convergence was marginal and resulted only after substantial experimentation with the values of the under- and overrelaxation factors, at supersonic and subsonic points, respectively. In the case of the flat plate, additional computations were performed at slightly higher frequencies; actual divergence of error measure was observed, as indicated in figure 1.

Further validation of the results of the matrix analysis was obtained as follows. It is an immediate inference from equation (13) that a decrease in the dimensions of the solution region implies an increase in the frequency for which convergence of overrelaxation can be obtained. As a test of this inference, and hence of equation (13), the dimensions of the solution region were reduced from 5.4 to 2.8 in the x -direction and 12.5 to 6.0 in the z-direction. For these dimensions and M = 0.9, the critical frequency predicted by equation (13) is 0.254. Flat-plate computations were performed for ω = 0.25 and ω = 0.30, with the result that convergence was observed in the former case and divergence occurred in the latter case.

The existence and general location of a critical frequency, dependent on Mach number and predicted by the analysis of the simplified problem, are in good agreement with the computational results from the full problem. Prediction of the exact location of the critical frequency is not to be expected since, of the five assumptions made in the formulation of the simplified problem in appendix D, all in the airfoil case and b through d in the flatplate case are violated in the actual computational scheme. The results strongly indicate that the cause of the frequency limitation in the full problem is the same as that in the simplified problem: the failure of the system matrix to remain positive definite.

It should be noted that the conclusions of this section so far are relevant to relaxation solutions. For a direct solution where A is formed from the complete set of simultaneous albegraic equations and the solution is obtained by matrix inversion, the matrix A need only be nonsingular rather than positive definite for solutions to exist. Thus use of a direct solution procedure may well lead to solutions at reduced frequencies above ω_{cr}. However, since the far-field must be updated as the velocity potential distribution changes, the matrix form is more nearly $A\bar{\varphi}_1(n) = R\bar{\varphi}_1(n-1)$, where $\bar{\varphi}_1(n)$ and $\bar{\varphi}_1(n-1)$ are the vectors of values of the unknown velocity potential and the values determined in the preceding solution, respectively. This iterative form resulting from the calculation of the far-field boundary conditions imposes the additional condition for solution convergence that the effective eigenvalues of the matrix product $A^{-1}R$ must be less than one in modulus.

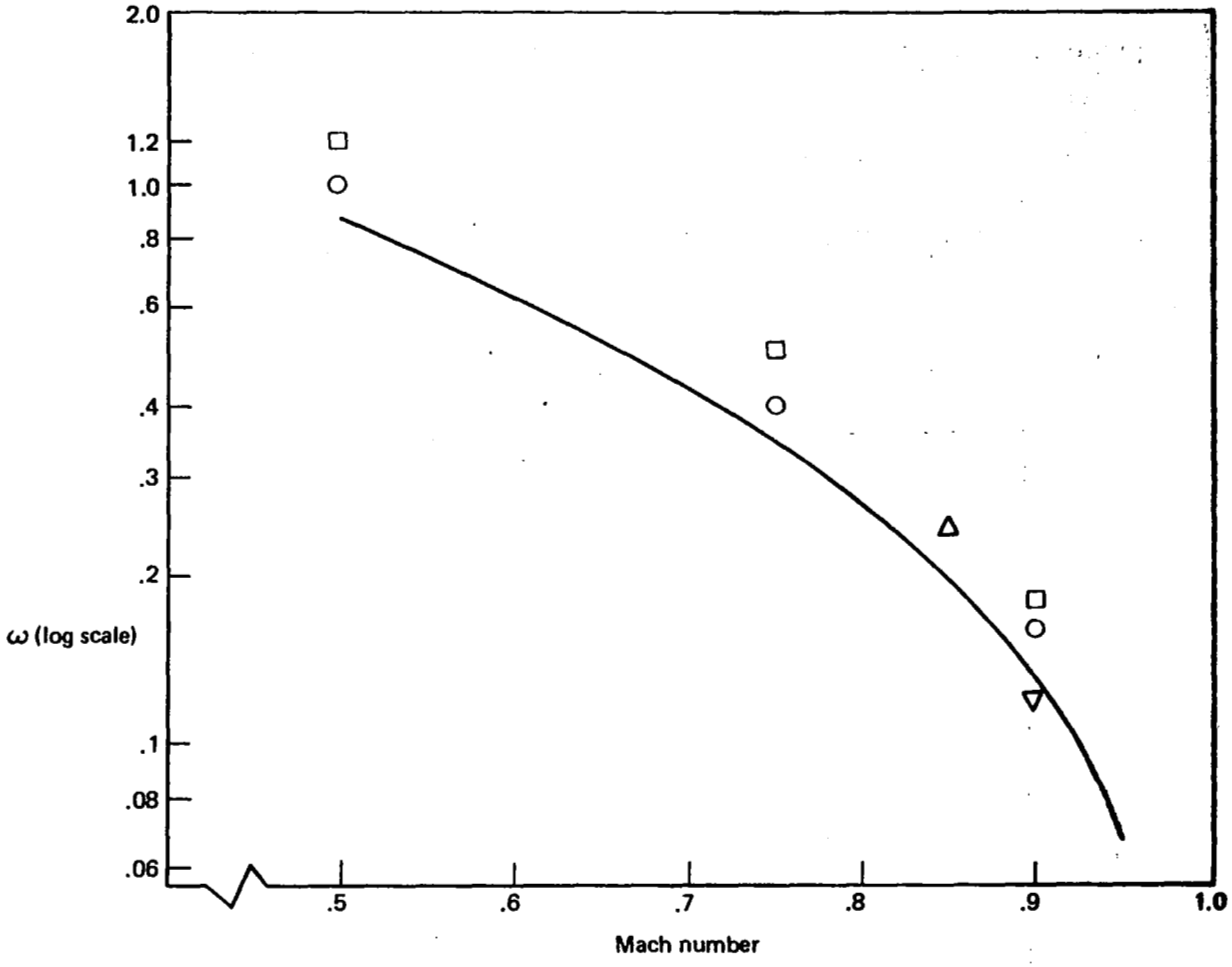

Figure 1. — Comparison of Predicted Critical Frequency with Computational Results

4.3 A VON NEUMANN STABILITY ANALYSIS

A third means of examining the convergence of a differencing method is the Von Neumann analysis of error propagation. Let $E_{k\ell}$ be the error at the k, ℓ grid point; then for a uniform x and a uniform y mesh the errors may be expressed in the form

$$E_{kl} = \sum_{p=-k_{max}}^{p=+k_{max}} \sum_{q=-\ell_{max}}^{q=+\ell_{max}} A_{pq}\, e^{2\pi i\left(kp\frac{\Delta x}{a}+\ell q\frac{\Delta y}{c}\right)} \tag{14}$$

where a and c are the width and height of the mesh region. Since the difference equation is linear, only a single term need be analyzed.

A solution of the difference equation of the form

$$\varphi_{1\,k\ell}^{(n)} = g^n\, e^{2\pi i\left(kp\frac{\Delta x}{a}+\ell q\frac{\Delta y}{c}\right)}$$

where n is the order of iteration, has the appropriate initial value consistent with equation (14). In order for errors to decrease with increasing n, g must have a magnitude less than one. In appendix E, the equations of column relaxation, row relaxation, and an ADI (alternating direction implicit) method were analyzed. The condition $|g| < 1$ in all cases reduced to the same inequality limiting the range of frequency, namely:

$$\omega^2 + \frac{2\omega}{\Delta x}\sin\theta_1 < 2\frac{1-M^2}{M^2}\left[\frac{1-\cos\theta_1}{\Delta x^2} + \frac{1-\cos\theta_2}{K\Delta y^2}\right] \tag{15}$$

where $\theta_1 = 2\pi p\frac{\Delta x}{a}$ and $\theta_2 = 2\pi q\frac{\Delta y}{c}$.
This relation shows that the range of frequency is increasingly limited as the Mach number approaches 1.

In the hopes of obtaining better convergence for the higher reduced frequency problem, an ADI (alternating direction implicit) method was tried. In the flat-plate case, we consider for the time-dependent equation for two-dimensions

$$\frac{\partial\varphi_1}{\partial t} = K\varphi_{1\,xx} + \varphi_{1\,yy} - \frac{i\omega}{\epsilon}\varphi_{1\,x} + \frac{\omega^2}{\epsilon}\varphi_1 \tag{16}$$

A uniform mesh is swept through using a row solution of the difference equation

$$\frac{\varphi_{1\,ij}^{(n+1)} - \varphi_{1\,ij}^{(n)}}{\Delta t} = \frac{K\left(\varphi_{1\,i+1j}^{(n+1)} - 2\varphi_{1\,ij}^{(n+1)} + \varphi_{1\,i-1j}^{(n+1)}\right)}{\Delta x^2} + \frac{\omega^2}{\epsilon}\varphi_{1\,ij}^{(n+1)}$$
$$- \frac{i\omega}{\epsilon}\left(\varphi_{1\,i+1j}^{(n+1)} - \varphi_{1\,i-1j}^{(n+1)}\right) + \frac{\left(\varphi_{1\,ij+1}^{(n)} - 2\varphi_{1\,ij}^{(n)} + \varphi_{1\,ij-1}^{(n)}\right)}{\Delta y^2} \tag{17}$$

and then through the mesh by a column solution of the difference equation

$$\frac{\varphi_{1ij}^{(n+2)} - \varphi_{1ij}^{(n+1)}}{\Delta t} = \frac{K\left(\varphi_{1i+1j}^{(n+1)} - 2\varphi_{1ij}^{(n+1)} + \varphi_{1ij}^{(n+1)}\right)}{\Delta x^2} + \frac{\omega^2}{\epsilon}\varphi_{1ij}^{(n+2)}$$

$$- \frac{i\omega}{\epsilon}\left(\varphi_{1i+1j}^{(n+1)} - \varphi_{1i-1j}^{(n+1)}\right) + \frac{\left(\varphi_{1ij+1}^{(n+1)} - 2\varphi_{1ij}^{(n+1)} + \varphi_{1ij-1}^{(n+1)}\right)}{\Delta y^2} \qquad (18)$$

Applying the Von Neumann stability analysis to the preceding two equations yields the same inequalities as found for conventional row and column relaxation. This indicates that the ADI method yields no improvement in the convergence for higher frequencies. The ADI method was coded and tried but failed to converge. Lack of time has prevented an adequate investigation of this failure.

5.0 SOLUTION PROCEDURE INVESTIGATION

An empirical investigation was conducted of the finite difference solution procedure to determine the effect of varying solution parameters and techniques and in minimizing solution computer resources. The investigation included:

- Relaxation factors
- Grid point distribution and spacing
- Extent of mesh area
- Sequential refinement with respect to Mach number, reduced frequency, and number of mesh points
- Row relaxation
- Direct solution
- Convergence acceleration

The results of these investigations are summarized in this section and detailed in appendix F.

5.1 SOLUTION CONVERGENCE CRITERIA

For this report, solution convergence was determined by monitoring the ERROR, which is defined as maximum value of all i, j, k of

$$\frac{\left| \varphi_{1\,ijk}^{(n)} - \varphi_{1\,ijk}^{(n-1)} \right|}{r} \tag{19}$$

where $\varphi_{1\,ijk}^{(n)}$ is the unsteady velocity potential for the nth iteration, $\varphi_{1\,ijk}^{(n-1)}$ is the corresponding potential for the preceding iteration, and r is the relaxation factor. The solution was considered converged when ERROR = 10^{-5}. In some cases, particularly for finer meshes and pitch mode, convergence was considered complete when ERROR $< 10^{-4}$.

The maximum residual was considered to have greater potential as an indication of solution convergence than ERROR. The residual is a measure of the degree to which a solution (here, a set of velocity potentials) satisfies the finite difference equations. The iteration may be written in general matrix form as $A\bar{\varphi}_1^{(n)} = R\bar{\varphi}_1^{(n-1)}$. The residual at the ith point is thus the summation $\sum_j (A_{ij} - R_{ij})\varphi_{1j}$. Preliminary attempts to calculate the residual resulted in values several orders of magnitude larger than the corresponding ERROR. Multiplying through by an area associated with each mesh point reduced the difference between the two values to some two orders of magnitude. However, the precise relationship between ERROR and the maximum residual is not yet entirely clear and thus further investigation is required before the residual can be used as a convergence criterion.

In the discussion on relaxation factors it will be noted the value of ERROR may be reduced rapidly by reducing the value of r. However, the resulting pressures were inconsistent with the minimal level of ERROR that had been reached with a single value of r. This again indicated that some form of residual measure might provide a more realistic insight into convergence.

5.2 SOLUTION PARAMETERS

5.2.1 RELAXATION FACTORS

In the iteration solution procedure used for this report a relaxation factor was applied to the velocity potential using the following replacement formula

$$\varphi_{1\,ijk}^{(n)} = r \cdot \varphi_{1\,ijk}^{(n)} + (1 - r) \cdot \varphi_{1\,ijk}^{(n-1)} \tag{20}$$

where $\varphi_{1\,ijk}^{(n-1)}$ is the velocity potential form the previous iteration at point (i,j,k), and $\varphi_{1\,ijk}^{(n)}$ on the right-hand side is the result of the current iteration. The factor r is the relaxation factor and is set to some value between 0 and 2. The procedure here was to use overrelaxation ($1.0 < r < 2.0$) for points at which the steady flow was subsonic and the unsteady differential equation was elliptic, and to use underrelaxation ($0 < r < 1$) for points at which the steady flow was supersonic and the differential equation was hyperbolic.

The characteristics of convergence for overrelaxation will be discussed with figures 2 and 3. These sketches show ERROR versus number of iterations. It is convenient to plot the ERROR in terms of log scale and the number of iterations as a conventional linear scale. It is noted that a straight difference of successive potential values includes the relaxation factor as a multiplier. Thus, we divided r out in calculating ERROR to provide a "normalized" measure of the error. For small ORF's (overrelaxation factors) these curves were made up of two nearly linear portions; for the initial iterations the convergence was rapid, resulting in a steep slope during the early iterations and a very shallow slope for the later iterations. As the ORF was raised, the slope of the initial iterations became less, while that of the later iterations increased. This trend continued as ORF was raised until the convergence during the initial iterations eventually became mildly unstable, but still converged well. Finally, when ORF was too high, convergence became quite unstable and the slope of ERROR versus number of iterations decreased sharply.

An ORF should be selected, if possible, so that the convergence criteria is attained within the number of iterations for which the steep initial slope holds.

Another interesting characteristic (fig. 3) is that if the ORF is changed during a solution calculation, there is an immediate change in the ERROR versus number of iterations curve. If the ORF is lowered, there is a significant drop in the ERROR curve. However, after the drop, the line levels out at a slope less than the slope for the higher ORF. It is possible, of course, to take advantage of this phenomenon to achieve a specific ERROR value for which convergence has been defined. However, we encountered inconsistent results where the convergence ERROR had been set as low as 10^{-5}, and thus caution is advised in making use of this characteristic.

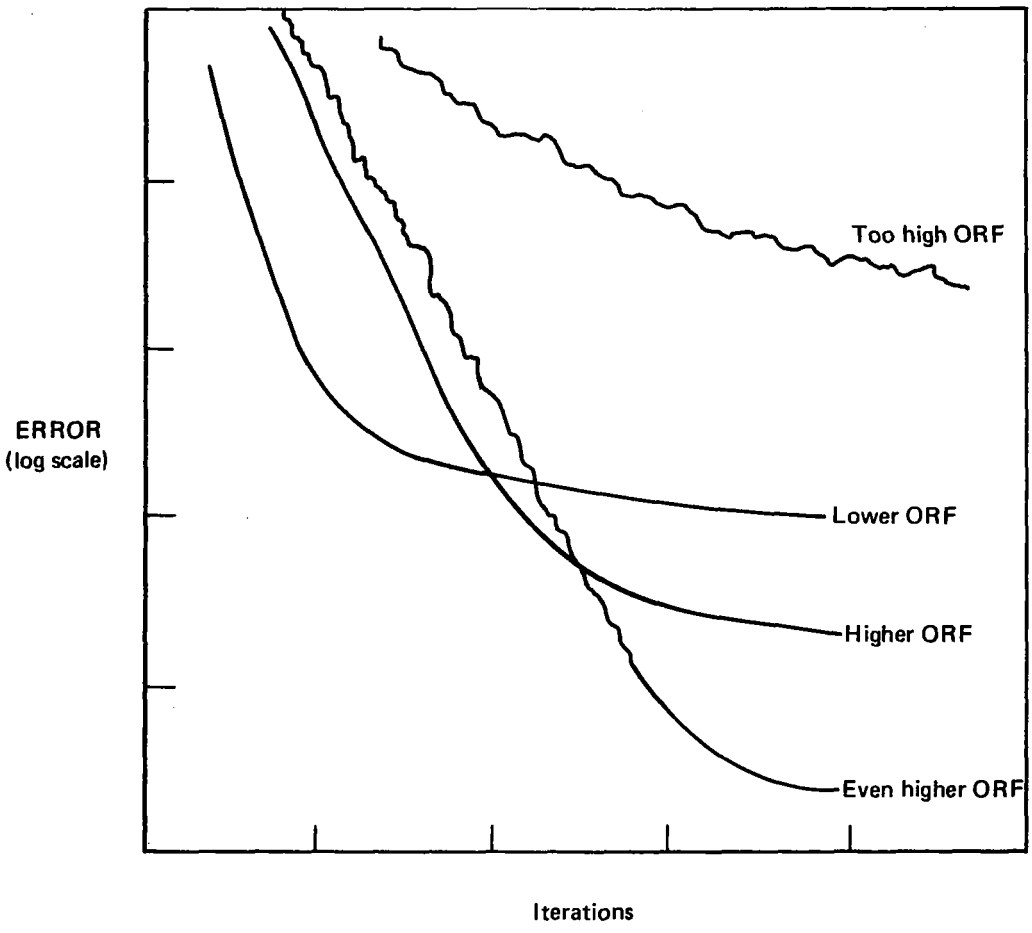

Figure 2. — Effect of Overrelaxation Factor on Convergence

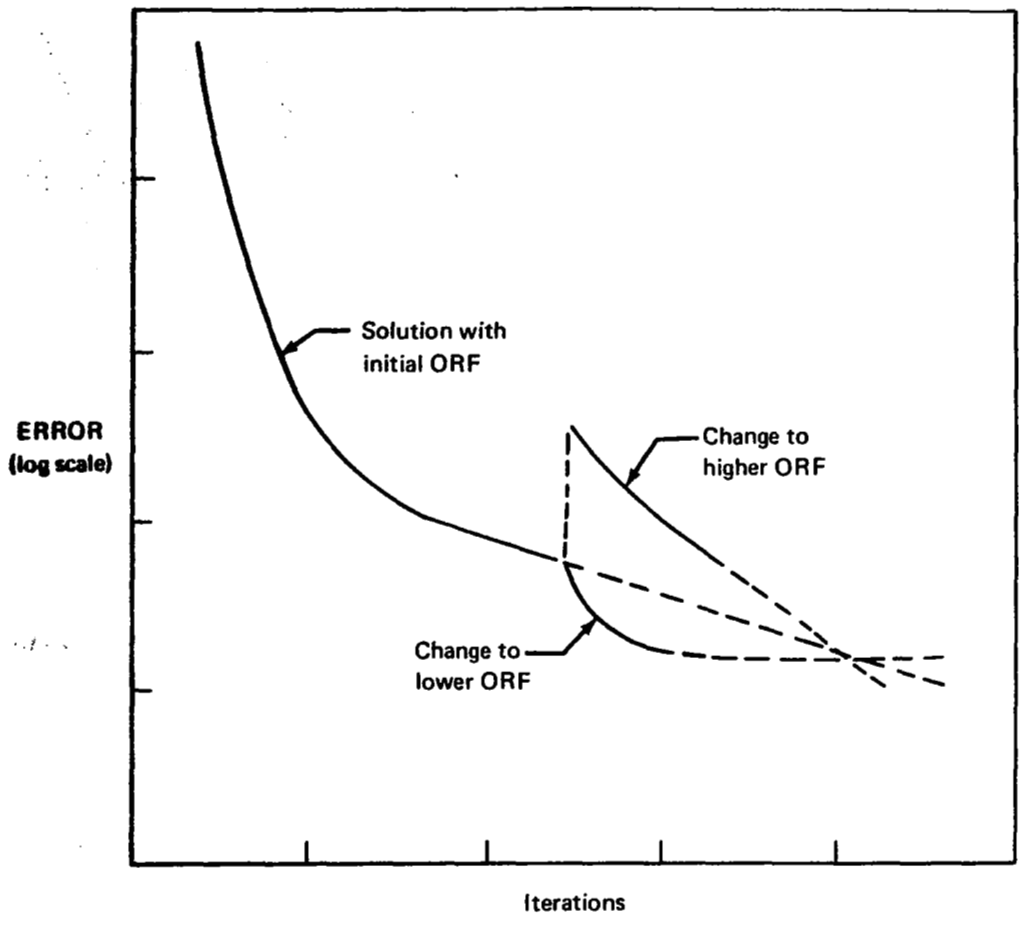

Figure 3. — Effect of Changing the Overrelaxation Factor During Convergence

The selection of the optimum overrelaxation factor was dependent on:

(a) The number of mesh points

(b) Level at which the convergence criteria was set

(c) Relaxation procedure (row, column, etc.)

(d) Solution sequence (start at upstream boundary, trailing edge, etc.)

(e) Frequency for a given Mach number

Values of the relaxation factor ranged from 1.9 down to 1.4 depending on the particular example. Item (c), the variation with frequency, appeared to be involved with the frequency limitation problem and is not discussed in appendix F. However, for a given Mach number and as the frequency was increased into the range of marginal stability, the value of the optimum relaxation factor decreased.

Generally, the coarser the mesh, the longer the initial slope lasted, and thus the smaller the optimum ORF. In this sense, the optimum ORF was dependent on the level at which the convergence criteria was set.

The pattern of the variation of optimum ORF with relaxation procedure and solution sequence was not explicitly defined within the limited number of examples run. Some illustrations of the variations encountered are presented in section F.1.1 of the appendix.

The use of complex ORF's does not improve the solution convergence characteristics. This was first demonstrated empirically and later shown with the Von Neuman stability analysis presented in appendix E.

The selection of ORF is best done by trial and error since it is a function of so many variables. We would recommend as large an ORF as possible and we have had considerable success with ORF's of 1.85 and 1.9, as shown in the appendix.

The solution convergence was not generally as sensitive to the underrelaxation factor as to the overrelaxation factor, although one case is cited in appendix F when the solution diverged for an URF of 1.0 and converged rapidly for an URF of 0.7.

5.2.2 GRID DISTRIBUTION AND SPACING

The examples of grid distribution and spacing showed that the representation of the pressures in the neighborhood of the flow singularities was significantly improved by clustering the points about the singularities and increasing the number of grid points.

For the first case, the mesh-area dimensions were fixed and the total number of points held nearly constant. The mesh points were spaced such that the ratio of sizes of adjacent intervals was λ, where λ could be varied between 2/3 and 3/2. The smallest intervals (for $\lambda > 1.0$) were centered about the known flow singularities; i.e. at the wing leading edge and the con-

trol surface hingeline in the flow direction and at the airfoil centerline in the crossflow direction. Successively improved representations of the leading-edge singularity in the pressure distribution was obtained as λ changed from 1.05 to 1.25 to 1.4. At the hingeline, the pressure distribution changed significantly between λ = 1.05 and 1.25 and minimally between λ = 1.25 and 1.4.

For the second case, the mesh area dimensions and the point spacing factor, λ, were held fixed, and the number of mesh points varied. A significant improvement in the pressure representations was obtained in going from a mesh of 25 x 16 to a mesh of 34 x 28. The change in pressure distribution in going from a 34 x 28 to a 42 x 30 mesh was minimal.

5.2.3 EXTENT OF MESH

The effect of varying the extent of the finite difference mesh was investigated by altering the location of the upper and lower mesh boundaries. Solutions were obtained for the boundaries at $y_{o\,max} = \pm 9, \pm 18.5$, and ± 29.6 (in physical coordinates) while the number of mesh points was held fixed. The pressure distributions and the velocity potential were compared. There was surprisingly little variation in the pressure distributions for the three cases. However, the distribution for $y_{o\,max} = \pm 9$ was slightly smaller in amplitude than the other two, which in turn were essentially the same. The velocity potential showed much more difference between the three cases, a difference not reflected in the pressure distributions. The best representation of the leading edge singularity in pressure was with $y_{o\,max} = +9$, the calculation apparently benefiting from the compression of points in the crossflow direction.

5.2.4 SEQUENTIAL REFINEMENT

In starting a new analysis, a set of zeros is often used as the initial values for the velocity potential distribution. The question is whether solution convergence for the desired set of parameters may be most economically achieved by calculating the velocity potential for intermediate values of the parameters, and using the resulting potentials as the initial distributions for the final calculation. This process of sequential refinement was applied in terms of Mach number, reduced frequency, and the number of mesh points.

The example presented in section F.1.4 of the appendix shows relatively little difference in the number of iterations to convergence, whether the initial velocity potential distribution is set to zero or taken from a corresponding problem with a relative small difference in Mach number or reduced frequency. The conclusion is that if potential distributions exist for intermediate values of Mach number and frequency, it would be worthwhile to use them. However, it would not be worthwhile to calculate them as an intermediate step in calculating the potential distributions for the desired values of Mach number and reduced frequency.

Sequential refinement with respect to the number of mesh points does appear worthwhile. Here, the velocity potential distribution is calculated for a relatively coarse grid. Then, the potential distribution is interpolated to a finer mesh and the resulting distribution used as initial values for another iteration sequence. An example is given in section F.1.4 of the appendix where the number of iterations for the refined grid is cut in half using the results

from a coarse grid. The actual savings is a function of the relative number of points of the coarse mesh with respect to the fine mesh and the number of iterations required to obtain a converged solution for the coarse mesh relative to the number required for the fine mesh.

5.3 SOLUTION PROCESS

5.3.1 ROW RELAXATION

The finite difference equations as presented in reference 1 were written for column relaxation where the solution is for a line of points parallel to the z -axis in three-dimensional flow (or the y -axis in two-dimensional flow) and extending from the lower boundary to the upper boundary. By rearranging terms, the equations may be rewritten for row relaxation where the solution is for a line of points extending from the upstream boundary to the downstream boundary. For subsonic flow, the resulting row formulation provides relatively rapid solution convergence. However, for mixed flow, additional terms must be included in the finite difference equation to obtain convergence. These terms, resulting from a time-like analysis of the finite difference equation, are derived in appendix C. The application of these terms is discussed in section F.2.1 of appendix F.

Examples of solution convergence using both row and column procedures, and using several solution sequences (i.e., the order in which the rows and columns are solved) are also presented in section F.2.1. Generally, row relaxation was found to be significantly more efficient than column relaxation for both subsonic and mixed flow. The only exceptions to this were for values of Mach number and frequency for which relaxation solutions were marginally stable. Here, although neither procedure was particularly rapid, column relaxation provided solution convergence for values of reduced frequency at which the row procedure had started to diverge.

Row relaxation was implemented in three ways. The most efficient manner was to start at the upper and lower boundaries and work toward the wing surface, alternately taking a row from the top section and a row from the bottom section. The alternatives of starting at the wing and working out toward the upper and lower boundaries and of starting at the lower boundary and simply taking successive rows in working to the top boundary were also tried. Column relaxation was run in two ways. The most efficient procedure proved to be the sequence that started at the trailing edge and worked toward the upstream boundary, then moved to the column just aft the trailing edge and worked to the downstream boundary. The alternate sequence started at the upstream boundary and moved by successive columns to the downstream boundary.

5.3.2 DIRECT SOLUTION

A version of the pilot two-dimensional program was written to provide a direct solution for the interior velocity potential distribution. By direct solution, we mean that the complete set of equations is solved all at once rather than in subsets, as with the row or column relaxation. For the direct solution as implemented here, there is still an iterative loop since the boundary conditions are calculated using an existing set of velocity potential distributions (i.e., the velocity potential distribution calculated in the preceding pass). The program for the direct solution was set up only for the purely subsonic flow.

The direct solution program has been used on the standard test problem of a flat plate with oscillating quarter-chord control surface for grids of 17 x 10 and 25 x 16 mesh points. It has also been used for the flat-plate pitch case. The results compare almost exactly with the relaxation solutions. The number of iterations required to reach convergence was less than 20 for all cases and computing time appears minimal.

In general, the direct solution was found to be a relatively fast and efficient solution procedure for small problems (coarse grids), but storage requirements make it impractical for incore solution of two-dimensional problems with what we currently feel to be realistic sized finite difference grids. The upper limit would be of the order of some 700 mesh points. As noted in a preceding section, current studies indicate that practical grids are of the order of 1200 or more points. Also, storage requirements for the mixed flow problem are even larger. Because of its speed, however, the direct solution has provided a very useful experimental tool for testing modifications to the program. Use of an out-of-core direct solution method has not been attempted, but is one possible direction for further investigation, particularly in light of the frequency limitation problem discussed in section 4.2.

5.3.3 CONVERGENCE ACCELERATION METHODS

The relatively regular, uniform, and monotonic behavior of the pressure difference distributions with successive iterations has suggested the use of convergence acceleration techniques. Also, these procedures have been successfully applied in limited examples of steady transonic flows by Hafez and Cheng (ref. 10) and Martin and Lomax (ref. 11). Further, our studies have shown relatively good behavior of both the velocity potential distribution and the ERROR with successive iterations. Despite the optimism with which this study was approached, the results were not favorable.

The Aitkin-Shanks nonlinear transformation (δ^2 -process) was tried first and applied to the velocity potential distribution. Typically, the extrapolated velocity potential had a large value of ERROR. Additional iterations resulted in a rapid drop in ERROR back to the convergence path that the solution was following before extrapolation. Although little was lost by using the extrapolation process, nothing was gained either.

Since examination of the extrapolated velocity potential showed it to be inconsistent with that which would be estimated by eye, a modified form of the Aitkin-Shanks transformation equation was introduced in order to constrain the shape of the extrapolation. This was tried on both the velocity potential and the pressure distributions without showing an improvement in solution convergence over straight relaxation.

Generally, the results of these studies have been discouraging despite the fact that convergence appears to be monotonic for the pressure and velocity potential distribution as well as ERROR. Results have not been improved by working with solutions with the smoother convergence characteristics obtained by either reducing the overrelaxation factor or using results from higher numbers of iterations. Finally, the real part of the solution appears to behave much better than the imaginary part, indicating that convergence acceleration procedures may well be much more promising for the steady-flow problem.

6.0 TWO-DIMENSIONAL EXAMPLES

A series of two-dimensional examples has been computed in order to further explore the accuracy and characteristics of the finite difference method examined in this report. The most important result from these examples was the discovery that solution convergence is limited as a function of Mach number and frequency. This particular point is discussed in section 4.0. This problem has reduced the number of examples in terms of number of different frequencies examined. The examples included both the NACA 64A006 airfoil and a flat plate (i.e., a section of vanishing thickness). The range of Mach numbers was 0.85 to 0.90 and the oscillatory motion included both section pitch and quarter-chord control surface rotation.

Generally, the rate of convergence was very dependent on the value of the relaxation factor. This was particularly true for elliptic points where an overrelaxation factor was used. Indeed, the selection of the overrelaxation factor is significant enough so that it ought to be determined for each case separately. Mixed-flow solutions appeared relatively less sensitive to the underrelaxation factor used with hyperbolic points. However, the case M = 0.9 and $\omega = 0.06$ for the airfoil in pitch diverged with an URF of 1.0, whereas 0.7 led to rapid convergence.

The sequential refinement in terms of mesh size (the number of points rather than the total mesh area that was held constant) proved worthwhile, whereas refinement in terms of frequency did not. The solutions presented here were obtained using some 150 to 200 iterations of a 25 x 20 grid followed by some 200 iterations of a 42 x 30 grid.

It was during the calculations for these examples that the limitations on convergence in terms of frequency and Mach number were encountered. Since the convergence problem existed for flat plate as well as the airfoil section, the handling of the shock and the attendant mixed flow was not the cause. At first it was assumed that the difficulties were due to poor selection of ORF or mesh size, or to some other parameter of the solution procedure. Thus considerable experimentation was done in an effort to obtain a significant improvement in the solution convergence. This included, besides ORF and mesh-size variations, various forms of column as well as row relaxation, the inclusion of a second-order approximation to the far field, and variation in mesh-point spacing. Sequential refinement in terms of frequency did not help. In addition, a considerable reshuffling of terms from one side to the other in the finite difference equation (eq. A1) was tried. Also, the program was modified to solve the differential equation and boundary conditions used by Traci et al. in reference 7. None of these changes provided the significant improvement that we felt was necessary to the problem.

As an example, consider the case of pitch for a flat plate with a harmonically oscillating quarter-chord control surface at M = 0.9. For a 25 x 20 mesh, relatively rapid convergence was obtained at frequencies up through $\omega = 0.12$. Although difficulty was encountered, convergence was obtained at $\omega = 0.14$ with column relaxation working considerably better than row relaxation. However, at $\omega = 0.16$, solutions converged rapidly to an ERROR of 10^{-3} and then the solution curve flattens out to provide, at best, very slow convergence. At $\omega = 0.18$, the solution diverged (this for a 42 x 30 mesh; ORF = 1.0 under row relaxation). By dropping the $q\varphi_1$, term of equation (3) and simplifying the boundary conditions.

the program was readily modified to approximate the solution of Traci et al. (ref. 7). Here the solution converged for $\omega = 0.16$, and at $\omega = 0.18$ the convergence became very slow again. Finally reduction of the mesh area, as suggested by the analyses discussed in section 4.0, provides rapid solution convergence at $\omega = 0.18$.

The flat-plate results are compared directly with solutions from the NASA linear subsonic three-dimensional unsteady aerodynamic program (refs. 4 and 5). This program solves the pressure-downwash integral equation using assumed pressure modes. Since the steady transonic flow past a flat plate is uniform, the finite difference results should match the subsonic results directly. Figures 4 through 8 present the results for a flat plate (section of vanishing thickness) in pitch. In all cases the correlation between the finite difference program and the NASA program is good.The finite difference method appears to underestimate slightly the amplitude as calculated with the NASA program. Also, the degree of correlation appears independent of Mach number and frequency. Solution convergence was considered to be a maximum error of 10^{-4} between velocity potentials for successive iterations. This appears to be adequate for the calculations involving the pitch mode.

Figures 9 and 10 show the jump in pressure coefficient across a flat plate with an oscillating quarter-chord trailing-edge control surface. Results are presented for $M = 0.9$ and reduced frequencies of 0.06 and 0.12. Again correlation between the finite difference program and the NASA program appears good.

Calculations for the NACA 64A006 airfoil section are presented in figures 11 through 17. Results for pitch motion at $M = 0.85$ and reduced frequency of 0.06 and 0.24 are shown in figures 11 and 12. In figure 11, results for three different mesh grids are shown while the total mesh area is held constant. First, it is noted that increasing the number of points (perpendicular to the flow) improves the representation of the leading-edge singularity. Secondly, the clustering of points about the shock, which in this case is just forward of midchord, results in a kind of singularity, with the pressure going to large positive numbers in front of the shock and reappearing from negative numbers behind the shock. For this example (in the 45-point distribution), points are clustered about the 3/4 chord, while in the 46-point distribution, the points are clustered about $x = -0.1$, the approximate location of the shock center. This latter phenomenon is illustrated in figure 12, which presents the results for two flow-wise point distributions. There are no experimental or other analytical data for correlation with these pitch motion results.

A two-dimensional example was also calculated to compare the change in pressure distribution that results from using the specific heat ratio of Freon ($\gamma = 1.135$) instead of that for air ($\gamma = 1.4$). Figure 13 shows the steady-state pressure coefficient at $M = 0.9$ for Freon and air for the NACA 64A006 airfoil. The shock in Freon is slightly ahead of the shock in air. Figure 14 shows the jump in pressure coefficient across the airfoil due to the harmonic pitch of the airfoil section with a reduced frequency of 0.06.

The remaining figures (figs. 15 through 17) show pressure difference coefficient distributions for oscillatory quarter-chord control surface motion. The cases for figures 15 and 16 are calculated at $M = 0.875$, and $M = 0.9$ for $\omega = 0.06$, and are shown with the corresponding measured data from Tijdeman and Schippers (ref. 6). Solutions at $M = 0.9$ and $\omega = 0.12$ were marginally convergent and converged pressure distributions were not obtained. Correla-

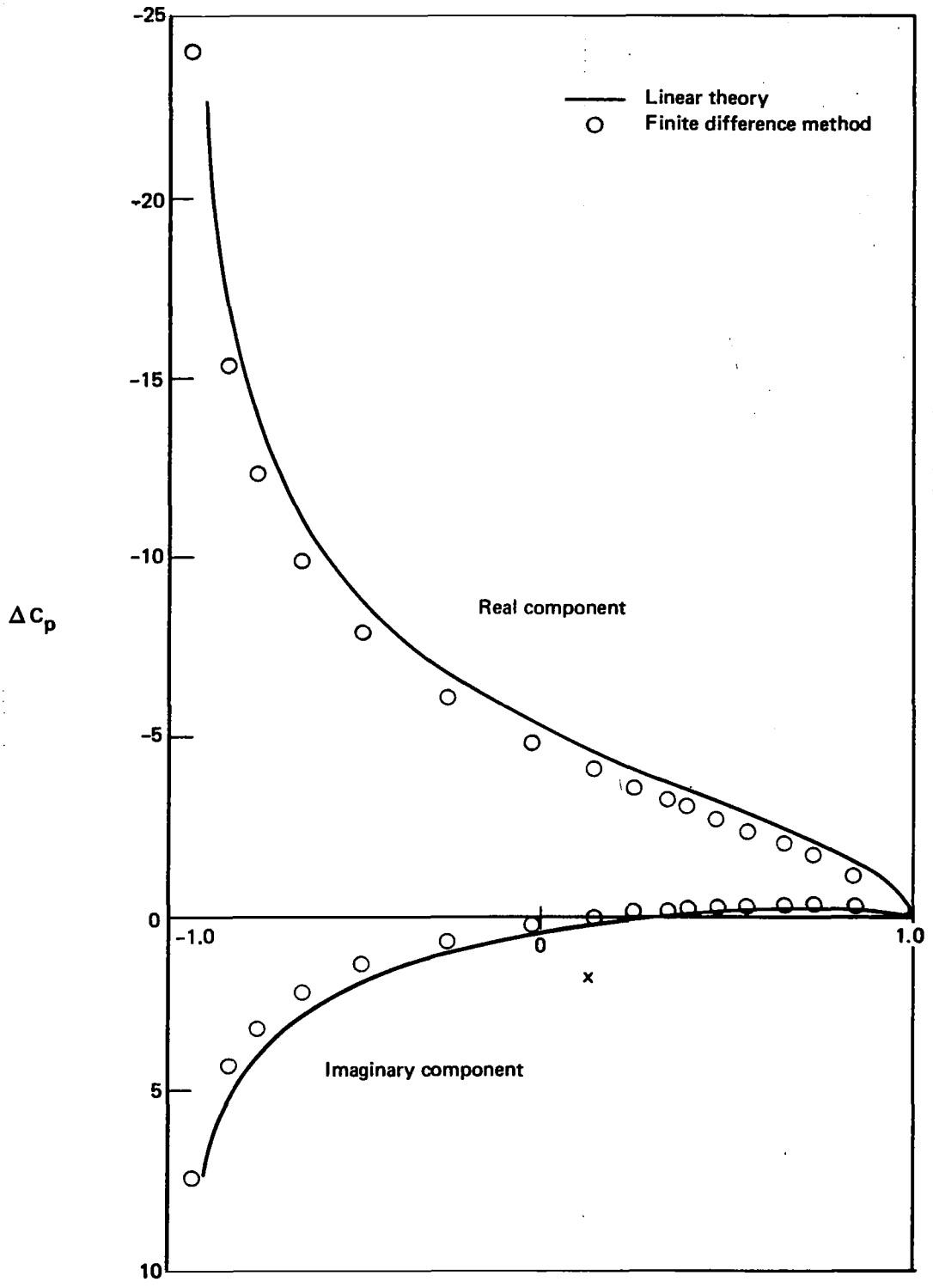

Figure 4. — Jump in Pressure Coefficient Across a Flat-Plate Oscillating in Harmonic Pitch — M = 0.80, ω = 0.06

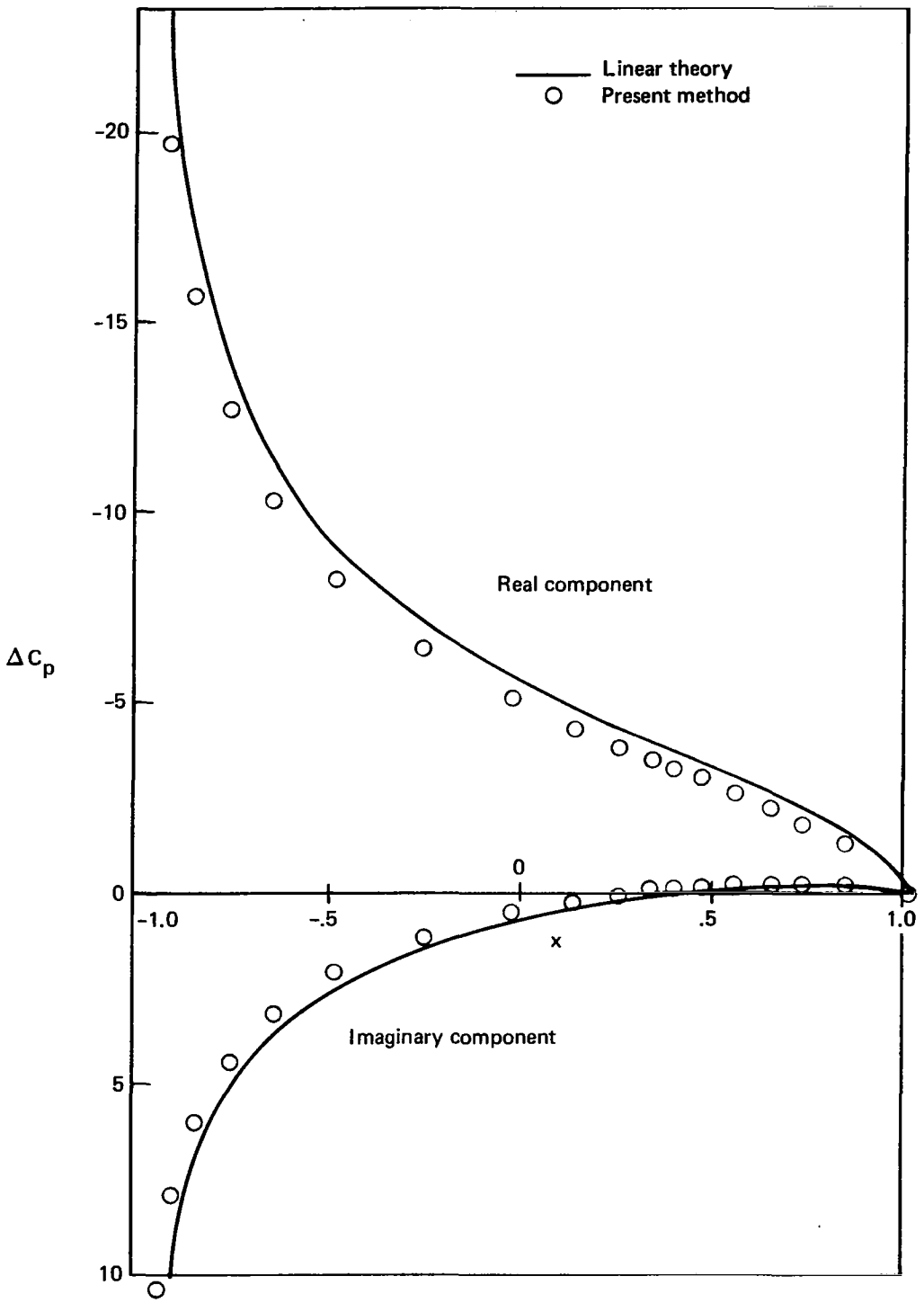

Figure 5. — Jump in Pressure Coefficient Across a Flat-Plate Oscillating in Harmonic Pitch — M = 0.85, ω = 0.06

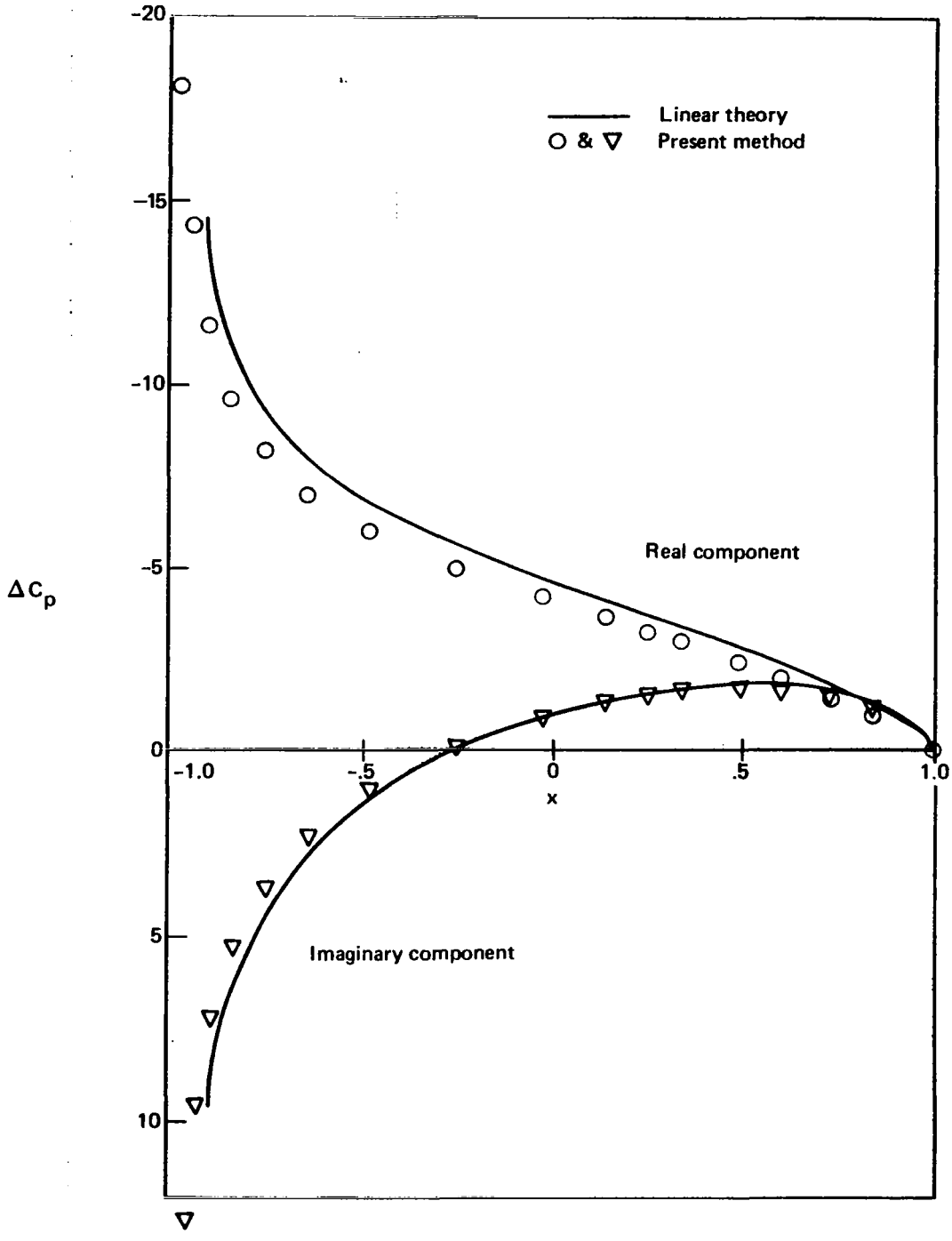

Figure 6. — Jump in Pressure Coefficient Across a Flat-Plate Oscillating in Harmonic Pitch — M = 0.85, ω = 0.18

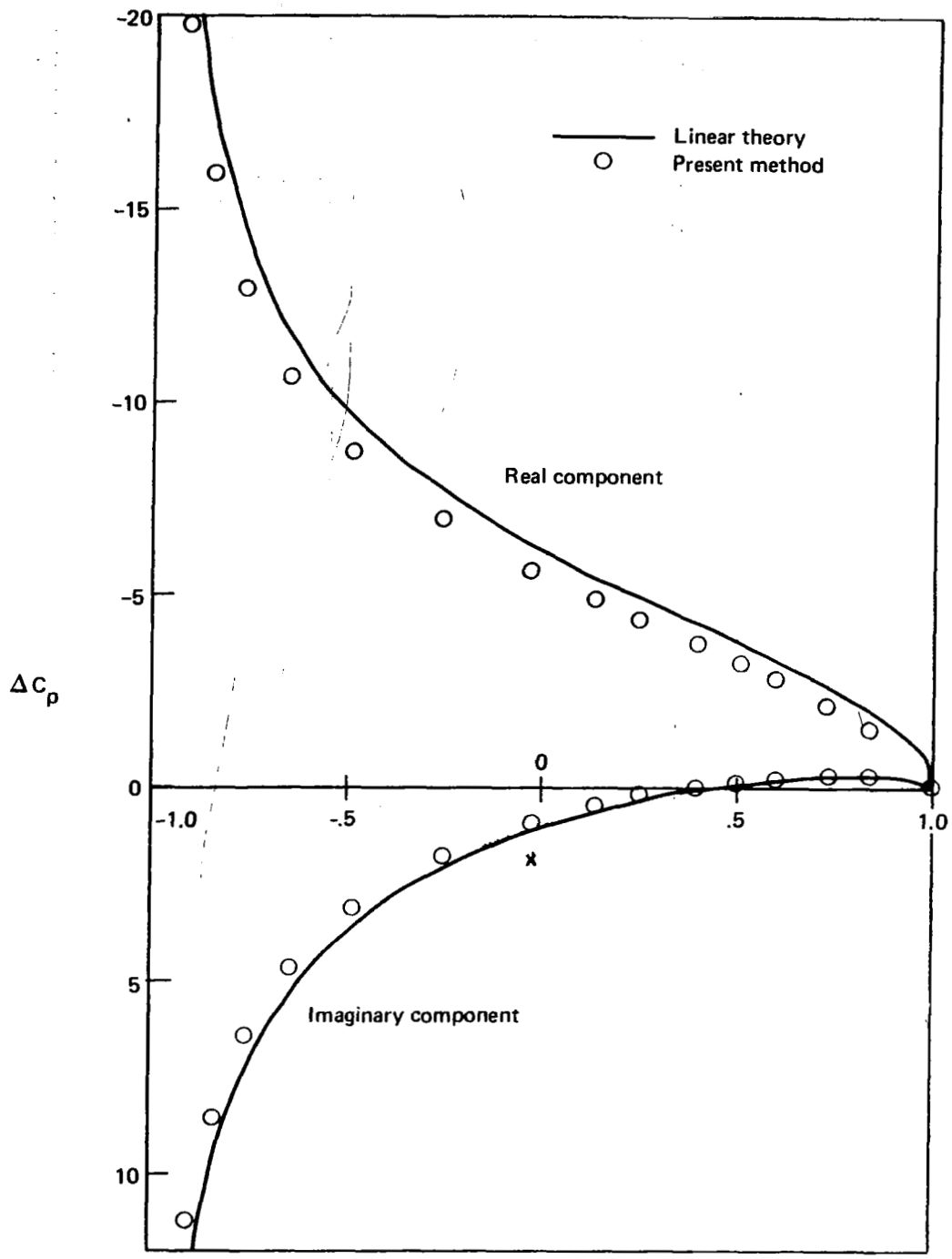

Figure 7. — Jump in Pressure Coefficient Across a Flat-Plate Oscillating in Harmonic Pitch — $M = 0.90$, $\omega = 0.06$

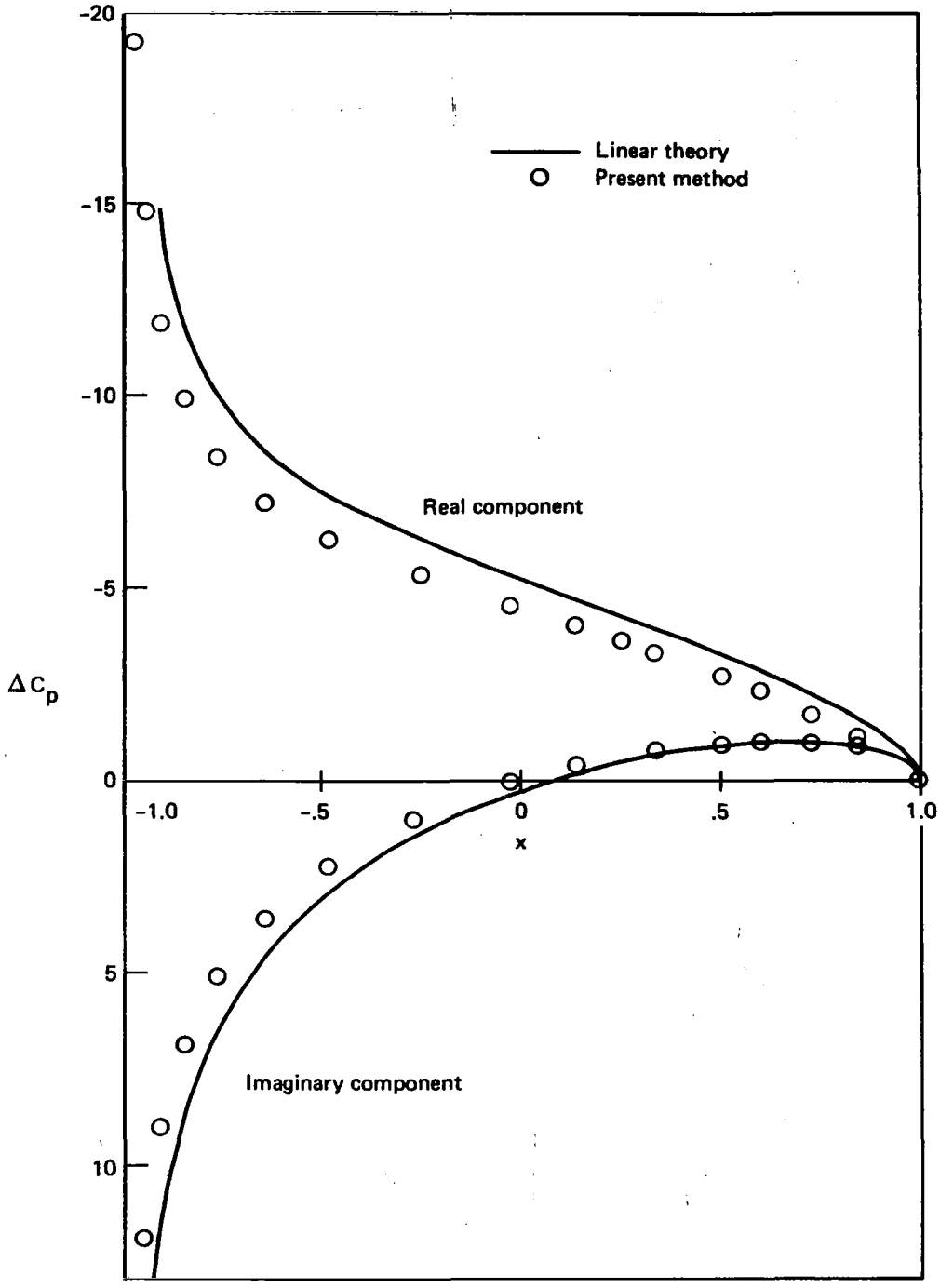

Figure 8. — Jump in Pressure Coefficient Across a Flat-Plate Oscillating in Harmonic Pitch — M = 0.9, ω = 0.12

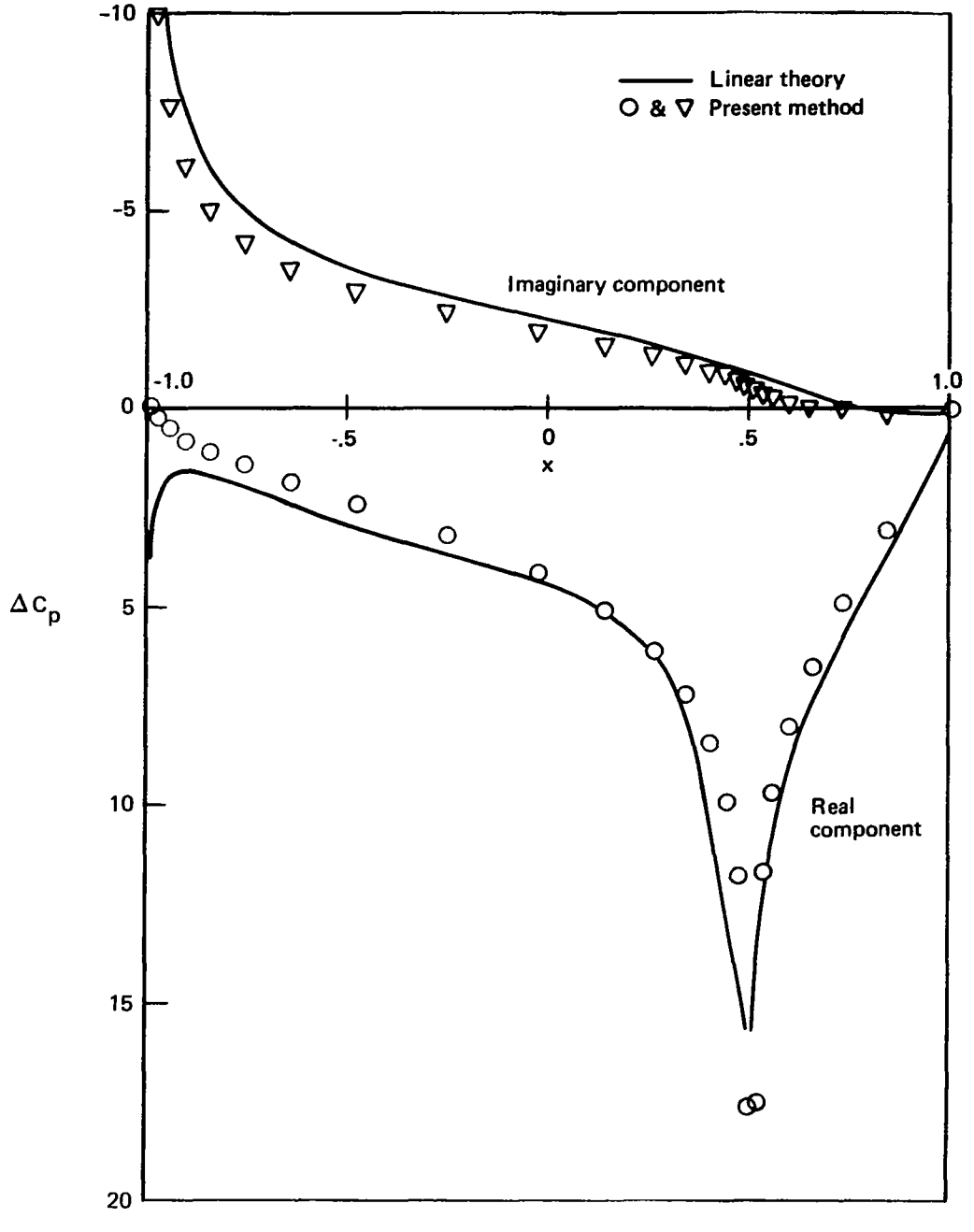

Figure 9. — Jump in Pressure Coefficient Across a Flat-Plate with Harmonically Oscillating Quarter-Chord Control Surface — M = 0.9, ω = 0.06

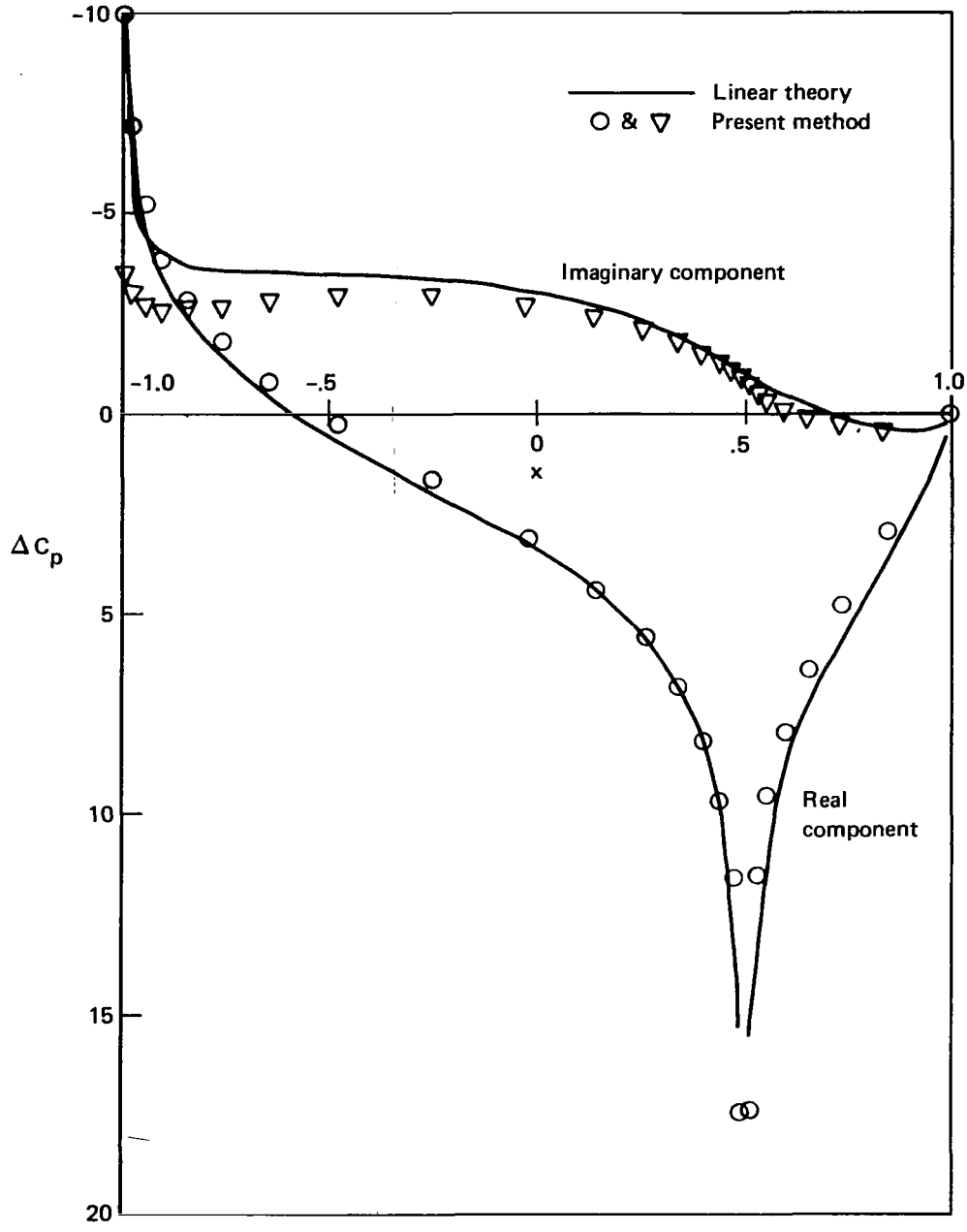

Figure 10. — Jump in Pressure Coefficient Across a Flat-Plate with Harmonically Oscillating Quarter-Chord Control Surface — M = 0.9, ω = 0.120

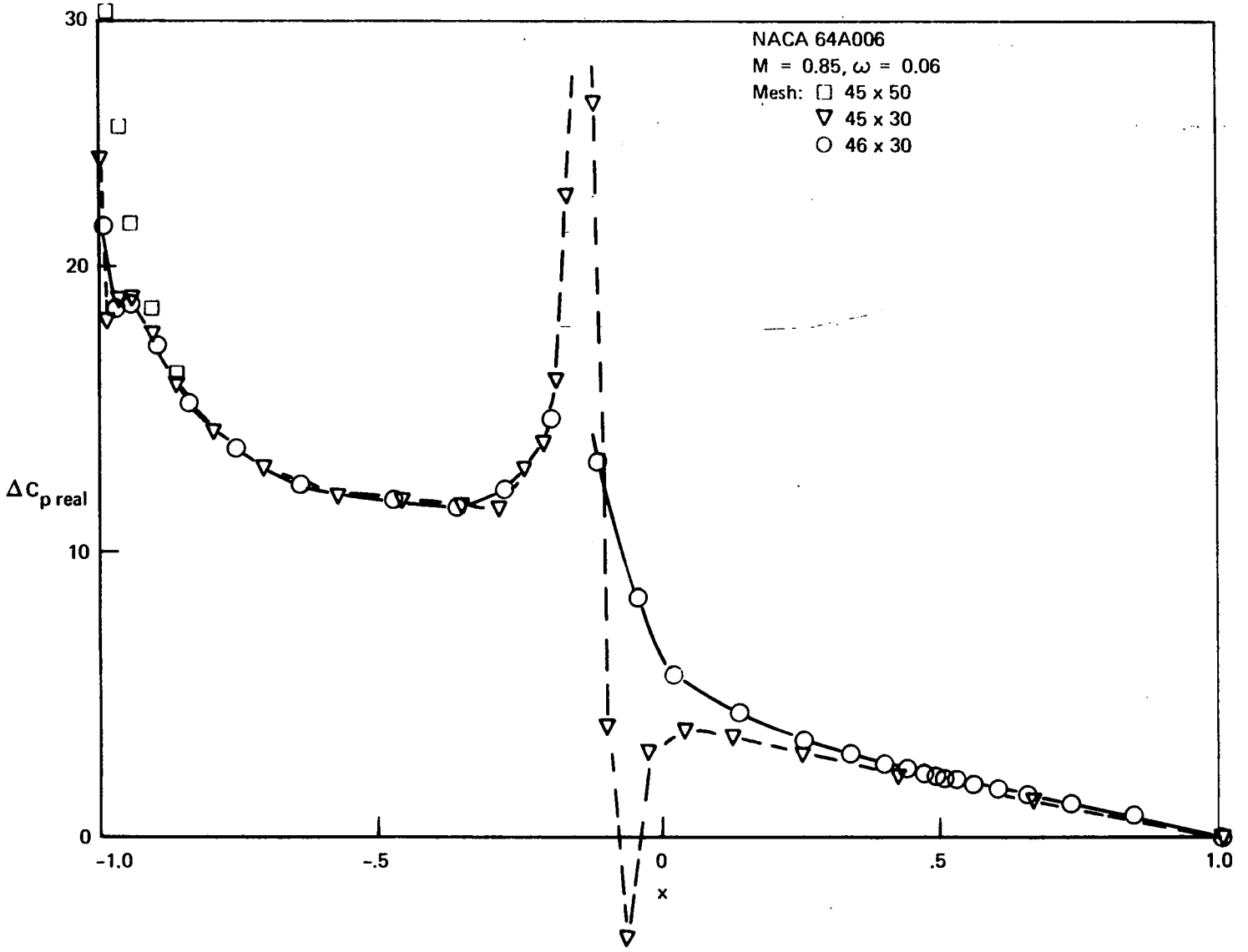

Figure 11a.— Jump in Pressure Coefficient Across an Airfoil Oscillating in Harmonic Pitch — M = 0.85, ω = 0.06

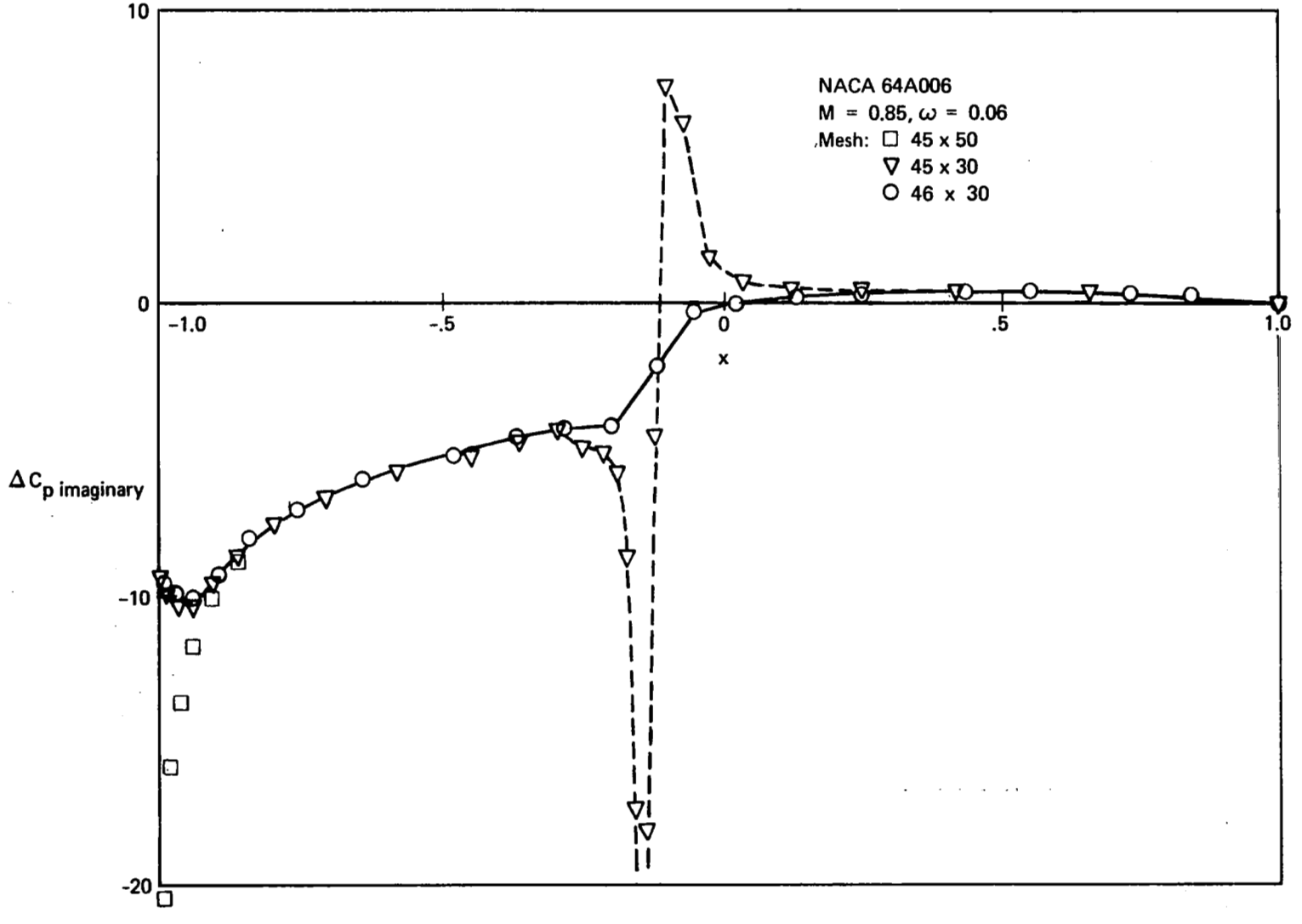

Figure 11b. — Jump in Pressure Coefficient Across an Airfoil Oscillating in Harmonic Pitch — M = 0.85, ω = 0.06

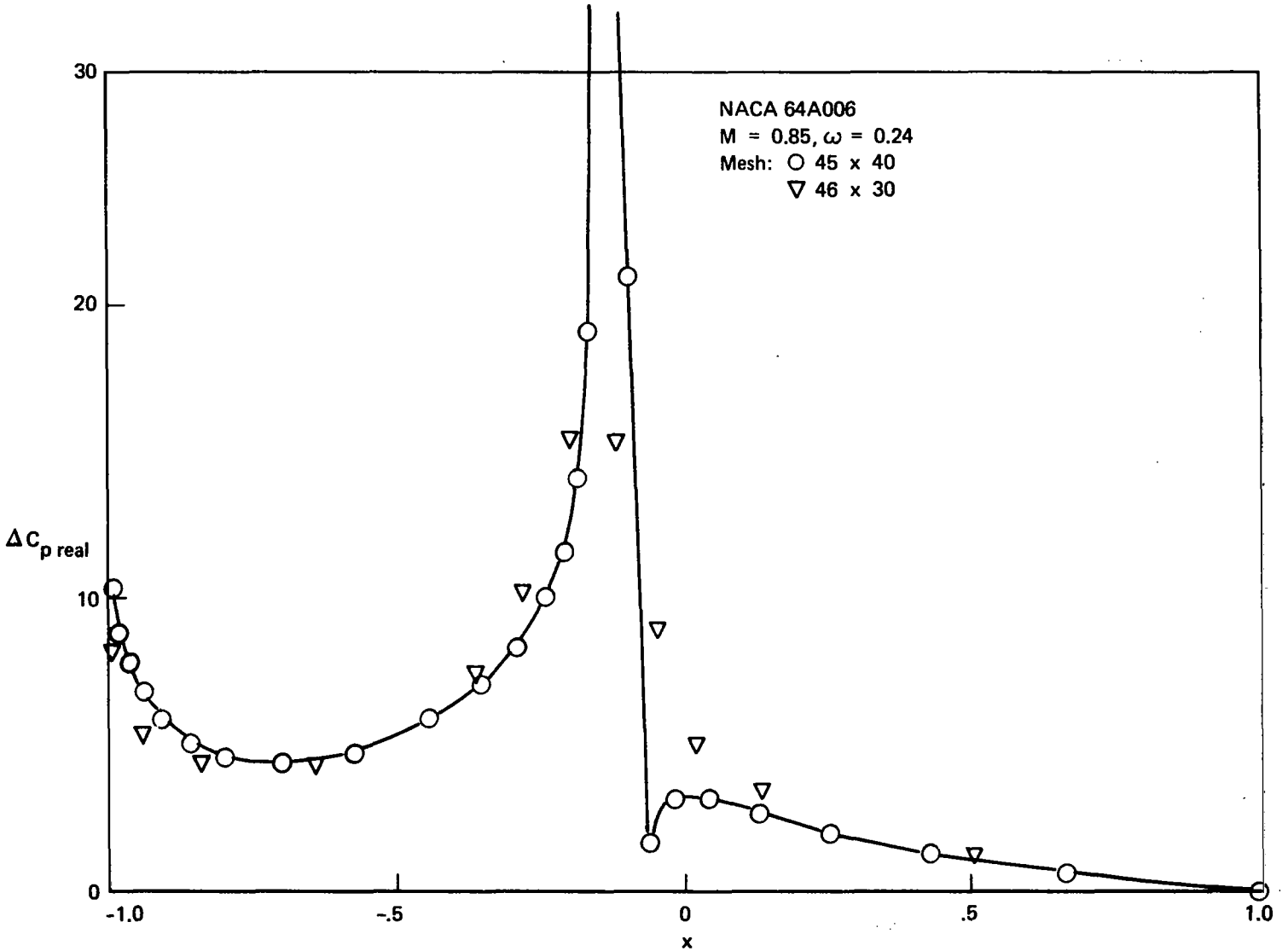

Figure 12a. — Jump in Pressure Distribution Across an Airfoil Oscillating in Harmonic Pitch — M = 0.85, ω = 0.24

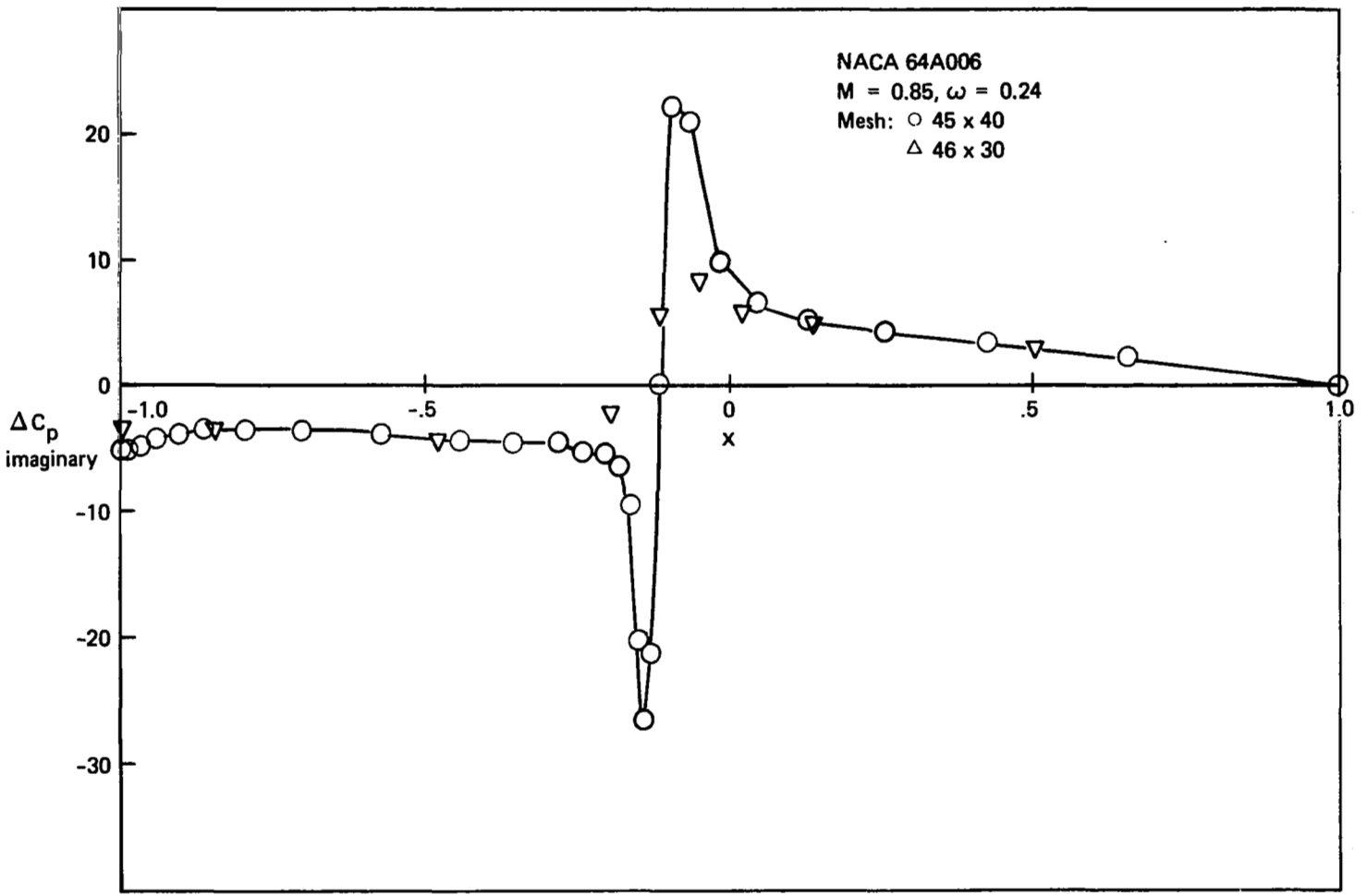

Figure 12b. — Jump in Pressure Coefficient Across an Airfoil Oscillating in Harmonic Pitch — M = 0.85, ω = 0.24

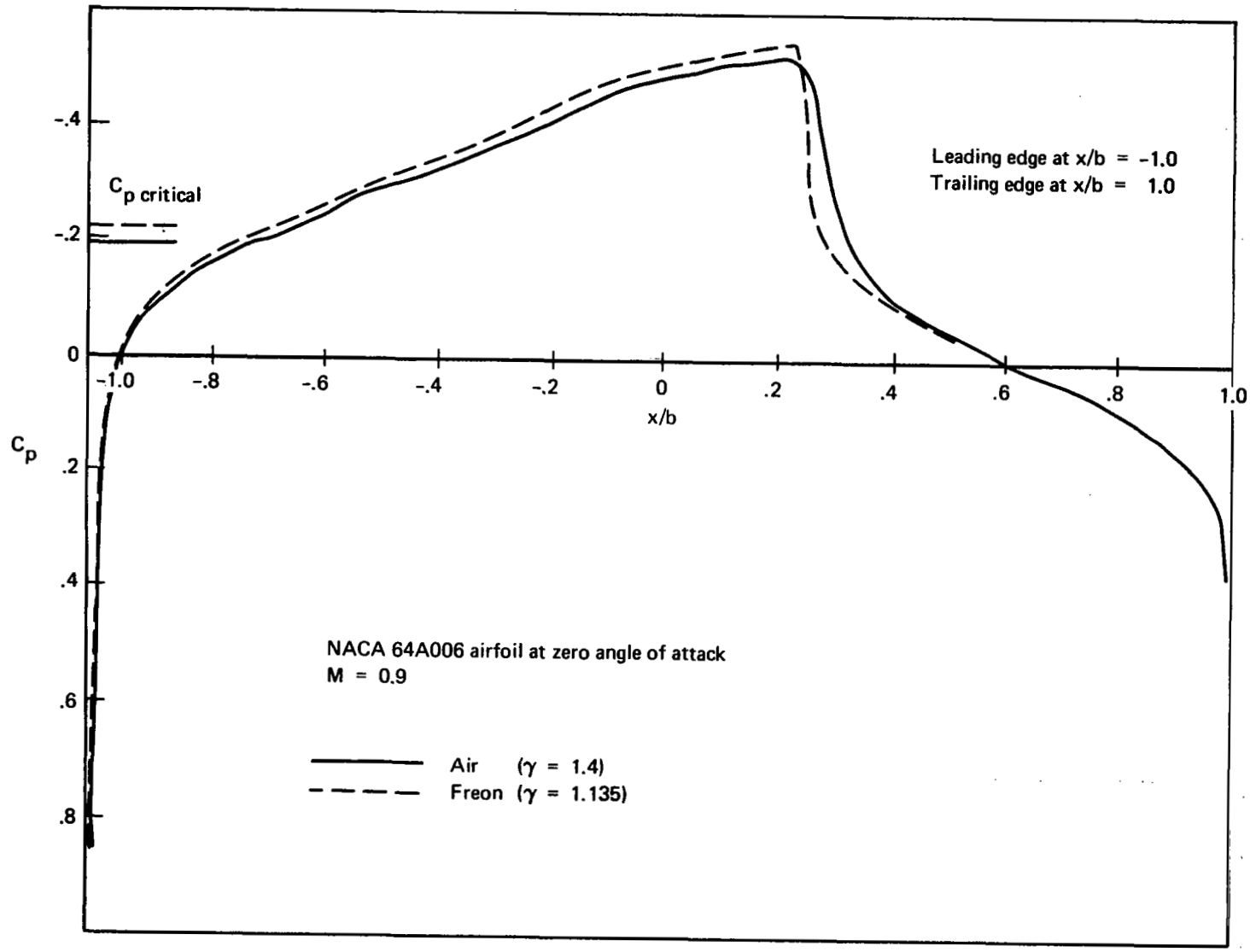

Figure 13. — Steady-State Pressure Coefficient for Airfoil Section

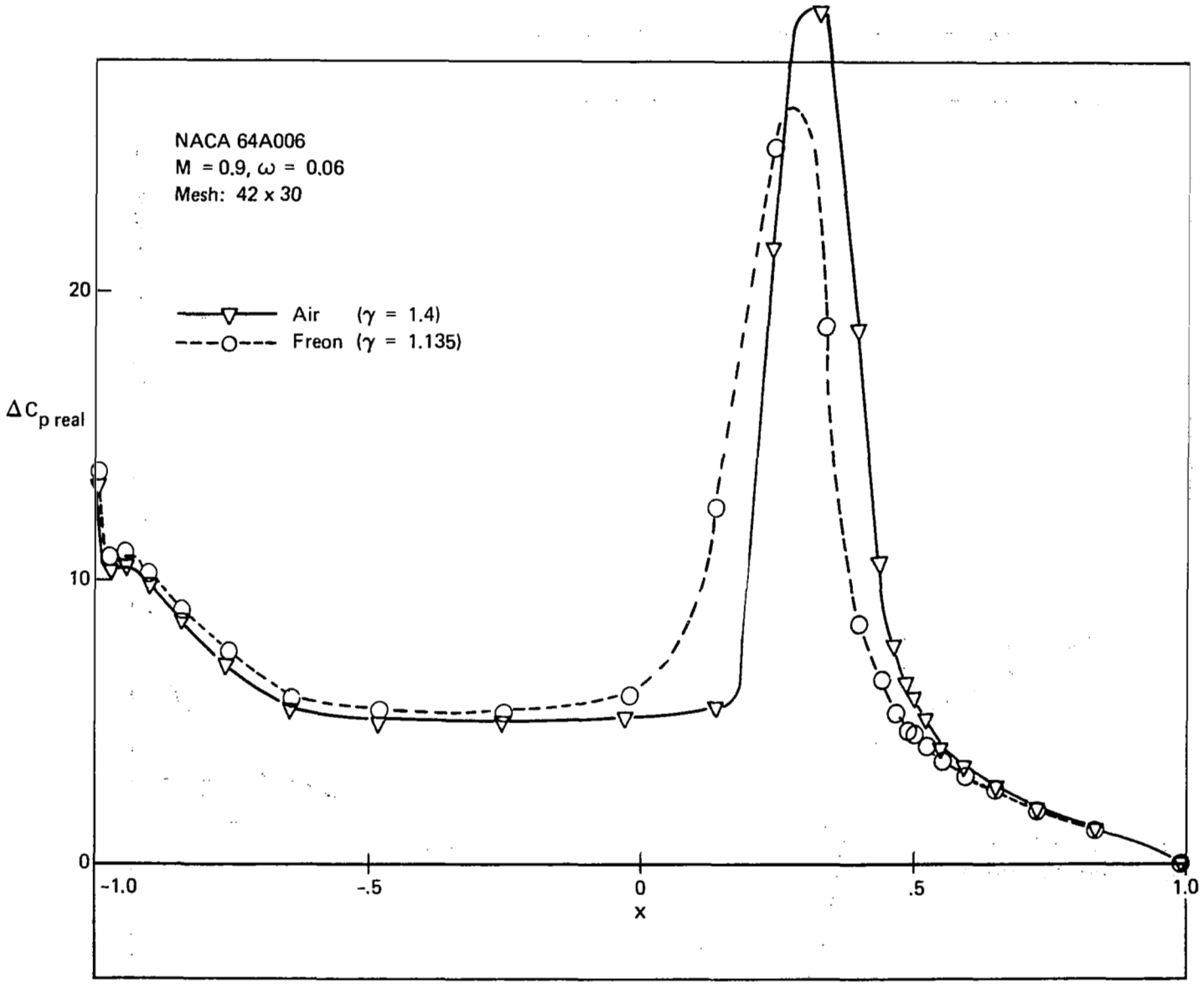

Figure 14a. — Jump in Pressure Coefficient Across an Airfoil Oscillating in Harmonic Pitch — M = 0.9, ω = 0.06

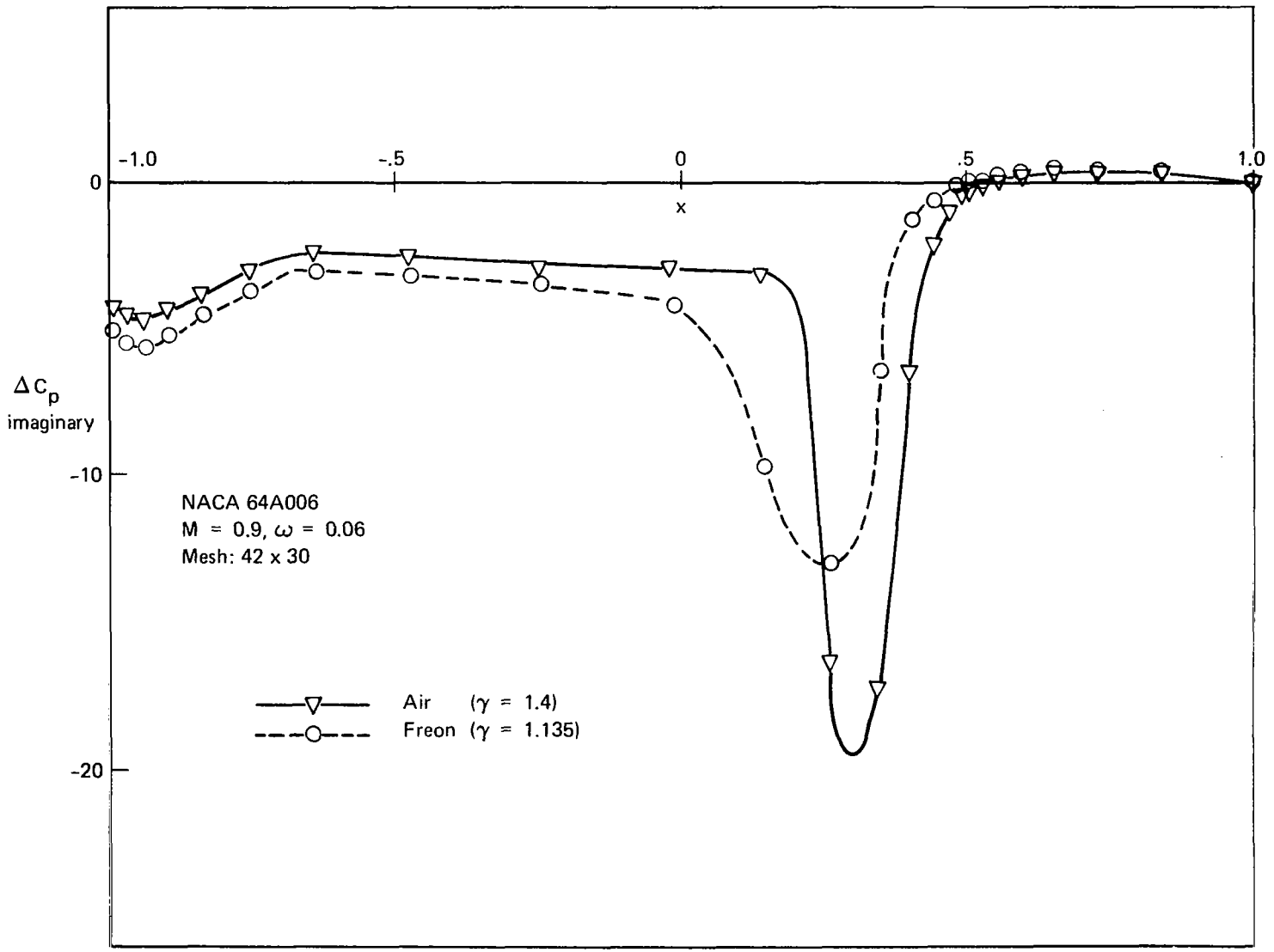

Figure 14b. —Jump in Pressure Coefficient Across an Airfoil Oscillating in Harmonic Pitch — M = 0.9, ω = 0.06

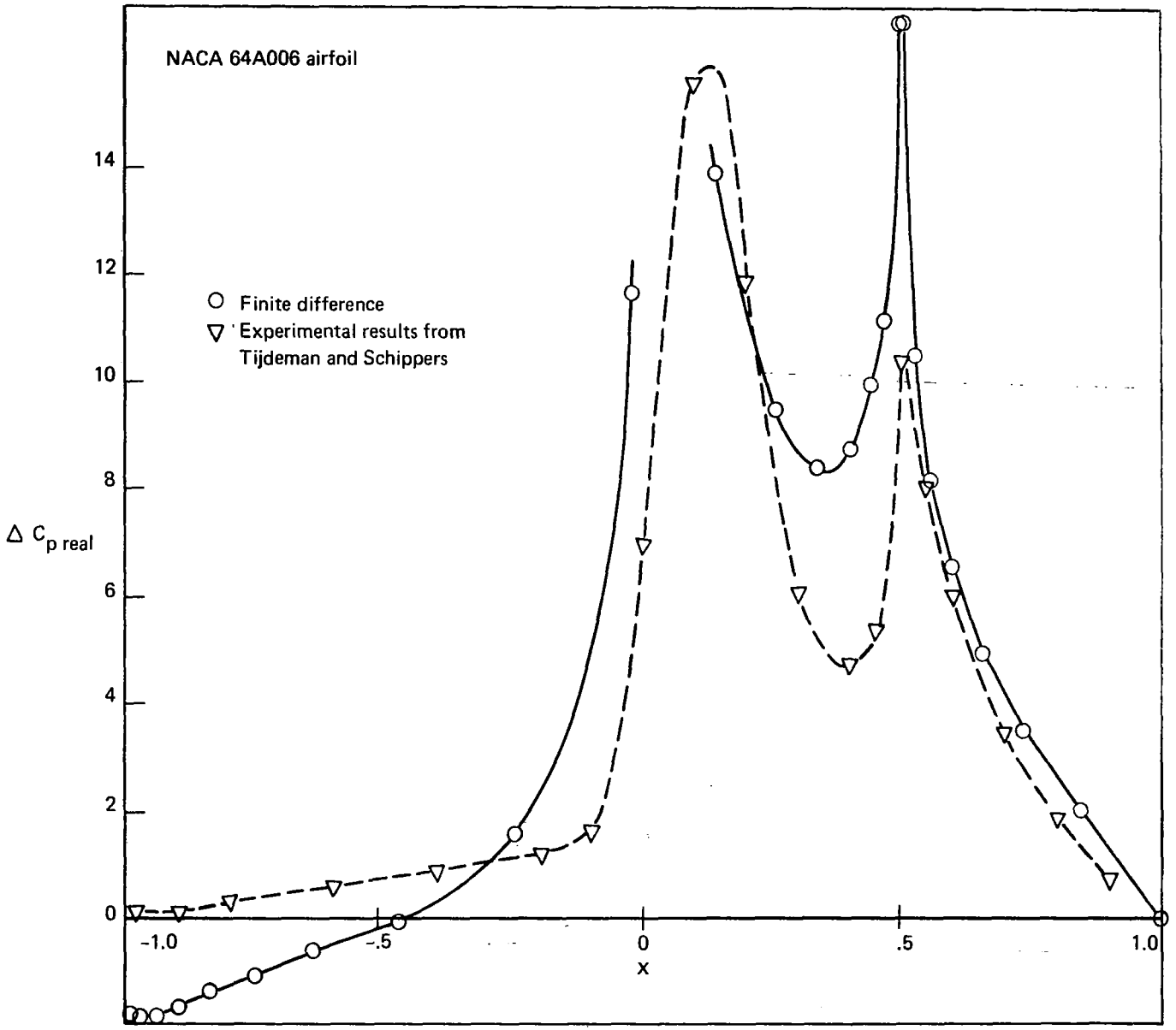

Figure 15a.— Jump in Pressure Coefficient Across an Airfoil with Harmonically Oscillating Quarter-Chord Control Surface — M = 0.875, ω = 0.06

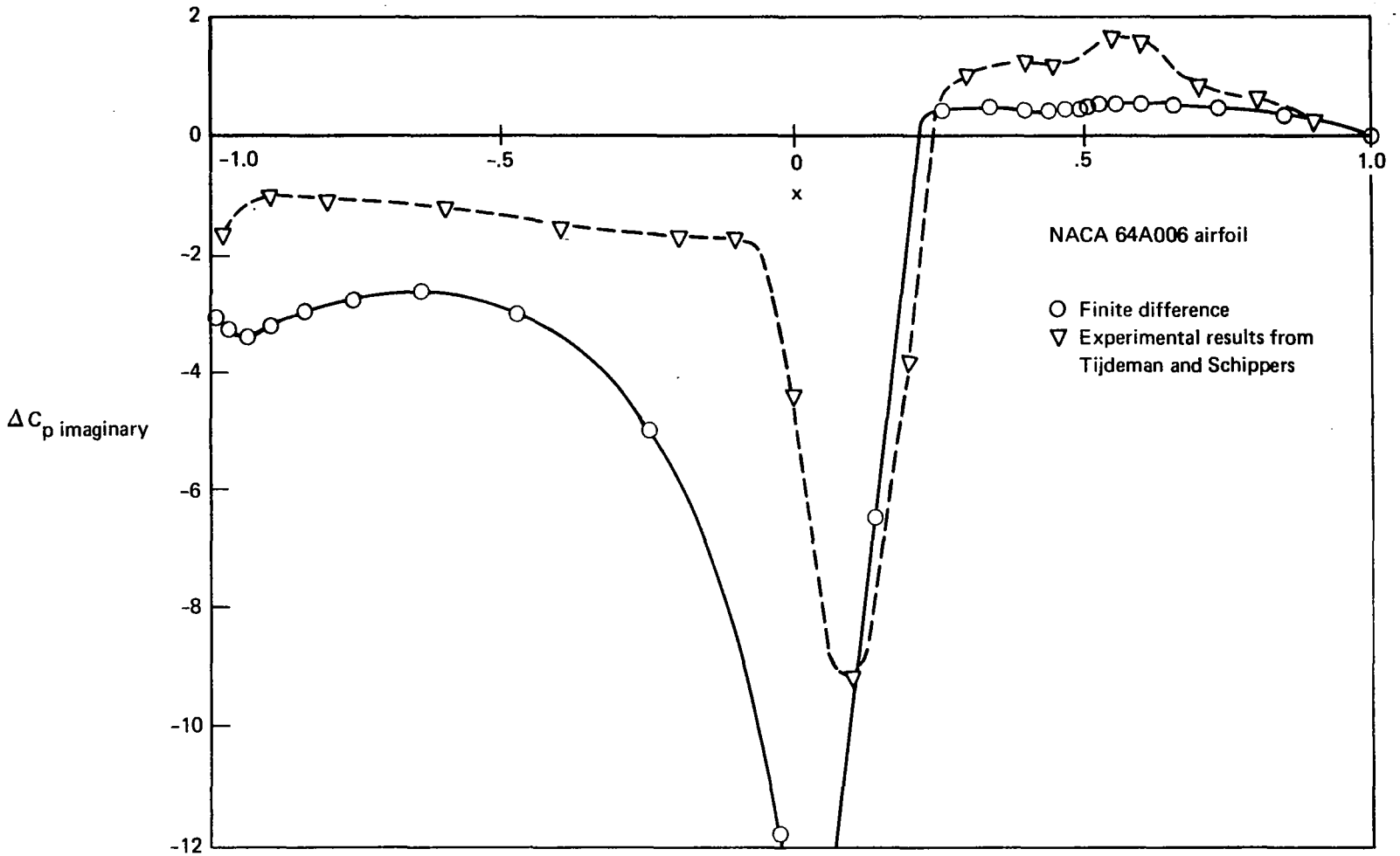

Figure 15b.— Jump in Pressure Coefficient Across an Airfoil with Harmonically Oscillating Quarter-Chord Control Surface — $M = 0.875$, $\omega = 0.06$

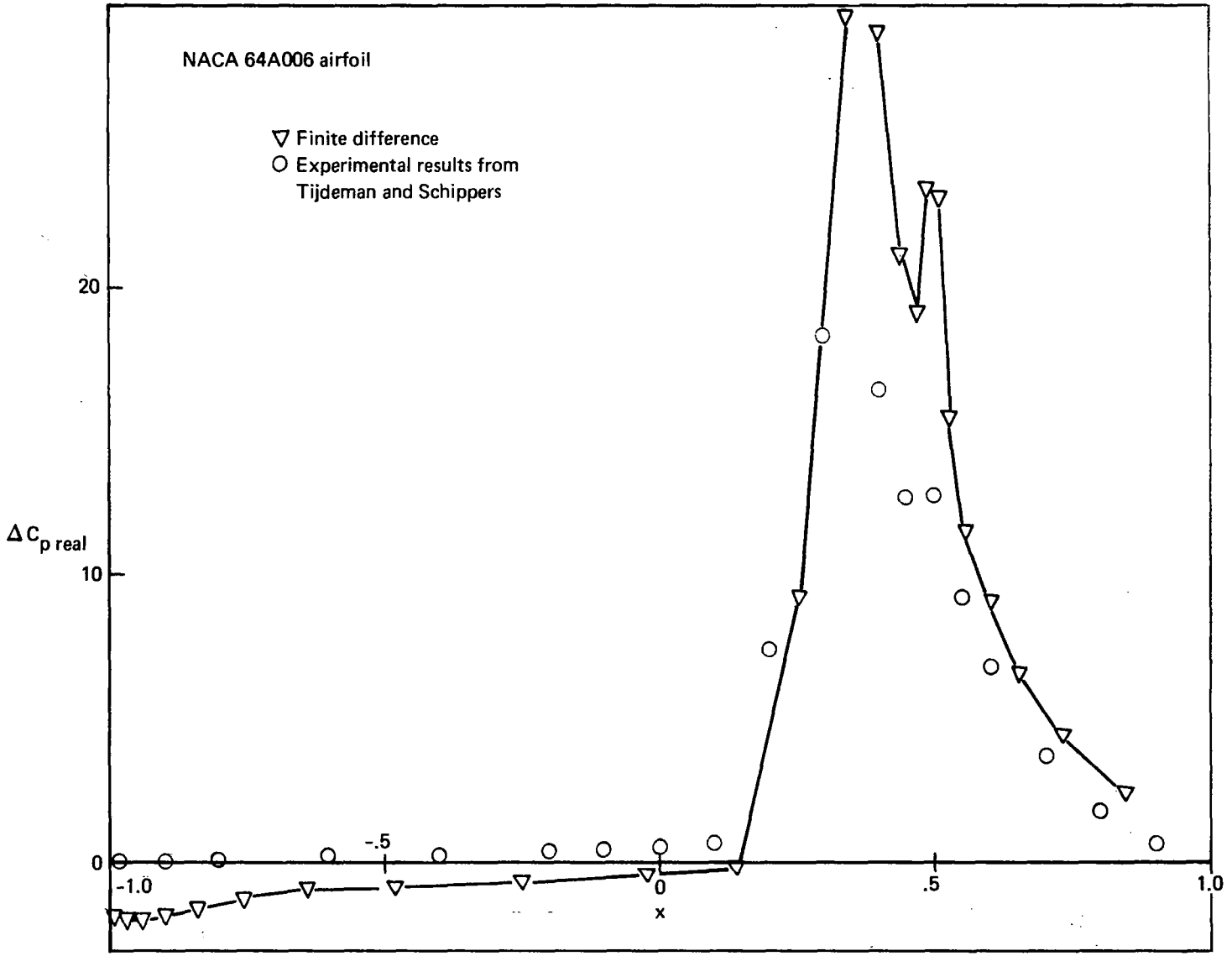

Figure 16a.— Jump in Pressure Coefficient Across an Airfoil with Harmonically Oscillating Quarter-Chord Control Surface — $M = 0.9$, $\omega = 0.06$

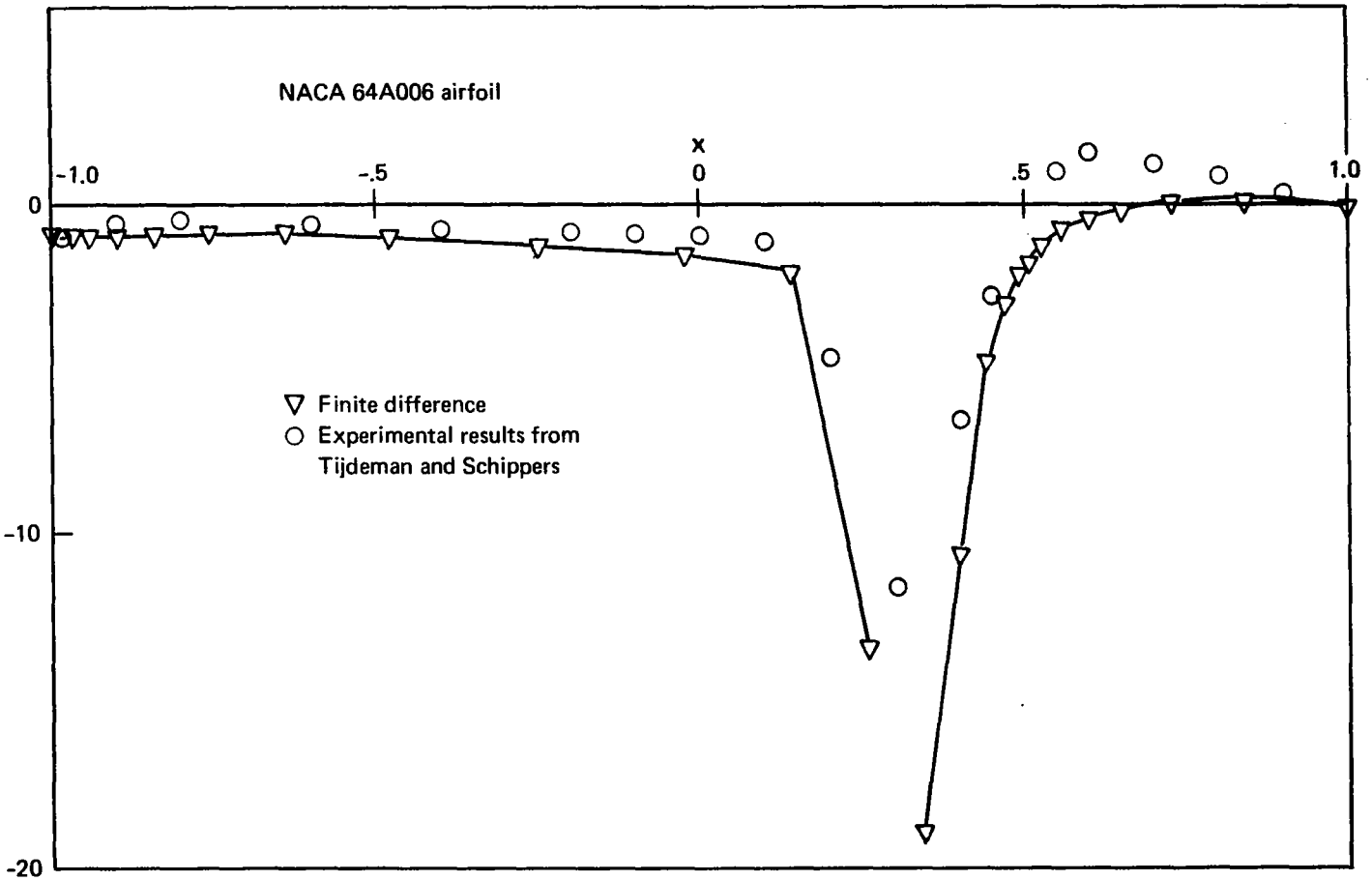

Figure 16b — Jump in Pressure Coefficient Across an Airfoil with Harmonically Oscillating Quarter-Chord Control Surface — $M = 0.9$, $\omega = 0.06$

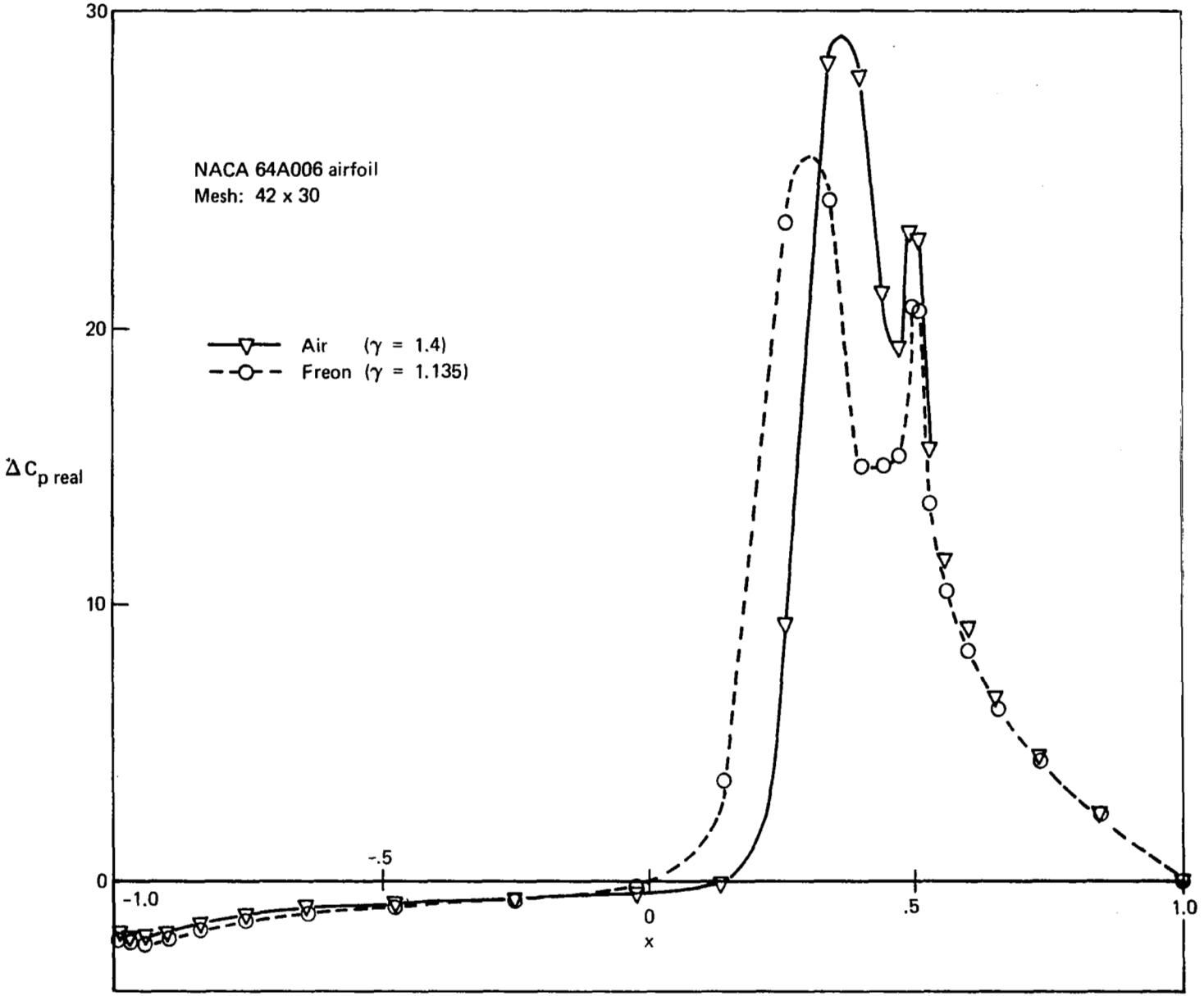

Figure 17a. — Jump in Pressure Coefficient Across an Airfoil with Harmonically Oscillating Quarter-Chord Control Surface — M = 0.9, ω = 0.06

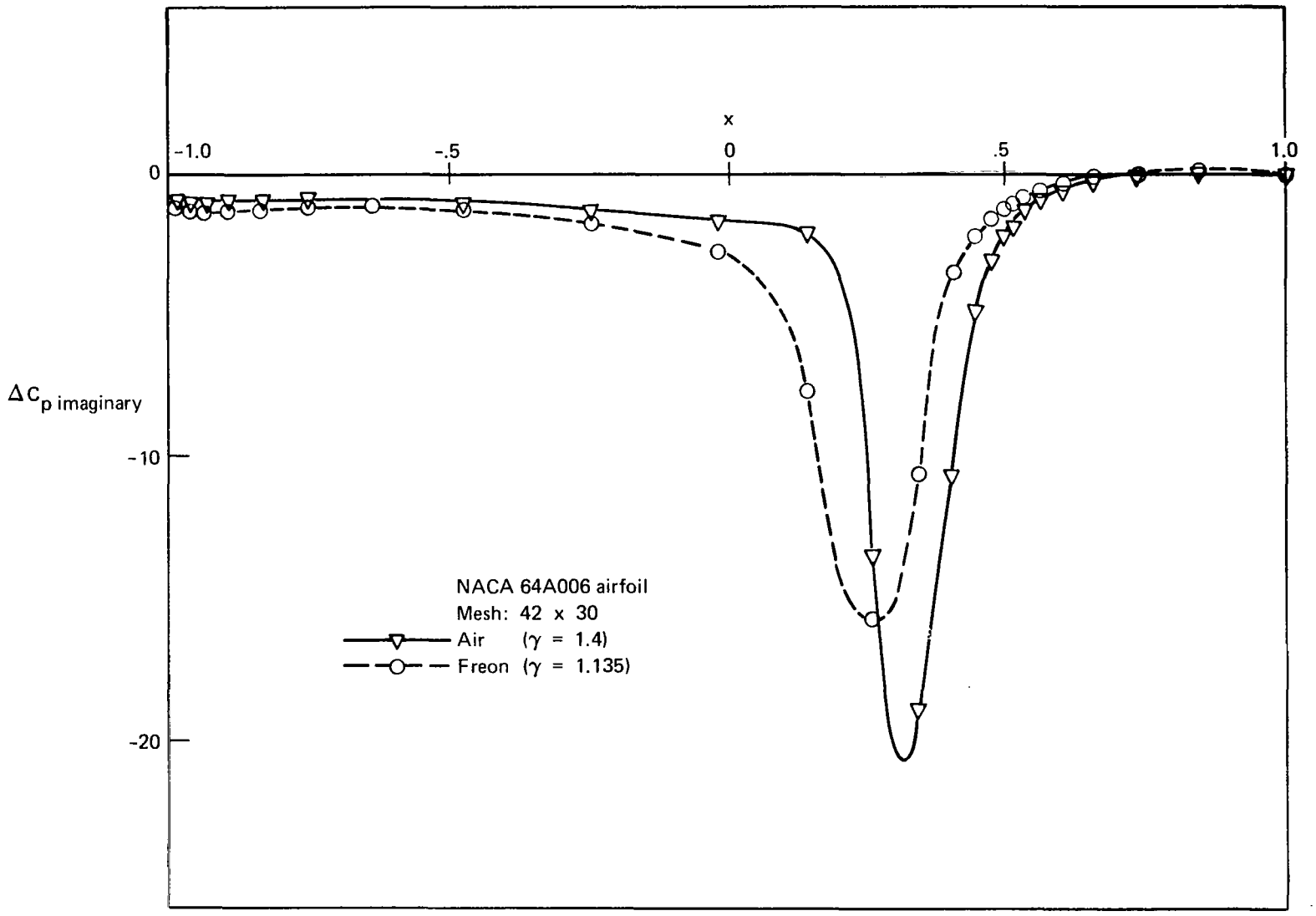

Figure 17b. — Jump in Pressure Coefficient Across an Airfoil with Harmonically Oscillating Quarter-Chord Control Surface — M = 0.9, ω = 0.06

tion. is about the same as that shown by Ehlers (ref. 1) for lower Mach numbers. Thus the essential features of the experimental data are reflected in the calculations while the amplitudes from the two sets of data do not match well.

Finally, figure 17 compares results from Freon and air calculations for the control surface case at $M = 0.9$ and $\omega = 0.06$. The Freon calculations for both the pitch and control surface motions reflect the slight forward shift of the shock shown in the steady results presented in figure 13. Except in the regions of the shock and hingeline, the Freon results also exhibit the slight increase in magnitude over the air results shown in the steady results. Surprisingly, the magnitude of the pressure coefficients in the neighborhood of the shock and hingeline appear less for Freon than for air.

Generally, then, the results of this section are consistent with the results presented by Ehlers in reference 1. The results for the flat-plate configuration correlate well with corresponding results from linear theory for both harmonic pitch and quarter-chord control surface motion. In all cases, the linear theory calculations provide slightly larger amplitudes than the finite difference calculations. For the airfoil, the correlation between the finite difference theory and the experimental results appeared to improve with Mach number. However, the calculations, as in reference 1, continue to provide pressure coefficient magnitudes larger than measured values except over the aft portions of the airfoil for the imaginary part. The correlation between theory and experiment remains inconclusive, and the discrepencies may still be attributed to unknown problems associated with either the theory or the experiment. Finally, the set of two-dimensional examples presented here are limited in terms of frequency range due to the phenomenon of frequency limitation discussed at the beginning of this section, and also in section 4.2 and appendix D.

7.0 AN INITIAL APPLICATION TO A RECTANGULAR WING

7.1 INTRODUCTION

A pilot computer program has been developed for computing the unsteady transonic aerodynamic flow over a three-dimensional rectangular wing. The program is based on the finite difference equations derived by Ehlers in reference 1 and represents a direct extension of the two-dimensional program discussed both in that report and in the preceding sections of this report.

A picture showing the geometrical setup is presented in figure 18. A rectangular, untapered wing is shown in the $z = 0$ plane, with leading edge at $x = -1$ and trailing edge at $x = +1$. The wing tip is at $y_0 = y_s$, and a partial span control surface is included with a hingeline at $x = x_a$, an inboard side edge at $y_0 = y_a$, and an outboard side edge at $y_0 = y_s$. The steady-state velocity potential distribution, φ_0, is calculated for a wing of the same planform but finite thickness and evaluated at the finite difference points that span the mesh space. The flow is assumed symmetric with respect to the x-z plane at $y_0 = 0$, and thus the solution is carried out only over half the wing. The program is arranged so that mesh points lie in the plane at $y = 0$ and the boundary conditions of

$$\left.\frac{\partial \varphi_1}{\partial y}\right|_{y=0} = 0$$

results in $\varphi_1(x,y,z) = \varphi_1(x,-y,z)$. This condition is readily included in the finite difference formulation.

The equations used in the pilot program are given in appendix A. For the most part, the equations are directly from reference 1. However, the second term in the expression for the velocity potential includes an integral in the flow direction with an upper limit of infinity. This term presents special problems in its evaluation. Morino et al.(refs. 12 and 13) present two evaluation procedures; a third is proposed here in hopes of obtaining improved efficiency. The formulation is presented in detail as part of appendix B. Briefly, here, the wake integral of the form

$$\int_{x_t(y_1')}^{\infty} e^{-i\omega x_1'} \frac{\partial \psi}{\partial z_1'} \partial x_1'$$

is converted to a form that may be evaluated using Laguerre integration. As in the two-dimensional case, advantage is taken of the pressure function

$$\frac{\partial \varphi_1}{\partial x} + i\omega \varphi_1$$

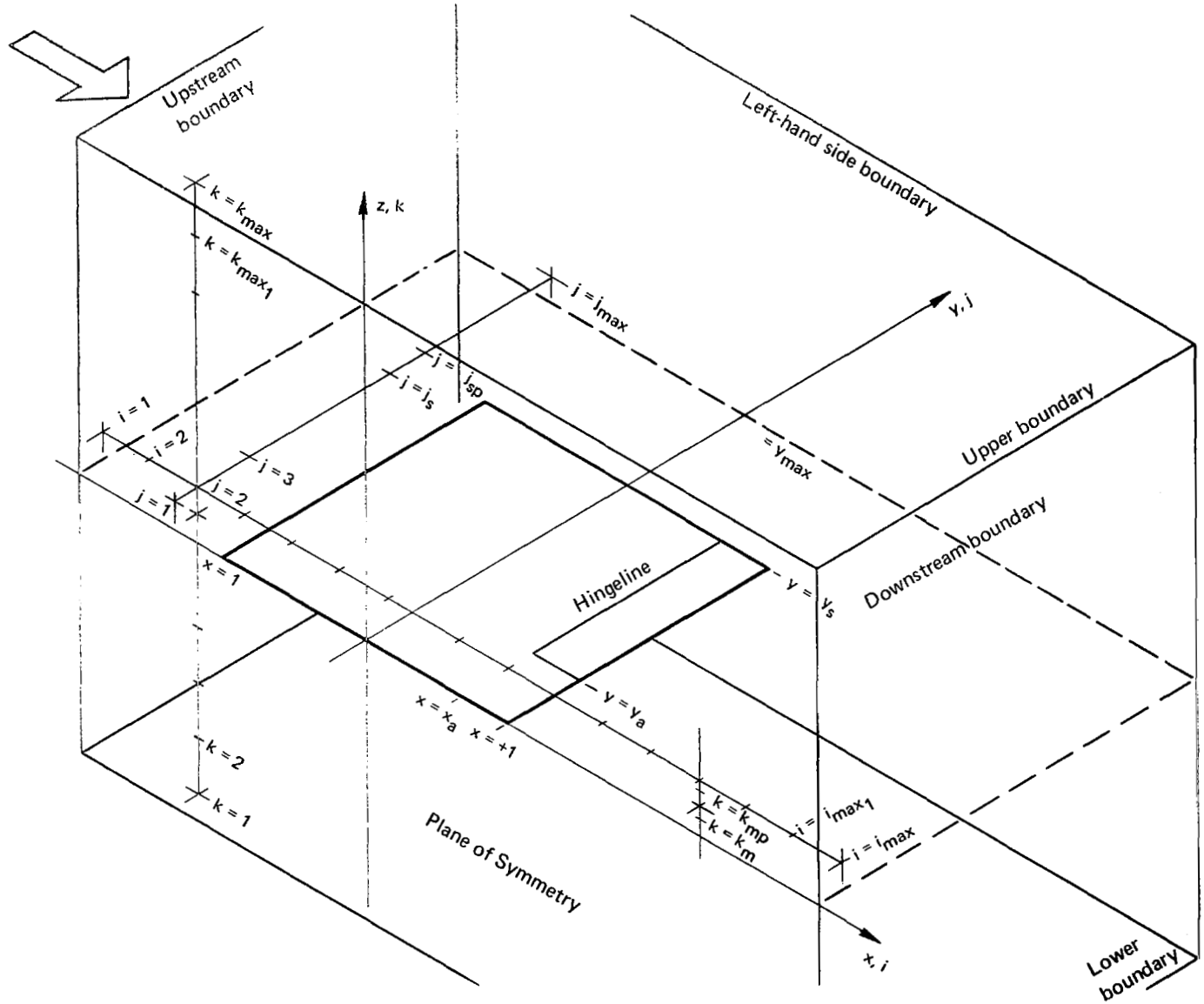

Figure 18. — Schematic of Mesh for Three-Dimensional Problem

to evaluate far-field boundary conditions on the upstream and downstream mesh boundaries. Further, this expression is used on the upper, lower, and side boundaries to determine the velocity potential distribution on the boundary once a velocity potential has been determined at one point on each flow-wise set of finite difference points. Again, for convenience, the velocity potential is evaluated on the boundaries only at x -values equal to the trailing edge (i.e., at x = +1). The pressure function in finite difference form then permits the calculation of φ, for different values of x for the constant values of z and y.

Ehlers in reference 1 presents an alternative derivation for swept (but untapered) wing planforms. However, W. Schmidt (ref. 14) indicates that considerable success in the steady-flow problem has been obtained using a straightforward rectangular finite difference grid not necessarily aligned with the wing planform. This particular point would have to be investigated with respect to the unsteady transonic problem, but there is reason to expect the pilot program to be applicable with relatively little modification to planforms other than the unswept, rectangular planform for which it was developed.

The major obstacle to performing three-dimensional solutions using finite difference techniques is the size of the complex velocity potential matrix, which must be stored between iterations. The finite difference mesh for practical cases is estimated to be on the order of 45 x 30 x 20, or some 81 000 words of core storage for the φ_1 and φ_0 matrices alone if the problem is to be stored in the machine all at once. The alternative is to store these matrices on tape and to bring in three (or more) planes at once. The current pilot program is capable of both modes of operation.

Column relaxation has been selected as the solution procedure because (1) column relaxation has proved most reliable for combinations of Mach number and frequency where the convergence is marginal, and (2) x-z planes require only three planes for the relaxation calculations of each plane. Note that x-y planes have this same feature while y-z planes require four planes because of the backward differencing of the x derivatives at supersonic points.

For our CDC 6600, a mesh of 25 x 19 x 20 is about the maximum size for an incore solution. The 25 x 20 grid in the x-z planes appears small for practical problems, based on our experience with two-dimensional analyses. The problem size may be increased by going to an out-of-core program. Both the incore and the out-of-core versions may be run online.

7.2 RECTANGULAR WING EXAMPLES

The three-dimensional program was used to calculate the pressures over an aspect ratio 5 rectangular wing undergoing harmonic pitch. Calculations were performed for both a flat-plate and a NACA 64A006 profile, with a Mach number of 0.875 and a reduced frequency of 0.06. A mesh of 44 points in the x -direction, 16 points in the y -direction, and 26 points in the z -direction was used. The extent of the finite difference solution area in physical coordinates was $x = \pm 3.80$ (the chord ran from -1.0 to +1.0), $y_0 = +10.5$ (the wing tips were at ± 5.0), and $z_0 = +10.0$. The computing time for these calculations ran on the order of 7 to 8 sec of CPU time for each iteration and 8 to 9 sec for each far-field update. This was for a CDC 6600 computer using the KRONOS 2.1 operating system. The number of iterations required for convergence (in this case ERROR $< 10^{-4}$) was on the order of 180 when starting with zeros for the initial velocity potential field.

The flat-plate results are presented in figure 19. The chordwise distribution of the jump in pressure coefficient is presented for five spanwise locations. In each case, the finite difference results are matched with results from the NASA subsonic program (refs. 4 and 5). Correlation between the results from the two methods is good, and corresponds to that experienced with the two-dimensional examples of section 6.0 and reference 1.

The steady-state pressure distribution for a NACA 64006 profile configuration is shown in figure 20. It was obtained by using a program developed at NASA-Ames by Ballhaus and Bailey (ref. 15) with the mesh arrangement modified in the manner of Schmidt, Rohlfs, and Vanino (ref. 14). The corresponding jump in the unsteady pressure coefficient is presented in figure 21 for five spanwise stations.

The results from a two-dimensional calculation are included in figure 21a. Comparison of the two- and three-dimensional results reflect the anticipated softening of shock effects from the three-dimensional representation. In particular, the imaginary part of the pressure coefficient shows no apparent shock influences, and resembles what would be expected for the elliptic problem. Compare, for example, the linear three-dimensional solution shown in figure 49a with the linear two-dimensional solution shown in figure 4. Here the ΔC_p changes sign at a significantly more forward chordwise location for the three-dimensional example than for the two-dimensional example. Three-dimensional experimental data are needed for further confirmation of the analytical program.

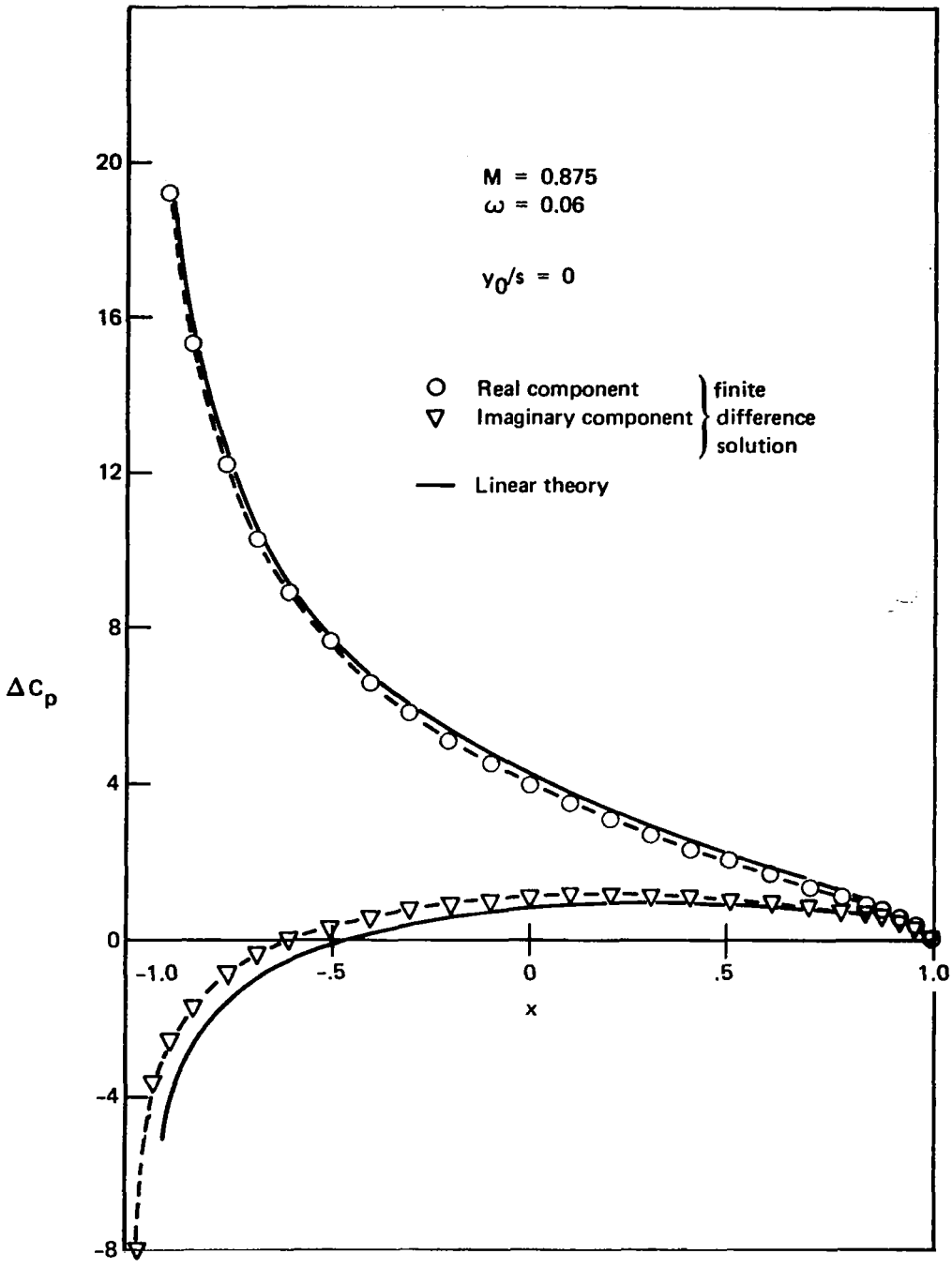

Figure 19a. — Pressure Distributions for an Aspect Ratio 5, Flat Plate in Pitch

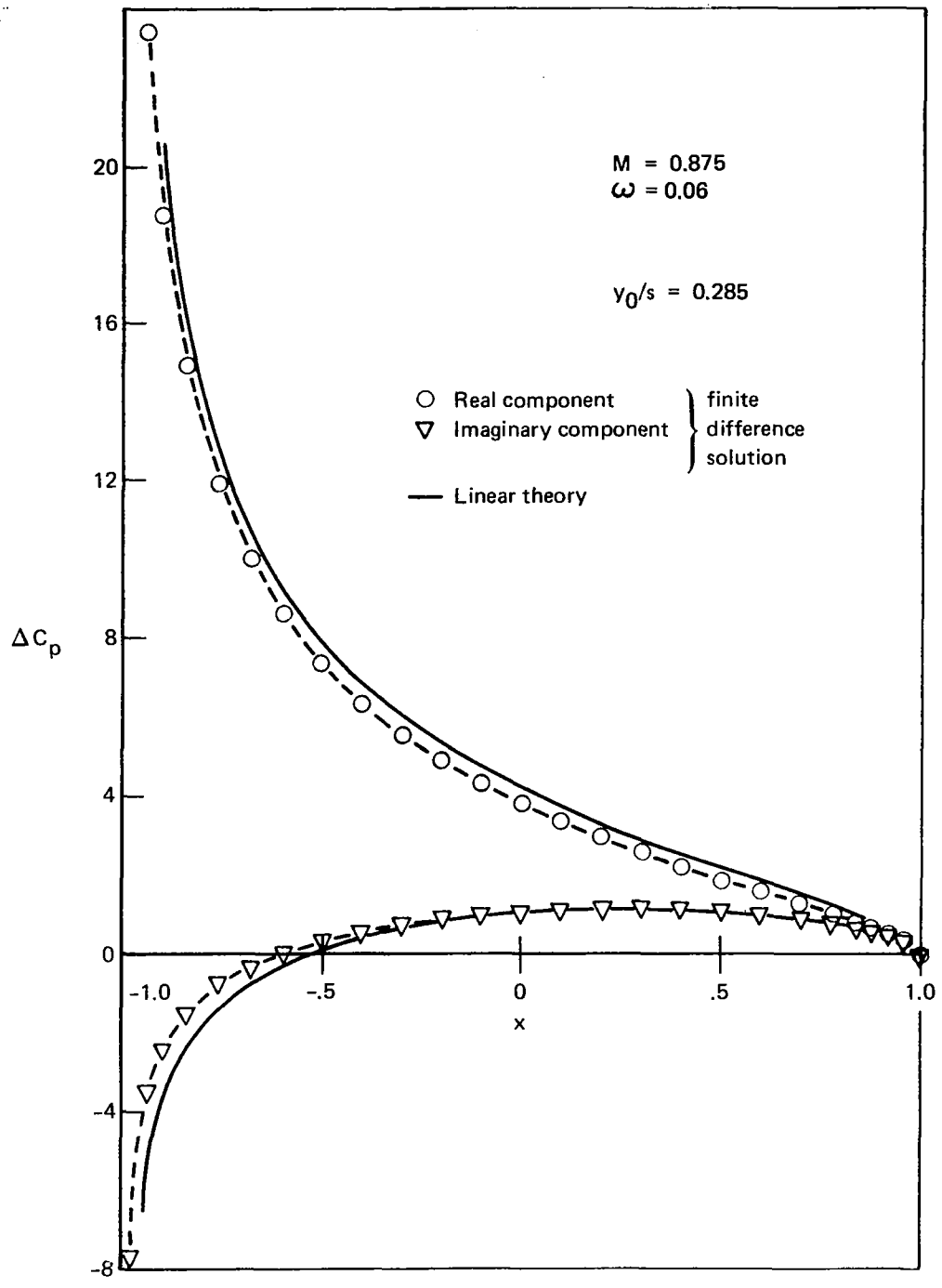

Figure 19b. — Pressure Coefficient Distributions for an Aspect Ratio 5, Flat Plate in Pitch

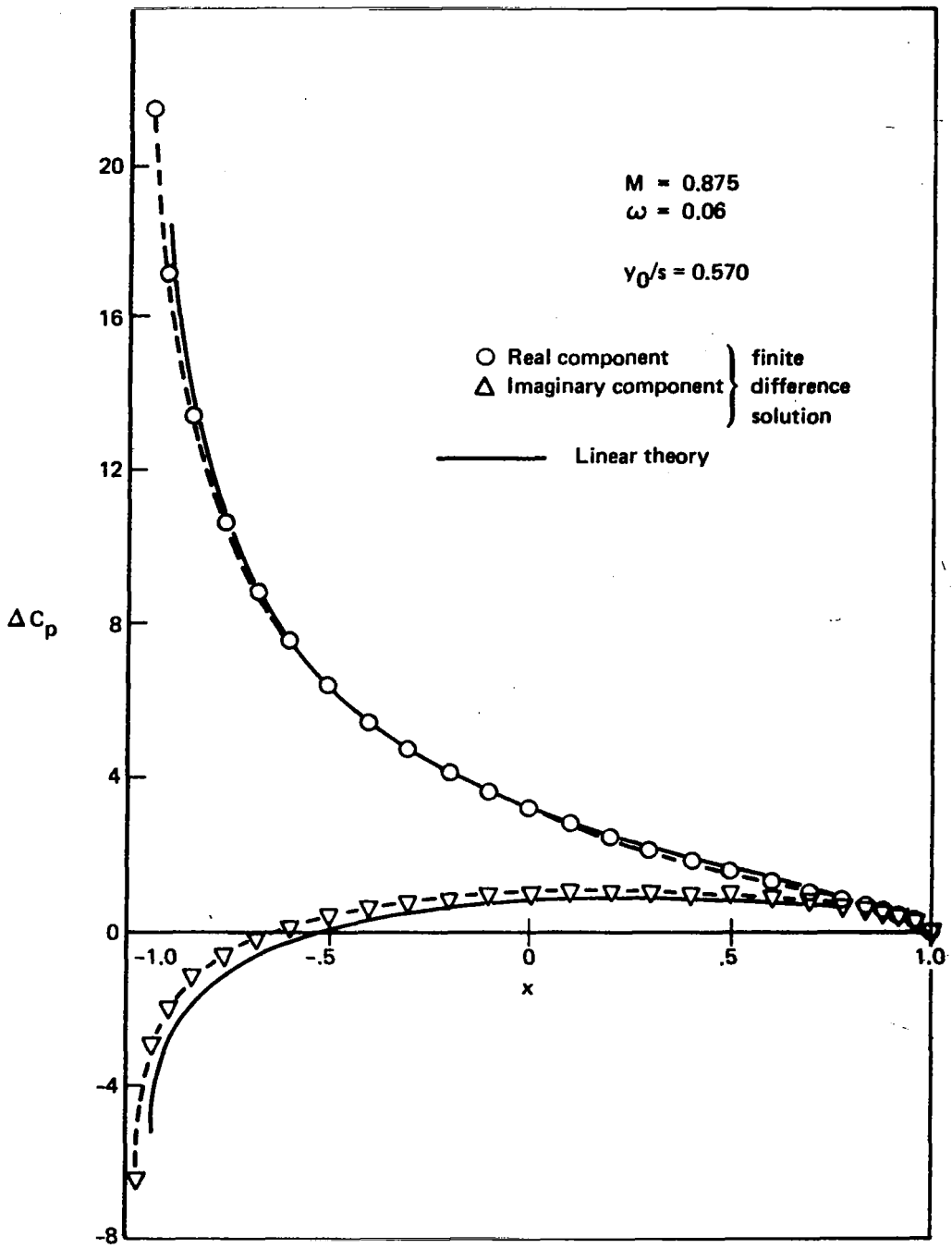

Figure 19c. — Pressure Coefficient Distributions for an Aspect Ratio 5, Flat Plate in Pitch

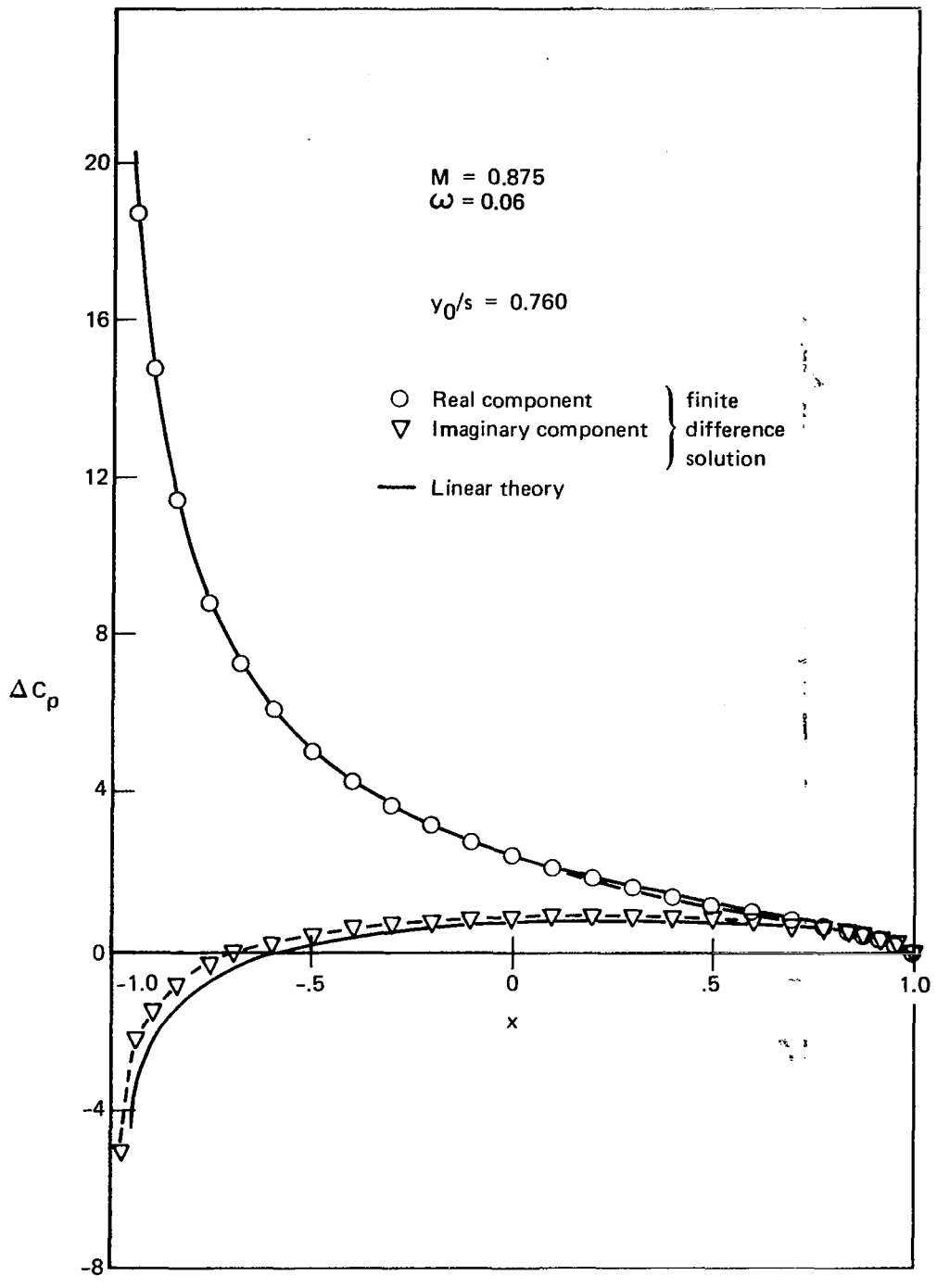

Figure 19d. — Pressure Coefficient Distributions for an Aspect Ratio 5, Flat Plate in Pitch

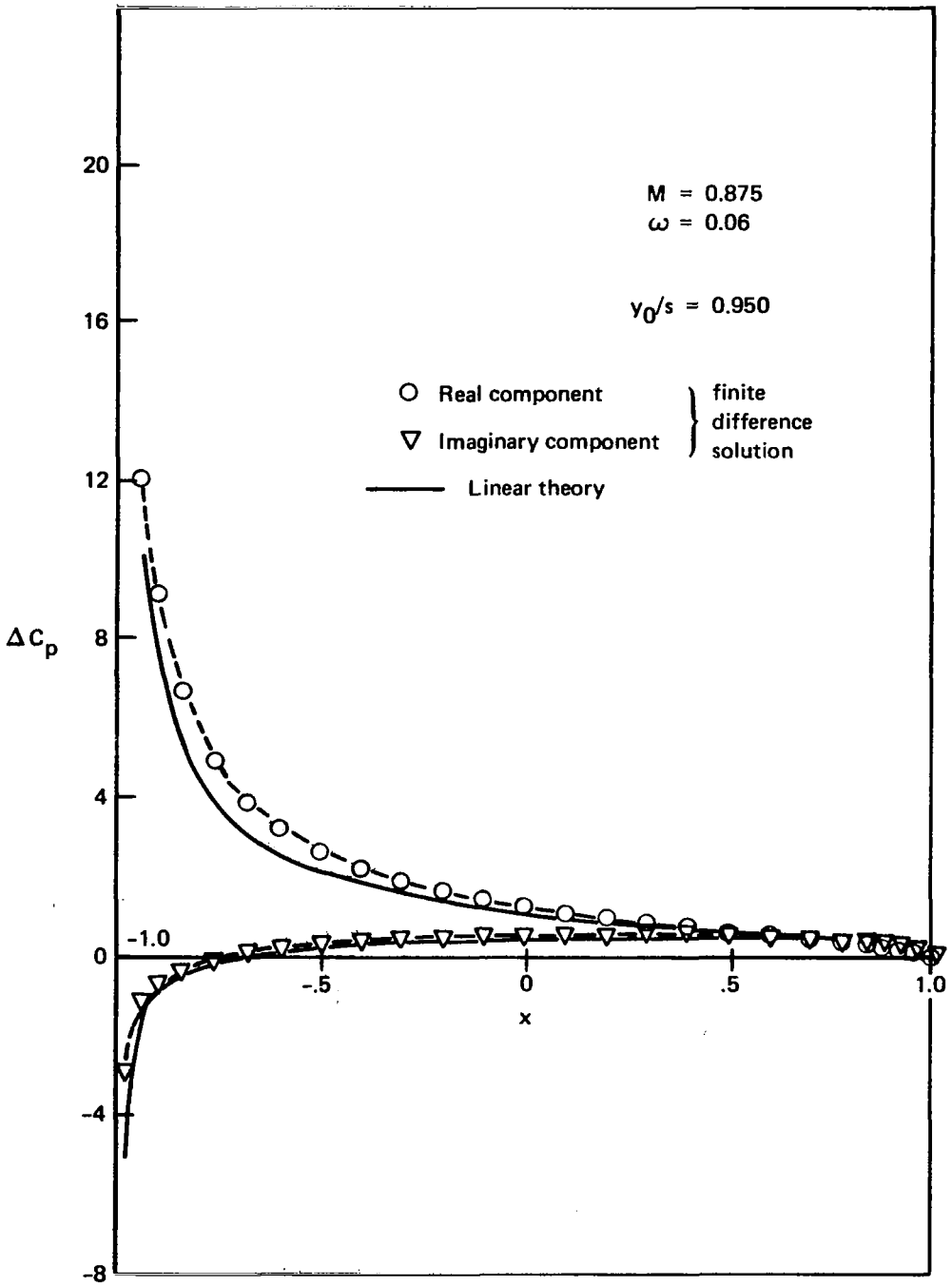

Figure 19e. — Pressure Coefficient Distributions for an Aspect Ratio 5, Flat Plate in Pitch

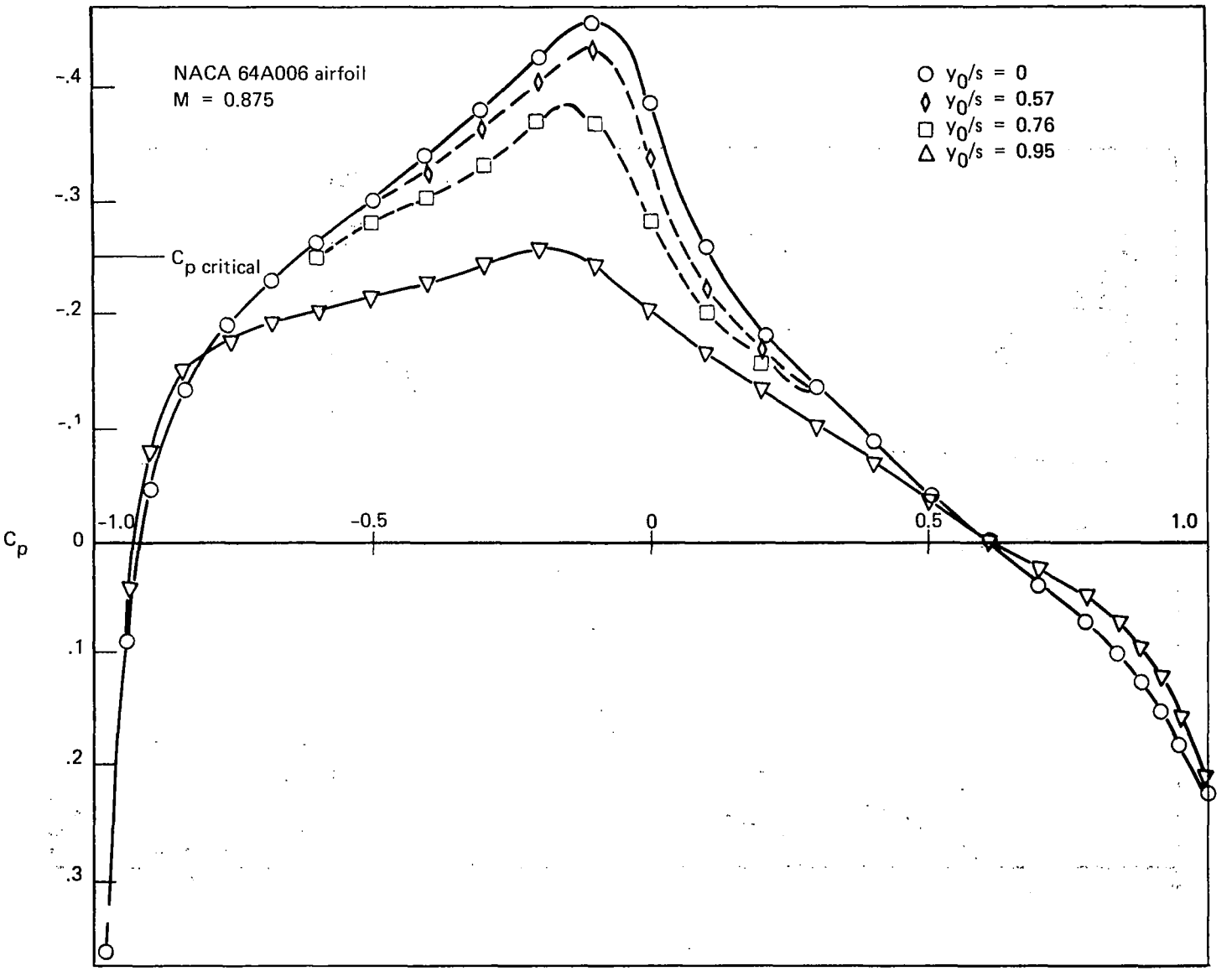

Figure 20. — Steady-State Pressure Coefficient Distributions for an Aspect Ratio 5, Rectangular Wing

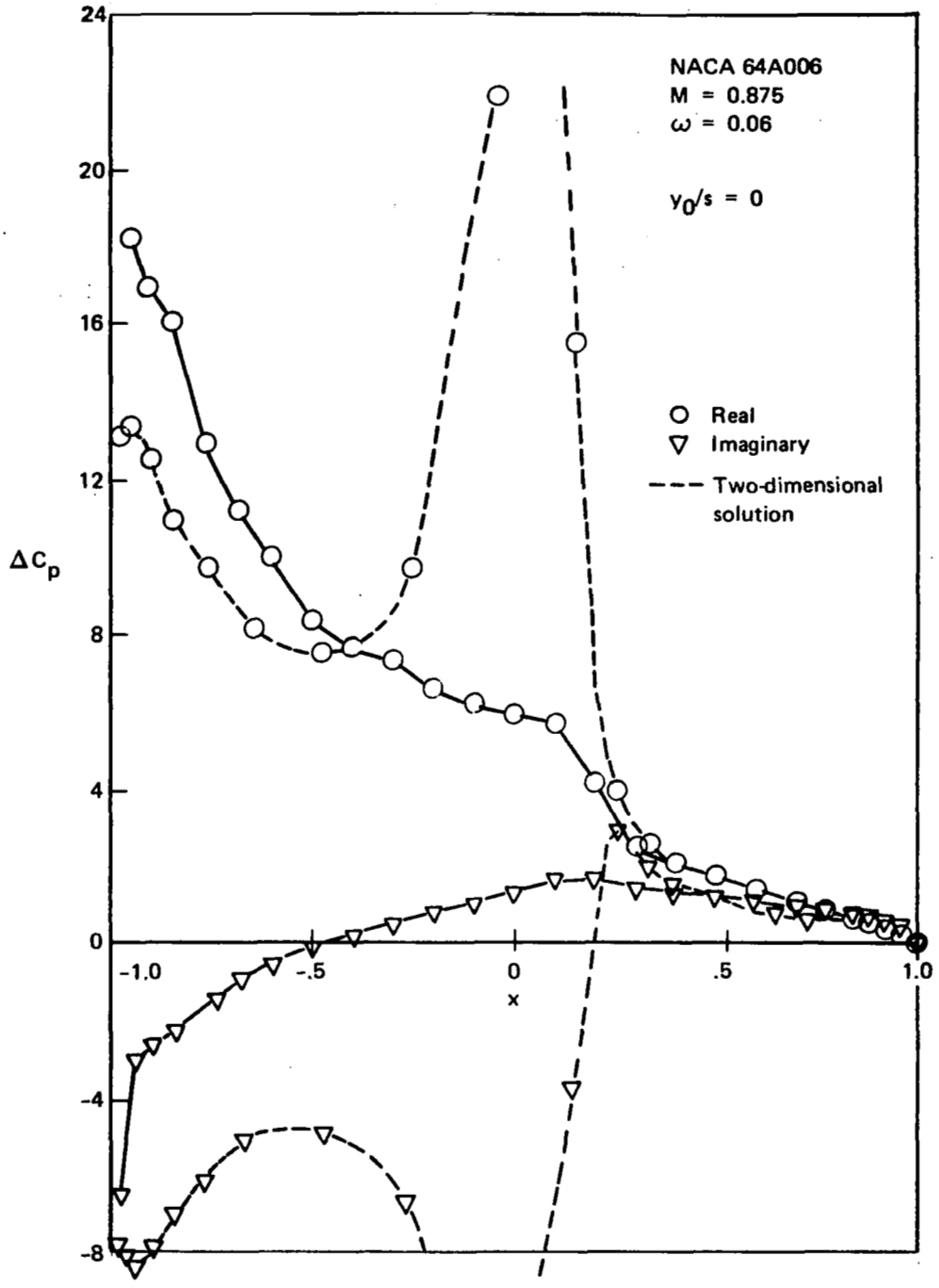

Figure 21a. — Pressure Coefficient Distributors for an Aspect Ratio 5, Rectangular Wing in Pitch

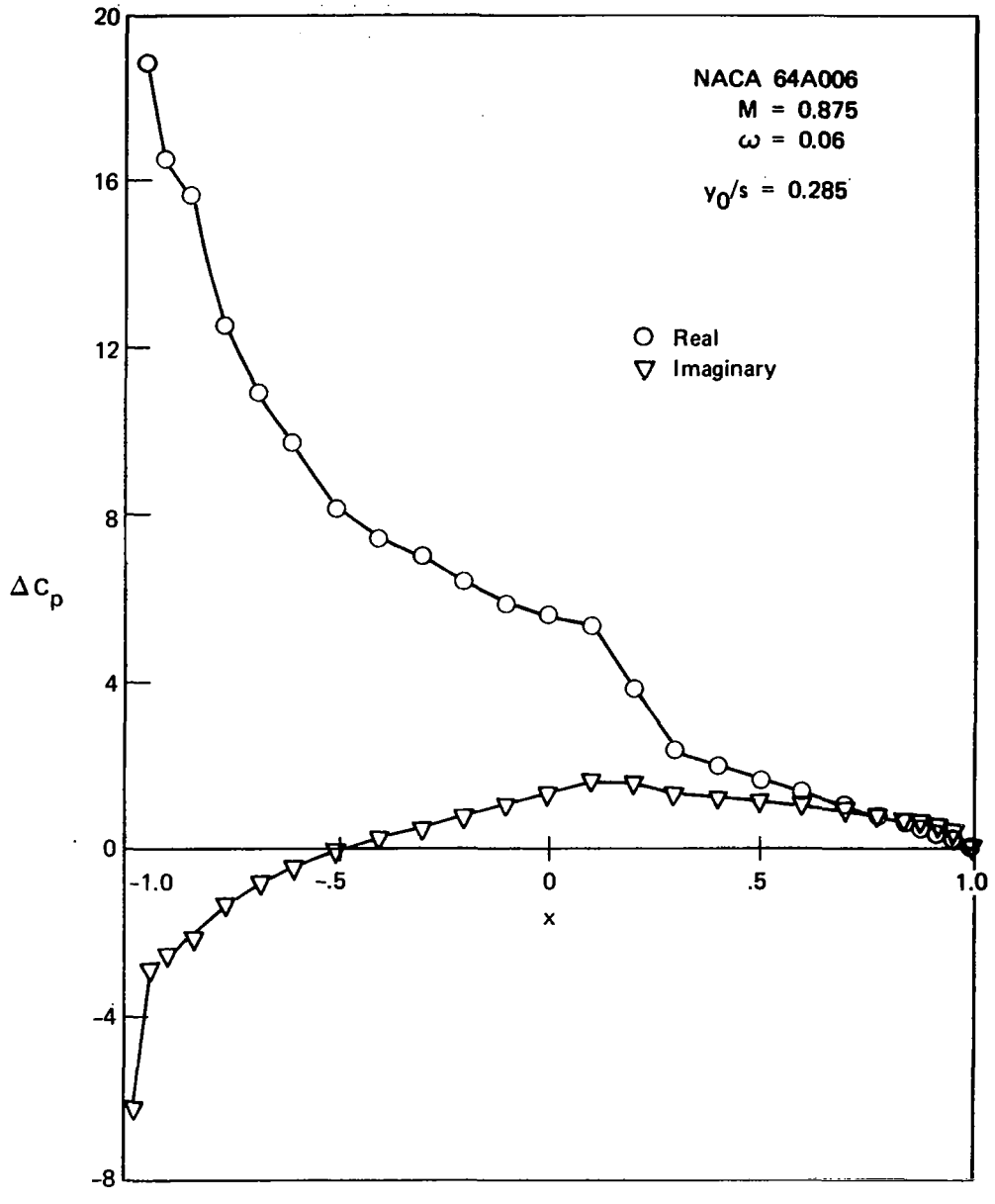

Figure 21b. — Pressure Coefficient Distributions for an Aspect Ratio 5, Rectangular Wing in Pitch

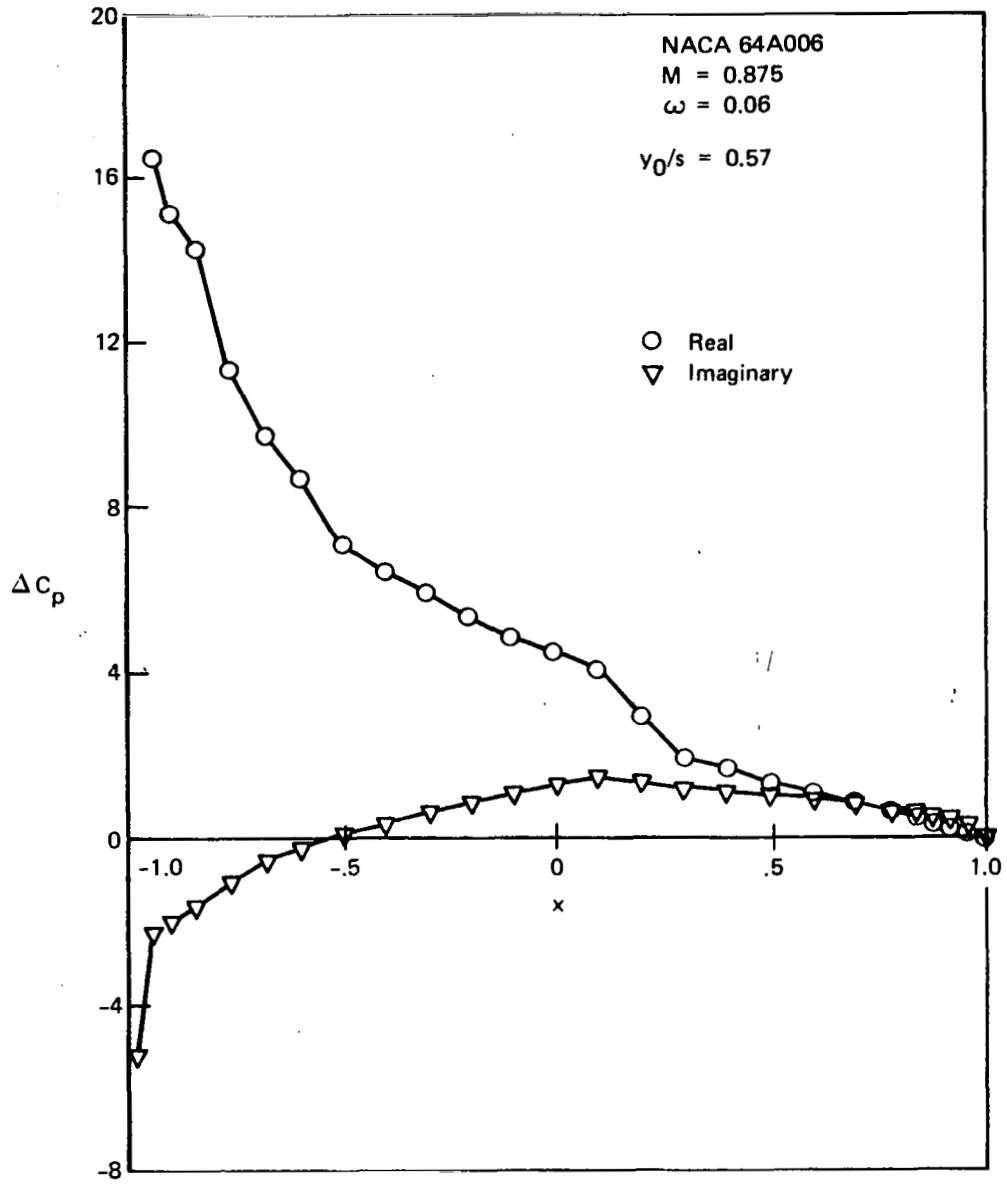

Figure 21c. — Pressure Coefficient Distributions for an Aspect Ratio 5, Rectangular Wing in Pitch

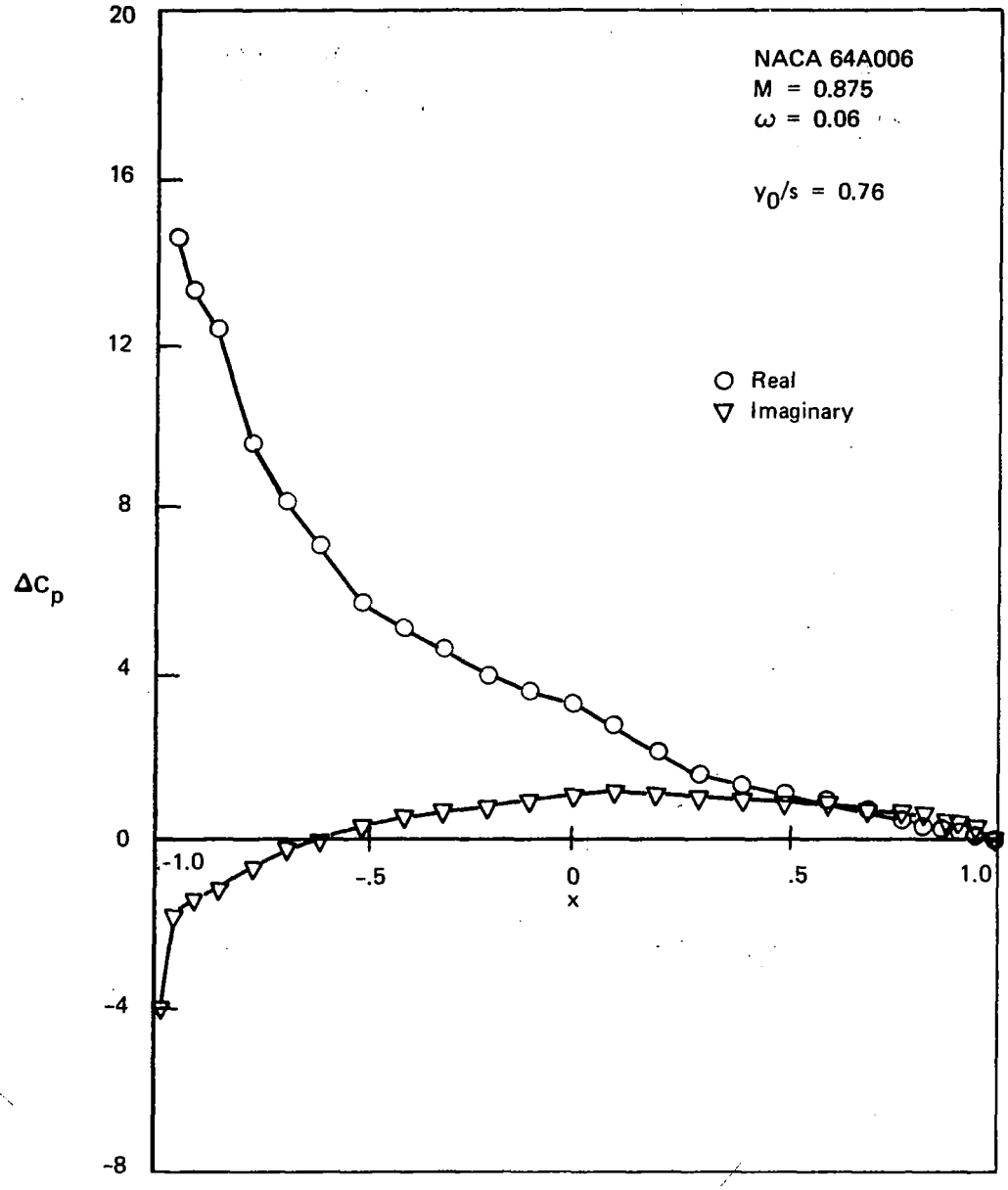

Figure 21d. — Pressure Coefficient Distributions for an Aspect Ratio 5, Rectangular Wing in Pitch

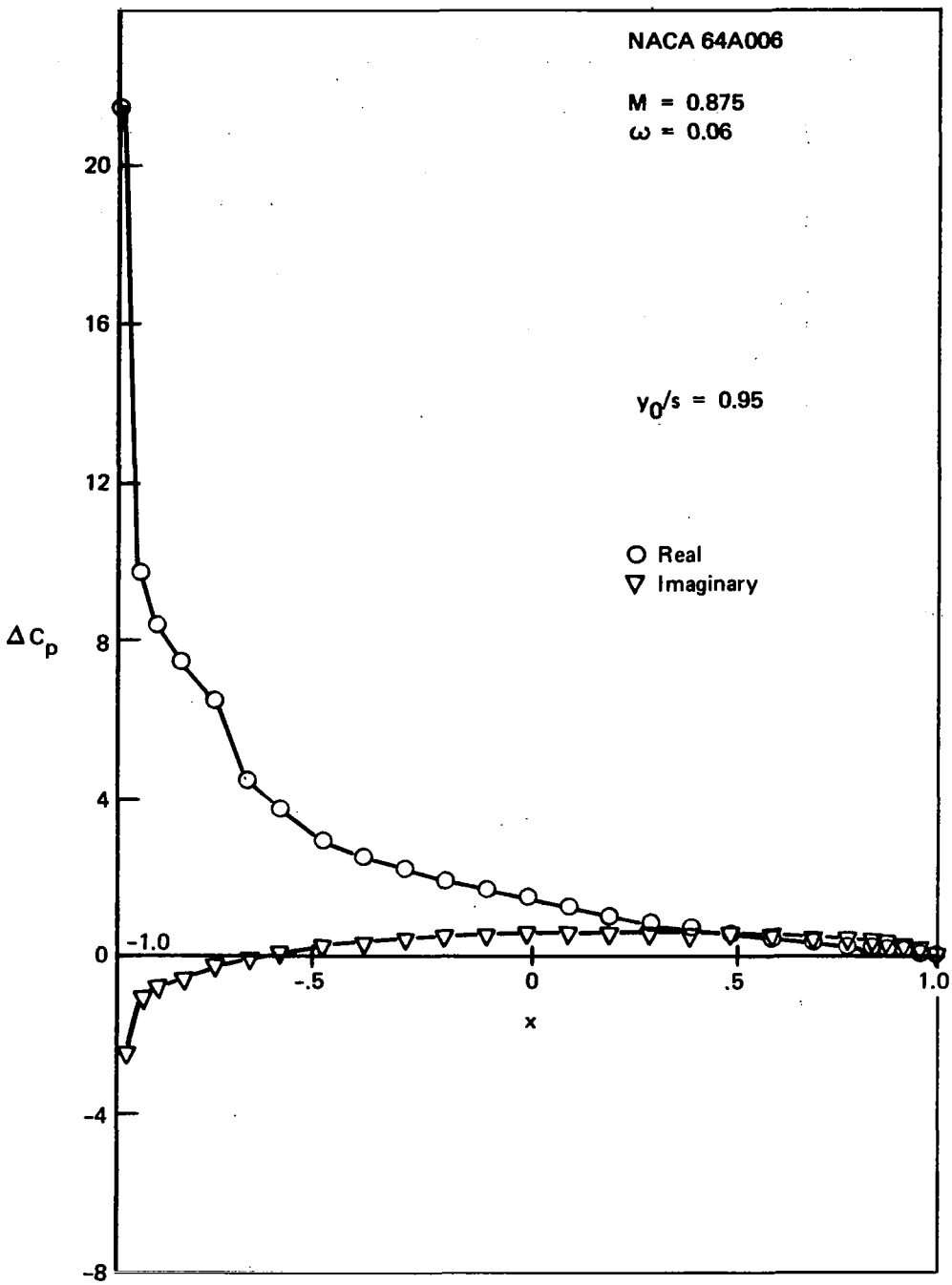

Figure 21e.— Pressure Coefficient Distributions for an Aspect Ratio 5, Rectangular Wing in Pitch

8.0 CONCLUSIONS

Following the work of Ehlers (ref. 1), this report has further explored the characteristics of a finite difference solution to the unsteady transonic flow problem. Relatively rapid solution convergence rates were obtained using selected values of the overrelaxation factor together with row line relaxation. Additional examples were calculated for Mach numbers from 0.8 to 0.9. Correlation of flat-plate results with corresponding results from linear subsonic programs was good for both pitching and control surface motions. Correlations between analyses for a NACA 64A006 airfoil and available experimental data were about the same at the higher Mach numbers, as reported in the preceding report (ref. 1) for the lower Mach numbers. Also, a pilot program for three-dimensional flow was developed and applied to a rectangular wing.

Of significant concern was the encountering of an upper limit on reduced frequency, depending on Mach number and mesh region dimensions, above which the relaxation procedure will not converge. The relaxation procedure has been analyzed from several points of view, providing an explanation for the lack of convergence under certain circumstances.

Boeing Commercial Airplane Company
P.O. Box 3707
Seattle, Washington 98124, July 1975

APPENDIX A

EQUATIONS FOR THREE-DIMENSIONAL FLOW

The finite difference equations for three-dimensional unsteady transonic flow are given by Ehlers in reference 1. They are listed here for convenience. At interior points where the steady flow is subsonic, we have

$$a_{z_k} \varphi_{1\,ijk-1} - \left(a_{y_j} + b_{y_j} + a_{z_k} + b_{z_k} + E_1 + E_2 - q_{ijk}/2\right) \varphi_{1\,ijk} + b_{z_k} \varphi_{1\,ijk+1} = -E_1 \varphi_{1\,i+1jk} - E_2 \varphi_{1\,i-1jk} - a_{y_j} \varphi_{1\,ij-1k} - b_{y_j} \varphi_{1\,ij+1k} \tag{A1}$$

and at points where the steady flow is supersonic,

$$a_{z_k} \varphi_{1\,ijk-1} - \left(a_{y_j} + b_{y_j} + a_{z_k} + b_{z_k} - E_3 - q_{ijk}/2\right) \varphi_{1\,ijk} + b_{z_k} \varphi_{1\,ijk+1} = (E_3 + E_4) \varphi_{1\,i-1jk} - E_4 \varphi_{1\,i-2jk} - a_{y_j} \varphi_{1\,ij-1k} - b_{y_j} \varphi_{1\,ij+1k} \tag{A2}$$

where

$$a_{z_k} = \frac{1}{(z_{k+1} - z_{k-1})(z_k - z_{k-1})} \qquad a_{y_j} = \frac{1}{(y_{j+1} - y_{j-1})(y_j - y_{j-1})} \tag{A3}$$

$$b_{z_k} = \frac{1}{(z_{k+1} - z_{k-1})(z_{k+1} - z_k)} \qquad b_{y_j} = \frac{1}{(y_{j+1} - y_{j-1})(y_{j+1} - y_j)}$$

$$E_1 = c_i u_{i+\frac{1}{2}jk} - i\omega c_{1\,i}/\epsilon$$

$$E_2 = d_i u_{i+\frac{1}{2}jk} - i\omega d_{1\,i}/\epsilon$$

$$E_3 = c_{i-1} u_{i-\frac{1}{2}jk} - i\omega c_{2\,i}/\epsilon$$

$$E_4 = d_{i-1} u_{i-\frac{3}{2}jk} - i\omega d_{2\,i}/\epsilon$$

$$c_i = \frac{1}{(x_{i+1} - x_{i-1})(x_{i+1} - x_i)} \qquad c_{1\,i} = (x_i - x_{i-1})\, c_i$$

$$d_i = \frac{1}{(x_{i+1} - x_{i-1})(x_i - x_{i-1})} \qquad d_{1\,i} = (x_{i+1} - x_i)\, d_i$$

$$u_{i+\frac{1}{2}jk} = K - (\gamma+1)(\varphi_{0\,i+1jk} - \varphi_{0\,ijk})/(x_{i+1} - x_i)$$

$$u_{i-\frac{1}{2}jk} = K - (\gamma+1)(\varphi_{0\,ijk} - \varphi_{0\,i-1jk})/x_i - x_{i-1})$$

$$c_{2\,i} = \frac{1}{x_i - x_{i-1}} + \frac{1}{x_i - x_{i-2}}$$

$$d_{2\,i} = -d_{1\,i-1}$$

Equations (A1) and (A2) are equations (24) and (27) from reference 1.

The boundary conditions on the upper and lower wing surfaces lead to the following equations for subsonic flow at finite difference points immediately below the wing, $k = k_m$

$$a_{z_{k_m}} \varphi_{1\,ijk_m-1} - \left(a_{y_j} + b_{y_j} + a_{z_{k_m}} + E_1 + E_2 - q_{ijk_m}/2\right) \varphi_{1\,ijk_m}$$
$$= -E_1 \varphi_{1\,i+1jk_m} - E_2 \varphi_{1\,i-1jk_m} - a_{y_j} \varphi_{1\,ij-1k_m} - b_{y_j} \varphi_{1\,ij+1k_m} - h_1 \, b_{z_{k_m}} F_{ij}^{(L)} \qquad \text{(A4)}$$

and points immediately above the wing, $k = k_m + 1$

$$-\left(a_{y_j} + b_{y_j} + a_{z_{k_m+1}} + E_1 + E_2 - q_{ijk_m+1}/2\right) \varphi_{1\,ijk_m+1} + b_{z_{k_m+1}} \varphi_{1\,ijk_m+2}$$
$$= -E_1 \varphi_{1\,i+1jk_m+1} - E_2 \varphi_{1\,i-1jk_m+1} - a_{y_j} \varphi_{1\,ij-1k_m+1} - b_{y_j} \varphi_{1\,ij+1k_m+1} + h_1 \, a_{z_{k_m+1}} F_{ij}^{(U)} \qquad \text{(A5)}$$

where

$$F_{ij}^{(L)} = f_{1_x}^{(L)}(x_i, y_j) + i\omega f_1^{(L)}(x_i, y_j)$$

$$F_{ij}^{(U)} = f_{1_x}^{(U)}(x_i, y_j) + i\omega f_1^{(U)}(x_i, y_j) \qquad \text{(A6)}$$

The (L) and (U) refer to upper and lower wing surfaces, respectively. The equations similar to (A4) and (A5) at supersonic points can be written down analogously.

The total harmonic deflection of the wing is written as

$$z_0 = \delta f(x,y,t) = \delta \left\{ f_0(x,y) + f_1(x,y)\, e^{i\omega t} \right\} \qquad \text{(A7)}$$

The steady velocity potential, φ_0 is calculated from the steady deflection shape, f_0, while the unsteady potential φ_1, is calculated from the harmonic mode shape, f_1 (x,y).

Over the wake, the conditions that the trailing vortex sheet supports no pressure,

$$\frac{\partial \Delta\varphi_1}{\partial x_1} + i\omega \Delta\varphi_1 = 0 \qquad \text{(A8)}$$

results in a term being added to the right-hand side of equations (A1) and (A2). For finite difference points just below the wing plane ($k = k_m$), the additional term is

$$b_{z_{k_m}} \Delta\varphi_{1\,ij} \tag{A9}$$

and for points just above the wing plane ($k = k_m + 1$) the term is

$$-a_{z_{k_m+1}} \Delta\varphi_{1\,ij} \tag{A10}$$

where

$$\Delta\varphi_{1\,ij} = \Delta\varphi_{1\,i_1+1j}\, e^{-i\omega(x_i - x_{i_1+1})} \tag{A11}$$

and $\Delta\varphi_{1i_1+1j}$ is the jump in velocity potential at the first point aft of the wing trailing edge at station j determined so as to satisfy the Kutta condition on the trailing edge. The additions of equations (A9) and (A10) implicitly satisfied the condition. The normal velocity is continuous across the wake.

The finite difference equation for the jump in φ_1 across the wing to the second order in mesh size is

$$\Delta\varphi_1 = \varphi_1^{(U)} - \varphi_1^{(L)} = \varphi_{1\,ijk_m+1} - \varphi_{1\,ijk_m} - c_{s1}\left(\varphi_{1\,ijk_m+2} - \varphi_{1\,ijk_m+1}\right)$$
$$- c_{s2}\left(\varphi_{1\,ijk_m} - \varphi_{1\,ijk_m-1}\right) - \left(d_{s1} F_{ij}^{(U)} - d_{s2} F_{ij}^{(L)}\right) \tag{A12}$$

where

$$c_{s1} = \frac{1}{4s_1(s_1+1)} \qquad c_{s2} = \frac{1}{4s_2(s_2+1)}$$
$$d_{s1} = \frac{h(2s_1+1)}{4(s_1+1)} \qquad d_{s2} = \frac{h(2s_2+1)}{4(s_1+1)} \tag{A13}$$

$$s_1 = \left(z_{k_m+2} - z_{k_m+1}\right)/h \qquad s_2 = \left(z_{k_m} - z_{k_m-1}\right)/h$$
$$h = z_{k_m+1} - z_{k_m} \tag{A14}$$

Two integral relations are used to satisfy the far-field boundary conditions on the outer boundaries of finite difference mesh. The first for the velocity potential is

$$\varphi_1(x_1,y_1,z_1) = \frac{1}{4\pi}\int_{-y_t}^{+y_t}\int_{x_\ell(y_1')}^{x_t(y_1')}\left[\Delta\varphi_1\ \psi_{z_1'} - \psi\Delta\varphi_{1\,z_1'}\right]dx_1'\,dy_1'$$

$$+\frac{1}{4\pi}\int_{-y_t}^{+y_t} e^{i\omega x_t(y_1')}\,\Delta\varphi_{1\,t}(y_1')dy_1'\int_{x_t(y_1')}^{\infty} e^{-i\omega x_1'}\,\psi_{z_1'}\,dx_1' \qquad \text{(A15)}$$

$$+\frac{1}{4\pi}\int_v\left\{(\gamma+1)\varphi_{0\,x_1'}\,\varphi_{1\,x_1'}\,\psi_{x_1'} - i\omega(\gamma-1)\varphi_1\,\psi\varphi_{0\,x_1'\,x_1'}\right\}dv'$$

and the second for the pressure function is

$$P(x_1,y_1,z_1) = \varphi_{1\,x_1} + i\omega\varphi_1 \qquad \text{(A16)}$$

$$= \frac{1}{4\pi}\int_{-y_t}^{+y_t}\int_{x_\ell(y_1')}^{x_t(y_1')}\left[\Delta\varphi_1\ \chi_{z_1'} - \chi\Delta\varphi_{1\,z_1'}\right]dx_1'\,dy_1'$$

$$-\frac{1}{4\pi}\int_{-y_t}^{+y_t} e^{i\omega x_t(y_1')}\Delta\varphi_{1\,t}(y_1')\psi_{z_1}(x_t(y_1')-x_1,y_1-y_1',z_1)\,dy_1' \qquad \text{(A17)}$$

$$+\frac{1}{4\pi K}\int_v\left\{(\gamma+1)\varphi_{0\,x_1'}\,\varphi_{1\,x_1'}\,\chi_{x_1'} - i\omega(\gamma-1)\varphi_1\,\chi\varphi_{0\,x_1'\,x_1'}\right\}dv'$$

Defining $\bar{x} = x_1 - x_1'$, $\bar{y} = y_1 - y_1'$, $\bar{z} = z_1 - z_1'$ and $R = \sqrt{\bar{x}^2 + \bar{y}^2 + \bar{z}^2}$

$$\psi(\bar{x},\bar{y},\bar{z}) = \frac{e^{i\lambda_1(M\bar{x}-R)}}{R}$$

$$\psi_{z_1'} = \frac{\bar{z}}{R}(1/R + i\lambda_1)\psi$$

$$\psi_{x_1'} = \left[i\lambda_1 M - \frac{\bar{x}}{R}(1/R + i\lambda_1)\right]\psi \qquad \text{(A18)}$$

$$\chi = \psi_{x_1} + i\omega\psi$$

$$\chi = \left[i\lambda_1 M - \frac{\bar{x}}{R}(1/R + i\lambda_1) + i\omega\right]\psi$$

$$\chi_{z_1'} = -\frac{\bar{z}}{R}\left\{\left[\frac{3\bar{x}}{R^2} - i\lambda_1 M - i\omega\right](i\lambda_1 + 1/R) - \lambda_1^2\,\bar{x}/R\right\}\psi$$

Equations (A15) and (A17) have been simplified for purposes of the pilot program. First, as noted in the two-dimensional derivation

$$\frac{\partial \Delta\varphi_1}{\partial z_1} = \Delta\left(\frac{\partial \varphi_1}{\partial z_1}\right) = 0 \tag{A19}$$

and thus the second integral in the first term of both (A15) and (A17) are zero. Second, the third term, which is the volume integral and has not been of significance in the two-dimensional problem, has been dropped. Third, since we are interested in the far-field, we approximate $x_1 - x_1'$ with x_1 and $y_1 - y_1'$ with y_1 so that the terms of ψ and x may be moved outside the integral sign. The evaluation of the wake integral in equation (A15) is discussed in detail in the next section. The equation for the velocity potential on the far-field (A15) for $x_1 = 1.0$ is

$$\varphi_1(x_1, y_1, z_1) = \frac{1}{4\pi} \psi_{z_1'} \int_{-y_t}^{+y_t} \int_{x_\ell(y_1')}^{x_t(y_1')} \Delta\varphi_1 \, dx_1' dy_1' + \varphi_{1_w}$$

$$+ \frac{1}{4\pi K} \int_v \left\{ (\gamma+1) \varphi_{0_{x_1'}} \varphi_{1_{x_1'}} \psi_{x_1'} - i\omega(\gamma-1)\varphi_1 \psi \varphi_{0_{x_1' x_1'}} \right\} dv' \tag{A20}$$

Where

$$\varphi_{1_w} = \frac{1}{4\pi} \int_{-y_t}^{+y_t} \Delta\varphi_{1_t}(y_1') \, I_w(y_1, z_1; y_1') \, dy_1' \tag{A21}$$

and I_w is defined in the next section. The pressure function (A9) becomes

$$P(x_1, y_1, z_1) = \frac{1}{4\pi} \chi_{z_1'} \int_{-y_t}^{+y_t} \int_{x_\ell(y_1')}^{x_t(y_1')} \Delta\varphi_1 \, dx_1' \, dy_1'$$

$$- \frac{1}{4\pi} \psi_{z_1} \int_{-y_t}^{+y_t} e^{i\omega x_t(y_1')} \Delta\varphi_{1_t}(y_1') \, dy_1' \tag{A22}$$

Equation (A20) is used to evaluate the velocity potential along the line resulting from the intersection of the y-z plane through the trailing edge of the wing and the x-y and x-z planes bounding the finite difference volume. Equation (A16) is then integrated by the trapezoidal rule to determine values ahead of this line and behind this line on the upper, lower, and side boundaries. For example, on the lower boundary when k = 1, for points ahead of the trailing edge ($x < 1.0$ or $i < i_1$)

$$\varphi_{1_{i-1j1}} = \varphi_{1_{ij1}} e^{i\omega(x_i - x_{i-1})} - \left[P(x_i, y_j, z_1) \, e^{i\omega(x_i - x_{i-1})} + P(x_{i-1}, y_j, z_1) \right] \frac{x_i - x_{i-1}}{2} \tag{A23}$$

and the equation for points downstream of the trailing edge ($i_1 > i$) is

$$\varphi_{1\,ij1} = \varphi_{1\,i-1j1}\, e^{-i\omega(x_i - x_{i-1})} + \left[P(x_i,y_j,z_1) + P(x_{i-1},y_j,z_1)\, e^{-i\omega(x_i - x_{i-1})}\right]\frac{x_i - x_{i-1}}{2} \quad \text{(A24)}$$

The application of equation (A22) to the upstream and downstream boundaries results in the following equations: on the upstream boundary

$$\varphi_{1\,ijk} = c_{k1}\,\varphi_{1\,ijk} - c_{k2}\,P_{1jk} \quad \text{(A25)}$$

and for the downstream boundary

$$\varphi_{1\,i_{max}jk} = c_{k3}\,\varphi_{1\,i_{max}-1jk} + c_{k4}\,P_{i_{max}jk} \quad \text{(A26)}$$

where

$$P_{1jk} = P(x_1, y_j, z_k)$$

and

$$P_{i_{max}jk} = P(x_{i_{max}}, y_j, z_k)$$

$$c_{k1} = \frac{1 + i\omega\delta_1/2}{1 - i\omega\delta_1/2} \qquad \delta_1 = x_2 - x_1$$

$$c_{k2} = \delta_1/(1 - i\omega\delta_1/2) \quad \text{(A27)}$$

$$c_{k3} = (1 - i\omega\delta_2/2)/(1 + i\omega\delta_2/2) \qquad \delta_2 = x_{i_{max}} - x_{i_{max}-1}$$

$$c_{k4} = \delta_2/(1 + i\omega\delta_2/2)$$

Equations (A25) and (A26) may be used to substitute for $\varphi_{1\,ijk}$ and $\varphi_{1\,i_{max}jk}$ in equations (A1) and (A2).

APPENDIX B

EVALUATION OF FAR-FIELD WAKE INTEGRAL

The wake integral of concern, φ_{1_W}, is the second term of equation (A15), i.e.,

$$\varphi_{1_W}(x_1,y_1,z_1) = \frac{1}{4\pi}\int_{-y_t}^{+y_t} e^{i\omega x_t(y_1')}\,\Delta\varphi_{1_t}(y_1')\,dy_1' \cdot \int_{x_t(y_1')}^{\infty} e^{-i\omega x_1'}\frac{\partial\psi}{\partial z_1'}(x_1-x_1',y_1-y_1',z_1-z_1')\,dx_1' \tag{B1}$$

where the partial derivative is to be evaluated at $z_1' = 0$ and ψ is defined in equation (A18). The evaluation will be carried out for $x_1 = 1.0$ for a rectangular wing for which the trailing edge is $x_t(y_1') = 1.0$. Equation (B1), after taking $e^{i\omega\cdot 1.0}$ into the x_1' integral, becomes

$$\varphi_{1_W}(1,y_1,z_1) = \frac{1}{4\pi}\int_{-y_t}^{+y_t}\Delta\varphi_{1_t}(y_1')\,dy_1' \int_{1}^{\infty} e^{-i\omega(x_1'-1)}\frac{\partial\psi}{\partial z_1'}(1-x_1',y_1-y_1',z_1-z_1')\,dx_1' \tag{B2}$$

Let I_W be the inner, x_1', integral

$$I_W = \int_{1}^{\infty} e^{-i\omega(x_1'-1)}\,\frac{\partial\psi}{\partial z_1'}(1-x_1',y_1-y_1',z_1-z_1)\,dx_1' \tag{B3}$$

setting $\rho = x_1' - 1$ and inserting the expression for ψ from equation (A18)

$$I_W = \int_{0}^{\infty} e^{-i\omega\rho}\frac{\partial}{\partial z_1'}\,\frac{e^{-i\lambda_1(R_1+M\rho)}}{R_1}\,d\rho \tag{B4}$$

with $R_1 = \sqrt{\rho^2 + R_0^2}$ and $R_0^2 = (y_1-y_1')^2 + (z_1-z_1')^2$

Taking the $\frac{\partial}{\partial z_1'}$ outside and combining the ρ exponentials, we obtain

$$I_W = \frac{\partial}{\partial z_1'}\int_{0}^{\infty}\frac{e^{-i\frac{\lambda_1}{M}\left[MR_1 + \frac{M(\omega+\lambda_1 M)}{\lambda_1}\rho\right]}}{R_1}\,d\rho \tag{B5}$$

or since

$$\frac{M(\omega+\lambda_1 M)}{\lambda_1} = \frac{M\left(\omega+\frac{\omega M^2}{1-M^2}\right)}{\omega M/(1-M^2)} = 1 \quad , \tag{B6}$$

$$I_w = \frac{\partial}{\partial z_1'} \int_0^\infty \frac{e^{-i\frac{\lambda_1}{M}(MR_1+\rho)}}{R_1} d\rho \tag{B7}$$

Next, let

$$u = \frac{MR_1+\rho}{\beta R_0} \tag{B8}$$

When

$$\rho = 0 \qquad u = \frac{MR_0}{\beta R_0} = \frac{M}{\beta} \quad , \tag{B9}$$

and as $\rho \to \infty \qquad u \to \infty$

Further

$$\sqrt{1+u^2} = \frac{1}{\beta R_0}\left[\beta^2 R_0^2 + M^2(\rho^2+R_0^2) + 2MR_1\rho + \rho^2\right]^{1/2} \tag{B10}$$

which becomes, using $\beta^2 = 1 - M^2$

$$\sqrt{1+u^2} = \frac{1}{\beta R_0}\left[R_0^2 + \rho^2 + 2MR_1\rho + M^2\rho^2\right]^{1/2} \tag{B11}$$

$$= \frac{1}{\beta R_0}\left[R_1^2 + 2MR_1\rho + M^2\rho^2\right]^{1/2} = \frac{R_1+M\rho}{\beta R_0}$$

and

$$\frac{du}{d\rho} = \frac{1}{\beta R_0}\left[M\rho/R_1 + 1\right] = \frac{1}{R_1}\cdot\frac{R_1+M\rho}{\beta R_0} = \frac{\sqrt{1+u^2}}{R_1} \tag{B12}$$

so

$$I_w = \frac{\partial}{\partial z_1'} \int_{M/\beta}^\infty \frac{e^{-i\frac{\lambda_1\beta R_0}{M}u}}{\sqrt{1+u^2}}\, du \tag{B13}$$

Now, let $u = \nu + M/\beta$ so that

$$I_w = \frac{\partial}{\partial z_1'} \int_0^\infty \frac{e^{-i\frac{\lambda_1 \beta R_0}{M}(\nu + M/\beta)}}{\sqrt{1 + (\nu + M/\beta)^2}} d\nu \tag{B14}$$

The singularities of the integrand are where

$$1 + (\nu + M/\beta)^2 = 0 \tag{B15}$$

or

$$\nu = -\frac{M}{\beta} \pm i$$

which is in the left half of the complex plane. Thus applying Cauchy's Theorem to the contour integral

$$I_{w_c} = \int_c \frac{e^{-i\frac{\lambda_1 \beta R_0}{M}(\nu + M/\beta)}}{\sqrt{1 + (\nu + M/\beta)^2}} d\nu \tag{B16}$$

where the contour is shown in the following sketch

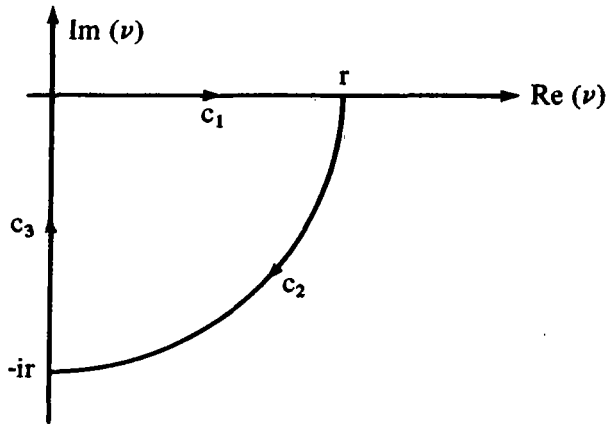

Then, $c = c_1 + c_2 + c_3$ and

$$I_{w_c} = I_{w_{c_1}} + I_{w_{c_2}} + I_{w_{c_3}} = 0 \tag{B17}$$

and

$$I_w = \lim_{r \to \infty} \frac{\partial}{\partial z_1'} I_{c_1} = \lim_{r \to \infty} \left[-\frac{\partial}{\partial z_1'} I_{c_2} - \frac{\partial}{\partial z_1'} I_{c_3} \right] \tag{B18}$$

As $r \to \infty$, then integral $I_{w_{c_2}} \to 0$. On the contour c_2, $\nu = r e^{-i\theta}$, $0 \leq \theta \leq \pi/2$, and

$$I_{W_{C_2}} = \int_{C_2} \frac{e^{-i\lambda_1 \beta R_0 (\nu + M/\beta)/M}}{\sqrt{\left(1 + \frac{M}{\beta\nu}\right)^2 + 1/\nu^2}} \frac{d\nu}{\nu}$$

$$= -ie^{-i\lambda_1 R_0} \int_0^{\frac{\pi}{2}} e^{-i\frac{\lambda_1 \beta R_0}{M} r\cos\theta} \; e^{-i\frac{\lambda_1 \beta R_0}{M} r\sin\theta} \, d\theta + O(1/r)$$

Then as $\nu \to \infty$

$$\left| I_{W_{C_2}} \right| = \int_0^{\frac{\pi}{2}} e^{-\frac{\lambda_1 \beta R_0}{M} r\sin\theta} \, d\theta < \int_0^{\frac{\pi}{2}} e^{-\frac{2\lambda_1 \beta R_0}{\pi M} r\theta} \, d\theta$$

$$= -\frac{\pi M}{\lambda_1 \beta R_0} \left(e^{-\frac{\lambda_1 \beta R_0}{M} r} - 1 \right) \to 0$$

Thus, we have

$$I_W = -\lim_{r\to\infty} \frac{\partial}{\partial z_1'} I_{W_{C_3}} \tag{B19}$$

On C_3, $\nu = i\eta$ and $d\nu = id\eta$ so that

$$I_{W_{C_3}} = i \int_{-r}^{0} \frac{e^{-i\frac{\lambda_1 \beta R_0}{M}(i\eta + M/\beta)}}{\sqrt{1 + (i\eta + M/\beta)^2}} d\eta \tag{B20}$$

or letting $\eta \to -\eta$

$$I_{W_{C_3}} = i \int_0^{r} \frac{e^{-i\frac{\lambda_1 \beta R_0}{M}(M/\beta - i\eta)}}{\sqrt{1 + (M/\beta - i\eta)^2}} d\eta \tag{B21}$$

Thus

$$\frac{\partial I_{C_3}}{\partial z_1'} = i \int_0^{r} \frac{-i\frac{\lambda_1 \beta}{M}(M/\beta - i\eta) \; e^{-i\frac{\lambda_1 \beta R_0}{M}(M/\beta - i\eta)}}{\sqrt{1 + (M/\beta - i\eta)^2}} d\eta \cdot \frac{\partial R_0}{\partial z_1'} \tag{B22}$$

$$= \frac{\lambda_1 \beta}{M} \int_0^r \frac{(M/\beta - i\eta)\, e^{-i\frac{\lambda_1 \beta R_0}{M}(M/\beta - i\eta)}}{\sqrt{1 + (M/\beta - i\eta)^2}}\, d\eta \cdot \frac{\partial R_0}{\partial z_1'} \tag{B23}$$

$$= \frac{\lambda_1 \beta}{M} \left(\frac{\partial R_0}{\partial z_1'}\right) e^{-i\lambda_1 R_0} \int_0^r \frac{(M/\beta - i\eta)\, e^{-\lambda_1 \frac{\beta R_0}{M} \eta}}{\sqrt{1 + (M/\beta - i\eta)^2}}\, d\eta \tag{B24}$$

or, noting that $\frac{\partial R_0}{\partial z_1'} = \frac{z_1' - z_1}{R_0}$ and taking

the limit as $r \to \infty$, I_w may be written as

$$I_w = \frac{\lambda_1 \beta}{M} \frac{(z_1 - z_1')}{R_0} e^{-i\lambda_1 R_0} \overset{\Delta}{I_w} \tag{B25}$$

where

$$\overset{\Delta}{I_w} = \int_0^\infty \frac{(M/\beta - i\eta)\, e^{-\frac{\lambda_1 \beta R_0 \eta}{M}}}{\sqrt{1 + (M/\beta - i\eta)^2}}\, d\eta \tag{B26}$$

Integrating by parts with

$$u = e^{-\frac{\lambda_1 \beta R_0}{M} \eta} \quad \text{and} \quad dv = \frac{(M/\beta - i\eta)}{\sqrt{1 + (M/\beta - i\eta)^2}}\, d\eta \tag{B27}$$

so

$$du = -\frac{\lambda_1 \beta R_0}{M} e^{-\frac{\lambda_1 \beta R_0}{M} \eta} d\eta \quad \text{and} \quad v = i\sqrt{1 + (M/\beta - i\eta)^2} \tag{B28}$$

from which

$$\overset{\Delta}{I_W} = i\, e^{-\frac{\lambda_1 \beta R_0 \eta}{M}} \sqrt{1 + (M/\beta - i\eta)^2} \Big|_{\eta = 0}^{\infty}$$

$$+ i\frac{\lambda_1 \beta R_0}{M} \int_0^{\infty} \sqrt{1 + (M/\beta - i\eta)^2}\; e^{-\frac{\lambda_1 \beta R_0}{M}\eta}\, d\eta \qquad \text{(B29)}$$

$$= -\frac{i}{\beta} + i\frac{\lambda_1 \beta R_0}{M} \int_0^{\infty} \sqrt{1 + (M/\beta - i\eta)^2}\; e^{-\frac{\lambda_1 \beta R_0}{M}\eta}\, d\eta \qquad \text{(B30)}$$

Note that while integrating by parts increases the order of the integrand, it reduces the number of numerical integrations from 4 to 2.

Anticipating the ultimate use of Gauss-Laguerre Quadrature, the following transformation is made:

$$\tau = \frac{\lambda_1 \beta R_0}{M}\eta \quad , \text{or} \qquad \eta = \frac{M}{\lambda_1 \beta R_0}\tau$$

so that

$$\overset{\Delta}{I_W} = -\frac{i}{\beta} + i \int_0^{\infty} \sqrt{1 + \left(\frac{M}{\beta} - i\frac{M}{\lambda_1 \beta R_0}\tau\right)^2}\; e^{-\tau}\, d\tau \qquad \text{(B31)}$$

or

$$\overset{\Delta}{I_W} = \frac{i}{\beta}\left[-1 + \int_0^{\infty} \sqrt{\beta^2 + \left(M - i\frac{M}{\lambda_1 R_0}\tau\right)^2}\; e^{-\tau}\, d\tau\right], \qquad \text{(B32)}$$

where z_1' is taken to be 0 in the evaluation of R_0

Letting

$$f(\tau) \equiv \sqrt{\beta^2 + \left(M - i\frac{M}{\lambda_1 R_0}\tau\right)^2}$$

the integral in (B32) has the form

$$\int_0^{\infty} f(\tau)\, e^{-\tau}\, d\tau \qquad \text{(B33)}$$

This may be evaluated approximately as

$$\sum_{i=1}^{N} w_i\, f(\tau_i) \qquad \text{(B34)}$$

where w_i and τ_i are the weights and abcissas for Laguerre integration for a given N.

APPENDIX C

TIME-LIKE CHARACTERISTICS OF THE RELAXATION TECHNIQUE

Following Jameson (refs. 8 and 9), we study the convergence of the difference methods by considering the iteration numbers as a time-like variable. Thus the relation between consecutively iterated values at an arbitrary point ij is defined in terms of a time derivative by

$$\varphi_{1\,ij}^{(n-1)} = \varphi_{1\,ij}^{(n)} - \Delta t \cdot \frac{\partial}{\partial t}\left(\varphi_{1\,ij}^{(n)}\right) \tag{C1}$$

where the superscript denotes the number of the iterations.

C.1 COLUMN RELAXATION WITH INCREASING i

The difference equation for column relaxation at subsonic points with i increasing is given for two dimensions by modifying equation (A1); namely

$$\begin{aligned} &2c_i\, u_{i+1j}\left(\varphi_{1\,i+1j}^{(n-1)} - \varphi_{1\,ij}^{(s)}\right) - 2d_i u_{ij}\left(\varphi_{1\,ij}^{(s)} - \varphi_{1\,ij}^{(n)}\right) \\ &-\frac{2i\omega}{\epsilon}\left[c_{1\,i}\left(\varphi_{1\,i+1\,j}^{(n-1)} - \varphi_{1\,ij}^{(s)}\right) + d_{1\,i}\left(\varphi_{1\,ij}^{(s)} - \varphi_{1\,i-1j}^{(n)}\right)\right] \\ &+2a_j\left(\varphi_{1\,ij-1}^{(s)} - \varphi_{1\,ij}^{(s)}\right) - 2b_j\left(\varphi_{1\,ij}^{(s)} - \varphi_{1\,ij+1}^{(s)}\right) + q_{ij}\varphi_{1\,ij}^{(s)} = 0 \end{aligned} \tag{C2}$$

where the superscript s denotes the value obtained from the solution of the equations for the ith column and n and n-1 denote updated and non-updated values, respectively.

When we apply a relaxation parameter r, then we obtain a modified value of φ_1 according to the formula

$$\varphi_{1\,ij}^{(n)} = r\,\varphi_{1\,ij}^{(s)} + (1 - r)\,\varphi_{1\,ij}^{(n-1)}$$

Solving for $\varphi_{1\,ij}^{(s)}$

$$\varphi_{1\,ij}^{(s)} = \varphi_{1\,ij}^{(n)}/r - (1 - r)\,\varphi_{1\,ij}^{(n-1)}/r \tag{C3}$$

Finally, eliminating $\varphi_{1\,ij}^{(n-1)}$ by means of equation (C1) leads to

$$\varphi_{1\,ij}^{(s)} = \varphi_{1\,ij}^{(n)} - \frac{(r - 1)}{r}\Delta t \cdot \varphi_{1\,ij_t}^{(n)} \tag{C4}$$

To obtain the differential equation corresponding to the difference equation (C2), we introduce equations (C4) and (C1) into equation(C2) and take the limit as Δx and Δy go to zero. We have

$$(u_x \varphi_{1x})_x - \frac{2i\omega}{\epsilon}\varphi_{1x} + \varphi_{1yy} + q\varphi_1 - \Delta t \cdot \varphi_{1yy_t}\left(\frac{r-1}{r}\right) - \Delta t \cdot q\varphi_{1t}$$

$$+ \lim_{\substack{\Delta x \\ \Delta y}} \to 0 \left\{ -2c_i u_{i+1j}\, \Delta t \left[\varphi_{1\,i+1j_t}^{(n)} - \left(\frac{r-1}{r}\right)\varphi_{1\,ij_t}^{(n)} \right] + 2d_i u_{ij}\, \Delta t \left(\frac{r-1}{r}\right)\varphi_{1\,ij_t}^{(n)} \right. \tag{C5}$$

$$\left. + \frac{2i\omega}{\epsilon}\left[c_{1\,i}\left(\varphi_{1\,i+1j_t}^{(n)} - \left(\frac{r-1}{r}\right)\varphi_{1\,ij_t}^{(n)}\right) + d_{1\,i}\left(\frac{r-1}{r}\right)\varphi_{1\,ij_t}^{(n)} \right] \Delta t \right\} = 0$$

Now

$$c_i = \frac{1}{(x_{i+1} - x_{i-1})(x_{i+1} - x_i)} = \frac{1}{(\Delta x_1 + \Delta x_2)\Delta x_1}$$

$$d_i = \frac{1}{(x_{i+1} - x_{i-1})(x_i - x_{i-1})} = \frac{1}{(\Delta x_1 + \Delta x_2)\Delta x_2} \tag{C6}$$

Substituting equation (C6) into equation (C5), expanding u and φ_1 about the point ij, and then simplifying, yields

$$(u\varphi_{1x} - \frac{2i\omega}{\epsilon}\varphi_1)_x + \varphi_{1yy} + q\varphi_1 - 2u\,\frac{\Delta t}{\Delta x_1 + \Delta x_2}\varphi_{1xt}$$

$$-2\frac{u}{\Delta x_1}\left(\frac{\Delta t}{\Delta x_1 + \Delta x_2}\right)\left[\frac{1}{r} - \frac{(r-1)}{r}\left(\frac{\Delta x_1}{\Delta x_2}\right)\right]\varphi_{1t} \tag{C7}$$

$$+2\frac{i\omega}{\epsilon}\left(\frac{\Delta t}{\Delta x_1 + \Delta x_2}\right)\left[\frac{1}{r}\left(\frac{\Delta x_2}{\Delta x_1}\right) + \frac{(r-1)}{r}\frac{\Delta x_1}{\Delta x_2}\right]\varphi_{1t} + 0(\Delta t, \Delta x, \Delta y) = 0$$

Since the real part of the coefficient of φ_{1t} must be negative to produce damping, then we must have

$$\frac{1}{r} - \frac{(r-1)}{r}\left(\frac{\Delta x_1}{\Delta x_2}\right)$$

or

$$r < \frac{1 + \Delta x_1 / \Delta x_2}{\Delta x_1 / \Delta x_2}$$

In practice, values of r in excess of this limitation have worked successfully. For example, with a spacing factor of 1.4, $1 + \Delta x_2/\Delta x_1 = 1.71$ [illegible] whether the sweep direction is in the direction of increasing or decreasing mesh size [illegible] have successfully used values of r up to 1.9. At elliptic points, we overrelax and hence r is restricted to values between 1 and 2.

It was suggested that complex values of the overrelaxation parameter might be useful in speeding convergence and a few values were tried without success. We will investigate the effect of a complex value of r on the real part as the coefficient of the φ_{1t} which provides damping. In equation (C7), the coefficient of the first term becomes

$$-2u\alpha_2 \left[\frac{e^{-i\gamma}}{r} - \left(\frac{r-e^{-i\gamma}}{r}\right)\frac{\Delta x_1}{\Delta x_2}\right] \qquad = -2u\alpha_2 \left[\frac{e^{i\gamma}}{r} - \delta\left(\frac{r-e^{-i\gamma}}{r}\right)\right]$$

where $re^{i\gamma}$ is the complex relaxation factor. The real part of the coefficient provides the damping and must be negative.

$$\frac{(1+\delta)\cos\gamma - r}{r} > 0$$

We see that the imaginary component always reduces the amount of damping. Since generally

$$u/\Delta x_1 > \omega/\epsilon$$

the first φ_{1t} provides most of the damping. With a complex relaxation parameter, the term proportional to $2i\omega/\epsilon$ also may contribute to the damping. The coefficient from this term becomes

$$\frac{2i\omega\alpha_1}{\epsilon\delta}\left[\left(\frac{e^{-i\gamma}}{r}\right) + \delta^2\left(\frac{r-e^{-i\gamma}}{r}\right)\right]$$

The real part is seen to be

$$\frac{2\omega\alpha_1 (1-\delta_1^2)\sin\gamma}{\epsilon\delta r}$$

This term provides damping when

$$\delta < 1 \text{ for which } \gamma < 0$$

or when

$$\delta > 1 \text{ for which } \gamma \text{ must be } > 0$$

Since γ is a constant and δ takes on values both greater and less than 1, the effect of the imaginary component of the overrelaxation factor is to reduce damping; and hence no improvement in convergence can be expected from the use of complex values. The few runs made with complex relaxation factors support this conclusion.

For convenience, equation (C7) may be written

$$(u\varphi_{1x})_x - \frac{2i\omega}{\epsilon}\varphi_{1x} + \varphi_{1yy} + q\varphi_1 - 2u\alpha_1\varphi_{1xt} \qquad \text{(C8)}$$

$$-2u\alpha_2\varphi_{1t} + 2i\omega\alpha_3\varphi_{1t} = 0$$

where

$$\alpha_1 = \frac{\Delta t}{\Delta x_1 + \Delta x_2}$$

$$\alpha_2 = \frac{\alpha_1}{\Delta x_1}\left[\frac{1}{r} - \frac{(r-1)}{r}\frac{\Delta x_1}{\Delta x_2}\right]$$

$$\alpha_3 = \frac{\alpha_1}{\epsilon}\left[\left(\frac{\Delta x_2}{\Delta x_1}\right)\frac{1}{r} + \frac{(r-1)}{r}\frac{\Delta x_1}{\Delta x_2}\right]$$

Equation (C8) is hyperbolic in time and this is readily seen by eliminating the φ_{1xt} derivative by a new time variable

$$\tau = t + \alpha_1 x$$

This leads to

$$(u\varphi_{1x})_x - \frac{2i\omega}{\epsilon}\varphi_{1x} + \varphi_{1yy} + q\varphi_1 - u\alpha_1^2\varphi_{1\tau\tau}$$

$$-2(u\alpha_2 - i\omega\alpha_3)\varphi_{1\tau} = 0 \qquad \text{(C9)}$$

Since u is positive, the coefficients of $\varphi_{1\tau\tau}$ and $\varphi_{1\tau}$ have the correct signs for a damped wave equation.

We now consider hyperbolic points. When the local flow is supersonic, backward differences for the x derivatives are used to eliminate downstream influences. The difference equation from equation (A2) is given by

$$2c_{i-1}\,u_{ij}\left(\varphi_{1\,ij}^{(s)} - \varphi_{1\,i-1j}^{(n)}\right) - 2d_{i-1}\,u_{i-1j}\left(\varphi_{1\,i-1j}^{(n)} - \varphi_{1\,i-2j}^{(n)}\right)$$

$$-\frac{2i\omega}{\epsilon}\left[c_{2\,i}\left(\varphi_{1\,ij}^{(s)} - \varphi_{1\,i-1j}^{(n)}\right) - d_{1\,i-1}\left(\varphi_{1\,i-1j}^{(n)} - \varphi_{1\,i-2j}^{(n)}\right)\right] \qquad \text{(C10)}$$

$$+2a_j\left(\varphi_{1\,ij-1}^{(s)} - \varphi_{1\,ij}^{(s)}\right) - 2b_j\left(\varphi_{1\,ij}^{(s)} - \varphi_{1\,ij+1}^{(s)}\right) + q_{ij}\,\varphi_{1\,ij}^{(s)} = 0$$

Using equation (A3) for the definition of the coefficients and eliminating $\varphi_1^{(s)}$ by equation (C4) yields the following differential equation;

$$(u\varphi_{1x})_x - \frac{2i\omega}{\epsilon}\varphi_{1x} + \varphi_{1yy} + q\varphi_1$$

$$-2\left[u\frac{\Delta t}{\Delta x_1(\Delta x_1 + \Delta x_2)} - \frac{i\omega}{\epsilon}\Delta t\left(\frac{1}{\Delta x_1} + \frac{1}{\Delta x_1 + \Delta x_2}\right)\right]\left(\frac{r-1}{r}\right)\varphi_{1t} = 0 \qquad \text{(C11)}$$

where

$$\Delta x_1 = x_i - x_{i-1},\quad \Delta x_2 = x_{i-1} - x_{i-2}$$

This equation is of parabolic type. Since $u < 0$, we must have $r < 1$ to have damping. Thus, at hyperbolic points, we use an underrelaxation parameter.

Similar results are obtained for column relaxation with decreasing i (upstream). In place of equation (C8), we obtain

$$(u\varphi_{1x})_x - \frac{2i\omega}{\epsilon}\varphi_{1x} + \varphi_{1yy} + q\varphi_{1_t} + 2u\alpha_1\,\varphi_{1xt} \qquad (C12)$$
$$-2(u\alpha_4 - i\omega\alpha_5)\,\varphi_{1t} = 0$$

where

$$\alpha_4 = \frac{\alpha_1}{\Delta x_2}\left[\frac{1}{r} - \frac{r-1}{r}\frac{\Delta x_2}{\Delta x_1}\right]$$

$$\alpha_5 = \frac{\alpha_1}{\epsilon}\left[\left(\frac{\Delta x_1}{\Delta x_2}\right)\frac{1}{r} + \frac{r-1}{r}\cdot\frac{\Delta x_2}{\Delta x_1}\right]$$

The transformation $\tau = t - \alpha_1 x$ yields a hyperbolic equation of the same form as (C9). For supersonic points sweeping in the direction of decreasing i, the superscript (n) in equation (C10) is replaced by (n - 1). The time-dependent differential equation then in place of equation (C11) is:

$$(u\varphi_{1x})_x - \frac{2i\omega}{\epsilon}\varphi_{1x} + \varphi_{1yy} + q\varphi_1$$
$$+2u\left(\frac{\Delta t}{\Delta x_1(\Delta x_1 + \Delta x_2)}\right)\frac{\varphi_{1t}}{r} + \frac{2i\omega}{\epsilon}\Delta t\left(\frac{1}{\Delta x_1} + \frac{1}{\Delta x_1 + \Delta x_2}\right)\varphi_{1t} = 0 \qquad (C13)$$

Decreasing r serves to increase the damping in supersonic regions.

C.2 ROW RELAXATION

For the smaller frequencies, the use of row relaxation improves the rate of convergence. This may be attributed to the coarse mesh in the y direction. For row relaxation in the increasing j (or y) direction, equation (C2) for elliptic points takes the form

$$2c_i u_{i+1j}\left(\varphi_{1\,i+1j}^{(s)} - \varphi_{1\,ij}^{(s)}\right) - 2d_i u_{ij}\left(\varphi_{1\,ij}^{(s)} - \varphi_{1\,i-1j}^{(s)}\right)$$
$$-\frac{2i\omega}{\epsilon}\left[c_{1\,i}\left(\varphi_{1\,i+1j}^{(s)} - \varphi_{1\,ij}^{(s)}\right) + d_{1\,i}\left(\varphi_{1\,ij}^{(s)} - \varphi_{1\,i-1j}^{(s)}\right)\right] \qquad (C14)$$
$$+2a_j\left(\varphi_{1\,ij-1}^{(n)} - \varphi_{1\,ij}^{(s)}\right) - 2b_j\left(\varphi_{1\,ij}^{(s)} - \varphi_{1\,ij+1}^{(n-1)}\right) + q_{ij}\varphi_{1\,ij}^{(s)} = 0$$

Substituting equations (C1) and (C4) into equation (C14) and taking the limit as $\Delta y, \Delta x \to 0$ yields

$$(u\varphi_{1x})_x - 2\frac{i\omega}{\epsilon}\varphi_{1x} + \varphi_{1yy} + q\varphi_1$$
$$+\Delta t\left[2a_j - \left(\frac{2}{r}\right)(a_j + b_j)\right]\varphi_t - 2\left(\frac{\Delta t}{\Delta y_j}\right)\varphi_{1yt} = 0 \qquad (C15)$$

where a_j and b_j are defined in equation (A3) and $\Delta y_j = y_{j+1} - y_{j-1}$. Since the coefficient of $\varphi_{1\,t}$ must be negative, this would appear to limit the range of overrelaxation factor to

$$r < \frac{a_j + b_j}{a_j} = 1 + \frac{y_{j+1} - y_{j-1}}{y_j - y_{j-1}} < 2$$

The transformation

$$\tau = t + \left(\frac{\Delta t}{\Delta y_j}\right) y$$

yields the equation

$$(u\varphi_{1\,x})_x - 2\frac{i\omega}{\epsilon}\varphi_{1\,x} + \varphi_{1\,yy} + q\varphi_1 - \Delta t\left[2\frac{a_j + b_j}{r} - 2a_j\right]\varphi_{1_\tau}$$

$$-(\Delta t/\Delta y_j)^2\,\varphi_{1\,\tau\tau} = 0 \qquad \text{(C16)}$$

which is hyperbolic in τ.

For supersonic points, we write in place of equation (C10) for increasing j

$$2c_{i-1}\,u_{ij}\left(\varphi_{1\,ij}^{(s)} - \varphi_{1\,i-1j}^{(s)}\right) - 2d_{i-1}\,u_{i-1j}\left(\varphi_{1\,i-1j}^{(s)} - \varphi_{1\,i-2j}^{(s)}\right)$$

$$-2\frac{i\omega}{\epsilon}\left[c_{2\,i}\left(\varphi_{1\,ij}^{(s)} - \varphi_{1\,i-1j}^{(s)}\right) - d_{1\,i-1}\left(\varphi_{1\,i-1j}^{(s)} - \varphi_{1\,i-2j}^{(s)}\right)\right] \qquad \text{(C17)}$$

$$+2a_j\left(\varphi_{1\,ij-1}^{(n)} - \varphi_{1\,ij}^{(s)}\right) - 2b_j\left(\varphi_{1\,ij}^{(n-1)} - \varphi_{1\,ij+1}^{(n-1)}\right) + q\,\varphi_{1\,ij}^{(s)} = 0$$

Substituting equations (C1) and (C4) into equation (C17) yields

$$(u\varphi_{1\,x})_x - \frac{2i\omega}{\epsilon}\varphi_{1\,x} + \varphi_{1\,yy} + q\varphi_1$$

$$+2a_j\left(\frac{r-1}{r}\right)\varphi_{1\,t}\,\Delta t - 2\left(\frac{\Delta t}{\Delta y_j}\right)\varphi_{1\,yt} = 0$$

Since $u < 0$, this equation is hyperbolic with respect to y since the coefficients of $\varphi_{1\,\tau\tau}$ and $\varphi_{1\,xx}$ terms will both be negative and opposite to that of $\varphi_{1\,yy}$. To render the x variable time-like, we write the equation in the form

$$(u\varphi_{1\,x})_x - \frac{2i\omega}{\epsilon}\varphi_{1\,x} + \varphi_{1\,yy} + q\varphi_1$$

$$-2\frac{\Delta t}{\Delta y_j}\left[\varphi_{1\,yt} + \beta_1\,\varphi_{1\,xt} + \beta_2\,\varphi_{1\,t}\right] = 0 \qquad \text{(C18)}$$

and determine β_1 and β_2 to eliminate the φ_{1xt}, φ_{1yt}, φ_{1t} terms and to obtain a coefficient of $\varphi_{1\tau\tau}$ with the correct sign. Choosing $\tau = t - \left(\frac{\Delta t}{\Delta y_j}\right) y + \alpha_1 x$ we find that

$$\beta_1\left(\frac{\Delta t}{\Delta y_j}\right) = u\alpha_1$$

$$\beta_2 = \frac{\beta_1 (u_x - 2i\omega/\epsilon)}{2u}$$

Substituting $\alpha_1 = \beta_1 \left(\frac{\Delta t}{\Delta y_j}/u\right)$ the relation for τ, we obtain the following differential equation equation for φ_1.

$$(u\varphi_{1x})_x - \frac{2i\omega}{\epsilon}\varphi_{1x} + \varphi_{1yy} + q\varphi_1 - \left(\frac{\Delta t}{\Delta y_j}\right)^2\left(\frac{\beta_1^2}{u} + 1\right)\varphi_{1\tau\tau} = 0$$

In order for the coefficient of the $\varphi_{1\tau\tau}$ term to be positive, we must have

$$\beta_1^2 > -u$$

$$\beta_1 > \sqrt{|u|} \qquad \text{(C20)}$$

In the light of equations (C17) through (C20), the differential equation to be differenced is

$$(u\varphi_{1x})_x - \frac{2i\omega}{\epsilon}\varphi_{1x} + \varphi_{1yy} + q\varphi_1$$

$$-2\frac{\Delta t}{\Delta y_j}\, c\, \sqrt{|u|}\, \left[\varphi_{1xt} + \frac{(u_x - 2i\omega/\epsilon)}{2u}\varphi_{1t}\right] \qquad \text{(C21)}$$

$$-2a_j\left(\frac{r-1}{r}\right)\Delta t\,\varphi_{1t} = 0$$

where c is a constant > 1. The difference relations for φ_{1xt} and φ_{1t} are seen to be

$$\Delta t \cdot \varphi_{1t} = \varphi_{1\,ij}^{(n)} - \varphi_{1\,ij}^{(n-1)}$$

$$\Delta t \cdot \varphi_{1xt} = c_{2\,i}\left(\varphi_{1\,ij}^{(n)} - \varphi_{1\,ij}^{(n-1)} - \varphi_{1\,i-1j}^{(n)} + \varphi_{1\,i-1j}^{(n-1)}\right) \qquad \text{(C22)}$$

$$-d_{1\,i-1}\left(\varphi_{1\,i-1j}^{(n)} - \varphi_{1\,i-1j}^{(n-1)} - \varphi_{1\,i-2j}^{(n)} + \varphi_{1\,i-2j}^{(n-1)}\right)$$

The addition of the time-like differences caused the relaxation method for mixed flows to converge, whereas the difference equation (C17) caused the iteration to diverge.

APPENDIX D

MATRIX ANALYSIS OF RELAXATION TECHNIQUES

As noted in the text, in the course of the solution of the unsteady transonic problem using line relaxation (block successive overrelaxation, or BSOR), it was found that convergence was obtained only for relatively low values of ω, the reduced frequency. In this appendix, a derivation is given that provides the theoretical basis for this empirical observation. By simplification of the basic boundary value problem and use of a theorem on the convergence of relaxation procedures, the conditions are determined for which the system matrix ceases to be positive definite, and thus for which a necessary condition for convergence is violated. The condition is defined in terms of the dimensions of the solution region, the transonic similarity parameter K, the Mach number, and the reduced frequency. It is convenient to think in terms of a critical reduced frequency, ω_{cr}, below which the solution procedure converges and above which it diverges. As shown in section 2.2 the ω_{cr}, as derived here, corresponds very closely with those values encountered during the running of sample problems.

The two- and three-dimensional problems will be developed together. The mesh regions for a two-dimensional problem is a rectangle with sides of lenths a and c. The region for the three-dimensional problem is a rectangular parallelepiped with the additional spanwise dimension of b. In order to carry out the convergence analysis and obtain an analytic formula for ω_{cr}, we make the following simplifying assumptions:

- The steady-state perturbation potential, φ_0, is constant;
- The far-field boundary values are constant;
- The airfoil and wake boundary conditions are omitted;
- The mesh spacings resulting from the discretization are uniform in each of the coordinate directions;
- The relaxation factor is the same for all points and for each iteration.

These assumptions, particularly the third, are rather strong; nevertheless, analysis of the problem resulting from these simplifications is found to yield results in generally good qualitative and quantitative agreement with experimental observations, indicating that the essential frequency-limiting characteristics of the problem have been retained.

In mathematical terms, the effect of the assumptions is to reduce the problem to the solution of

$$K\varphi_{1\,xx} + \varphi_{1\,yy} - \frac{2i\omega}{\epsilon}\varphi_{1_x} + \frac{\omega^2}{\epsilon}\varphi_1 = 0 \tag{D1}$$

over a rectangle (or the analogous differential equation and region in three dimensions) with Dirichlet boundary conditions, and it is this problem to which we apply the convergence analysis.

Following the sections giving mathematical background and details of the region discretization, we give the analyses for both the exact problem above and a modified problem resulting from transformation of (D1). The rather complicated formula for ω_{cr} from the exact problem is seen to reduce to the much simpler formula for ω_{cr} from the modified problem as $h_x \to 0$.

D.1 MATHEMATICAL BACKGROUND

In this section we give a brief statement of various mathematical facts that will be required in the course of our analysis.

D.1.1 MATRIX FORMULATION OF BSOR

Our discussion is a specialization of that given in Varga (ref. 16), and the convergence theorem we state is an immediate consequence of the one given there.

Let an n x n Hermitian matrix A be partitioned for some N, into the form

$$A = \begin{bmatrix} A_{11} & A_{22} & \cdot & \cdot & \cdot & A_{1N} \\ A_{21} & A_{22} & \cdot & \cdot & \cdot & A_{2N} \\ \cdot & \cdot & \cdot & \cdot & \cdot & \cdot \\ \cdot & \cdot & \cdot & \cdot & \cdot & \cdot \\ \cdot & \cdot & \cdot & \cdot & \cdot & \cdot \\ A_{N1} & A_{N2} & \cdot & \cdot & \cdot & A_{NN} \end{bmatrix} \qquad \text{(D2)}$$

where the diagonal blocks A_{ii}, i = 1, . . ., N are square and nonvoid. Then defining the n x n matrices D and F by

$$D = \begin{bmatrix} A_{11} & & & & \\ & A_{22} & & \bigcirc & \\ & & \cdot & & \\ & \bigcirc & & \cdot & \\ & & & & A_{NN} \end{bmatrix}, \qquad F = -\begin{bmatrix} O & O & \cdot & \cdot & \cdot & O \\ A_{21} & O & \cdot & \cdot & \cdot & O \\ A_{31} & A_{32} & O & \cdot & \cdot & O \\ \cdot & \cdot & & \cdot & \cdot & \cdot \\ \cdot & \cdot & & \cdot & \cdot & \cdot \\ A_{N1} & A_{N2} & & \cdot & A_{NN-1} & O \end{bmatrix} \qquad \text{(D3)}$$

and with F* as the complex conjugate of F, so that A = D -F -F*, then BSOR applied to $A\bar{\varphi} = \bar{R}$, where $\bar{\varphi}$ and $\bar{R}$ are n dimensional vectors, may be written

$$(D - rF)\,\bar{\varphi}_1^{(m+1)} = \{rF^* + (1 - r)D\}\,\bar{\varphi}_1^{(m)} + r\bar{R} \qquad \text{(D4)}$$

m = 0, 1, . . ., where r is the overrelaxation factor. The following theorem gives necessary and sufficient conditions for convergence of the above iteration.

Theorem 1.—If D is positive definite and $0 < r < 2$, then the given iteration is convergent for all starting vectors $\bar{\varphi}_1^{(0)}$ if, and only if, A is positive definite.

Comments: 1) An implication of the theorem is that under the given conditions the eigenvalues of the iteration matrix

$$(D - rF)^{-1}\,\{rF^* + (1 - r)D\}$$

will all be less than 1 in modulus, a well-known necessary and sufficient condition for convergence; and 2) the statement "*all* . . . $\varphi_1^{(0)}$" does not limit the applicability of the theorem. In any practical problem a stationary iteration such as (D4) must converge for every choice of starting vector to be of use.

D.1.2 EIGENVALUES OF A CERTAIN TRIDIAGONAL MATRIX

The eigenvalues of the tridiagonal matrix

$$\begin{bmatrix} a & b & & & & \\ c & a & b & & & \\ & \ddots & \ddots & \ddots & & \\ & & \ddots & \ddots & \ddots & \\ & & & c & a & b \\ & & & & c & a \end{bmatrix} \qquad \text{(order n)}$$

are given in Bellman (ref. 17) by

$$\lambda_\ell = a - 2\sqrt{bc}\,\cos\frac{\ell\pi}{n+1}, \qquad \ell = 1, \ldots, n. \tag{D5}$$

D.1.3 KRONECKER (TENSOR) PRODUCT

From Bellman (ref. 17) we have the following:

Definition.—Let A be an N_1 dimensional matrix and B an N_2 dimensional matrix. The Kronecker product of A and B, written $A \otimes B$, is the $N_1 \cdot N_2$ dimensional matrix given by

and

$$\begin{bmatrix} a_{11}B & a_{12}B & \cdots & a_{1N_1}B \\ a_{21}B & a_{22}B & \cdots & a_{2N_1}B \\ \vdots & \vdots & \ddots & \vdots \\ a_{N_1 1}B & a_{N_1 2}B & \cdots & a_{N_1 N_1}B \end{bmatrix}$$

Theorem 2.—Let λ_ℓ, $\ell = 1, \ldots, N_1$ be the eigenvalues of an order N_1 matrix A, and let μ_j, $j = 1, \ldots, N_2$ be the eigenvalues of an order N_2 matrix B. Then the eigenvalues of the $N_1 \cdot N_2$ order matrix

$$(I_{N_2} \otimes A) + (B \otimes I_{N_1})$$

where I denotes the identity matrix of the given order, are given by

$$\lambda_\ell + \mu_j \quad \text{for } \ell = 1, \ldots, N_1 \text{ and } j = 1, \ldots, N_2.$$

Comment: If B is tridiagonal, then the matrix $(I_{N_2} \otimes A) + (B \otimes I_{N_1})$ is easily seen to be block tridiagonal, which is the case we will encounter.

D.2 REGION DISCRETIZATION AND MESH POINT ORDERING

D.2.1 TWO DIMENSIONS

In two dimensions the region is a rectangle in the x-y plane with sides of lengths a and c in the x and y directions, respectively. Taking the lower left cornerpoint as (x_0, y_0) and choosing N_x and N_y as the number of mesh increments in the indicated directions, the totality of mesh points is given by (x_ℓ, y_j), where

$$x_\ell = x_0 + \ell h_x, \quad \ell = 0,1,\ldots, N_x,$$
$$y_j = y_0 + jh_y, \quad j = 0,1,\ldots, N_y, \tag{D6}$$
$$\text{with } h_x = a/N_x \text{ and } h_y = c/N_y.$$

Of these, points with $\ell = 0$ or N_x, or $j = 0$ or N_y, are *boundary* points; all other are *interior* points. Thus the

$$N_s = (N_x - 1)(N_y - 1)$$

interior points are given by equation (D6), but with the ranges of ℓ and j being 1 to $N_x - 1$ and 1 to $N_y - 1$, respectively.

Now to obtain a matrix formulation of the discretized problem, the interior points must be ordered as a one-dimensional array. To be definite, we choose column ordering, which is consistent with column relaxation of the resulting system. A similar analysis may be done for row ordering, which is consistent with row relaxation and leads to precisely the same formulas for ω_{cr}. The column ordering is specified by having the j index vary most rapidly and ℓ index least rapidly. That is, by the mapping:

$$(x_\ell, y_j) \rightarrow p_S, \text{ where } S = j + (\ell - 1)(N_y - 1) \tag{D7}$$

for

$$\ell = 1,\ldots, N_x - 1 \text{ and } j = 1,\ldots, N_y - 1.$$

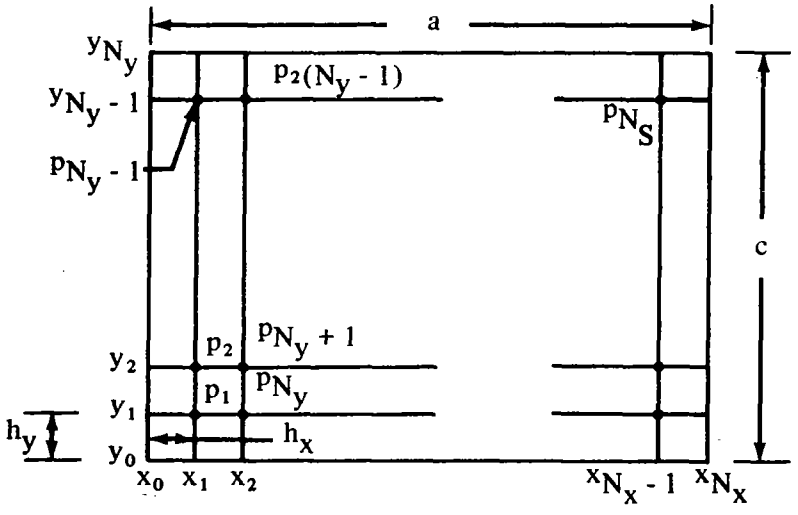

D.2.2 THREE DIMENSIONS

In three dimensions the region is a rectangular parallelepiped with sides of lengths a, b, and c in the x, y, and z directions, respectively. The discretization in the x and z directions is the same as that given by equation (D6). We will treat the y (spanwise) direction slightly differently since we have a symmetry condition in the x-z plane. In particular, taking $y_1 = 0$ and $y_{N_y} = b/2$, the totality of mesh points is given by (x_ℓ, y_j, z_k),

where

$$x_\ell = x_0 + \ell h_x, \quad \ell = 0,1, \ldots, N_x,$$

$$y_j = (j-1)h_y, \quad j = 0,1, \ldots, N_y, \tag{D8}$$

and

$$z_k = z_0 + kh_z, \quad k = 0,1, \ldots, N_z,$$

with

$$h_x = a/N_x, \; h_y = b/2(N_y-1),$$

and

$$h_z = c/N_z.$$

Of these, points with $\ell = 0$ or N_x, $j = 0$ or N_y, or $k = 0$ or N_z are boundary points; all others are interior points. Thus the interior points are given by equation (D8) but with the ranges of ℓ, j, and k being 1 to N_x-1, 1 to N_y-1, and 1 to N_z-1, respectively.

The three-dimensional mesh point ordering is a direct extension of that used for two dimensions. That is, the interior mesh points are sequenced such that the k index varies most rapidly and j index least rapidly. Thus the ordering is given by the mapping

where

$$(x_\ell, y_j, z_k) \rightarrow p_S,$$

$$S = k + (\ell - 1)(N_z-1) + (j-1)(N_x-1)(N_z-1),$$

$$\text{for } \ell = 1, \ldots, N_x-1, \; j = 1, \ldots, N_y-1,$$

and

$$k = 1, \ldots, N_z-1.$$

D.3 DERIVATION AND ANALYSIS OF THE SYSTEM MATRIX

D.3.1 MODIFIED PROBLEM—HELMHOLTZ EQUATION

Since it will be most economical to derive the system matrix for the modified and exact problems at the same time, we first define what we call the modified problem. This consists of the given region and the differential equation obtained from equation (D1) or its three-dimensional analog by making the transformation

$$\varphi_1 \rightarrow \psi \; e^{i\omega x/\epsilon K}$$

When this is done we have the equation

$$K\psi_{xx} + \psi_{yy} + \frac{\omega^2}{\epsilon(1-M^2)}\psi = 0 \qquad \text{(D10)}$$

in two dimensions and the equation

$$K\psi_{xx} + \psi_{yy} + \psi_{zz} + \frac{\omega^2}{\epsilon(1-M^2)}\psi = 0 \qquad \text{(D11)}$$

in three dimensions. We observe that the first derivative term is absent in these equations—a consequence of, and the motivation for, the given transformation. Further, we observe that except for the K coefficient, which may easily be removed by scaling, (D10) and (D11) are the two- and three-dimensional versions, respectively, of the well-known Helmholtz (or reduced wave) equation. Thus the modified problem is directly analogous to the mathematical formulation of the problem of a finite elastic membrane whose amplitude is assumed to vary sinusoidally in time.

D.3.2 TWO-DIMENSIONAL ANALYSIS

Note that both equations (D1) and (D10) have the form

$$K\varphi_{xx} + \varphi_{yy} - 2ic_1\varphi_x + c_2\varphi = 0 \qquad \text{(D12)}$$

where $c_1 = \omega/\epsilon$, $c_2 = \omega^2/\epsilon$ for equation (D1)

and $c_1 = 0$, $c_2 = \dfrac{\omega^2}{\epsilon(1-M^2)}$ for equation (D10)

From this fact it follows that the system matrices from the discretizations of (D1) and (D10) have the same form, which we now derive.

At each of the N_S interior points of the mesh given by equations (D6), we discretize (D12) by making the substitutions

$$\begin{aligned} K\varphi_{xx} &\rightarrow \left(\varphi_{\ell-1,j} - 2\varphi_{\ell,j} + \varphi_{\ell+1,j}\right)/\bar{h}_x^2 \\ \varphi_{yy} &\rightarrow \left(\varphi_{\ell,j-1} - 2\varphi_{\ell,j} + \varphi_{\ell,j+1}\right)/h_y^2 \\ \varphi_x &\rightarrow \left(\varphi_{\ell+1,j} - \varphi_{\ell-1,j}\right)/2h_x, \text{ and} \\ \varphi &\rightarrow \varphi_{\ell,j}\,, \end{aligned} \qquad \text{(D13)}$$

where $\bar{h}_x = h_x/\sqrt{K}$.

This yields the system of difference equations

$$-g_2\varphi_{\ell-1,j} - g_1\varphi_{\ell,j-1} + g_0\varphi_{\ell,j} - g_1\varphi_{\ell,j+1} - g_2^*\varphi_{\ell+1,j} = 0, \qquad \text{(D14)}$$

for $\ell = 1, \ldots, N_x-1$, and $j = 1, \ldots, N_y-1$, where

$g_0 = 2/\bar{h}_x^2 + 2/h_y^2 - c_2$, $g_1 = 1/h_y^2$

and $g_2 = 1/\bar{h}_x^2 + ic_1/h_x$. Here terms for which the first subscript becomes 0 or N_x, or the second becomes 0 or N_y, are transferred to the right-hand side.

Using the mapping given by equation (D7), equation (D14) may be written as

$$-g_2\varphi_{S-(N_y-1)} - g_1\varphi_{S-1} + g_0\varphi_S - g_1\varphi_{S+1} - g_2^*\varphi_{S+(N_y-1)} = 0, \tag{D15}$$

$S = 1,2, \ldots, N_S$, with terms being transferred to the right-hand side where appropriate.

Now since each subscript is linear in S with a coefficient of 1, it is clear that (D15) represents a five-diagonal system for the unknowns $\varphi_1, \ldots, \varphi_{N_S}$. Letting $\bar{\varphi}$ be a vector with these components, (D15) may be written in matrix notation as $A\bar{\varphi} = \bar{R}$, where $\bar{R}$ is the right-hand side vector and A is the N_S order system matrix given by

$$A = \begin{bmatrix} G_0 & G_1^* & & & \\ G_1 & G_0 & G_1^* & & \\ & \ddots & \ddots & \ddots & \\ & & G_1 & G_0 & G_1^* \\ & & & G_1 & G_0 \end{bmatrix} \tag{D16}$$

where

$$G_0 = \begin{bmatrix} g_0 & -g_1 & & & \\ -g_1 & g_0 & -g_1 & & \\ & \ddots & \ddots & \ddots & \\ & & -g_1 & g_0 & -g_1 \\ & & & -g_1 & g_0 \end{bmatrix} \quad \text{(order } N_y-1\text{)}, \tag{D17}$$

and

$$G_1 = -g_2 I_{N_y-1}.$$

Now we have the system matrix; it remains to apply theorem 1 to obtain an analytic form for ω_{cr}. First, we identify A as given by (D16) as a matrix of the form given by equation (D2) by making the identifications

$N = N_x-1$; $A_{ii} = G_0$, $i = 1, \ldots, N$;

$A_{i+1,\,i} = A^*_{i,\,i+1} = G_1$, $i = 1, \ldots, N-1$; and

$A_{ij} = 0$ otherwise

Next we check that D is positive definite. From the identification, we have that D as given in (D3) is

$$D = \text{diag}\,(G_0, G_0, \ldots, G_0).$$

Thus the eigenvalues of D are the same as those of G_0, which from (D17) and using (D5) are

$$g_0 - 2g_1 \cos\frac{\ell\pi}{N_y}, \ell = 1, \ldots, N_y - 1.$$

The minimum eigenvalue occurs when $\ell = 1$, so that the condition on D is satisfied if, and only if,

$$g_0 - 2g_1 \cos\frac{\pi}{N_y} > 0$$

or, using the definitions of g_0 and g_1, if, and only if,

$$\frac{2}{h_x^2} + \frac{2}{h_y^2}\left(1 - \cos\frac{\pi}{N_y}\right) > c_2 \qquad \text{(D18)}$$

where $c_2 = \frac{\omega^2}{\epsilon}$ for the exact problem and $c_2 = \frac{\omega^2}{\epsilon(1 - M^2)}$ for the transformed problem.

Condition (D18) will be satisfied, as will be apparent (eq. D19) since the frequency for which A ceases to be positive definite is substantially below that for which condition (D18) is violated.

The eigenvalues of A are easily found through the use of the Kronecker product. Noting first that A may be written as

$$\left(A = I_{N_x - 1} \otimes G_0\right) + \left(G_2 \otimes I_{N_y - 1}\right)$$

where

$$G_2 = \begin{bmatrix} \circ & -g_2^* & & & \\ -g_2 & \circ & -g_2^* & & \\ & \ddots & \ddots & \ddots & \\ & & \ddots & \ddots & \\ & & & -g_2 & \circ \end{bmatrix} \quad \text{(order } N_x - 1\text{)},$$

we have using equation (D5) and theorem 2 that the eigenvalues of A are given by

$$g_0 - 2g_1 \cos\frac{\ell\pi}{N_y} - 2\sqrt{g_2\, g_2^*}\cos\frac{j\pi}{N_x},$$

where

$$\ell = 1, \ldots, N_y - 1 \text{ and } j = 1, \ldots, N_x - 1.$$

The minimum eigenvalue occurs when $\ell = j = 1$ so that A is positive definite if, and only if,

$$g_0 - 2g_1 \cos\frac{\pi}{N_y} - 2\sqrt{g_2\, g_2^*}\cos\frac{\pi}{N_x} > 0,$$

or using the definitions of g_0, g_1 and g_2 if, and only if

$$\frac{2}{h_x^2}\left(1-\left[1+\frac{c_1^2 h_x^2}{K^2}\right]^{1/2}\cos\frac{\pi}{N_x}\right) + \frac{2}{Kh_y^2}\left(1-\cos\frac{\pi}{N_y}\right) > c_2/K. \tag{D19}$$

Now we consider the two cases corresponding to the two different choices for c_1 and c_2.

Case 1.—For the modified problem, $c_1 = 0$ and $c_2 = \dfrac{\omega^2}{\epsilon(1-M^2)}$ so that A is positive definite, and hence, by theorem 1, BSOR converges if, and only if,

$$\frac{2}{h_x^2}\left(1-\cos\frac{\pi}{N_x}\right) + \frac{2}{Kh_y^2}\left(1-\cos\frac{\pi}{N_y}\right) > \frac{\omega^2}{\epsilon K(1-M^2)}$$

or if, and only if, $\omega < \omega_{cr}$ where

$$\omega_{cr} = \frac{(1-M^2)}{M}\left[\frac{2}{h_x^2}\left(1-\cos\frac{\pi}{N_x}\right) + \frac{2}{Kh_y^2}\left(1-\cos\frac{\pi}{N_y}\right)\right]^{1/2} \tag{D20}$$

Equation (D20) gives the precise value for ω_{cr} in the transformed problem. A more transparent formula may be obtained by using the first two terms of each cosine series expansion and the relations $h_x N_x = a$, $h_y N_y = c$ so that to a very good approximation for reasonably large N_x and N_y.

$$\omega_{cr} = \pi\frac{(1-M^2)}{M}\left[\frac{1}{a^2} + \frac{1}{Kc^2}\right]^{1/2}. \tag{D21}$$

The dependence of ω_{cr} only on the absolute dimensions of the region and not on the mesh size is notable, and has been previously observed in another context by Molberg and Reynolds (ref. 18).

Note: In going from equation (D19) to equation (D20) we have used the relation

$$1/\epsilon K = M^2/(1-M^2) \tag{D22}$$

Case 2.—For the exact problem, $c_1 = \dfrac{\omega}{\epsilon}$ and $c_2 = \dfrac{\omega^2}{\epsilon}$, so that, making these substitutions in equation (D19), we have that BSOR converges if, and only if,

$$\frac{2}{h_x^2}\left(1-\left[1+\frac{\omega^2 h_x^2}{\epsilon^2 K^2}\right]^{1/2}\cos\frac{\pi}{N_x}\right) + \frac{2}{h_y^2}\left(1-\cos\frac{\pi}{N_y}\right) > \frac{\omega^2}{\epsilon K} \tag{D23}$$

We note that this inequality is satisfied for $\omega = 0$ and that as ω increases, the left-hand side is strictly decreasing while the right-hand side is strictly increasing, so that there is a unique value at which the inequality just fails, namely ω_{cr}.

An explicit formula for ω_{cr} may be derived from (D23). When the $>$ is replaced by an equal sign, (D23) may be transformed into a quadratic equation for ω_{cr}, which is easily solved.

When this is done it is found that the solution may be written as

$$\omega_{cr} = \frac{(1 - M^2)}{M}\sqrt{Q_1}\, Q_2 \qquad \text{(D24)}$$

where

$$Q_1 = \frac{2}{h_x^2}\left(1 - \cos\frac{\pi}{N_x}\right) + \frac{2}{Kh_y^2}\left(1 - \cos\frac{\pi}{N_y}\right)$$

and

$$Q_2 = \left[\frac{1 - M^2\, Q_3}{1 - M^2}\right]^{1/2}$$

with

$$Q_3 = \frac{2\cos(\pi/N_x)}{\left[1 - 2M^2\left(\sin\frac{\pi}{2N_x}\right)^2\right] + \left\{Q_1(1 - M^2)M^2\, h_x^2 + \left[1 - 2M^2\left(\sin\frac{\pi}{2N_x}\right)^2\right]^2\right\}^{1/2}}.$$

We observe that as $h_x \to 0$, $Q_3 \to 1$, so that $\omega_{cr} \to \frac{(1 - M^2)}{M^2}\sqrt{Q_1}$ which is the same as equation (D20), the result for the transformed equation.

D.3.3 THREE-DIMENSIONAL ANALYSIS

The three-dimensional analysis is a straightforward extension of that already done for two dimensions. First we note that the three-dimensional analog of equation (D1) is

$$K\varphi_{1xx} + \varphi_{1yy} + \varphi_{1zz} - \frac{2i\omega}{\epsilon}\varphi_{1x} + \frac{\omega^2}{\epsilon}\varphi_1 = 0, \qquad \text{(D25)}$$

so that both (D11) and (D25) have the form

$$K\varphi_{xx} + \varphi_{yy} + \varphi_{zz} - 2ic_1\varphi_x + c_2\varphi = 0, \qquad \text{(D26)}$$

where, as before

$c_1 = 0,\ c_2 = \omega^2/\epsilon(1 - M^2)$ for equation (D11) and

$c_1 = \omega/\epsilon,\ c_2 = \omega^2/\epsilon$ for equation (D26).

At each of the N_S *interior* points given by equation (D8) we discretize (D26) by making the substitutions

$$\begin{aligned} K\varphi_{xx} &\to \left(\varphi_{\ell-1,j,k} - 2\varphi_{\ell,j,k} + \varphi_{\ell+1,j,k}\right)/\bar{h}_x^2, \\ \varphi_{yy} &\to \left(\varphi_{\ell,j-1,k} - 2\varphi_{\ell,j,k} + \varphi_{\ell,j+1,k}\right)/h_y^2, \\ \varphi_{zz} &\to \left(\varphi_{\ell,j,k-1} - 2\varphi_{\ell,j,k} + \varphi_{\ell,j,k+1}\right)/h_z^2, \\ \varphi_x &\to \left(\varphi_{\ell+1,j,k} - \varphi_{\ell-1,j,k}\right)/2h_x, \text{ and} \\ \varphi &\to \varphi_{\ell,j,k}. \end{aligned} \tag{D27}$$

This yields the system of difference equations

$$\begin{aligned} &-g_3\varphi_{\ell,j-1,k} - g_2\varphi_{\ell-1,j,k} - g_1\varphi_{\ell,j,k-1} + g_0\varphi_{\ell,j,k} \\ &\qquad - g_1\varphi_{\ell,j,k+1} - g_2^*\varphi_{\ell+1,j,k} - g_3\varphi_{\ell,j+1,k} = 0 \end{aligned} \tag{D28}$$

for $\ell = 1, \ldots, N_x - 1$; $j = 1, \ldots, N_y - 1$; and $k = 1, \ldots, N_z - 1$, where g_2 is as before, while now

$$g_0 = \frac{2}{\bar{h}_x^2} + \frac{2}{h_y^2} + \frac{2}{h_z^2} - c_2, \; g_1 = \frac{1}{h_z^2}, \text{ and } g_3 = \frac{1}{h_y^2}.$$

Here terms for which the first subscript becomes 0 or N_x, or the second becomes N_y, or the third becomes 0 or N_z, are transferred to the right-hand side. The $\varphi_{\ell j-1k}$ term, for which the second subscript becomes 0, is handled according to the symmetry condition:

$$\varphi_{\ell,0,k} = \varphi_{\ell,2,k}$$

Using the mapping given by equation (D9) equation (D28) may be written

$$\begin{aligned} &-g_3\varphi_{S-N_2} - g_2\varphi_{S-N_1} - g_1\varphi_{S-1} + g_0\varphi_S \\ &\qquad - g_1\varphi_{S+1} - g_2^*\varphi_{S+N_1} - g_3\varphi_{S+N_2} = 0, \end{aligned} \tag{D29}$$

for $S = 1, \ldots, N_S$,

where $N_1 = N_z - 1$, and $N_2 = (N_x - 1)(N_z - 1)$.

Equation (D29) represents a seven-diagonal linear system, which may be written, as before, as $A\bar{\varphi} = \bar{R}$, where $\bar{R}$ is the right-hand-side vector and A is the N_S order matrix given by

$$A = \begin{bmatrix} G_4 & 2G_3 & & & & & \\ G_3 & G_4 & G_3 & & & \bigcirc & \\ & \ddots & \ddots & \ddots & & & \\ & & \ddots & \ddots & \ddots & & \\ & \bigcirc & & G_3 & G_4 & G_3 & \\ & & & & G_3 & G_4 & \end{bmatrix} \tag{D30}$$

where $G_3 = g_3 I_{N_2}$ and G_4 is the order N_2 matrix given by equations (D16) and (D17) with, however, the redefinition of g_0 for the present three-dimensional case.

We have the system matrix; now we apply theorem 1. With regard to the hypothesis, we observe that the modus operandi is still column relaxation, so that matrix D is still given by

$$D = \text{diag}\,(G_0, G_0, \ldots, G_0)$$

and thus, following the previous argument, D is positive definite if, and only if,

$$\frac{2}{h_x^2} + \frac{2}{h_y^2} + \frac{2}{h_z^2}\left(1 - \cos\frac{\pi}{N_z}\right) > c_2, \tag{D31}$$

which will hold for the frequencies of interest.

The eigenvalues of A may be found, as before, with the aid of the Kronecker product. We note that A may be written as

$$A = \left(I_{N_y-1} \otimes G_4\right) + \left(G_5 \otimes I_{N_2}\right)$$

where

$$G_5 = \begin{bmatrix} 0 & -2g_3 & & & \\ -g_3 & 0 & -g_3 & & 0 \\ & \ddots & \ddots & \ddots & \\ & & \ddots & \ddots & \\ 0 & & -g_3 & 0 & -g_3 \\ & & & -g_3 & 0 \end{bmatrix} \quad \text{(order } N_y\text{-1)}$$

Now the eigenvalues of G_5 are given by

$$-2g_3 \cos\frac{(j-\frac{1}{2})\pi}{N_y-1}, \quad j = 1,2,\ldots,N_y-1,$$

while those of G_4 are the same as those for the two-dimensional A, with g_0 redefined,

Thus, applying theorem 2, the eigenvalues of A are given by

$$g_0 - 2g_1 \cos\frac{k\pi}{N_z} - 2\sqrt{g_2 g_2^*}\cos\frac{\ell\pi}{N_x} - 2g_3 \cos\frac{(j-\frac{1}{2})\pi}{N_y-1}, \text{ for}$$

$$\ell = 1,\ldots,N_x-1;\ j = 1,\ldots,N_y-1;\ \text{and } k = 1,\ldots,N_z-1.$$

The minimum eigenvalue is clearly that for which $\ell = j = k = 1$. Thus using the definitions of g_0, g_1, g_2, and g_3, and applying theorem 1, we have that BSOR converges if, and only if,

$$\frac{2}{h_x^2}\left(1 - \left[1 + \frac{c_1^2 h_x^2}{K^2}\right]^{\frac{1}{2}} \cos\frac{\pi}{N_x}\right) + \frac{2}{Kh_y^2}\left(1 - \cos\frac{\pi}{2(N_y-1)}\right)$$

$$+ \frac{2}{Kh_z^2}\left(1 - \cos\frac{\pi}{N_z}\right) > c_2/K, \tag{D32}$$

which is the three-dimensional extension of equation (D19).

Specialization of equation (D32) for the two cases follows directly as before.

Case 1.—For the modified problem we have that BSOR converges if, and only if, $\omega < \omega_{cr}$ where

$$\omega_{cr} = \frac{(1 - M^2)}{M}\left[\frac{2}{h_x^2}\left(1 - \cos\frac{\pi}{N_x}\right) + \frac{2}{Kh_y^2}\left(1 - \cos\frac{\pi}{2(N_y-1)}\right)\right.$$

$$\left. + \frac{2}{Kh_z^2}\left(1 - \cos\frac{\pi}{N_z}\right)\right]^{1/2} \tag{D33}$$

or, for N_x, N_y, and N_z, reasonably large,

$$\omega_{cr} = \pi\,\frac{(1 - M^2)}{M}\left[\frac{1}{a^2} + \frac{1}{Kb^2} + \frac{1}{Kc^2}\right]^{1/2} \tag{D34}$$

Case 2.—For the exact problem we find, proceeding as in the two-dimensional case, that ω_{cr} is again given by equation (D24) with Q_2 and Q_3 defined as following that equation, but with Q_1 redefined as

$$Q_1 = \frac{2}{h_x^2}\left(1 - \cos\frac{\pi}{N_x}\right) + \frac{2}{Kh_y^2}\left(1 - \cos\frac{\pi}{2(N_y-1)}\right) + \frac{2}{Kh_z^2}\left(1 - \cos\frac{\pi}{N_z}\right). \tag{D35}$$

Thus, as before, the result for the exact problem reduces to that of the transformed problem as $h_x \to 0$.

D.3.4 SUMMARY

In summary, the predicted values for ω_{cr} resulting from the analysis of the simplified problem are given by equations (D21) (approximate) and (D24) (exact) for two dimensions, and by equations (D34) (approximate) and (D24) and (D35) (exact) for three dimensions.

APPENDIX E

VON NEUMANN STABILITY ANALYSIS

One way of investigating the stability of a differencing system is to study the propagation of errors through the mesh in the iteration process in a manner derived by Von Neuman (ref. 19). Let $E_{k\ell}$ be the error in $\varphi_{1\,k\ell}$ at the k, ℓ mesh point. Von Neuman assumed that these errors may be expressed in the form

$$E_{k\ell} = \sum_{p=-k_{max}}^{p=+k_{max}} \sum_{q=-\ell_{max}}^{q=+\ell_{max}} A_{pq}\, e^{2\pi i\left(kp\frac{\Delta x}{a} + \ell q\frac{\Delta y}{b}\right)} \tag{E1}$$

for a uniform mesh. Here a and b are x and y dimensions of the mesh. Since there are the same number of equations as unknowns, the system of equation (E1) is determinate. For simplicity, we shall assume a flat plate with a uniform mesh. Then $u_{ij} = K$ and the difference equation for the column relaxation sweeping in the direction of increasing i is

$$K\left(\varphi_{1\,i-1j}^{(n)} - 2\varphi_{1\,ij}^{(s)} + \varphi_{1\,i+1j}^{(n-1)}\right)/\Delta x^2 - \frac{i\omega}{\epsilon\Delta x}\left(\varphi_{1\,i+1j}^{(n-1)} - \varphi_{1\,i-1j}^{(n)}\right) \tag{E2}$$

$$+\left[\varphi_{1\,ij+1}^{(s)} - 2\varphi_{1\,ij}^{(s)} + \varphi_{1\,ij-1}^{(s)}\right]/\Delta y^2 + \frac{\omega^2}{\epsilon}\varphi_{1\,ij}^{(s)} = 0$$

Now

$$\varphi_{1\,ij}^{(s)} = \varphi_{1\,ij}^{(n)}/r - \left(\frac{1-r}{r}\right)\varphi_{1\,ij}^{(n-1)}$$

and we obtain

$$\begin{aligned} &K\left[\varphi_{1\,i-1j}^{(n)} - 2\varphi_{1\,ij}^{(n)}/r + 2\left(\frac{1-r}{r}\right)\varphi_{1\,ij}^{(n-1)} + \varphi_{1\,i+1j}^{(n-1)}\right]/\Delta x^2 \\ &- \frac{i\omega}{\epsilon\Delta x}\left(\varphi_{1\,i+1j}^{(n-1)} - \varphi_{1\,i-1j}^{(n)}\right) + \left[\varphi_{1\,ij+1}^{(n)} - 2\varphi_{1\,ij}^{(n)} + \varphi_{1\,ij-1}^{(n)}\right]/r\Delta y^2 \\ &- \frac{(1-r)}{r}\left(\varphi_{1\,ij+1}^{(n-1)} - 2\varphi_{1\,ij}^{(n-1)} + \varphi_{1\,ij-1}^{(n-1)}\right)/\Delta y^2 \\ &+ \frac{\omega^2}{\epsilon}\cdot\frac{\varphi_{1\,ij}^{(n)}}{r} - \frac{\omega^2}{\epsilon}\cdot\left(\frac{1-r}{r}\right)\varphi_{1\,ij}^{(n-1)} = 0 \end{aligned} \tag{E3}$$

Since the difference equation is linear, we may consider a single component of equation (E1) and find the solution of the difference equation in the form

$$\varphi_{ikl}^{(n)} = g^n e^{2\pi i \left(kp\frac{\Delta x}{a} + \ell q\frac{\Delta y}{b}\right)} \tag{E4}$$

This has the initial condition in the form of equation (E1). The iteration will converge if the magnitude of g is less than 1. Substituting equation (E4) into equation (E3) yields, after dividing out the common factor,

$$K\left[ge^{-i\theta} - \frac{2g}{r} + \frac{2(1-r)}{r} + e^{i\theta_1}\right]/\Delta x^2$$

$$-\frac{i\omega}{\epsilon\cdot\Delta x}\left(e^{i\theta_1} - ge^{-i\theta_1}\right) + 2g(\cos\theta_2 - 1)/r\cdot\Delta y^2 \tag{E5}$$

$$-\frac{2}{\Delta y^2}\left(\frac{1-r}{r}\right)(\cos\theta_2 - 1) + \frac{\omega^2 g}{\epsilon r} - \frac{\omega^2}{\epsilon}\left(\frac{1-r}{r}\right) = 0$$

where $\theta_1 = 2\pi p\frac{\Delta x}{a}$ and $\theta_2 = 2\pi q\frac{\Delta y}{c}$. Solving for g and simplifying, yields

$$g = \frac{-\overline{A} - \left(\frac{1-r}{r}\right)c}{A - c/r} \tag{E6}$$

where

$$A = a_1 + ib_1 = \left(\frac{K}{\Delta x^2} + \frac{i\omega}{\epsilon\cdot\Delta x}\right)e^{-i\theta_1}$$

$$C = \frac{2K}{\Delta x^2} + \frac{2(1-\cos\theta_2)}{\Delta y^2} - \frac{\omega^2}{\epsilon} \tag{E7}$$

The quantity C is always positive if $\frac{\omega^2}{\epsilon} < \frac{2K}{\Delta x^2}$. Since the magnitude of g must be less than one, we must have

$$\left[a_1 + \frac{1-r}{r}C\right]^2 + b_1^2 < \left(a_1 - \frac{1}{r}C\right)^2 + b^2$$

which simplifies to

$$\left(\frac{2-r}{r}\right)C\ \left(2a_1 - C\right) < 0$$

Since $\left(\frac{2-r}{r}\right)C > 0$ this leads to

$$2\left(\frac{K\cos\theta_1}{\Delta x^2}+\frac{\omega}{\epsilon\Delta x}\sin\theta_1\right)<\frac{2K}{\Delta x^2}+\frac{2(1-\cos\theta_2)}{\Delta y^2}-\frac{\omega^2}{\epsilon} \tag{E8}$$

Considering the preceding relation as a restriction on frequency, we express the inequality in the form

$$\omega^2+\frac{2\omega}{\Delta x}\sin\theta_1<2K\epsilon\left[\frac{1-\cos\theta_1}{\Delta x^2}+\frac{1-\cos\theta_2}{K\cdot\Delta y^2}\right] \tag{E9}$$

For p = q = 1 the limit $\Delta x, \Delta y \to 0$ yields

$$\omega^2+\frac{4\omega\pi}{a}<4K\epsilon\left(\frac{\pi^2}{a^2}+\frac{\pi^2}{Kc^2}\right)$$

or for M near the sonic value

$$\omega<\frac{1-M^2}{M^2}\pi\left(\frac{1}{a^2}+\frac{1}{Kc^2}\right)a \tag{E10}$$

since $\frac{1-M^2}{M^2}=K\epsilon<1$. Note that this limitation depends upon the outer dimensions of the mesh region and is similar to the result from the matrix method.

For now relaxation, with increasing j, we have

$$\begin{aligned}&K\left(\varphi_{1\,i-1j}^{(s)}-2\varphi_{1\,ij}^{(s)}+\varphi_{1\,i+1j}^{(s)}\right)/\Delta x^2-\frac{i\omega}{\epsilon\cdot\Delta x}\left(\varphi_{1\,i+1j}^{(s)}-\varphi_{1\,i-1j}^{(s)}\right)\\&+\left[\varphi_{1\,ij+1}^{(n-1)}-2\varphi_{1\,ij}^{(s)}+\varphi_{1\,ij-1}^{(n)}\right]/\Delta y^2+\frac{\omega^2}{\epsilon}\varphi_{1\,ij}^{(s)}=0\end{aligned} \tag{E11}$$

Eliminating $\varphi_1^{(s)}$

$$\begin{aligned}&K\left(\varphi_{1\,i-1j}^{(n)}-2\varphi_{1\,ij}^{(n)}+\varphi_{1\,i+1j}^{(n)}\right)/r\cdot\Delta x^2-\left(\frac{1-r}{r}\right)K\left(\varphi_{1\,i-1j}^{(n-1)}-2\varphi_{1\,ij}^{(n-1)}+\varphi_{1\,i+1j}^{(n-1)}\right)/\Delta x^2\\&-\frac{i\omega}{\epsilon\cdot\Delta x}\left[\left(\varphi_{1\,i+1j}^{(n)}-\varphi_{1\,i-1j}^{(n)}\right)/r-\left(\frac{1-r}{r}\right)\left(\varphi_{1\,i+1j}^{(n-1)}-\varphi_{1\,i-1j}^{(n-1)}\right)\right]\\&+\left[\varphi_{1\,ij+1}^{(n-1)}+2\left(\frac{1-r}{r}\right)\varphi_{1\,ij}^{(n-1)}-\left(\frac{2}{r}\right)\varphi_{1\,ij}^{(n)}+\varphi_{1\,ij-1}^{(n)}\right]/\Delta y^2\\&+\frac{\omega^2}{\epsilon}\left[\varphi_{1\,ij}^{(n)}/r-\left(\frac{1-r}{r}\right)\varphi_{1\,ij}^{(n-1)}\right]=0\end{aligned} \tag{E12}$$

Substituting equation (E4) into equation (E12) and simplifying, yields

$$2K\left[\frac{g}{r}-\left(\frac{1-r}{r}\right)\right](\cos\theta_1 - 1)/\Delta x^2 + \frac{2\omega}{\epsilon\cdot\Delta x}\cdot(\sin\theta_1)\left[\frac{g}{r}-\left(\frac{1-r}{r}\right)\right]$$

$$-\left[\frac{2g}{r}-2\left(\frac{1-r}{r}\right)-ge^{-i\theta_2}-e^{i\theta_2}\right]/\Delta y^2 \qquad \text{(E13)}$$

$$+\frac{\omega^2}{\epsilon}\left[\frac{g}{r}-\left(\frac{1-r}{r}\right)\right]=0$$

Solving for g yields

$$g=\frac{-e^{i\theta_2}/\Delta y^2 + \frac{1-r}{r}\left[\frac{\omega^2}{\epsilon}+\frac{2\omega}{\epsilon\cdot\Delta x}\sin\theta_1+\frac{2K(\cos\theta_1-1)}{\Delta x^2}-\frac{2}{\Delta y^2}\right]}{e^{-i\theta_2}/\Delta y^2 + \frac{1}{r}\left[\frac{\omega^2}{\epsilon}+\frac{2\omega}{\epsilon\cdot\Delta x}\sin\theta_1+\frac{2K(\cos\theta_1-1)}{\Delta x^2}-\frac{2}{\Delta y^2}\right]}=\frac{-\bar{A}-\frac{1-r}{r}C}{A-\frac{1}{r}C}$$

where

$$A=e^{-i\theta_2}/\Delta y^2;\ \bar{A}=e^{i\theta_2}/\Delta y^2;\ C=\frac{2}{\Delta y^2}+\frac{2K(1-\cos\theta_1)}{\Delta x^2}-\frac{\omega^2}{\epsilon}-\frac{2\omega}{\epsilon\cdot\Delta x}\sin\theta_1$$

The condition then $|g|<1$ becomes

$$2\cos\theta_2/\Delta y^2 < \frac{2}{\Delta y^2}+\frac{2K(1-\cos\theta_1)}{\Delta x^2}-\frac{\omega^2}{\epsilon}=\frac{2\omega}{\epsilon\cdot\Delta x}\sin\theta_1$$

or

$$\frac{\omega^2}{\epsilon}+\frac{2\omega}{\epsilon\cdot\Delta x}\sin\theta_1 < \frac{2K(1-\cos\theta_1)}{\Delta x^2}+\frac{2(1-\cos\theta_2)}{\Delta y^2},$$

which is the identical condition found for column relaxation.

Since complex values of ORF were tried, it is worthwhile to find the effect of complex r on the Von Neumann test for convergence. Equation (E6) for g becomes

$$g=\frac{-\bar{A}-\left(\frac{e^{-i\gamma}-r}{r}\right)C}{A-\frac{e^{-i\gamma}}{r}C}$$

and the condition that $|g|<1$ becomes

$$\left(a+\frac{\cos\gamma - r}{r}C\right)^2+\left(b+\frac{C\sin\gamma}{r}\right)^2<\left(a-\frac{\cos\gamma}{r}C\right)^2+\left(b+\frac{C\sin\gamma}{r}\right)^2$$

which simplifies to

$$\left(\frac{2\cos\gamma - r}{r}\right)C\ (2a - C)<0$$

For small frequencies, the same inequality (eq. E8) holds if

$$r<2\cos\gamma$$

Otherwise $|g|<1$ may hold for large values of frequency (for $r>2\cos\gamma$).

Oswatitsch and Singleton (ref. 20) replaced the actual time derivatives in the Euler equations of fluid flow with fictitious time derivatives to change the equations from hyperbolic in time to parabolic in order to improve the convergence rate for calculating steady flows. In the same manner, an artificial time derivative was added to the unsteady differential equation for harmonic motion and an ADI (alternating-direction-implicit) scheme was tried to solve the resulting equation. For the flat plate, the equation is

$$\frac{\partial\varphi_1}{\partial t}=K\varphi_{1xx}-\frac{2i\omega}{\epsilon}\varphi_{1x}+\varphi_{1xx}+\frac{\omega^2}{\epsilon}\varphi_1 \tag{E14}$$

The mesh was swept through by row relaxation and alternately by column relaxation. The appropriate difference equation for row relaxation in uniform mesh is given by

$$\begin{aligned}\mu\left(\varphi_{1ij}^{(n)}-\varphi_{1ij}^{(n-1)}\right)=K\left[\varphi_{1i+1j}^{(n)}-2\varphi_{1ij}^{(n)}+\varphi_{1i-1j}^{(n)}\right]/\Delta x^2\\ -\frac{i\omega}{\epsilon\cdot\Delta x}\left[\varphi_{1i+1j}^{(n)}-\varphi_{1i-1j}^{(n)}\right]\\ +\left[\varphi_{1ij+1}^{(n-1)}-2\varphi_{1ij}^{(n-1)}+\varphi_{1ij-1}^{(n-1)}\right]/\Delta y^2\\ +\frac{\omega^2}{\epsilon}\varphi_{1ij}^{(n)}=0\end{aligned} \tag{E15}$$

and for column relaxation

$$\mu\left(\varphi_{1\,ij}^{(n)} - \varphi_{1\,ij}^{(n-1)}\right) = K\left[\varphi_{1\,i+1j}^{(n-1)} - 2\varphi_{1\,ij}^{(n-1)} + \varphi_{1\,ij+1}^{(n-1)}\right]/\Delta x^2$$

$$- \frac{i\omega}{\epsilon \cdot \Delta x}\left[\varphi_{1\,i+1j}^{(n-1)} - \varphi_{1\,i-1j}^{(n-1)}\right] \qquad \text{(E16)}$$

$$+\left[\varphi_{1\,ij+1}^{(n)} - 2\varphi_{1\,ij}^{(n-1)} + \varphi_{1\,ij+1}^{(n)}\right]/\Delta y^2$$

$$+\frac{\omega^2}{\epsilon}\varphi_{1\,ij}^{(n)} = 0$$

Substituting equation (E4) into equation (E16) and simplifying, yields the following equation for g

$$g = \frac{\mu - 2K(1 - \cos\theta_1)/\Delta x^2 + \frac{2\omega}{\epsilon \cdot \Delta x}\sin\theta_1}{\mu + \frac{2(1 - \cos\theta_2)}{\Delta y^2} - \frac{\omega^2}{\epsilon}}$$

If $\mu > \omega^2/\epsilon_1$ then $g < 1$ requires

$$\frac{\omega^2}{\epsilon} + \frac{2\omega}{\epsilon \cdot \Delta x}\sin\theta_1 < \frac{2(1 - \cos\theta_2)}{\Delta y^2} + \frac{2K(1 - \cos\theta_1)}{\Delta x^2}$$

APPENDIX F

SOLUTION PROCEDURE INVESTIGATION EXAMPLES

F.1 SOLUTION PARAMETERS

F.1.1 RELAXATION FACTORS

The characteristics of the variation in solution convergence with relaxation factor magnitude are discussed in section 5.2.1. Some examples to illustrate these characteristics are included in this section.

Generally, the coarser the mesh, the longer the initial convergence slope lasted, and thus the smaller the optimum overrelaxation factor (ORF), as shown in figure F1. Also, for a given frequency, as Mach number increased, the initial slope decreased, as shown in figure F2. For a given Mach number, this slope decreased as the frequency increased. Generally, as the reduced frequency was increased, the ORF for most rapid convergence was reduced. As discussed later in this section, the size of the optimum ORF is also dependent on the relaxation procedure.

Also shown in figure F2 are two examples of the effect on the convergence rate when the ORF is decreased during an analysis. The change is particularly noticeable for the M = 0.80 curve when ORF is dropped to 1.4 from 1.85.

An example of the effect of the magnitude of the underrelaxation factor (URF) is given in figure F3, and consists of a NACA 64A006 airfoil in harmonic pitch at a Mach number of 0.9 and a reduced frequency of 0.06. The solution for the coarse, 25 x 20 grid converged relatively rapidly using an ORF = 1.6 and URF = 1.0. However, the solution for the finer 42 x 30 grid diverged for URF = 1.0, but converged rapidly for URF = 0.7. Variation of URF in similar calculations showed relatively little change in convergence rates as URF was varied between 0.7 and 0.3.

As an alternative to the overrelaxation factors used so far, the pilot program was rewritten to accept complex ORF's. Since there is little theoretical background for the use of complex relaxation factors, the procedure was to try several values to see what would happen. Here, only the real part of ORF was used in the calculation of ERROR. The results from using ORF's of 1.6 ±0.1i and 1.7 ±0.3i are shown in figures F4 and F5. Also included is the corresponding result for an all-real relaxation factor of 1.85, which appears to be optimum for this particular case. The ordinates for the figures are ERROR and the number of iterations. Although these calculations were not carried through to convergence, experience showed that the slope of this curve after it settled down (after some 30 or 40 iterations) was a valid indication of the rate convergence of the solution. Hence, an all-real ORF of 1.85 appeared to be distinctly more efficient than any of the complex factors. ORF's of 1.2 ±1.2i were also tried, but ERROR diverged almost immediately.

The alternative possibility of using different overrelaxation factors for the real and imaginary parts of the velocity potential was also examined. Figure F6 presents results for several

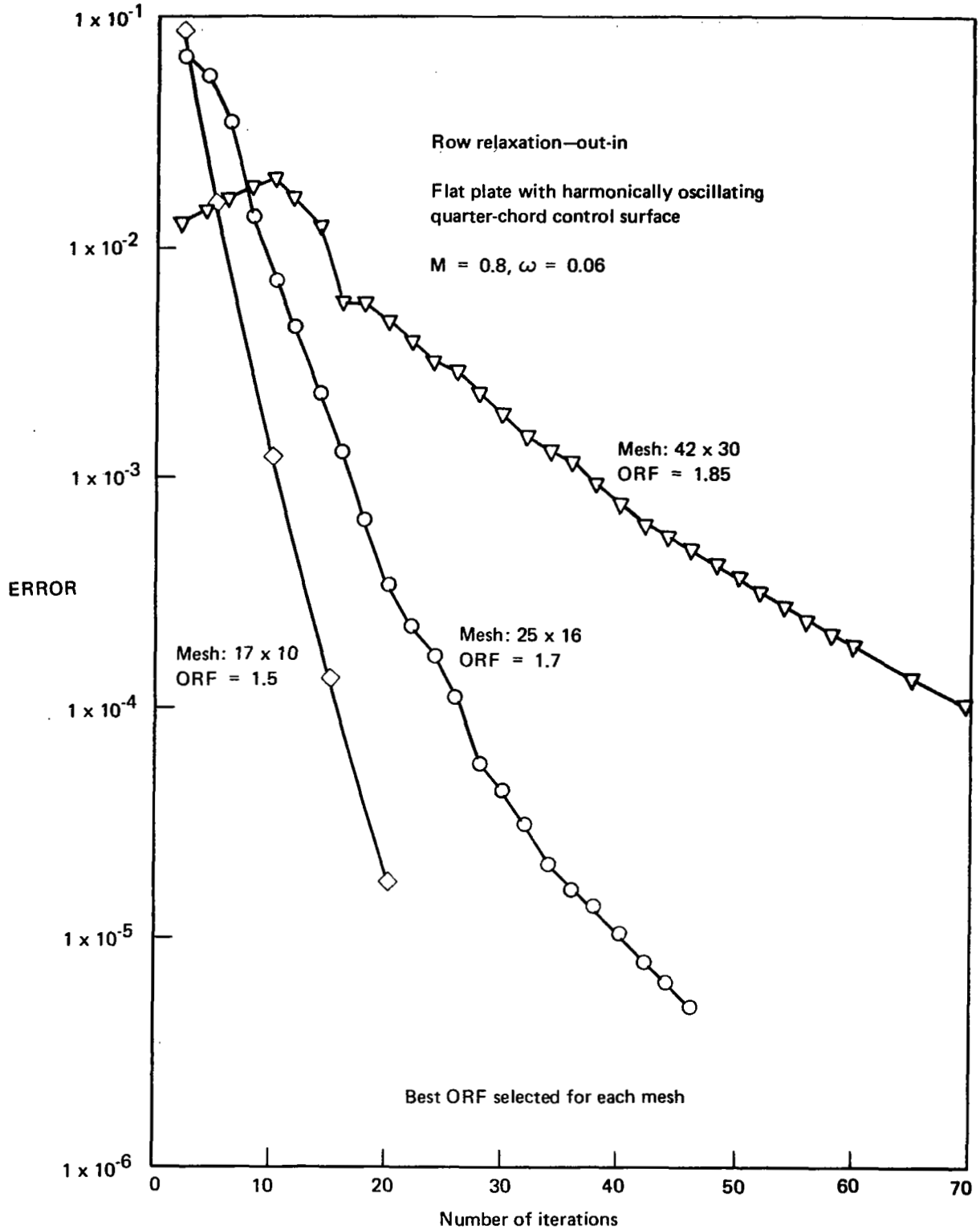

Figure F1. — Solution Convergence and Number of Points in Mesh

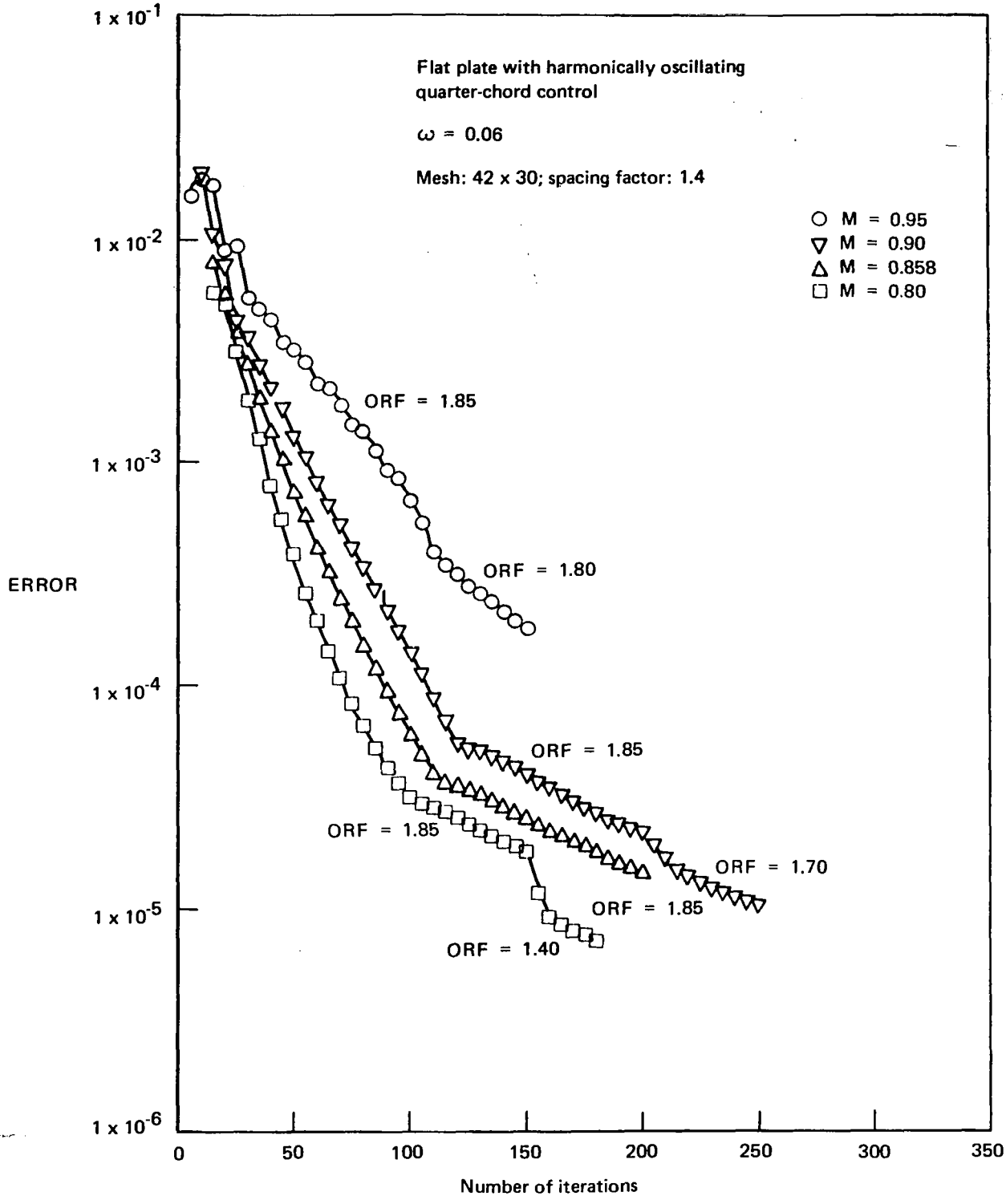

Figure F2— Variation of Solution Convergence With Mach Number

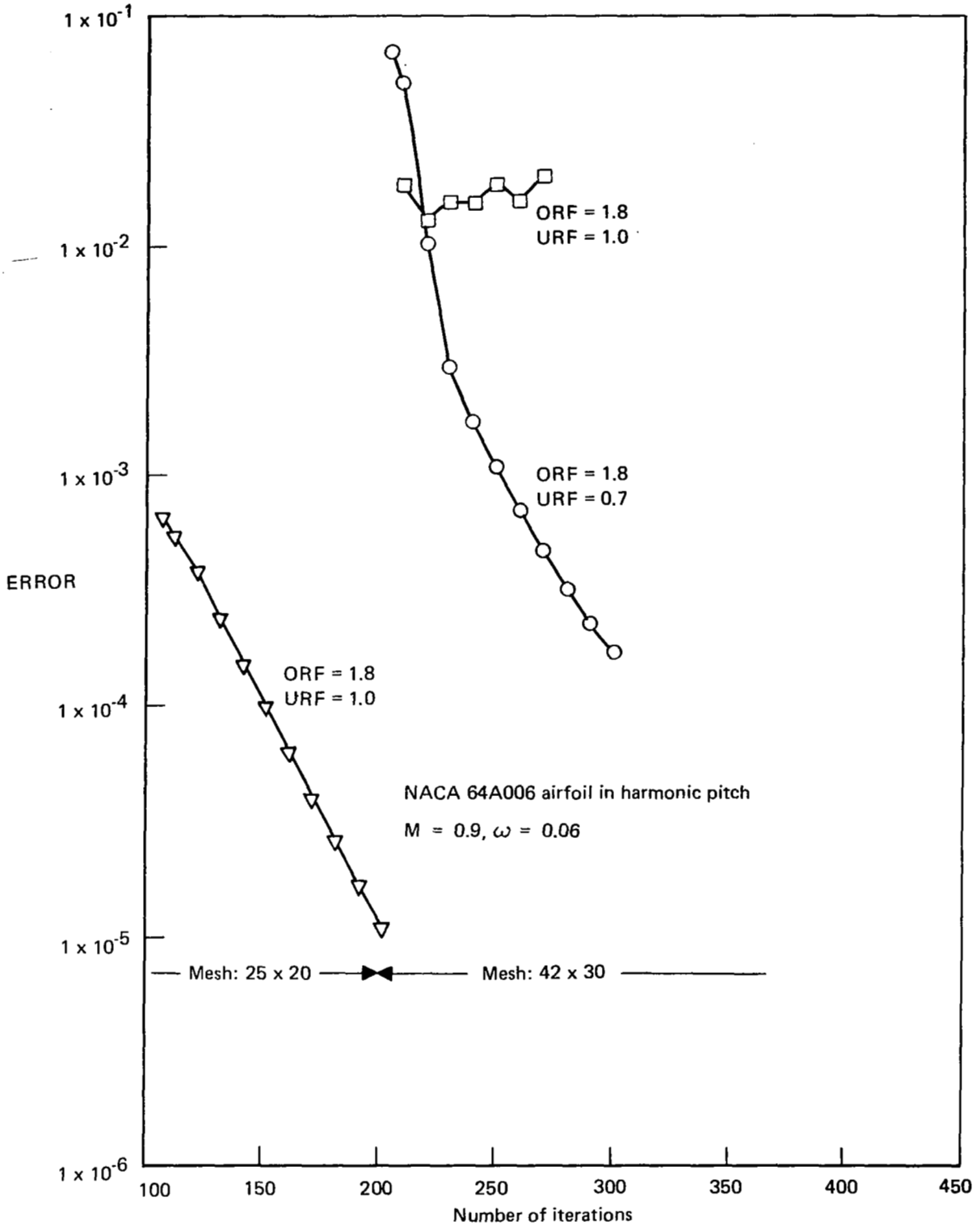

Figure F3. — Example of Effect of Underrelaxation Factor Variation on Solution Convergence

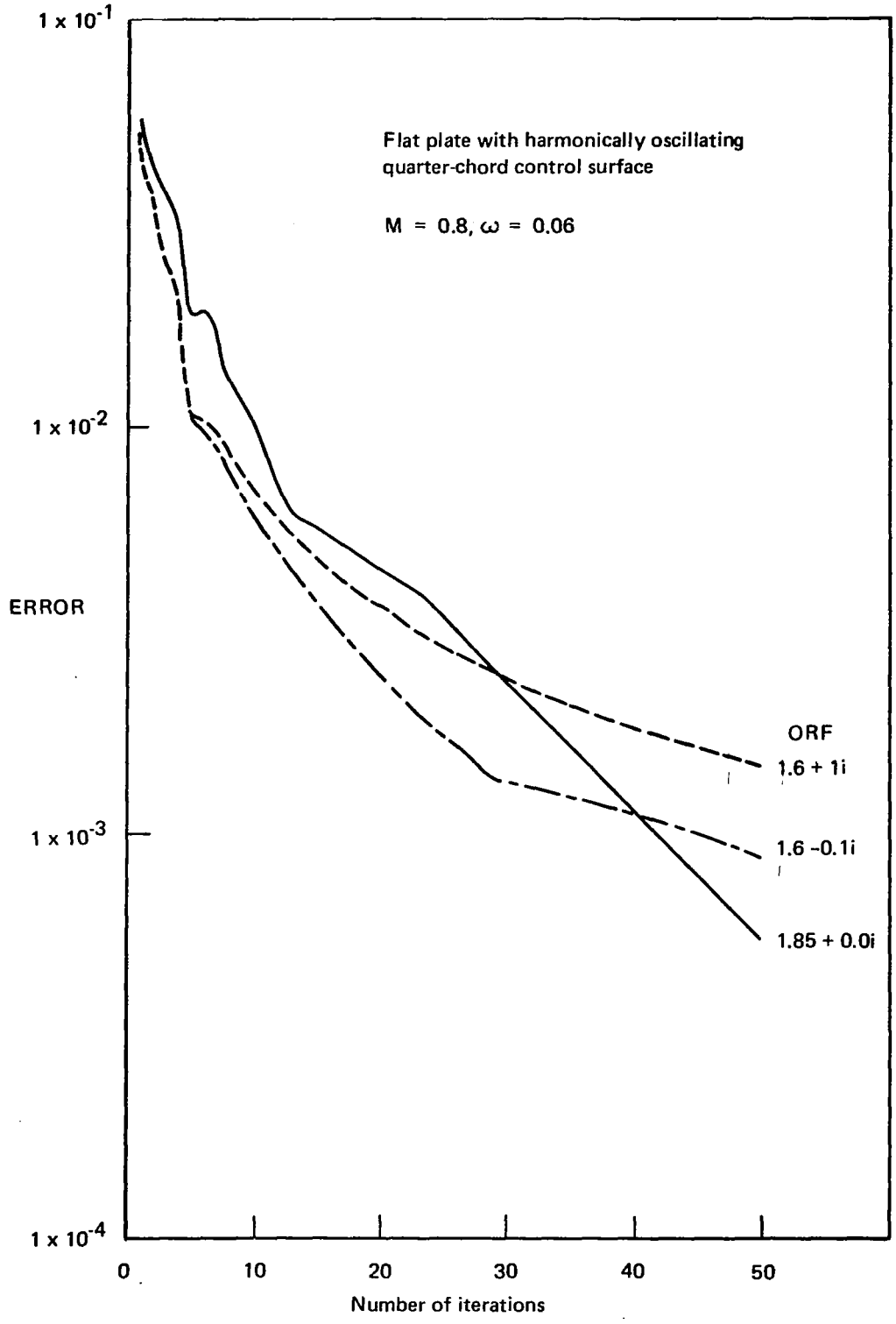

Figure F4. — Solution Convergence With Complex ORF's

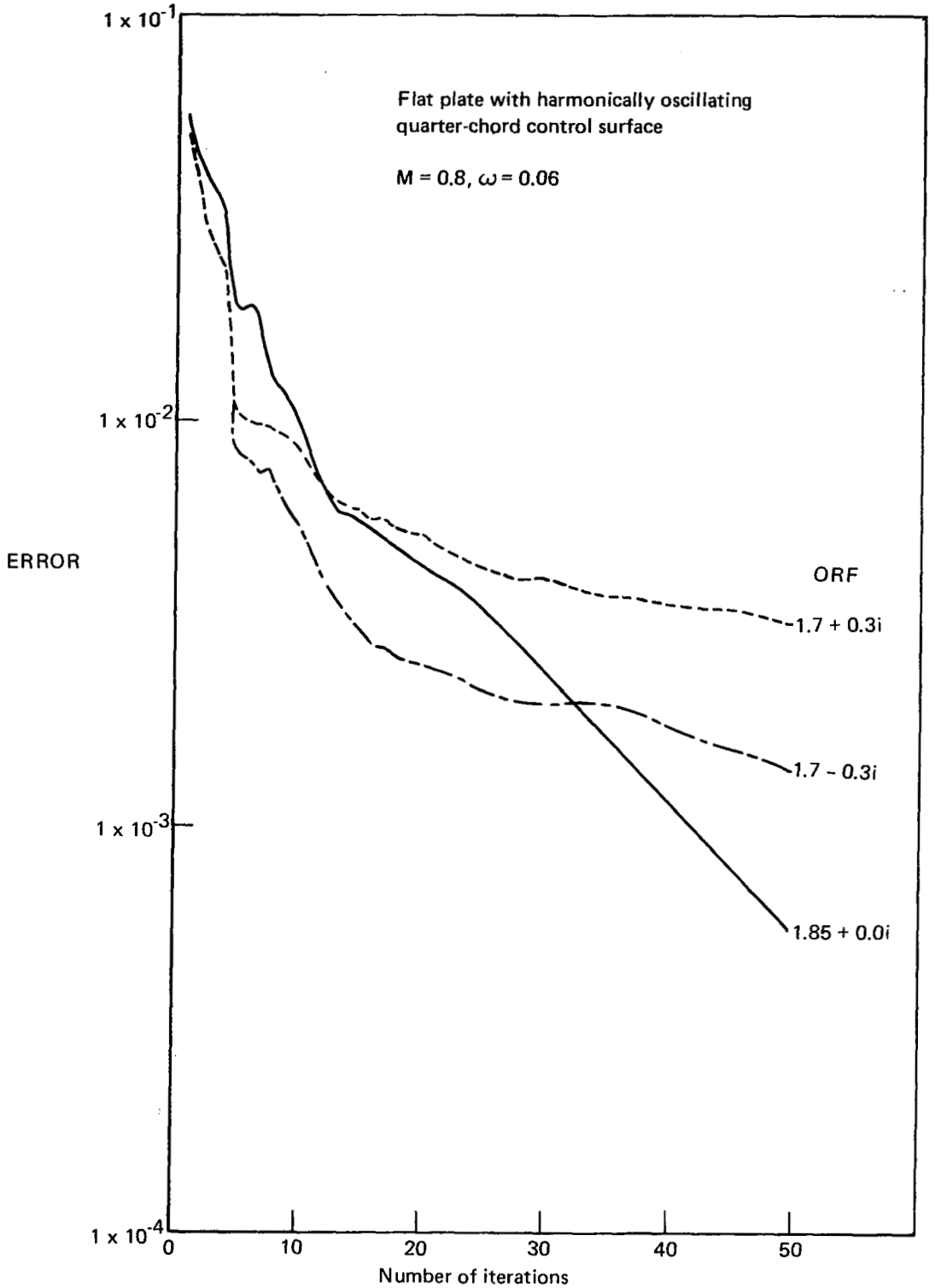

Figure F5. — Solution Convergence With Complex ORF's

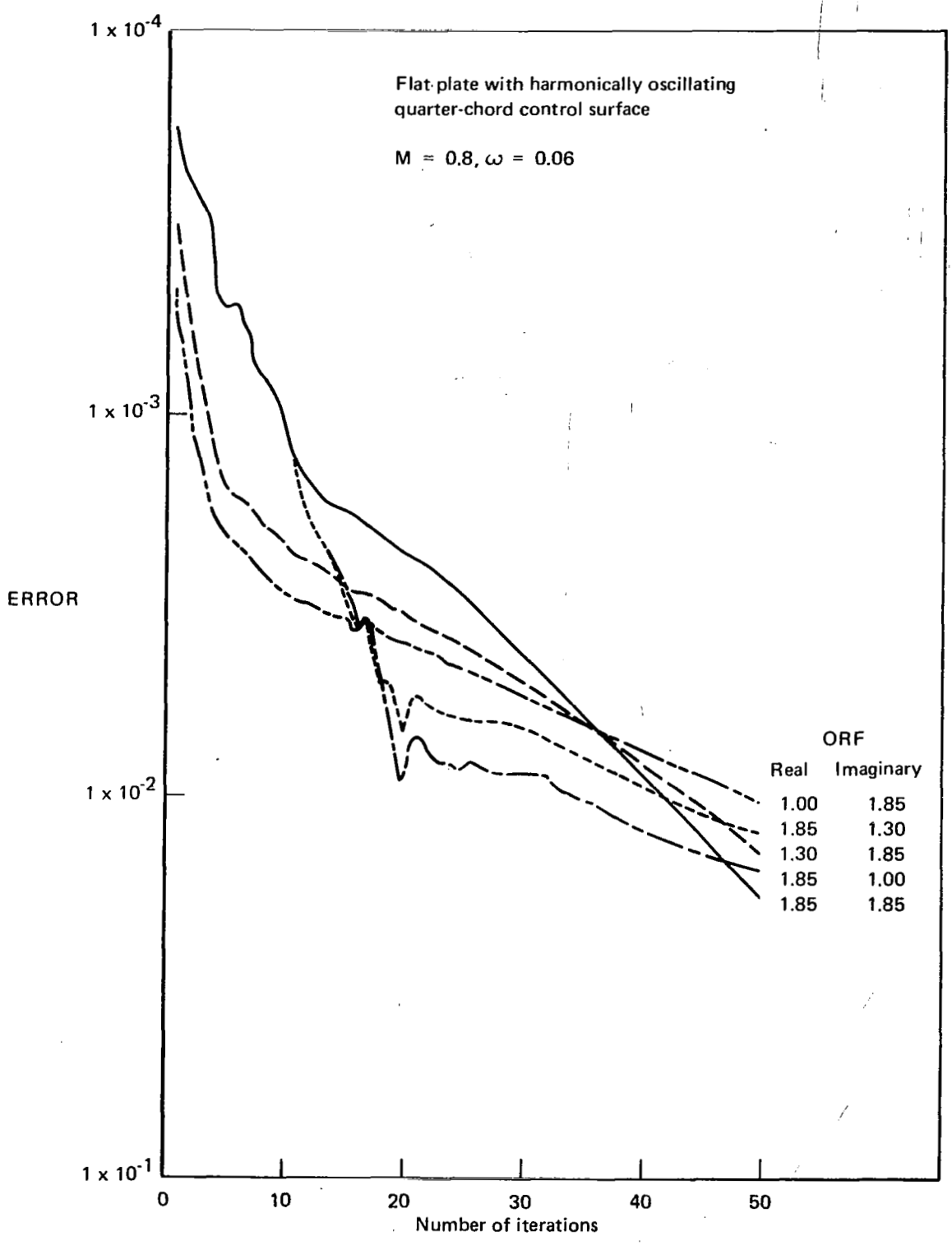

Figure F6. — Solution Convergence With Separate ORF's for Real and Imaginary Parts of the Velocity Potential

cases. The cases were run with ORF = 1.85 used for the real part and ORF = 1.3 and 1.0 for the imaginary part; then with ORF = 1.85 for the imaginary part and ORF 1.3 and 1.0 for the real part.

The most interesting result of this study is shown in figure F7, where the convergence of the real and imaginary parts of the ERROR were plotted separately versus number of iterations. The periodicity as well as the phasing of the real and imaginary parts of ERROR was unexpected and seemed to be significant. It perhaps helps to explain why convergence acceleration procedures such as those discussed in section 5.3.3. were unsuccessful. It would also seem to indicate that the complex ORF studies described above should be more successful.

Finally, reference is made to appendixes C and E in which analyses were made of the relaxation solutions using time-like characteristics and the Von Neumann stability analysis. In both cases the addition of an imaginary term to ORF decreased the damping and thus did not aid in solution convergence.

F.1.2 GRID DISTRIBUTION AND SPACING

In this section, examples are presented of pressure distributions in which there were variations in the spacing of adjacent finite difference intervals and in the number of points used to represent the flow field. The configuration used for these calculations was the flat plate with a Mach number of 0.8 and a reduced frequency of 0.06. As would be expected, in each case the representation of the singularities in the pressure distribution was improved by clustering the points about the singularities and by increasing the number of points.

A program was developed for calculating the mesh-point locations for an airfoil with a control surface. The points were spaced according to the rule that adjacent intervals are λ times the length of adjacent intervals with $2/3 < \lambda < 3/2$. The user specified the scale factor λ in each direction, the number of points over the wing surface (i.e., between $x = -1.0$ and x_a), and the number of points in the vertical direction. In the vertical direction, points were placed symmetrically about $y = 0$ (the vertical dimension in a two-dimensional coordinate system) with no point at $y = 0$. Moving away from the $y = 0$ plane, each interval was λ times the preceding interval, with the spacing set so as to put points on the upper and lower boundaries. The horizontal point spacing was more complicated, with points at the upstream and downstream boundaries, and a point over the trailing edge, $x = +1.0$. Then points were equally spaced on either side of the leading edge, $x = -1.0$, and the control surface hingeline, $x = x_a$. Also points over the wing (i.e., between $x = -1.0$ and $x = x_a$) were symmetrically spaced about $\frac{x_a - 1}{2}$. If λ's of close to 3/2 are used, the finite difference points are clustered about the flow singularities at the leading edge and the hingeline in the flow direction and about the airfoil in the vertical direction.

Examples of pressure distributions for several different mesh spacings are shown in figures F8 through F11. Throughout the example, the area of mesh grid was held fixed and the total number of points nearly constant. The pressure distributions for the flat plate with an oscillating quarter-chord control surface are shown in figures F8 and F9. Corresponding pressure distributions for the flat plate in pitch are shown in figures F10 and F11. In each

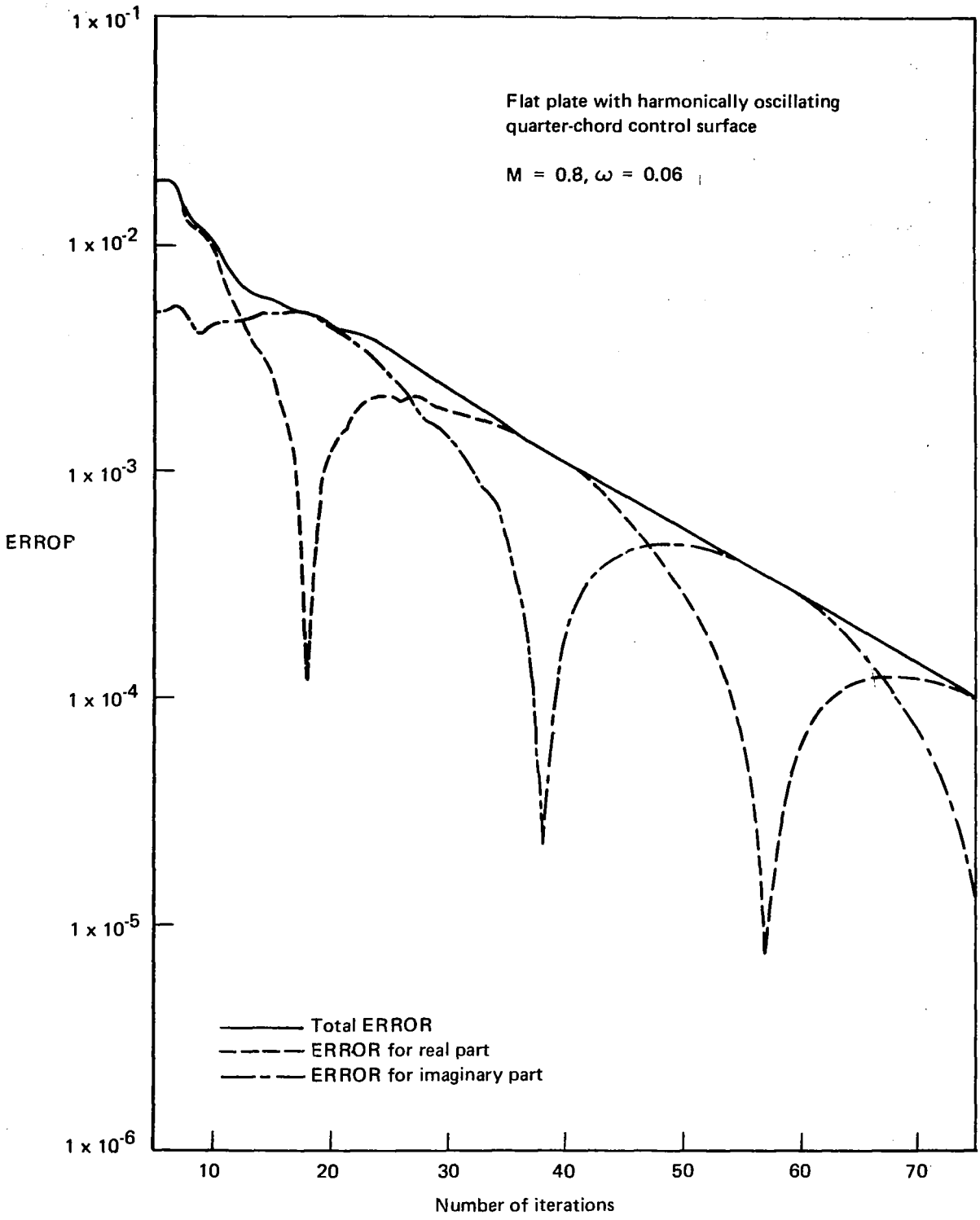

Figure F7. — Convergence of Real and Imaginary Parts of ERROR

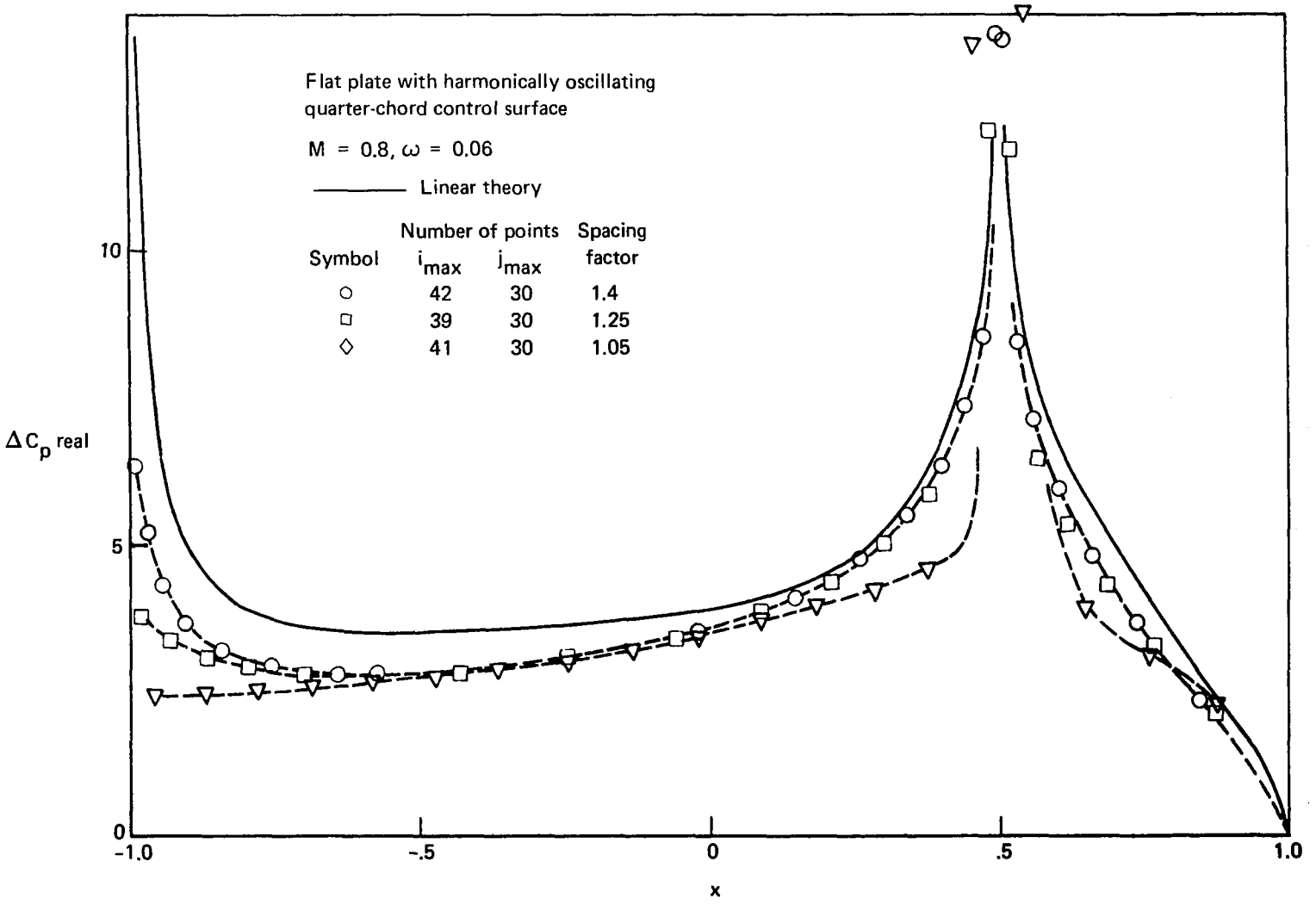

Figure F8. — Comparison of Solutions for Different Mesh-Point Spacings

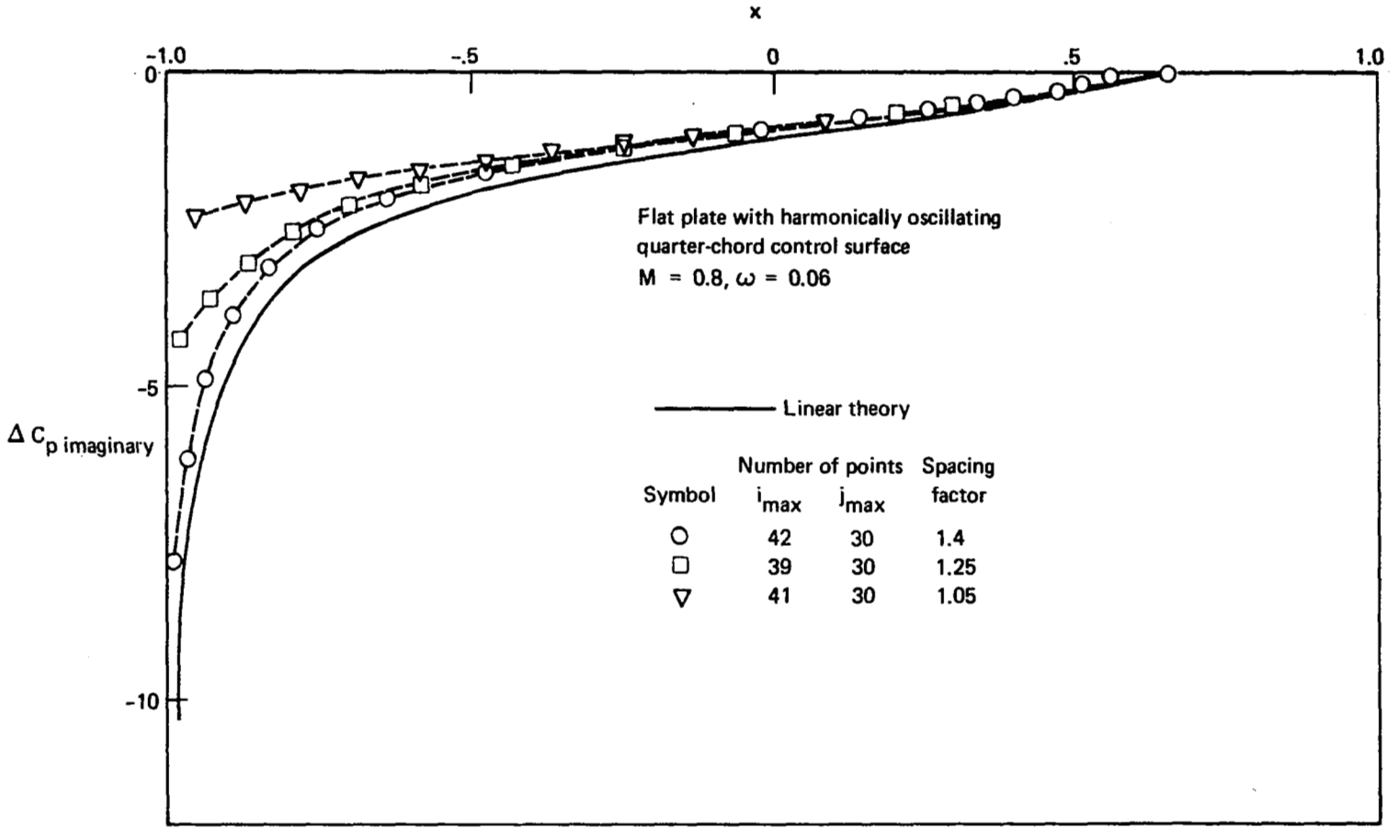

Figure F9. — Comparison of Solutions for Different Mesh-Point Spacings

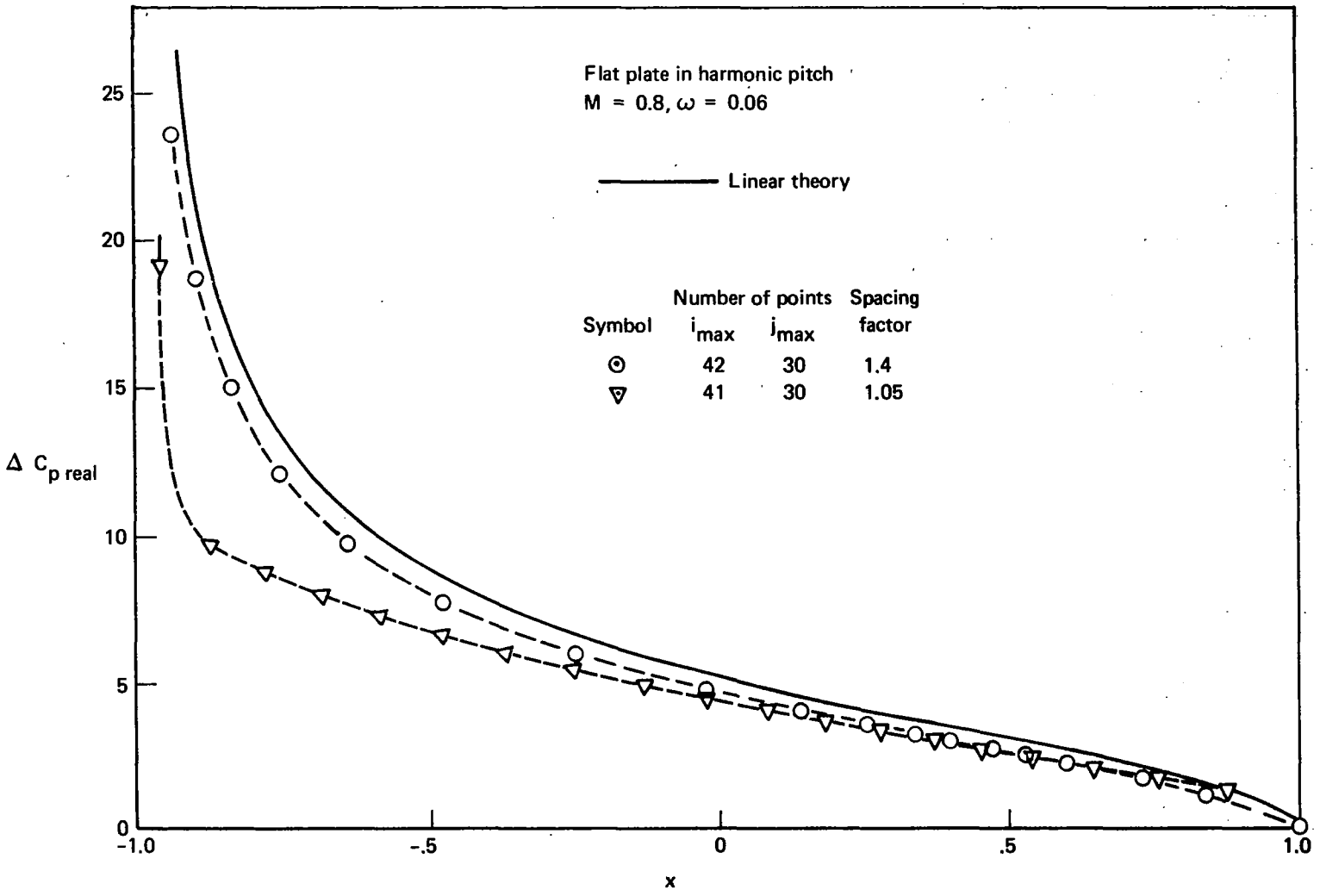

Figure F10. — Comparison of Solutions for Different Mesh-Point Spacings

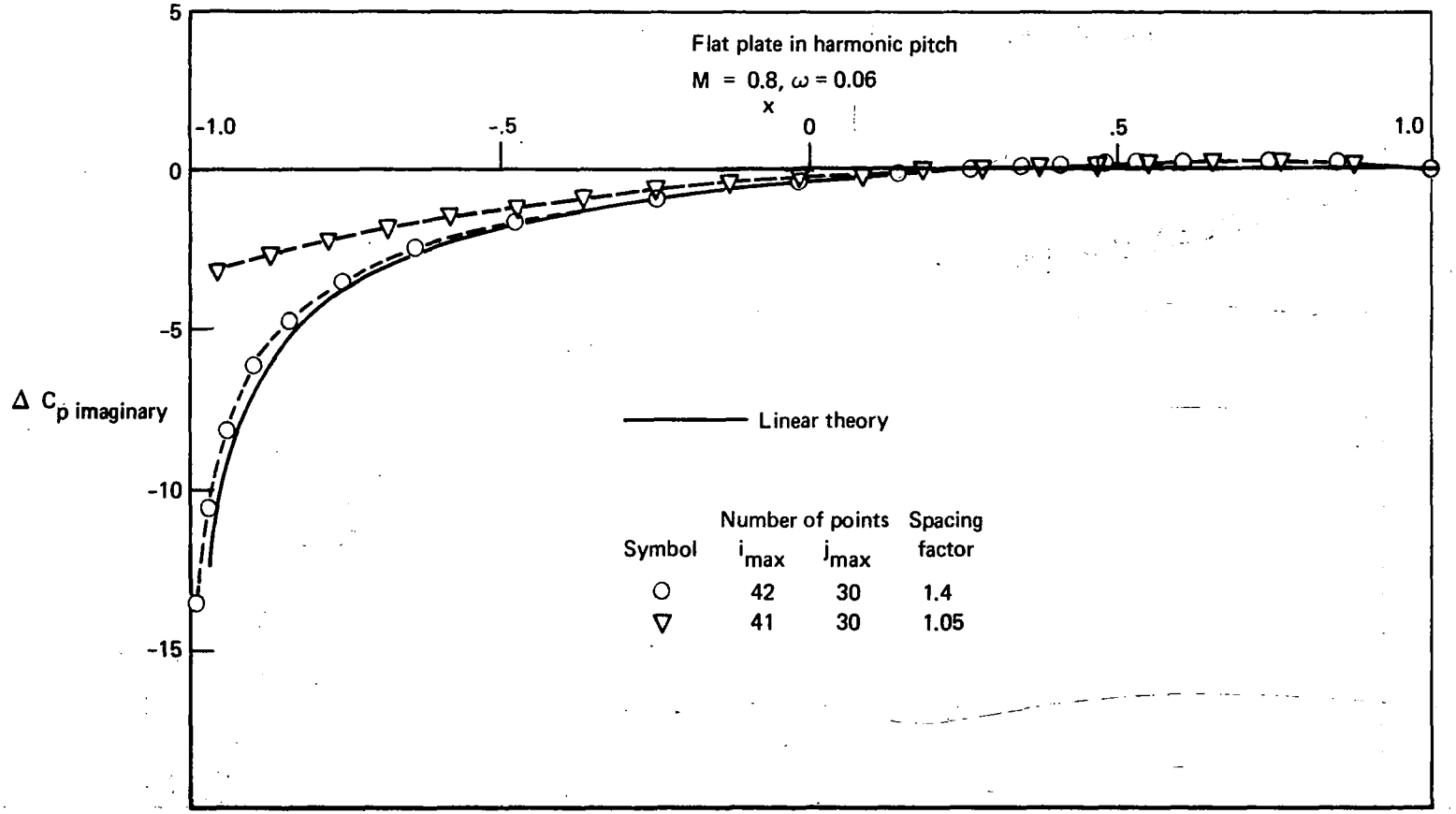

Figure F11. — Comparison of Solutions for Different Mesh-Point Spacings

case, the improvement in the representation of the singularity as the points were clustered about the singularities was very noticeable.

A comparison of pressure distributions resulting when the number of mesh points was varied is shown in figures F12 and F13. The example is the flat plate with the oscillating quarter-chord control surface. The area of the mesh grid was constant and the points were placed according to the program briefly described earlier. These results are essentially directly comparable to the results presented in figures 4 and 5 of reference 1 for a much finer grid. There was a significant improvement in correlation with the linear solution as the number of points increased. It is felt that the 42 x 30 grid represented a good compromise between correlation with the linear result and overall economy, and thus would make a satisfactory basis for parameter variation calculations.

F.1.3 EXTENT OF MESH

An example of variations in the location of the upper and lower boundaries is presented next. This calculation was carried out at M = 0.8 and $\omega = 0.06$ for a flat plate with a harmonically oscillating quarter-chord control surface. The upper and lower boundaries (i.e., $y_{1\,max}$) were set at ±3.0, ±6.25, and ±10.0 in scaled coordinates. This is equivalent to ±8.99, ±18.5, and ±29.6 in physical coordinates (i.e., 4, 9, and 15 chord lengths) for a 6% thick airfoil at M = 0.8. The number of mesh points was held constant for the three analyses using 42 points flow-wise and 30 points in the crossflow direction. Figures F14 and F15 show the distribution of the jump in pressure coefficient across the section. The curves for $y_{1\,max} = \pm 6.25$ and ±10.0 are essentially the same except in the region of the leading-edge singularity. Here, a better representation of the singularity was obtained from the smaller $y_{1\,max}$ value, apparently because the points in this case were more closely spaced about the wing section. The results at $y_{1\,max} = \pm 3.0$ were slightly smaller in the amplitude for both the real and imaginary cases except in the region of the leading-edge singularity. Again, the representation of the leading-edge singularity benefited from the closer vertical spacing of the finite difference points.

Figures F16 and F17 show plots of the velocity potential distribution for the variations in $y_{1\,max}$ discussed previously. The plots represent the variation in φ_1 (real and imaginary parts) in the vertical (crossflow) direction. The graph coordinates were set to emphasize the behavior of the velocity potential in the vicinity of the outer boundaries rather than the region next to the wing. The φ_1 for only two chordwise points are shown, but these curves are typical of the remaining curves. The curves for $y_{1\,max}$ of ±6.25 and ±10.0 lie very close together, while the corresponding curves for $y_{1\,max}$ of ±3.0 look quite different. Of course, it is the behavior of φ_1 adjacent to the wing that is most important, for this is where the pressure function is evaluated. However, for this case, the φ_1 distribution itself appears to have settled down by the time $y_{1\,max} = \pm 6.25$.

F.1.4 SEQUENTIAL REFINEMENT

As discussed in section 5.2.4, sequential refinement may be applied in terms of number of grid points, frequency, or Mach number. Although all three forms were tried, it is sequential refinement with respect to mesh spacing that held promise of significant savings in terms of computer resources. Examples of sequential refinement with respect to both Mach number

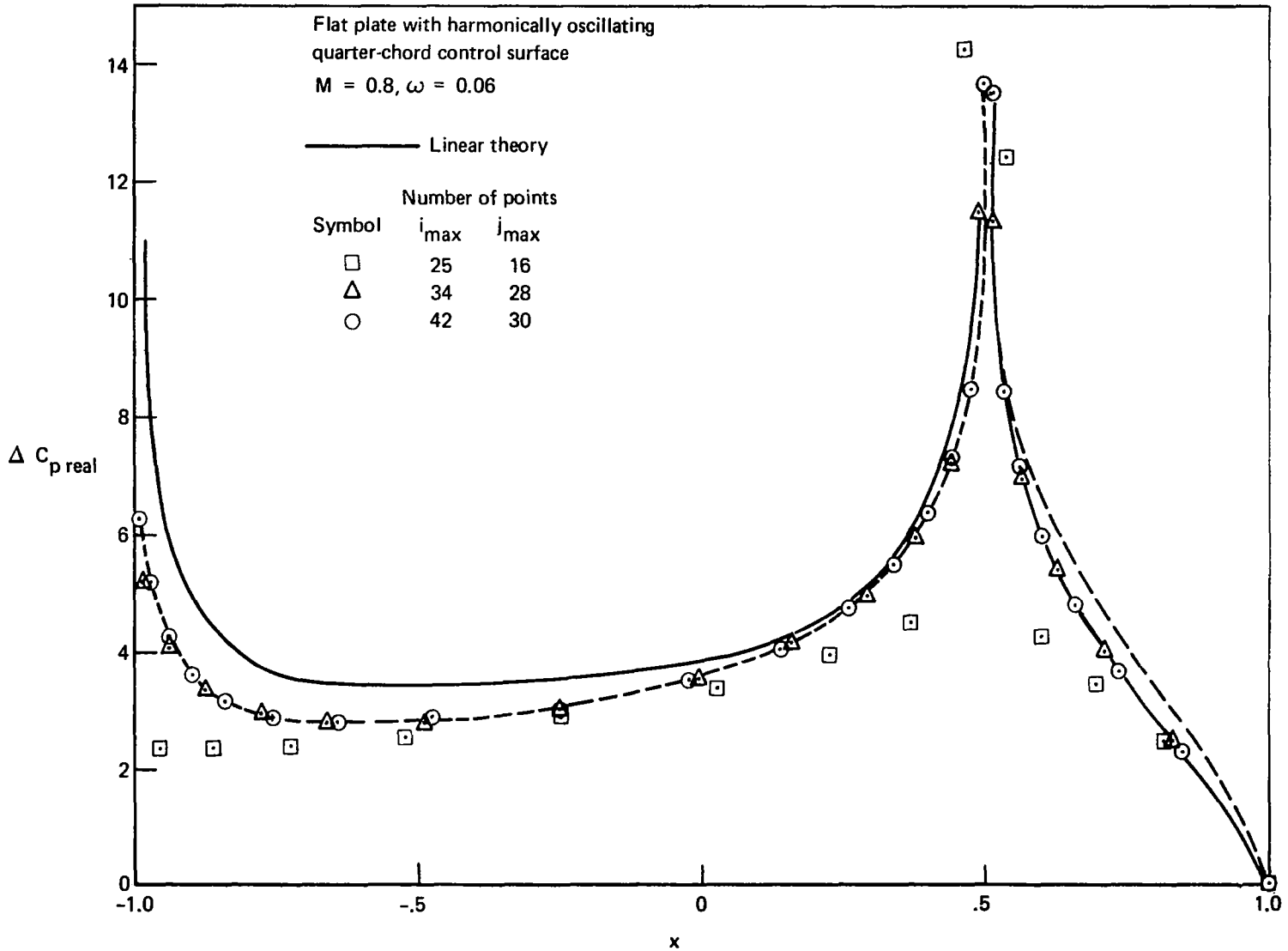

Figure F12. — Comparison of Solutions with Difference in Number of Mesh Points

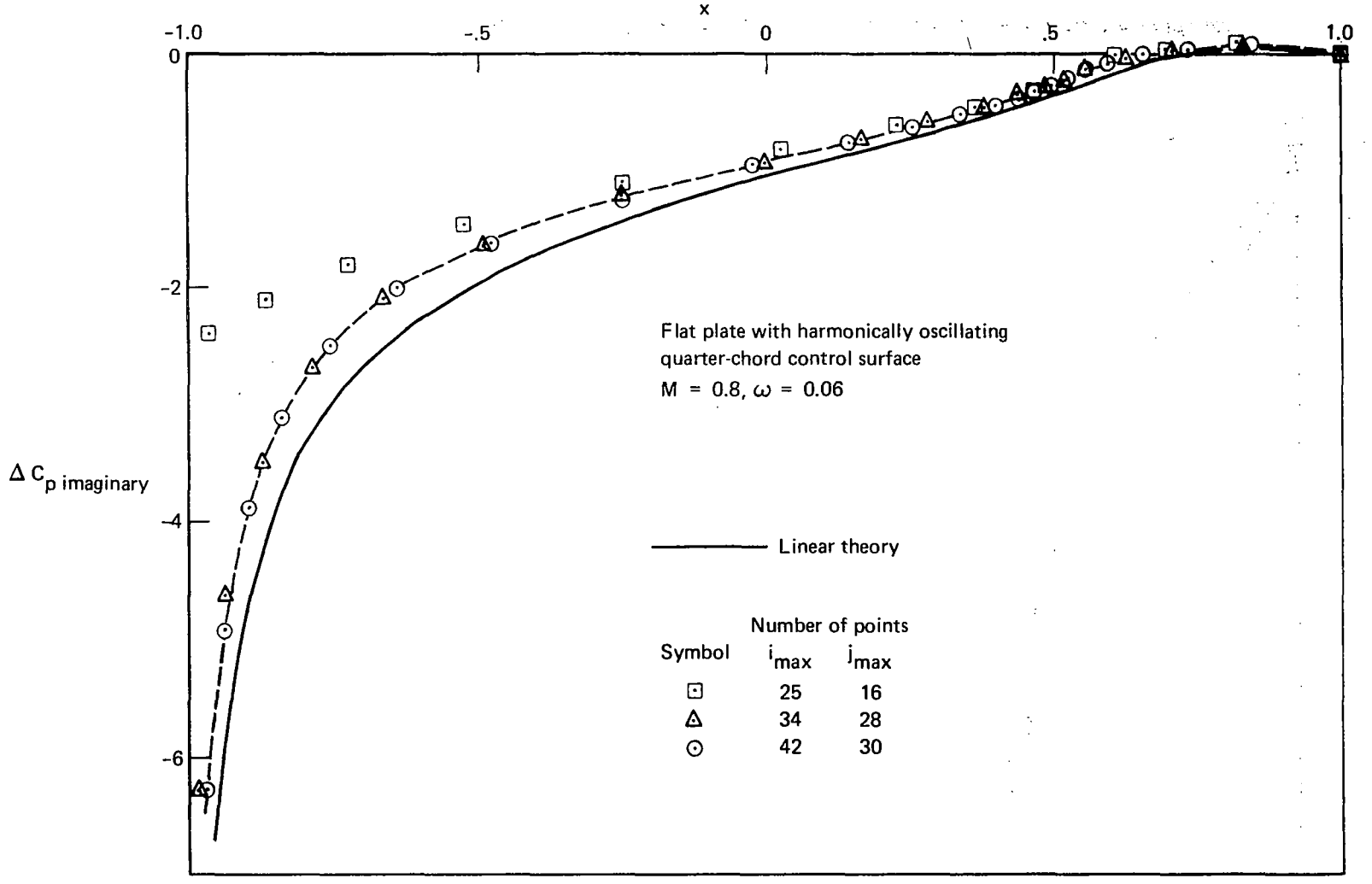

Figure F13. — Comparison of Solutions with Difference in Number of Mesh Points

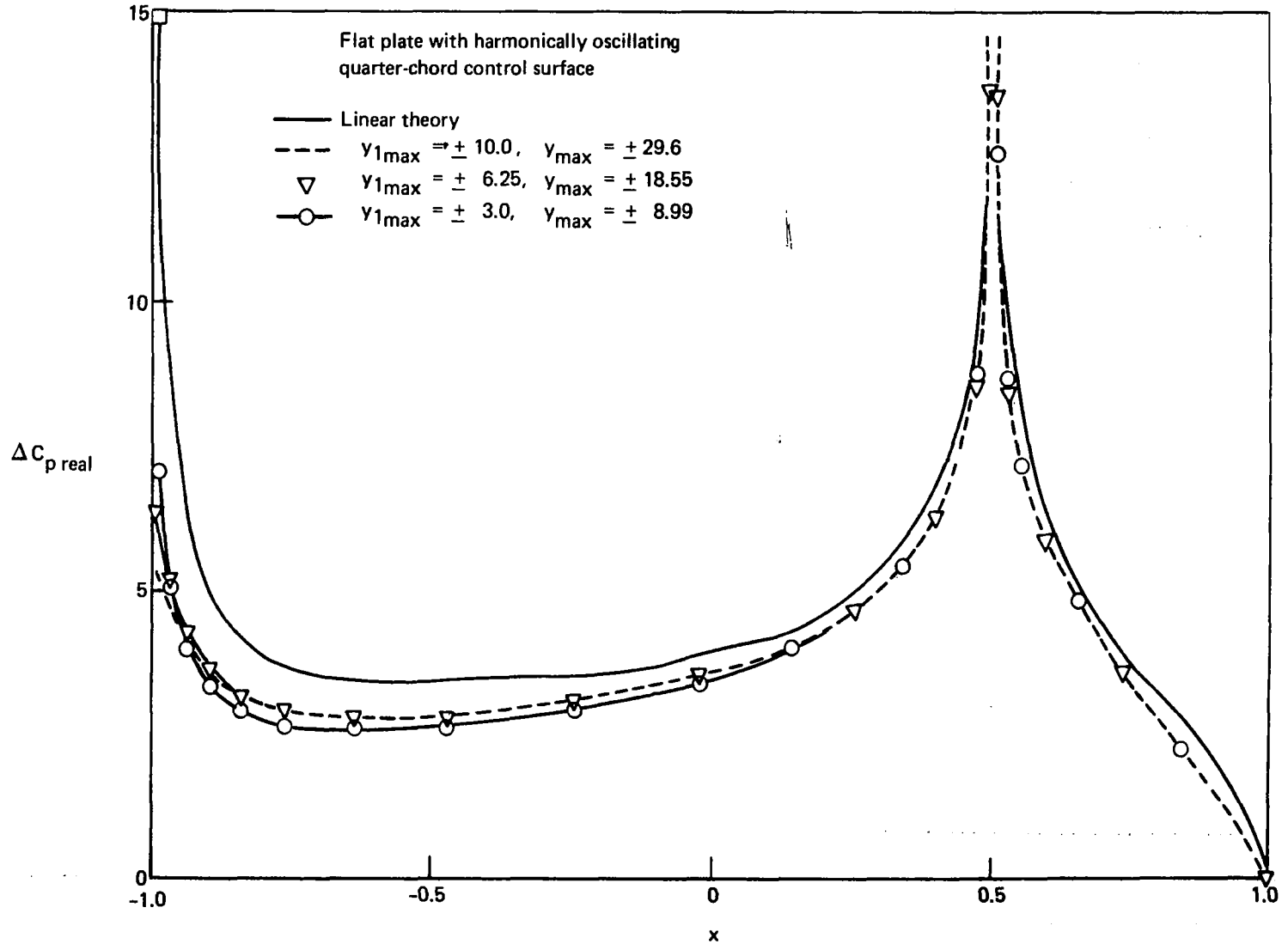

Figure F14. — Comparison of Solutions With Variation in Location of Upper and Lower Boundaries

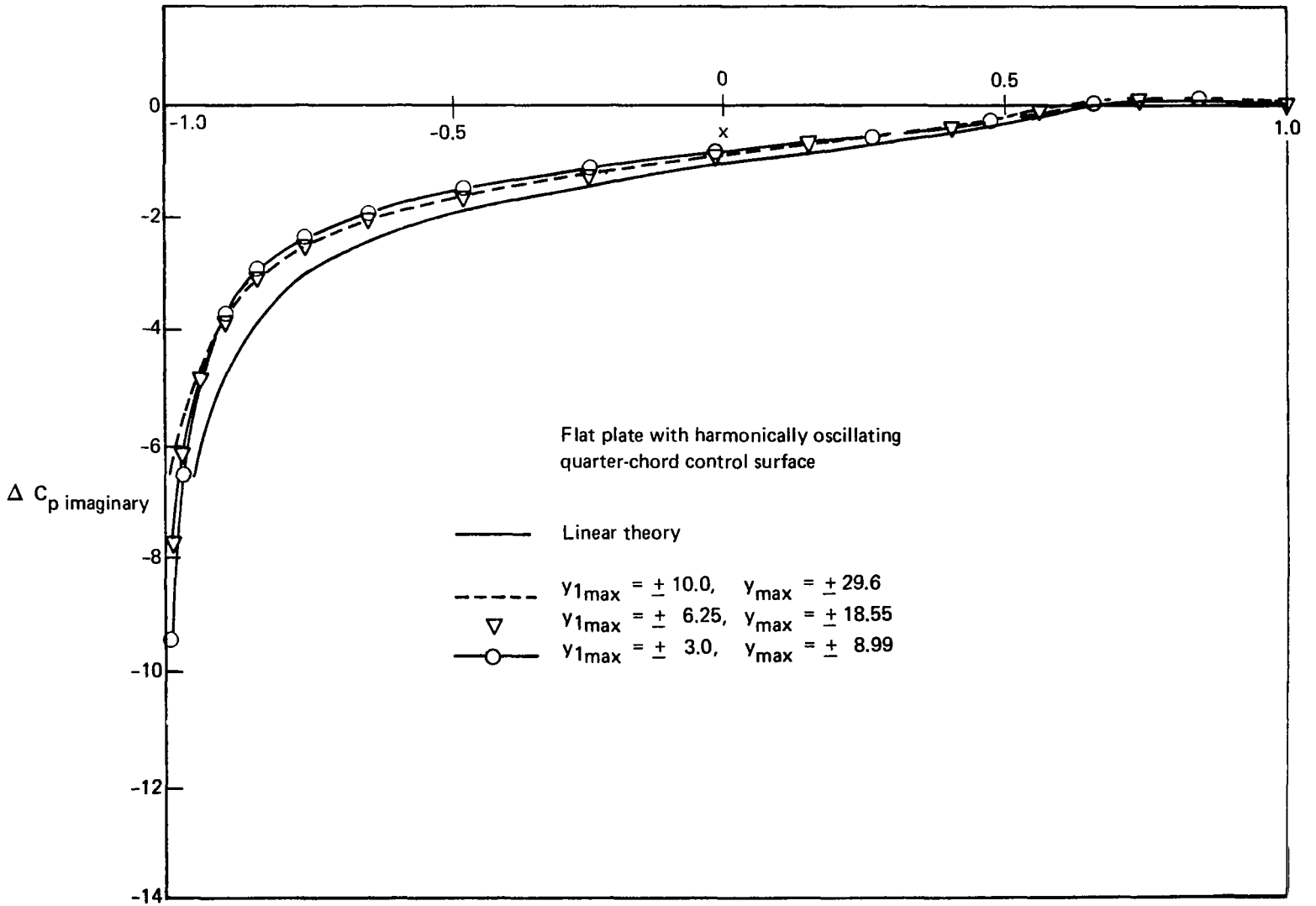

Figure F15. — Comparison of Solutions With Variation of Location of Upper and Lower Boundaries

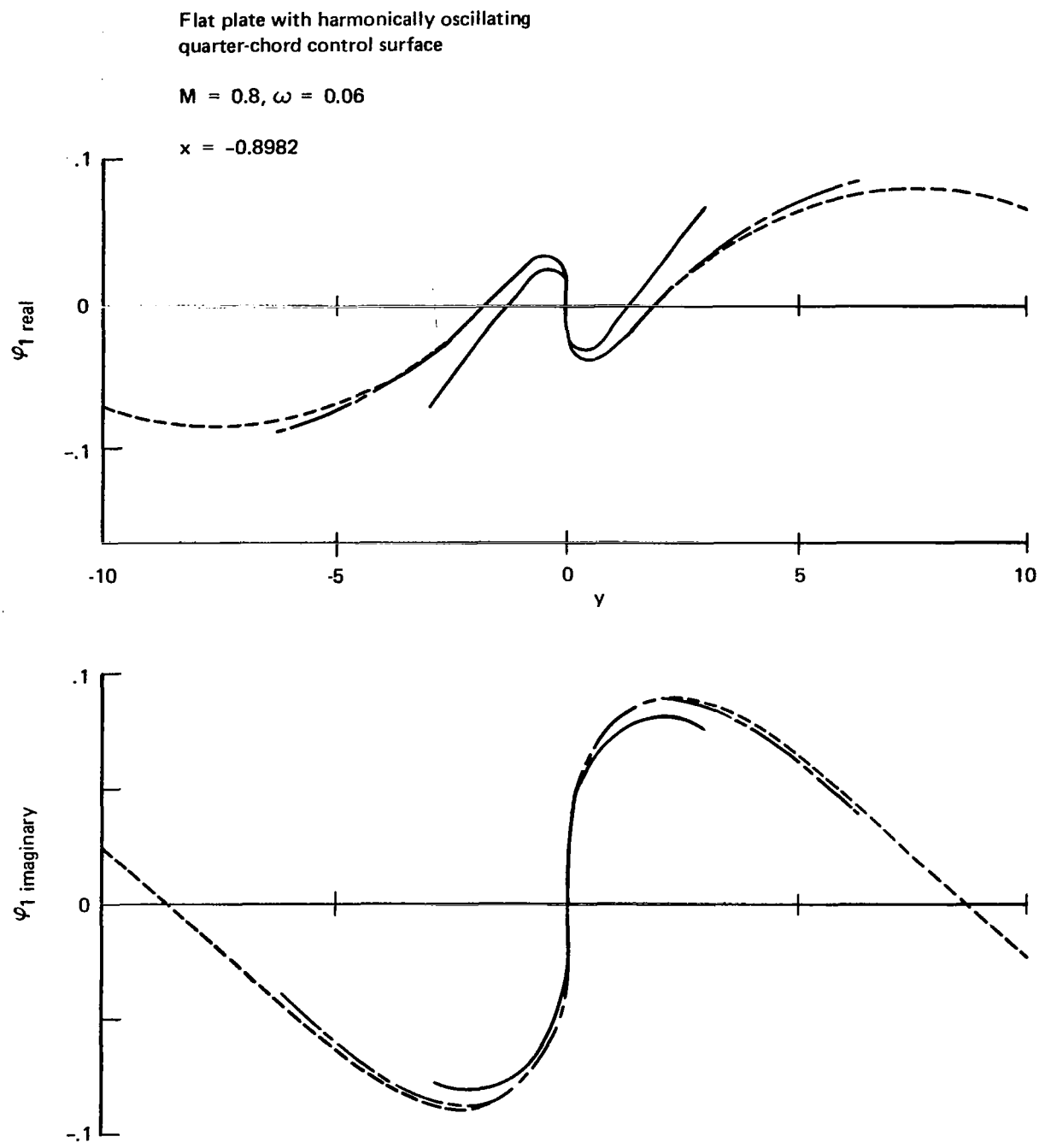

Figure F16. — Variation of Velocity Potential With Location of Upper and Lower Boundaries

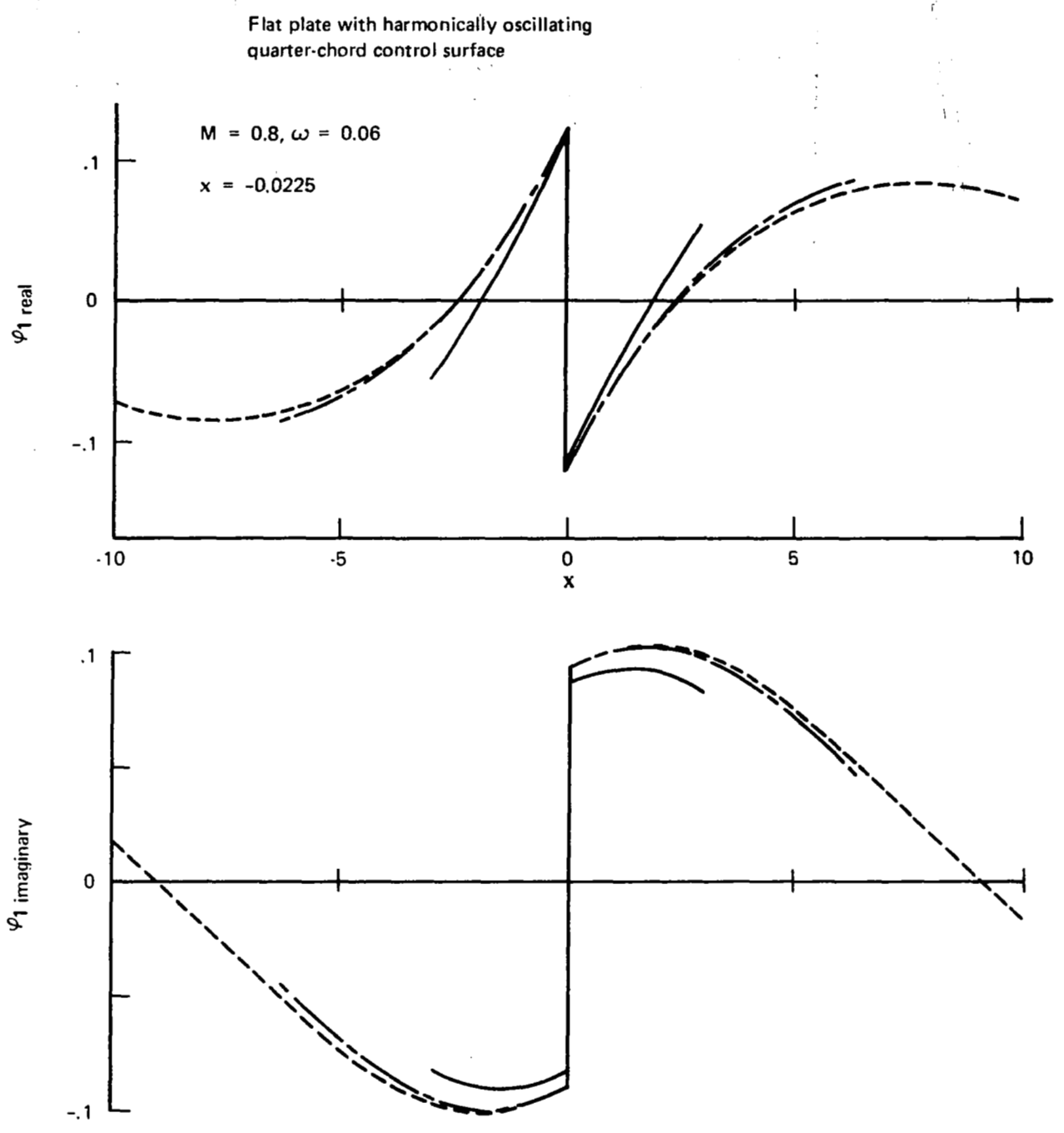

Figure F17. — Variation of Velocity Potential With Location of Upper and Lower Boundaries

and frequency is shown in figure F18. Depicted in this figure is the convergence for the case M = 0.9 and $\omega = 0.12$ for three different runs. For the first, the initial velocity potential distribution was zeros; for the second, the converged solution for M = 0.85 and $\omega = 0.12$; and for the third, the converged solution for M = 0.9 and $\omega = 0.10$. The difference in the number of iterations to convergence between the three runs was 25 out of 120, or about 22%, and is not significant unless the initial converged case is in existence. That is, it would not be worth generating the first solution in order to use it in the generation of the second case.

The same is not true for sequential refinement with respect to the number of points while keeping the total area constant. Significant saving is not automatic, however, and several possibilities are sketched in the next two figures. The first figure (fig. F19) shows two possible convergence paths using a combination of a course grid with a fine grid. A straightforward linear interpolotation was used to obtain the initial values of φ_1 for the iteration with the fine mesh from the last φ_1 distribution of the course mesh. Note that there is a sharp peak in the convergence curves at the time the grids are switched. The difference between the two paths is the convergence value reached for the coarse mesh before the switch to the fine mesh is made. The computer cost is a function of the size and number of iterations performed with each mesh. For example, both paths reach the value C of ERROR in the same number of iterations. Path B is obviously more efficient than path A since a larger proportion of the iterations were made with the coarse grid. We found it advisable to carry the convergence of the coarse mesh below that of final convergence criterion.

Another problem concerned the relative coarseness of the first grid to the second grid in a sequential refinement process. A second sketch (fig. F20) shows two convergence paths that differed as a result of different coarse grids. The evaluation of the total cost to convergence was more complicated than the preceding example. Here the efficiency must be evaluated by comparing the difference in cost of I_2 iterations of the fine mesh with the No. 2 coarse mesh, with difference in cost of I_1 iterations of No. 2 coarse mesh with No. 1 coarse mesh.

Thus it is very difficult to put quantitative numbers to the actual gain in computer efficiency using sequential refinement. We were satisfied with the results of using just two meshes to obtain final answers – a 25 x 20 mesh followed by a 42 x 30 mesh – for most of the examples of this report.

Figure F21 presents the solution convergence for an airfoil using a 46 x 30 mesh. The upper curve shows the convergence starting with an initial φ_1 distribution of zero. The lower curve shows the corresponding convergence starting with an initial distribution from a converged solution for a 17 x 20 mesh. The values at the points of the coarse mesh were linearly interpolated to provide values at the points of the fine mesh. The two meshes covered the same area. The point to be made is that the solution curves tend to merge for a large number of iterations and thus the advantage gained by using sequential refinement is lessened. As a side issue, the graph gives an indication of the effect of varying the scalar applied to the terms that are added to the finite difference equation to provide for convergence in the mixed-flow problem when using row relaxation. This factor, which is called CONPXT and is described in section F.2.1, was set at 5 and 10 for this particular case. Also, the graph shows the effect of using an ORF of 1.6 rather than 1.85 for this problem.

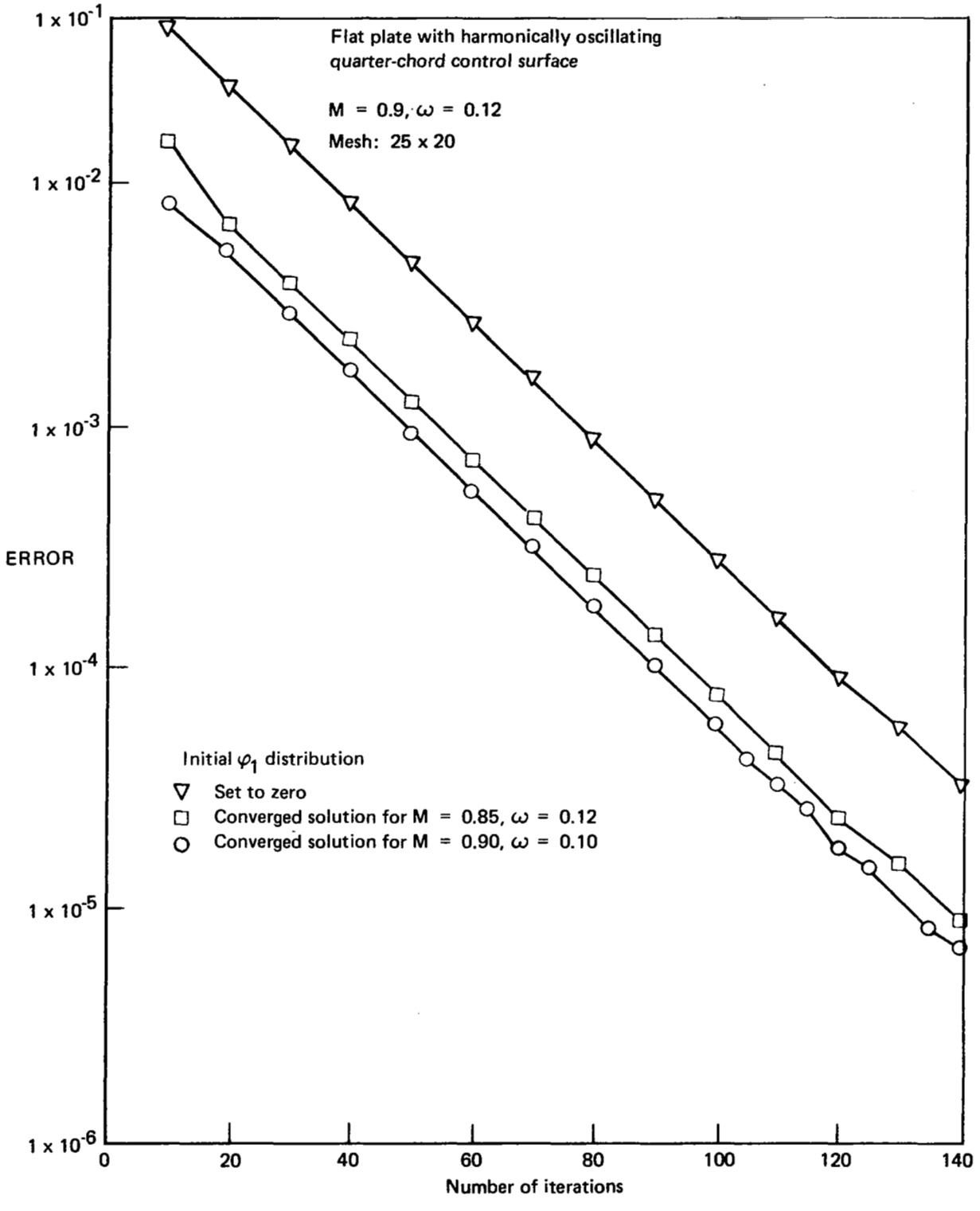

Figure F18. — Sequential Refinement with Respect to Mach Number and Frequency

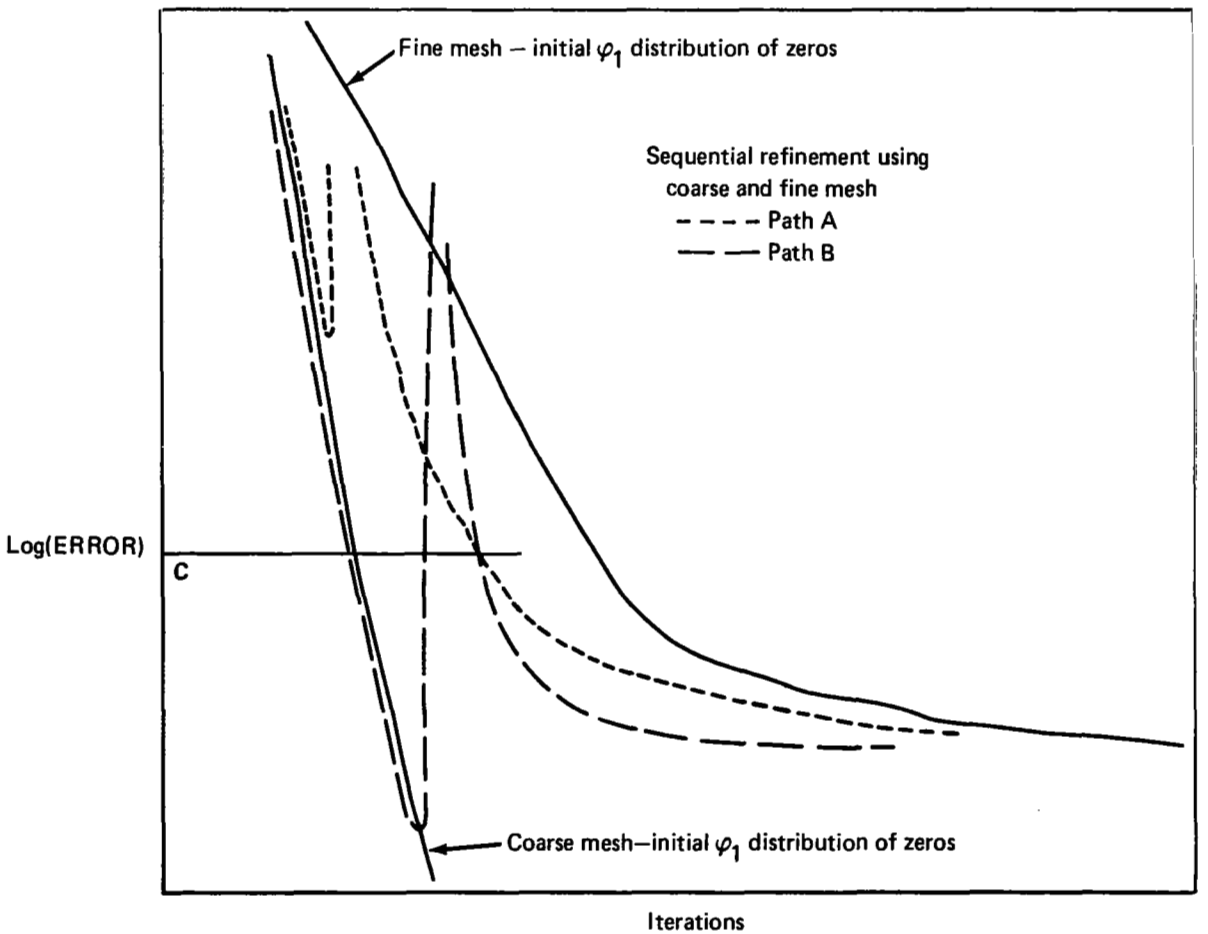

Figure F19. — Sequential Refinement With One Coarse Mesh and One Fine Mesh

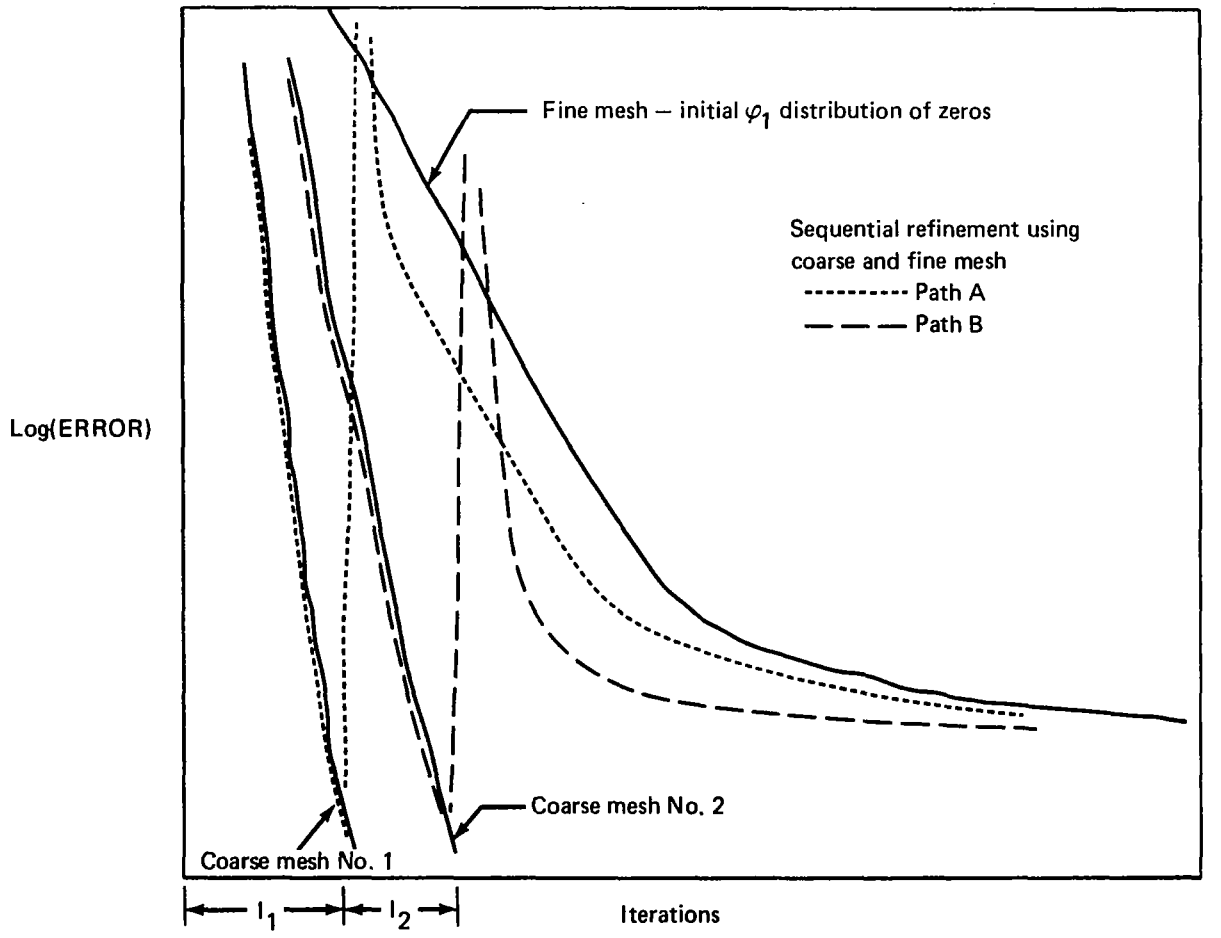

Figure F20. — Sequential Refinement and the Effect of Coarseness of First Mesh

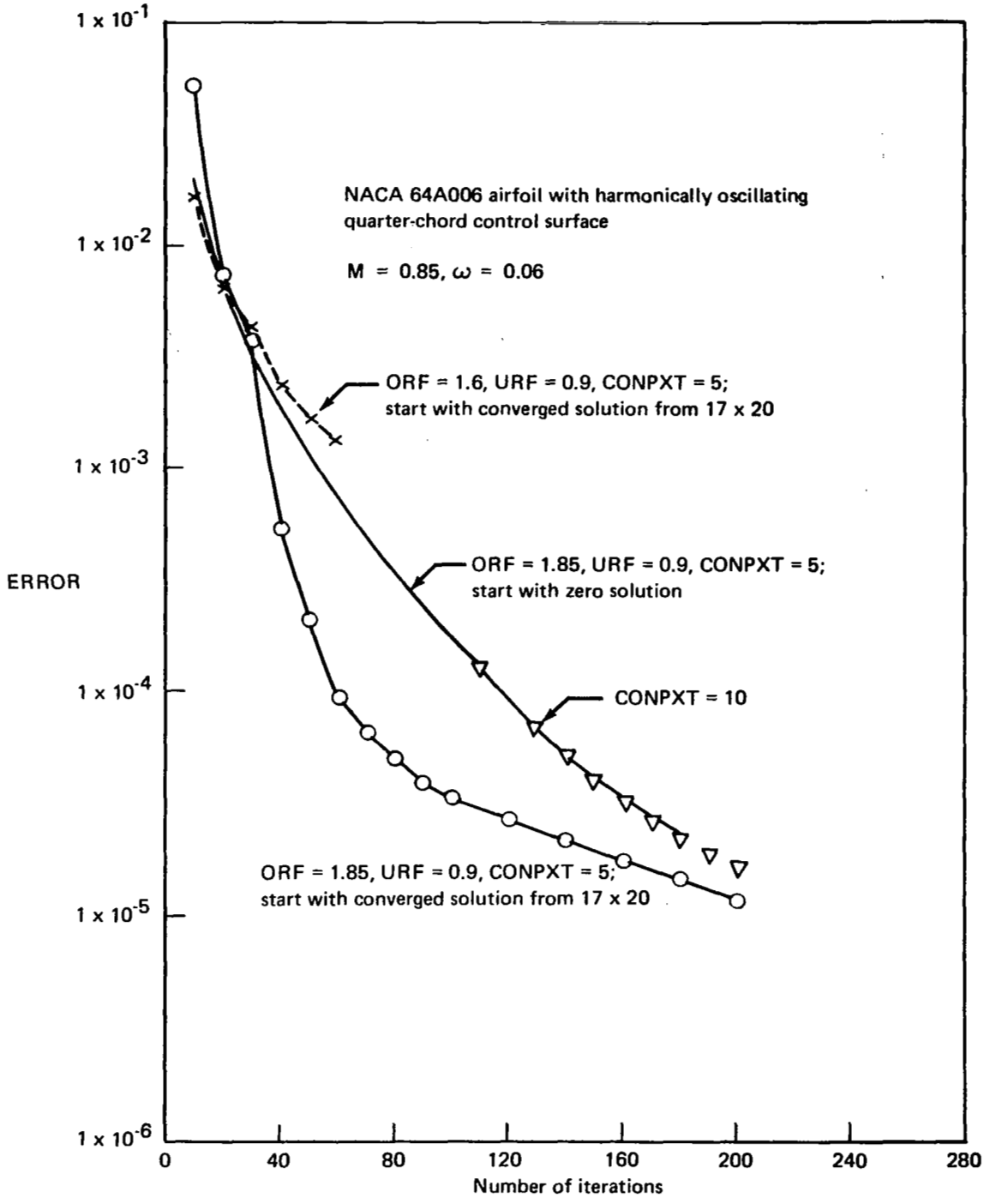

Figure F21. — Examples of Effect of Starting Velocity Potential on Solution Convergence

F.2 SOLUTION PROCESS

F.2.1 ROW RELAXATION

The finite difference equations presented by Ehlers in reference 1 are written for column line relaxation. Rewriting these equations for row line relaxation consisted of simply putting the i+1, i-1, i-2 terms on the left-hand side of the equations and moving the j+1, j-1 terms to the right-hand side of the equation. This change was accomplished in the program by minor DO loop changes and by rewriting the coefficient generator module. Although the mechanical aspects of the change were relatively straightforward, questions did arise regarding the effect on the solution convergence, a point made clear in discussions with Jameson. A general way of analyzing the iterative solution of finite difference equations is discussed by Jameson in references 8 and 9. Briefly the procedure is to treat the iterations steps as an artificial time coordinate. This permits rewriting the finite difference equation as a differential equation including time, and the particular way the relaxation is performed is reflected in time-dependent terms. Thus a relaxation procedure may be considered as a finite difference equation for a time-dependent equation and the behavior of the corresponding iterative solution inferred from the resulting time-dependent equation. Both the subsonic (elliptic) and supersonic (hyperbolic) forms of the two-dimensional equation were analyzed; the details are included in appendix C. In summary, it was found that the elliptic form was convergent in its original form, whereas the hyperbolic form required the addition of two terms to achieve convergence. These terms are derived in the appendix and the following discussion will concentrate on the result of using row relaxation.

Generally, row relaxation proved much more efficient than column relaxation. In addition, the row process was most efficient starting at the upper and lower boundaries and working in toward the wing surface, alternating the rows by taking one from the top section, one from bottom section, then one from the top section, etc. The one exception to this pattern was for combinations of Mach number and frequency for which convergence was marginal at best; then column relaxation proved superior to row relaxation.

Figures F22 and F23 present examples of row and column solutions for comparison purposes. Figure F22 compares row and column solutions for a 42 x 30 grid for a flat plate. It is believed that the solutions are carried out, initially at least, with a nearly optimum ORF. Figure F23 shows corresponding data for a 17 x 10 grid. In each case, row relaxation was significantly more efficient.

Convergence in the airfoil case, i.e., for mixed flow, was obtained by adding the following terms to the finite difference equation.

$$-\frac{CONPXT}{y_{j+1}-y_{j-1}}\sqrt{\frac{|u_{ij}+u_{i+1j}|}{2}}\left\{\frac{\left(\varphi^{(n)}_{ij}-\varphi^{(n)}_{i-1j}\right)-\left(\varphi^{(o)}_{ij}-\varphi^{(o)}_{i-1j}\right)}{x_i-x_{i-1}}\right. \tag{F1}$$

$$\left.+CONE6\cdot 4\cdot\left[\frac{u_{i+1j}-u_{ij}}{x_{i+1}-x_{i-1}}-\frac{i\omega}{\epsilon}\right]\frac{\varphi^{(n)}_{ij}-\varphi^{(o)}_{ij}}{u_{ij}+u_{i+1j}}\right\}$$

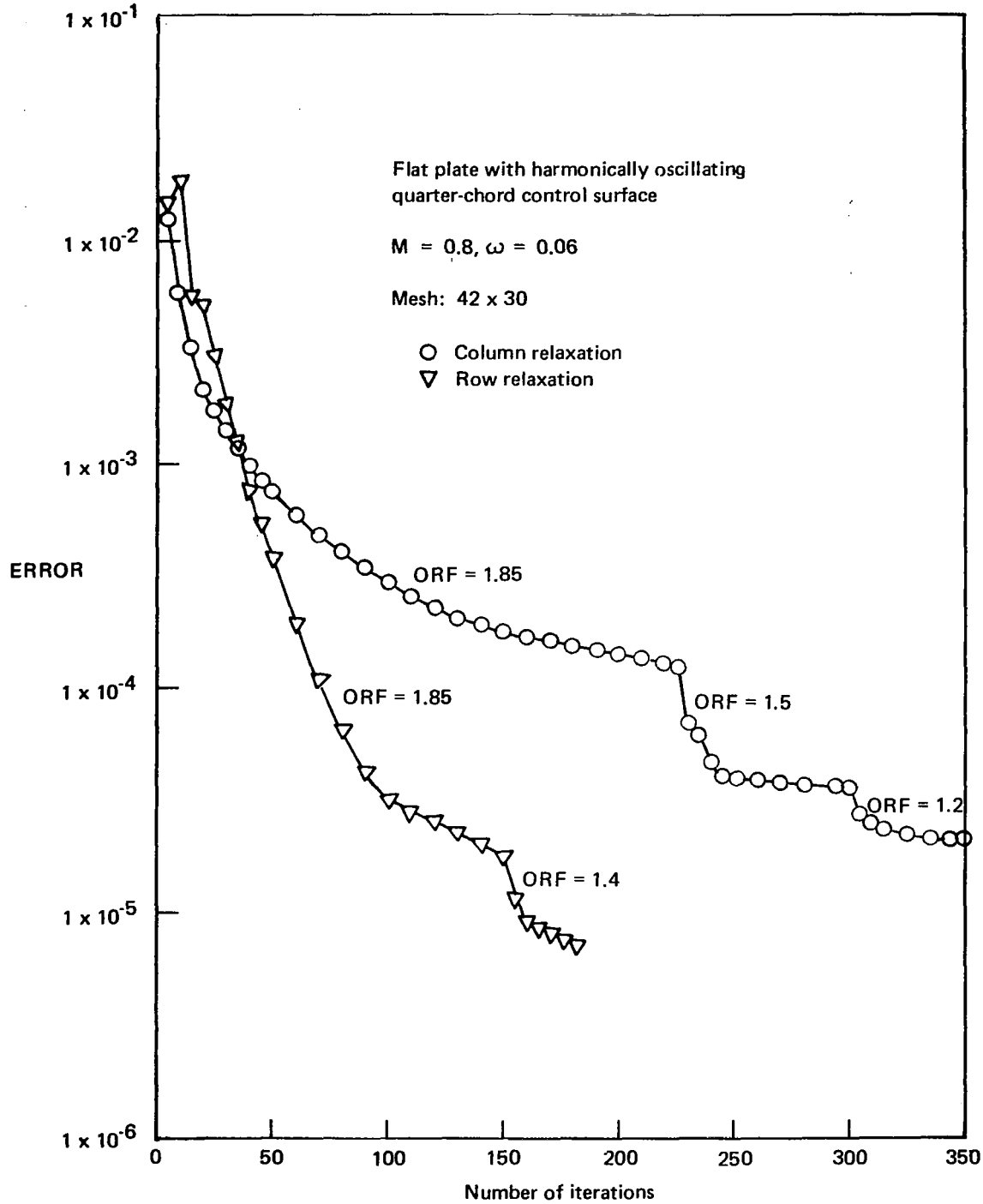

Figure F22. — Convergence Comparison of Row and Column Relaxation Procedures for a 42 x 30 Mesh

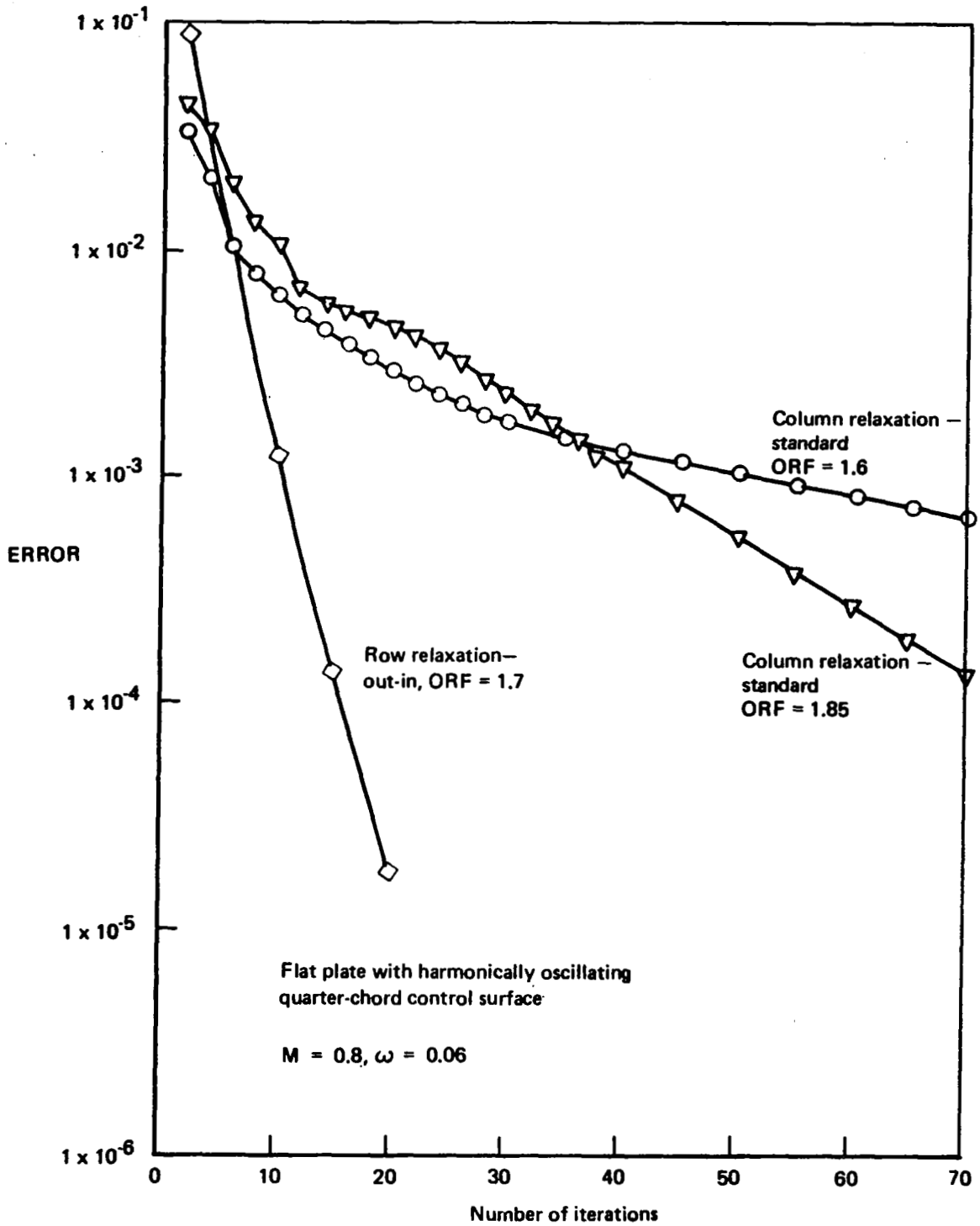

Figure F23. — Convergence Comparison of Row and Column Relaxation Procedures for a 17 x 10 Mesh

The values of the velocity potential with superscripts (n) are considered "new" values and are considered to be unknowns. The values with superscript (o) are considered "old" values that were calculated in the preceding iteration and go on the right-hand side of equations (A1) and (A2).

CONPXT and CONE6 are constants that may be varied from run to run. Column relaxation is convergent without these additional terms. A comparison between the solutions for row and column procedures (fig. F24) showed that row relaxation was again the most efficient process. The values used for CONPXT should be of the order 2 to 10 and for the value of CONE6 should be of the order of +0.1. As with ORF and URF, optimum values of CONPXT and CONE6 appeared to vary from case to case and, for maximum efficiency, should be determined separately for each calculation.

There are several ways of running column relaxation for the two-dimensional case. The two most logical sequences appear to be: (1) starting from the upstream mesh boundary and, taking the columns in succession, moving to the downstream boundary; and (2) starting at the section trailing edge and moving forward, column by column, to the upstream boundary and then returning to the first column aft of the trailing edge and moving, column by column, to the downstream boundary. It is this latter process that worked best and is referred to as the "standard" column procedure. The former sequence will be referred to as simply "fwd-aft." An example using this latter solution sequence is shown in figure F25. From this particular example, it would appear that fwd-aft is more efficient than the standard sequence (see fig. F23). The fwd-aft sequence appears, in many cases, to be nearly as efficient as the standard column, but we found it generally to be less reliable. This was particularly true for combinations of Mach number and frequency that led to marginal solution stability. Also, the fwd-aft sequence utilized lower ORF's, for several examples diverged when rerun with ORF's that had been optimum for the standard sequence. It is interesting to note that working the solution sequence forward and aft from the the trailing edge does not seem logical for mixed-flow problems; however, in practice, it worked out very well.

Similarly, there are other sequences for row solution besides the "out-in" sequence described above. These include, for example, "in-out" sequence (i.e., starting at the wing surface and working out, row by row, and alternating top and bottom), and just starting at one boundary (say the lower boundary) and solving successive rows to the upper boundary. A comparison of row in-out with row out-in is given in figure F26.

F.2.2 DIRECT SOLUTION

A version of the pilot program was also developed to provide direct solution for the interior velocity potential distribution. This concept was outlined by Ehlers (ref. 1). Generally, the iterative relaxation for the unknowns associated with the interior points was replaced by a solution of the complete set of simultaneous equations at one time. There was still an iterative loop since the conditions on the outer boundaries of the mesh area were a function of the unknown velocity potentials adjacent to the airfoil surface. The modified pilot program was appropriate only for problems with subsonic steady-flow fields.

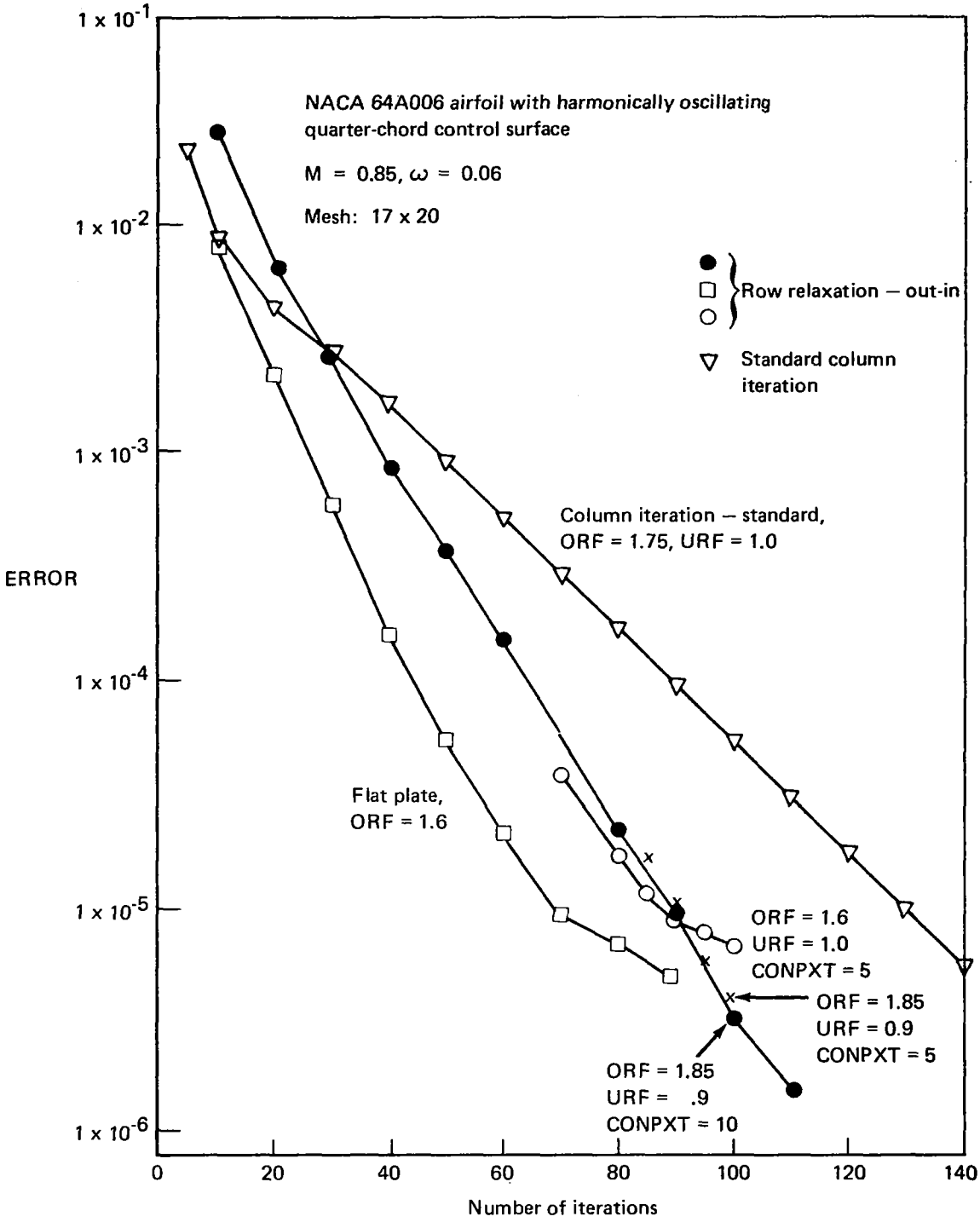

Figure F24. — Convergence Comparison of Row and Column Relaxation for Mixed Flow

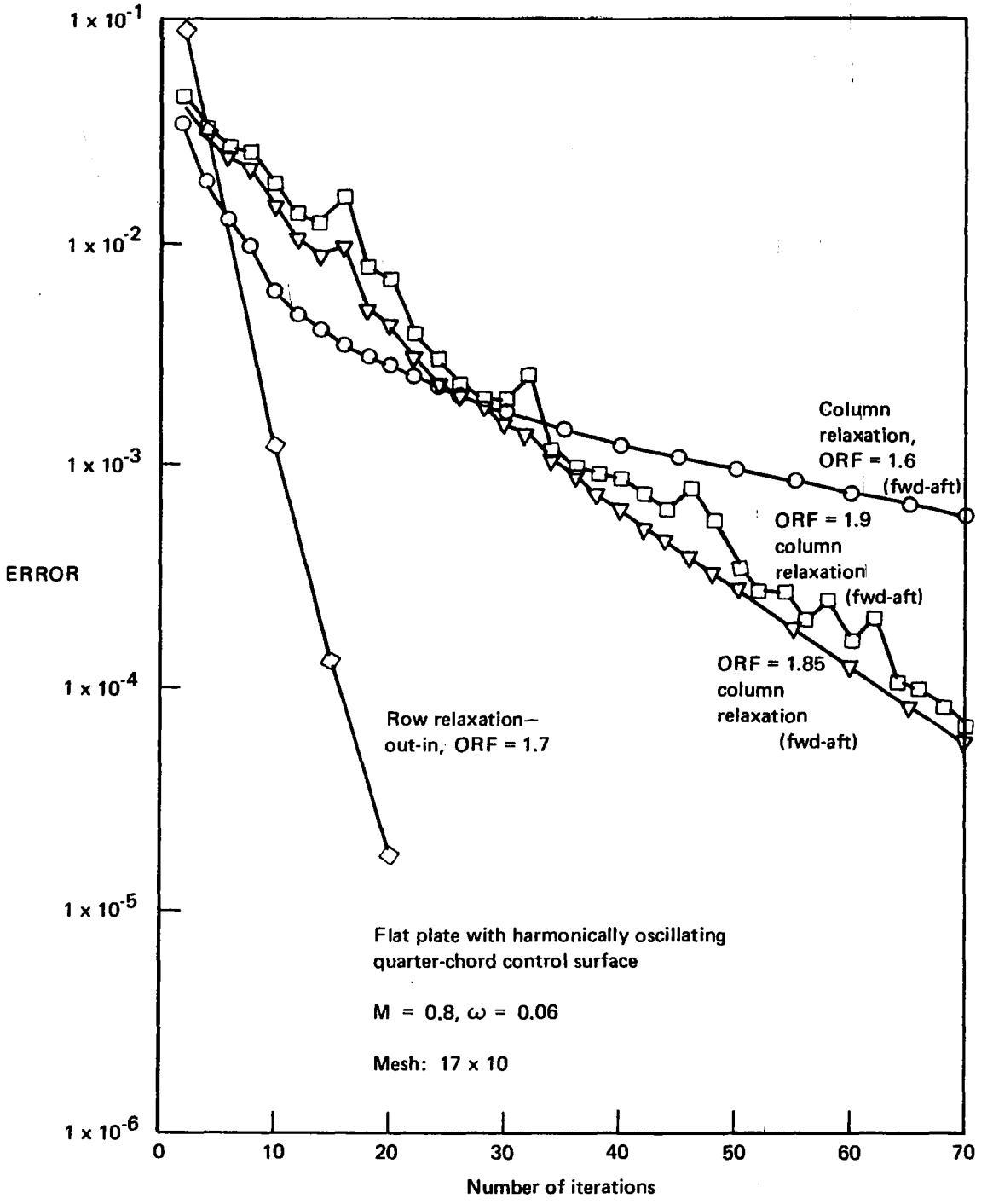

Figure F25. — Convergence Comparison of Row and Column Relaxation (Forward - Aft)

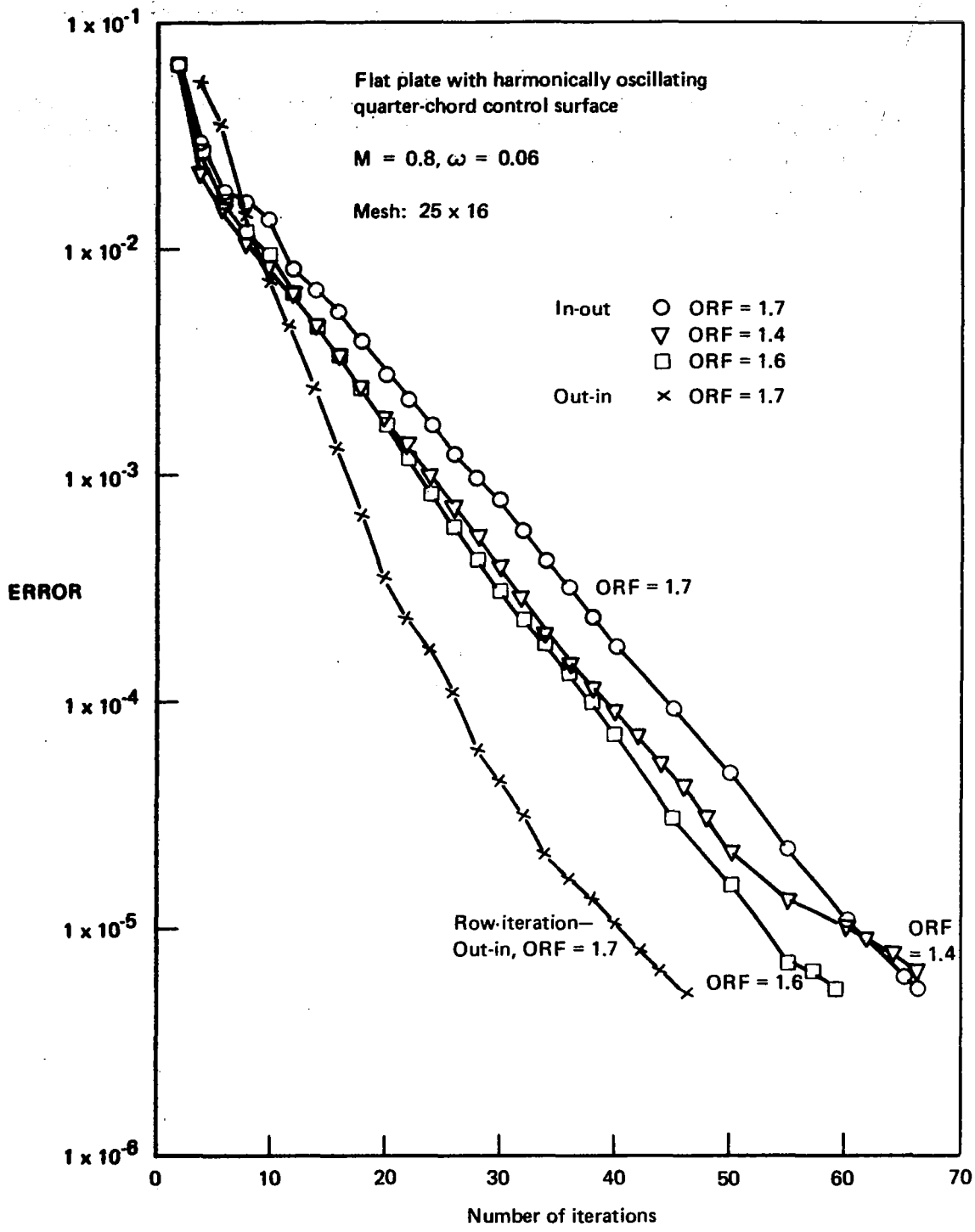

Figure F26. — Convergence Comparison of "In-Out" and "Out-In" Sequences for Row Relaxations

The matrix equation for the direct solution may be written as

$$[A]\ \{\bar{X}\} = \{\bar{R}\} \tag{F2}$$

where [A] is matrix of complex coefficients of order equal to the number of interior points, $\{\bar{X}\}$ is column matrix of unknown velocity potential, and $\{\bar{R}\}$ is a complex column matrix introducing the conditions on the flow-field boundaries. If the number of mesh points in the flow direction is i_{max} and the number in the crossflow direction is j_{max}, then N, the number of interior points and thus the order of equation (F2) is

$$N = (i_{max} - 2)\,(j_{max} - 2) \tag{F3}$$

The boundary values on the mesh region are dependent on the values of the velocity potential on the wing and wake; hence equation (F2) may be written as

$$[A]\ \{\bar{X}\} = \{\bar{R}(\bar{X})\} \tag{F4}$$

where [A] is a constant matrix and $\{\bar{R}\}$ is a complicated nonlinear vector valued function of $\{\bar{X}\}$. The solution is obtained by iteration. That is, a $\{\bar{X}^{(\ )}\}$ is chosen and improved approximations to $\{\bar{X}\}$ are determined from

$$[A]\ \{\bar{X}^{(n+1)}\} = \{\bar{R}(\bar{X}^{n})\} \tag{F5}$$

Note that for each fixed n, there is a linear equation of the form of equation (F2), and that as n changes, only the right-hand side changes, not [A].

The most efficient direct method for the solution of a linear system $[A]\ \{\bar{X}\} = \{\bar{R}\}$ is well known to be the Gaussian elimination algorithm. The form of this algorithm that is particularly suitable for several systems with the same coefficient matrix but with different right-hand sides is LU decomposition. In this scheme, [A] is decomposed, *once and for all,* into lower and upper triangular matrices [L] and [U], respectively, such that [L] [U] = [A]. Then $[A]\ \{\bar{X}\} = \{\bar{R}\}$ may be written as $[L]\ [U]\ \{\bar{X}\} = \{\bar{R}\}$ and the solution found by solving, in turn, $[L]\ \{\bar{Y}\} = \{\bar{R}\}$ and $[U]\ \{X\} = \{\bar{Y}\}$. Note that since [L] is lower triangular, solution of $[L]\ \{\bar{Y}\} = \{\bar{R}\}$ involves only forward substitution; similarly, since [U] is upper triangular, solution of $[U]\ \{\bar{X}\} = \{\bar{Y}\}$ involves only backward substitution. Thus solution of $[A]\ \{\bar{X}\} = \{\bar{R}\}$ is very fast once the decomposition [A] = [L] [U] is performed.

The main obstacle to solving large systems by direct methods is the large storage requirement. This is not due to the space required for [L] and [U], since these may replace [A] as they are calculated, but simply the storage required for [A]. The situation is improved somewhat when [A] is a band matrix as in this case, but for a sufficiently fine mesh, the storage required may still exceed core capacity. To be more precise, when the coefficient matrix is banded, it may be shown that the band structure carries over to [L] and [U]. Thus it is not necessary to store all of [A] ; in particular, the 0's below the far subdiagonal and above the far superdiagonal need not be stored. (The 0's within the band must be stored since these locations are filled in the course of the decomposition.) Hence the total storage required for [A] is $N[2(j_{max} - 2) + 1]$. In addition to the storage for [A] we required N locations for

$\{\bar{R}\}$ and N locations for a scratch array used in the course of the decomposition. In sum, if the values were all real the total additional storage requirement, T, would be

$$T = N \cdot [2(j_{max} - 2) + 1] + 2N \tag{F6}$$

$$= N \cdot [2(j_{max} - 2) + 3], \tag{F7}$$

but since the values are complex, we have

$$T = 2N \cdot [2(j_{max} - 2) + 3]. \tag{F8}$$

We proceed to put (F7) in slightly different form, in which the dependence on the number of interior points is more transparent.

Let $$C = (j_{max} - 2)/(i_{max} - 2).$$

Then $$(j_{max} - 2)^2 = C(i_{max} - 2)(j_{max} - 2) = CN \tag{F9}$$

which leads to

$$T = 4\sqrt{C} \cdot N^{3/2} + 6N \tag{F10}$$

Hence, we see that the storage requirement grows essentially as the number of interior points grows to the 3/2 power, for a fixed ratio of mesh spacings. For a mesh of 27 x 18 (i.e., with $i_{max} = 27$ and $j_{max} = 18$), T = 28 000 words, which is within the core capacity of the CDC 6600. For a mesh of 42 x 32, T = 151 200 words, which is beyond the core capacity of the CDC 6600.

F.2.3 CONVERGENCE ACCELERATION METHODS

The relatively regular, uniform, and monotonic behavior of the pressure difference distributions with successive iterations suggested the use of convergence acceleration techniques. Also, these procedures were successfully applied in limited examples of steady transonic flows by Hafez and Cheng (ref. 13), and Martin and Lomax (ref. 14). Further, our studies showed relatively good behavior of both the unsteady velocity potential distribution and the ERROR with successive iterations.

A rather straightforward program system was set up whereby three successive velocity potential distributions (or pressure distributions) could be calculated and saved. These would be for the n-2m, n-m, and n iterations, with both n and m being set by the user. A separate program is then used to generate a new distribution, which may be used as a starting point for a new sequence of iterations.

The sample problem used for all the calculations was that of a two-dimensional flat plate with a harmonically oscillating control surface at M = 0.8 and a reduced frequency of 0.06. A mesh with 42 points in the streamwise direction and 30 points perpendicular to the flow was used. It is estimated that convergence for this case was reached in less than 400 iterations.

The first convergence acceleration procedure used was an application of Aitken-Shanks nonlinear transformation (δ^2 process) to the velocity potential distribution (ref. 21).

$$\varphi_{1\,ij}^{(n)*} = \frac{\varphi_{1\,ij}^{(n)}\,\varphi_{1\,ij}^{(n-2m)} - \left(\varphi_{1\,ij}^{(n-m)}\right)^2}{\varphi_{1\,ij}^{(n)} - 2\left(\varphi_{1\,ij}^{(n-m)}\right) + \varphi_{1\,ij}^{(n-2m)}} \tag{F11}$$

The results were not encouraging. A typical result is shown in figure F27 and presents ERROR versus iteration. Equation (F11) was applied using the velocity potential distributions from iterations 25, 50, and 75. The resulting velocity potential distribution was used as a starting point for 25 more iterations. The resulting ERROR's are shown by the triangle symbols. After an initial sharp perturbation, the ERROR fell back to the level at which equation (F11) was applied, and the convergence continued as if nothing had happened.

As a second step, equation (F11) was used on the pressure distribution rather than velocity potential distribution. Since the functional iteration solution process cannot be restarted with the predicted pressure distribution, successive results were monitored to see if they would converge. The process was to use increments of 25 (i.e., m = 25 in eq. F11), starting with the 25th iteration. Thus pressure distributions were obtained using equation (F11) with the results from iterations (25, 50, 75), (50, 75, 100), etc. Here again results were discouraging. The real part of the pressure behaved very well; the imaginary part had obvious problems up through the (100, 125, 150) set. Typical results are presented in figures F28 and F29.

Examination of both the velocity potential and the pressures as calculated with equation (F11) showed that the results were very sensitive to the input values when the values tended to lie along a straight line. Under these circumstances, for example, three positive values, obviously leading to more positive values, may well result in a negative value when used in equation (F11). To eliminate this problem, the equation was rewritten in the following form:

$$\varphi_{1\,ij}^{(n)*} = \varphi_{1\,ij}^{(n)} + \frac{1}{\dfrac{\varphi_{1\,ij}^{(n-2m)} - \varphi_{1\,ij}^{(n-m)}}{\varphi_{1\,ij}^{(n)} - \varphi_{1\,ij}^{(n-m)}} - 1} \cdot \left(\varphi_{1\,ij}^{(n)} - \varphi_{1\,ij}^{(n-m)}\right) \tag{F12}$$

Then, a lower limit was set on the value of the denominator in the second term to restrain the resulting extrapolation within certain limits. An example of the use of equation (F12) is shown in figure F30. The results show no improvement over using just straight relaxation.

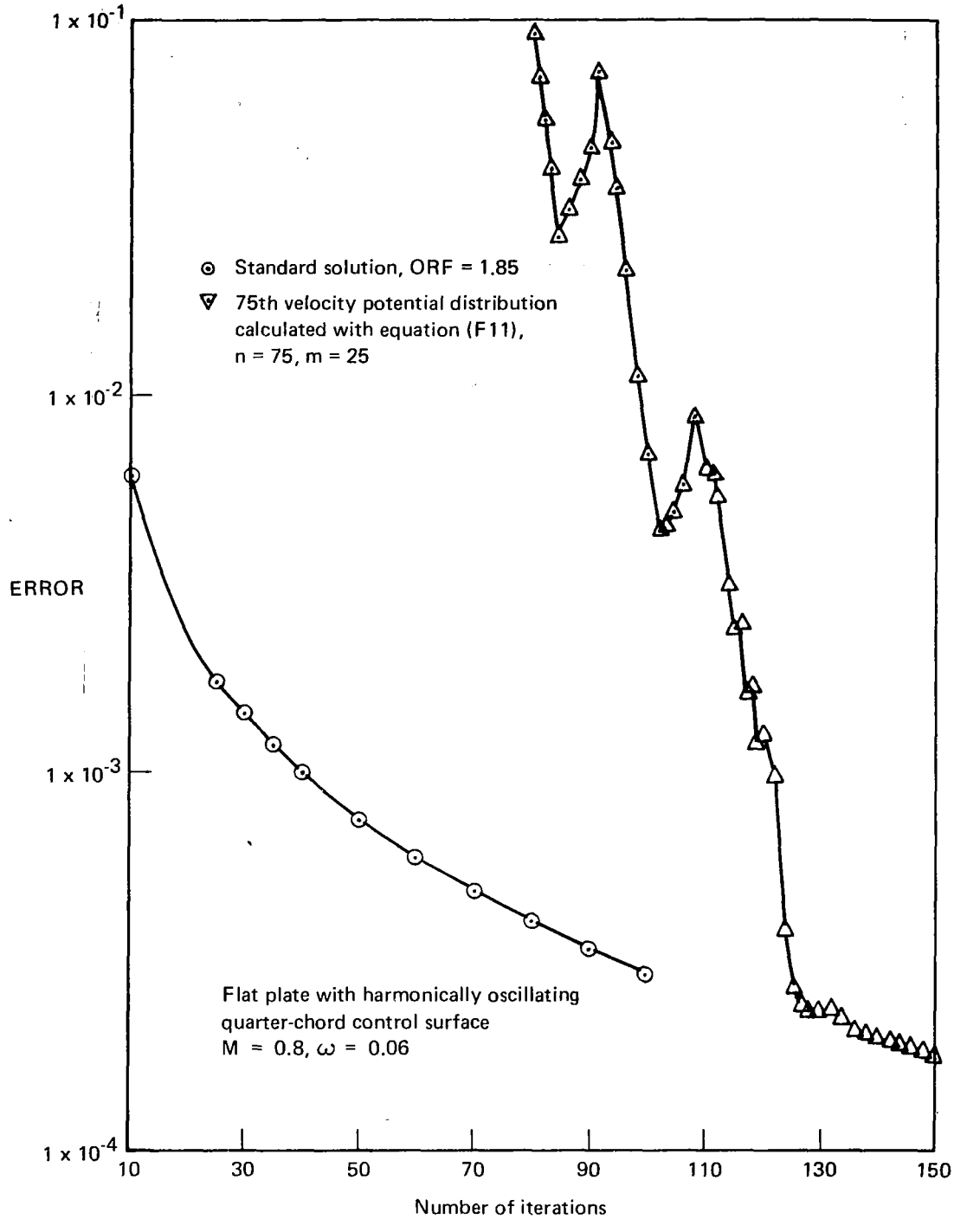

Figure F27. — Example of Solution Convergence Using the Aitken-Shanks Nonlinear Transformation

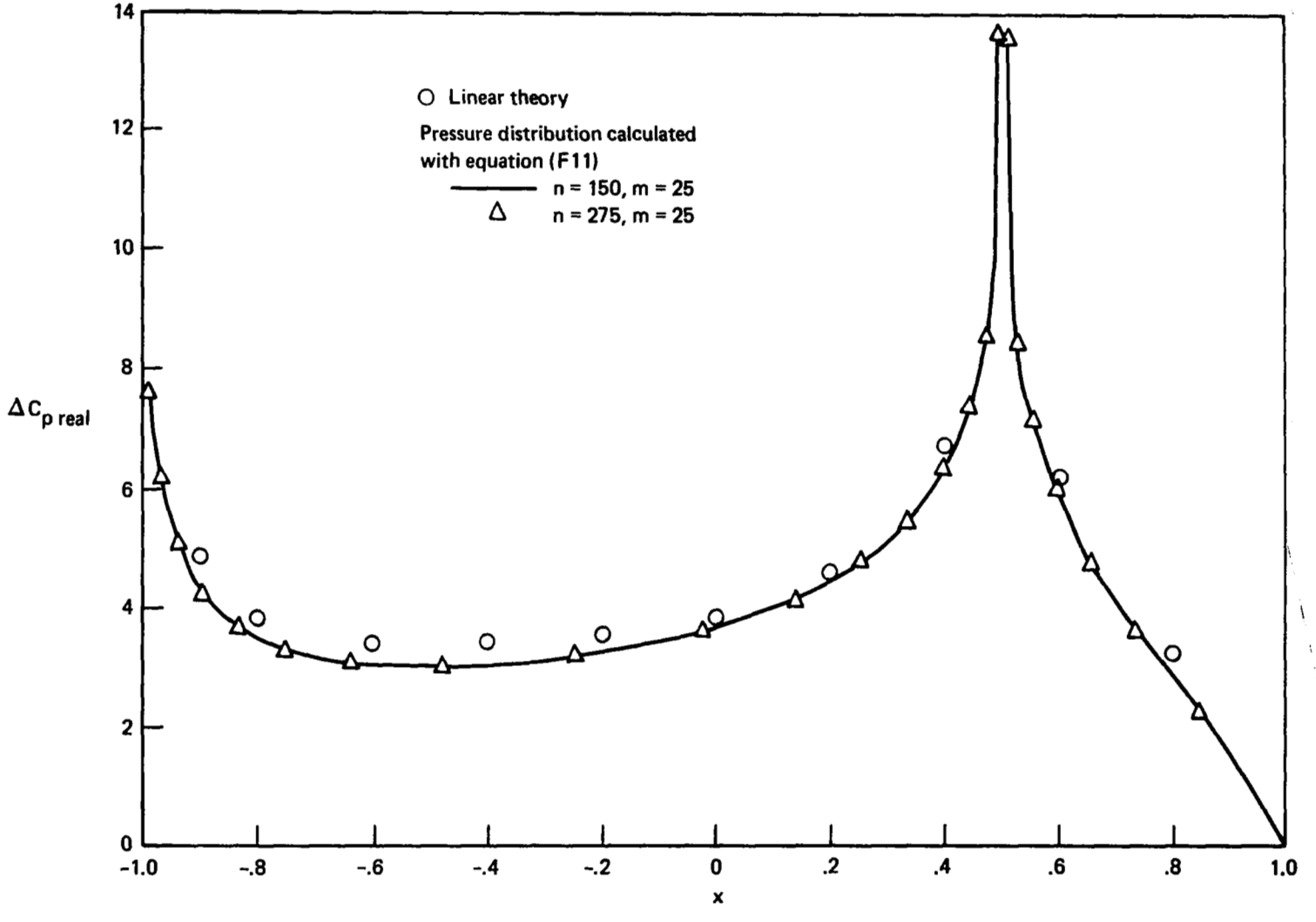

Figure F28. — Flat Plate With Harmonically Oscillating Quarter-Chord Control Surface — $M = 0.8$, $\omega = 0.06$

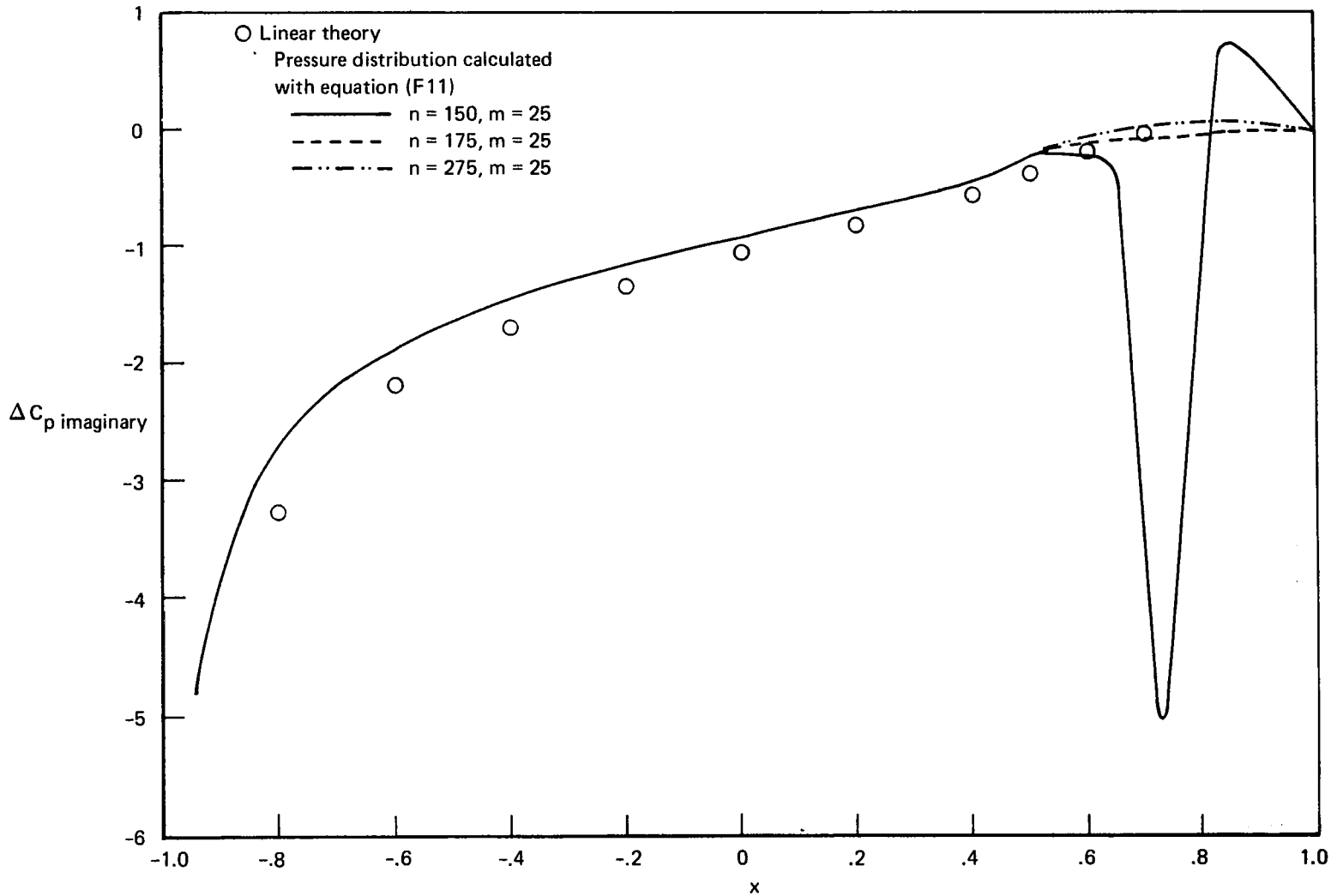

Figure F29. — Flat Plate With Harmonically Oscillating Quarter-Chord Control Surface — M = 0.8, ω = 0.06

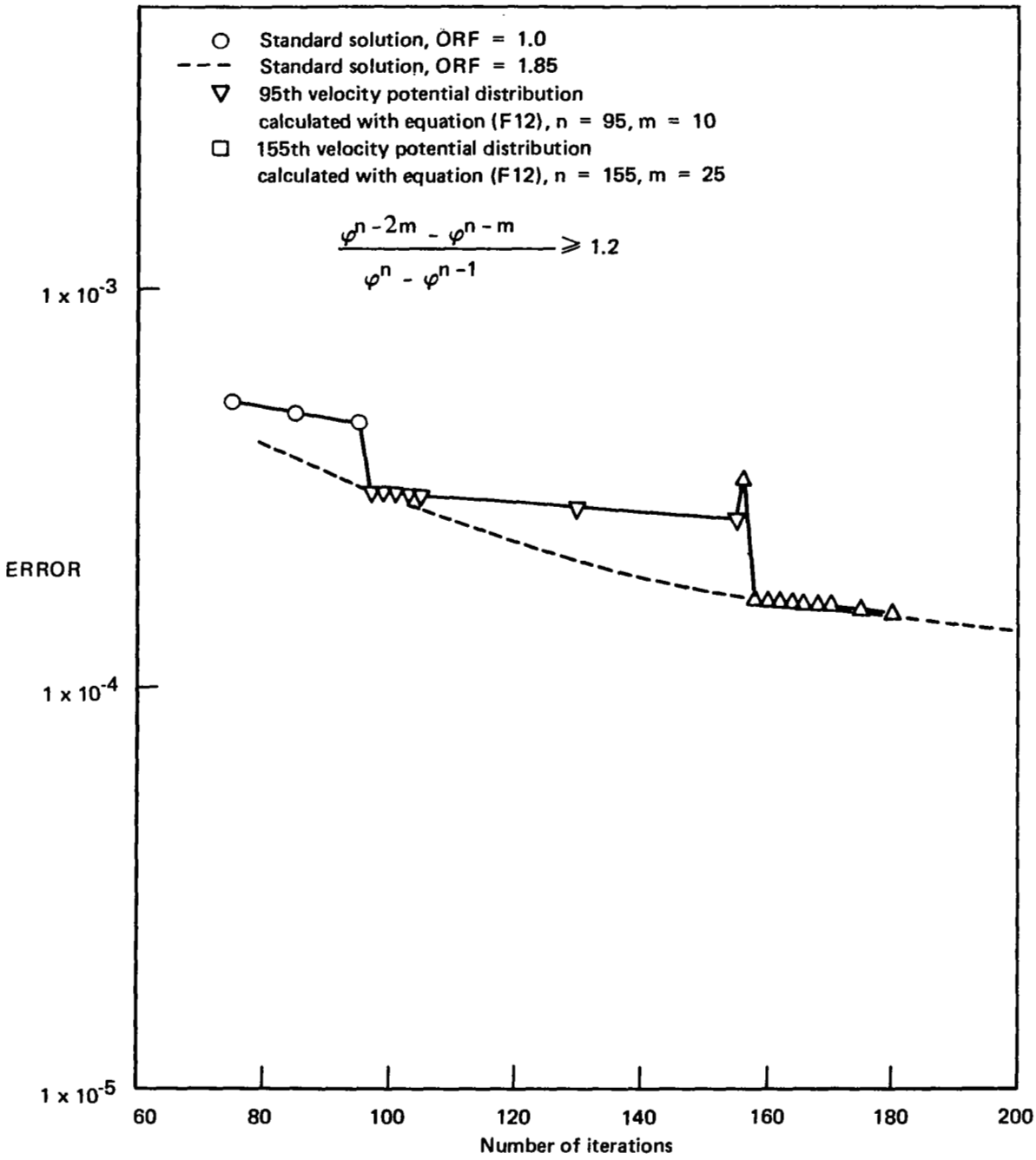

Figure F30. — Flat Plate With Harmonically Oscillating Quarter-Chord Control Surface — M = 0.8, ω = 0.06

REFERENCES

1. Ehlers, F. Edward: *A Finite Difference Method for the Solution of the Transonic Flow Around Harmonically Oscillating Wings.* NASA CR-2257, January 1974.

2. Murman, E.M.; and Cole, J.D.: *Calculation of Plane Steady Transonic Flow.* AIAA Paper 70-188, January 1970.

3. Krupp, J.A.; and Murman, E.M.: *Computation of Transonic Flows Past Lifting Airfoils and Slender Bodies.* AIAA Journal, Vol. 10, July 1972, pp. 880-887.

4. Rowe, W.S.; Winther, B.A.; and Redman, N.C.: *Prediction of Unsteady Aerodynamic Loadings Caused by Trailing Edge Control Surface Motions in Subsonic Compressible Flow—Analysis and Results.* NASA CR-2003, March 1972.

5. Redman, M.C.; Rowe, R.S.; and Winther, B.A.: *Prediction of Unsteady Aerodynamic Loadings Caused by Trailing Edge Control Surface Motions in Subsonic Compressible Flow—Computer Program Description.* NASA CR-112015, March 1972.

6. Tijdeman, H.; and Schippers, P.: *Results of Pressure Measurements on an Airfoil with Oscillating Flap in Two-Dimensional High Subsonic and Transonic Flow (Zero Incidence and Zero Mean Flap Positions).* NLR report TR 73078 U, August 1973.

7. Traci, R.M.; Albano, E.D.; and Farr, J.L., Jr.: *Perturbation Method for Transonic Flows About Oscillating Airfoils,* AIAA Paper No. 75-877, presented at AIAA 8th Fluid and Plasma Dynamics Conference, Hartford, Connecticut, June 16-18, 1975.

8. Jameson, Antony: *Iterative Solution of Transonic Flows Over Airfoils and Wings, Including Wings at Mach 1.* Comm. on Pure and Applied Math., Vol. 27, May 1974, pp. 283-309.

9. Jameson, Antony: *Three-Dimensional Flows Around Airfoils with Shocks.* In: Computing Methods in Applied Sciences and Engineering. Proceedings of the International Symposium, Versaukesm France, December 17-21, 1973. Part 2 (A74-45201), Berlin and New York, Springer-Verlag, 1974 pp. 185-212.

10. Hafez, M.M.; and Cheng, H.K.: *Convergence Acceleration and Shock Fitting for Transonic Aerodynamics Computations.* AIAA Paper No. 75-51, presented at the AIAA 13th Aerospace Sciences Meeting, Pasadena, California, January 20-22, 1975.

11. Martin, E. Dale; and Lomax, H.: *Rapid Finite-Difference Computation of Subsonic and Transonic Aerodynamic Flows.* AIAA Paper 74-11.

12. Morino, L.; and Kuo, C.C.: *Unsteady Subsonic Flow Around Oscillating Finite-Thickness Wings.* Boston University, Dept. of Aerospace Engineering, TR-73-03, February 1973.

REFERENCES—Continued

13. Chen, L.T.; Suciu, E.O.; and Morino, L.: *A Finite Element Method for Potential Aerodynamics Around Complex Configurations.* AIAA Paper No. 74-107, presented at AIAA 12th Aerospace Sciences Meeting, Washington, D.C., January 30—February 1, 1974.

14. Schmidt, W.; and Rohlfs, R.; and Vanino, R.: *Some Results Using Relaxation Methods for Two- and Three-Dimensional Transonic Flows.* Presented at the Fourth International Conference on Numerical Methods in Fluid Dynamics, Boulder, Colorado, June 24-28, 1974.

15. Ballhaus, W.F.; and Bailey, F.R.: *Numerical Calculation of Transonic Flow About Swept Wings.* AIAA Paper No. 72-677, presented at the AIAA 5th Fluid and Plasma Dynamics Conference, Boston, Massachusetts, June 26-28, 1972.

16. Varga, R.S.: *Matrix Iterative Analysis.* Prentice-Hall, Inc., Englewood Cliffs, New Jersey, 1962.

17. Bellman, R.: *Introduction to Matrix Analysis.* Second Edition, McGraw-Hill Book Company, New York, 1970.

18. Molberg, J.R.; and Reynolds, D.K.: *Iterative Solutions of the Scalar Helmholtz Equation in Lossy Regions.* IEEE Transactions on Microwave Theory and Techniques, Vol. 17, No. 8, 1969, p. 461.

19 Roache, Patrick J.: *Computational Fluid Dynamics.* Hermosa Publishers, Albuquerque, New Mexico, 1972.

20. Oswatitsch, K.; and Singleton, R.E.: *The Method of Parabolic Substitution for High Subsonic Flow.* Z. Flugwiss 30, Heft 11, November 1972, pp. 401-406.

21. Shanks, D.: *Non-Linear Transformations of Divergent and Slowly Convergent Sequences.* Journal of Math. and Phys., Vol. 34, 1955, pp. 1-42.

*U.S. GOVERNMENT PRINTING OFFICE: 1975 - 635-275/46